Characterization of the ESCRT pathway in *Candida albicans*

A DISSERTATION
SUBMITTED TO THE FACULTY OF THE GRADUATE SCHOOL
OF THE UNIVERSITY OF MINNESOTA
BY

Julie Marie Wolf

IN PARTIAL FULFILLMENT OF THE REQUIREMENTS
FOR THE DEGREE OF
DOCTOR OF PHILOSOPHY

Dana Davis, Adviser

February 2010

Acknowledgements

I would like to express my sincere gratitude to my advisor, Dr. Dana Davis, who has been a dedicated mentor during my time in his lab. He has been instrumental to my development as a scientist, not only with regards to protocols and techniques (and controls!), but also with regards to communication – a vital part of the scientific process. He has always challenged me to keep the bar high, and he has led by example, setting a high bar for himself. Additionally, I have learned something new from each of my labmates, past and present: Lucia Zacchi, Dr. Yong Un Baek, David Simmons, Dave Chmielewski, and Tim Rast. Thank you for hours of lab meetings, manuscript reading, and helpful conversations. Thank you to coworker Amy (Kullas) for balancing shared responsibility with a sense of humor and community. I am also grateful to my committee members: Dr. Sandy Armstrong, Dr. Judy Berman, and Dr. Lou Mansky, for feedback and support during my studies.

The studies in chapter 3 would not have been possible without the help of Diedre Johnson, a talented undergraduate who helped generate and do initial characterization of several of the ESCRT deletion mutants. Dave Chmielewski was central to getting the *in vivo* pathogenesis studies done for Chapter 3. Everything good I've learned about working with animals I've learned from Dave.

One of the best opportunities I've had during grad school was to be a part of the MinnCResT training program. This program not only funded my salary, but also provided a tightly knit biomedical research community. Thanks to Dr. Mark Herzberg, Michelle Lamere, and Ann Hagen for providing speaking opportunities, scientific discussion, and dinner to enhance my training.

Thanks to my friends who have supported me during my training: my MICaB cohort, who listened to practice seminars; my running buddy Colleen, who kept me motivated; my roommate Michelle and then Ami, who helped me explore the city outside of lab; Mouse, Mo, and Skitzo, whose annual reunions have kept me sane; Afia, my oldest friend who would generously lend an ear whenever I needed her.

I owe the greatest debt to my family: Mary Ann, Tony, Lisa, and Kevin. My parents have always believed in my abilities and encouraged me to reach for what I want. My sister keeps me grounded and helps me to take life less seriously. My brother makes me laugh and shares my awesome taste in music. Thank you for years of pretending to be interested in my research and listening patiently – even though you already know all about vacuoles.

Dedication

To my parents,
Tony and Mary Ann,
who taught me the two qualities most needed in science:
skepticism and optimism

Abstract

The human opportunistic pathogen *Candida albicans* has a signal transduction pathway unique to fungi, called the Rim101 pathway. The Rim101 pathway regulates the proteolytic activation of the transcription factor, Rim101, the activation of which is required for growth at neutral-alkaline pH. Many genes regulated by Rim101 play a role in *C. albicans* virulence, including genes involved in filamentation, cell wall structure, adhesion, and nutrient acquisition. The Rim101 pathway consists of two complexes: a signaling complex at the plasma membrane and a processing complex inside the cell, and both of these complexes are required for Rim101 activation. Rim101 activation also requires members of a second pathway, the endosomal sorting complex required for transport (ESCRT) pathway. The ESCRT pathway is required to generate multivesicular bodies prior to vesicle fusion with the vacuole. The ESCRT pathway consists of several polyprotein complexes recruited sequentially to the endosomal membrane to generate an intraluminal vesicle. The role of the ESCRT pathway has not been well characterized in *C. albicans*, and study of the ESCRT pathway is complicated by the secondary effect many ESCRT mutations have on Rim101 processing. These studies sought to separate ESCRT function from Rim101 function, and to investigate ESCRT pathway function in *C. albicans* virulence. In these studies, ESCRT and Rim101 pathway separation is demonstrated (1) at distinct domains on a single protein known to be part of both pathways by using alanine scanning mutagenesis and (2) at ESCRT pathway complexes by using deletion mutagenesis. The ESCRT pathway is demonstrated here to play a wholly Rim101-independent role in *C. albicans* virulence.

Table of Contents

Abstract iv
List of Figures vii
List of Tables ix

Chapter 1: Background **1**
- I. *Candida* disease and virulence mechanisms 1
- II. The ESCRT pathway 7
- III. The Rim101 pathway 17
- IV. Rim101 processing and *C. albicans* pathogenesis 24
- V. Goals of these studies 27

Chapter 2: Mutational analysis of *C. albicans SNF7* reveals genetically separable Rim101 and ESCRT functions and demonstrates divergence in bro1-domain protein interactions **29**
- I. Introduction ***29***
- II. Materials and methods ***33***
  - a. Strains and plasmids 33
  - b. Growth and filamentation assays 41
  - c. FM 4-64 staining 41
  - d. Protein Preparation 41
  - e. Cell fractionation 42
  - f. Western blot analysis 42
  - g. Immunofluorescence 43
  - h. Filamentation assays 43
  - i. FaDu cell damage assay 43
- III. Results ***44***
  - a. *snf7* alleles affecting vacuolar transport 46
  - b. *snf7* alleles affecting the Rim101 pathway 49
  - c. Filamentation-related *snf7* phenotypes 54
  - d. Snf7 protein localization 59
  - e. Rim101 processing and localization 63
  - f. Epithelial cell damage 68
- IV. Discussion ***71***
  - a. Separation of function and identification of functional domains 71
  - b. Effects on Rim101 processing and regulation 75
  - c. Effects on epithelial cell damage 76
  - d. Effects on filamentation 78

Chapter 3: The *C. albicans* ESCRT pathway plays a role in pathogenesis independent of Rim101 processing **80**
- I. Introduction ***80***
- II. Materials and methods ***84***
  - a. Media and growth conditions 84

b. Growth assays 85
c. Filamentation assays 90
d. Protein preparations 90
e. Western blot analysis 91
f. FaDu cell damage assay 91
g. Oropharyngeal candidiasis mouse modal 91
III. Results ***92***
a. ESCRT knockout mutations and ESCRT-dependent phenotypic defects 92
b. Rim101-dependent phenotypic defects 95
c. Rim101 processing 101
d. Iron-specific growth defects 103
e. Epithelial cell damage 105
f. Oropharyngeal candidiasis mouse model of disease 106
g. *VPS27* complementation 112
IV. Discussion ***113***
a. ESCRT complex relationship with Rim101 processing 113
b. ESCRT function in pathogenesis 116
c. *C. albicans* niche size 118

Chapter 4: *NHX1* plays a role in *C. albicans* filamentation and virulence **120**
I. Introduction ***120***
II. Materials and methods ***122***
a. Media and growth conditions 122
b. Strain manipulation 123
c. Growth assays 126
d. Filamentation assays 126
e. Protein preparation 126
f. Western blot analysis 127
III. Results ***128***
a. FM 4-64 trafficking phenotype 128
b. Rim101-dependent growth phenotypes 131
c. Rim101-dependent filamentation phenotypes 131
d. Rim101 processing 134
e. Epithelial damage assay 137
IV. Discussion ***141***

Chapter 5: General Discussion **145**
I. Can the ESCRT pathway and Rim101 pathways be separated? 145
II. Will the molecular interactions between ESCRT and Rim101 pathways be applicable to all fungi with a Rim101 pathway? 150
III. Where does Rim101 processing occur? 151
IV. How does the ESCRT pathway contribute to *C. albicans* virulence? 154

References **161**

List of Figures

Figure 1. Known functions of the ESCRT pathway 8
Figure 2. The ESCRT pathway 10
Figure 3. The Rim101 pathway 19
Figure 4. Model of ESCRT pathway and Rim101 pathway interaction at the endosome 25
Figure 5. Model of Snf7 role in Rim101 processing and in ESCRT complex functions 32
Figure 6. FM 4-64 localization in control strains and *snf7* mutants 48
Figure 7. Growth phenotypes of control strains and *snf7* mutants 50
Figure 8. Growth phenotypes of control strains and *snf7* mutants (streaks) 51
Figure 9. Mutant *snf7* alleles produce detectable protein 52
Figure 10. Comparison of mutant *snf7* alleles facilitates categorization into functional groups 58
Figure 11. Snf7 localization remains normal in alanine scanning *snf7* mutants 60
Figure 12. Rim101 processing is affected by some *snf7* mutants 64
Figure 13. Rim101 localization in alanine scanning *snf7* mutants 66
Figure 14. *C. albicans*-mediated FaDu cell damage is affected by Rim101-dependent defects 69
Figure 15. Model of Snf7 interactions 77
Figure 16. Model of ESCRT pathway and Rim101 pathway interactions 82
Figure 17. PCR genotyping of the *vps27*Δ/Δ strains 93
Figure 18. FM 4-64 trafficking defects of *C. albicans* ESCRT mutants 94
Figure 19. ESCRT-I, -II, and -III mutants, but not ESCRT-0 or -DS mutants, have Rim101-dependent defects 96
Figure 20. ESCRT mutant filamentation phenotypes 99
Figure 21. Rim101 processing in ESCRT mutants 102
Figure 22. ESCRT mutants have growth defects on iron-depleted medium 104
Figure 23. ESCRT mutants have FaDu epithelial cell damage defects 107
Figure 24. A *vps27*Δ/Δ mutant is attenuated in a mouse model of oral

candidiasis 109
Figure 25. PCR verification of strain genotype 129
Figure 26. The *nhx1*Δ/Δ mutation does not affect FM 4-64 trafficking in *C. albicans* 130
Figure 27. *NHX1* is not required for Rim101-dependent phenotypes 132
Figure 28. *NHX1* is not required for alkaline-induced filamentation but is required for serum-induced filamentation 133
Figure 29. *NHX1* does not play a role in Rim101 processing 135
Figure 30. *NHX1* is required for wild-type damage of FaDu epithelial cells 138
Figure 31. *NHX1* is not required for growth in the presence of CO_2 140
Figure 32. Two possible models of Rim101 processing 149
Figure 33. Model of ESCRT complex contributions to pathogenesis 160

List of Tables

Table 1. Homologous genes involved in the ESCRT/MVB pathway 9
Table 2. Homologous genes involved in the Rim101 pH response pathway 18
Table 3. Strains used in Chapter 2 studies 34
Table 4. Primers used in Chapter 2 studies 36
Table 5. Mutant *snf7* sequences 45
Table 6. Filamentation assays of *snf7* mutants 56
Table 7. Strains used in Chapter 3 studies 86
Table 8. Primers used in Chapter 3 studies 89
Table 9. ESCRT mutant filamentation phenotypes 100
Table 10. Strains used in Chapter 4 studies 124
Table 11. Primers used in Chapter 4 studies 125

CHAPTER 1

I. Candida disease and virulence mechanisms

Candida albicans is a human commensal fungus able to colonize many individuals as part of their endogenous microflora. As a commensal, *C. albicans* resides on the skin and the mucosal surfaces of the body, including the oral cavity, the gastrointestinal tract, and the vaginal cavity (34). In immunocompetent individuals, *C. albicans* is maintained at relatively low levels. Despite its ubiquity as a human commensal, it does not pose a threat to human health in most healthy hosts.

Certain conditions increase the risk of *C. albicans* overgrowth, promoting disease. Disease can range from a localized mucosal surface infection to a systemic bloodstream infection. Mucosal *C. albicans* infections cause a decreased quality-of-life among those infected, but have a low associated mortality rate. However, systemic bloodstream infections are associated with high morbidity and mortality. *C. albicans* is the fourth most common bloodstream nosocomial infection, and up to 50% of patients with bloodstream *Candida* infections will succumb to their infection (56, 149). *C. albicans* therefore remains a relevant human pathogen that can cause a variety of diseases.

A number of risk factors increase susceptibility to *C. albicans* overgrowth, including host immune dysfunction and host flora disruption. Immune system dysfunction or immunosuppression can occur through chemotherapy, genetic disposition, or infection. Decreased immune system function hinders the host's ability to maintain *C. albicans* at low levels, thereby facilitating *C. albicans* overgrowth. Host flora disruption can occur through chemotherapy, radiation, and is often associated with the use of antibiotics. Antibacterial drugs, particularly broad-spectrum antibiotics, alter the natural

flora composition within the host. This exposes a niche normally unavailable to *C. albicans*, into which the fungus can grow, uninhibited by its natural competitors. Thus, while *C. albicans* does not normally cause disease in healthy individuals, several risk factors increase susceptibility to *C. albicans* disease.

The most common forms of mucosal *C. albicans* infection are oral candidiasis (also known as thrush) and vaginal candidiasis. Oral candidiasis involves infection of tissues within the oral cavity. The tongue is commonly colonized, but the hard and soft palate can also be affected. Infection can be classified as membranous or erythromatous. During membranous infection, tissue surfaces are coated with a white layer of *C. albicans*, which is the result of biofilm formation at the infection site. During erythromatous infection, the tissue surfaces appear red and inflamed, but no concentrated white patches are observed. Thrush is commonly observed in newborns before their immune system has matured. Adults with compromised cell-mediated immunity, especially CD4 T cell dysfunction, are particularly vulnerable to oral candidiasis. Epithelial cells, including oral epithelial cells, also play an active immunological role by secreting antimicrobial peptides, such as histatins and defensins, which have anti-*Candida* activity (90, 170). Oral candidiasis can normally be treated with antifungal agents and resolve with few secondary effects.

Vaginal candidiasis involves infection of tissues within the vaginal cavity, such as the cervix or labia. Similar to oral *C. albicans* infections, the infection can be either membranous, with white *C. albicans* growth readily apparent, or erythromatous, with red, inflamed tissue but no observable yeast growth. Unlike oral candidiasis, host susceptibility to vaginal infection is not T cell-dependent (60). Innate immunity,

particularly the beta-glucan-binding pattern recognition receptor Dectin-1, appears to play an important role in protection against vaginal infection (59, 71). Like oral candidiasis, vaginal candidiasis is normally easily treated with local or systemic antifungal drug treatment with little to no secondary effects.

A more serious form of infection is systemic candidiasis. Systemic infections can be seeded from a *C. albicans* biofilm growing on an in-dwelling catheter or other implanted medical device, such as a heart valve. They may also arise by organisms escaping from normal GI colonization, such as when the epithelial cell barrier is damaged during total parenteral nutrition (100, 121). Once in the bloodstream, *C. albicans* can attach and invade into a number of internal organs. Patients who succumb to infection often die of organ failure due to microbe- and host-mediated tissue damage. Despite patient treatment with intensive systemic antifungal therapy, up to 50% of patients succumb to the disease (56, 81, 149).

Several virulence factors of *C. albicans* are required for both mucosal and systemic infections. These include the secretion of degradative enzymes, the ability to grow in several morphologies, and the ability to adapt to a wide variety of environmental conditions.

Degradative enzymes: *C. albicans* secretes a variety of degradative enzymes, including proteinases, lipases, and phospholipases (83, 169). Some of the best characterized are those in the Secreted Aspartic Proteinase, or *SAP*, family. These are a group of 10 proteinases regulated by environmental conditions. Some members (*SAP1-3*) are induced during growth in acidic conditions, while others (*SAP 4-6*) are induced during growth in alkaline conditions (22, 180). Proper *SAP* expression is required for

colonization of distinct niches and plays a role during disease. For example, a Δ*sap1-sap3* mutant, but not a Δ*sap4-sap6* mutant is less adherent to buccal epithelial cell and forms fewer oral lesions during oral candidiasis than wild type (201). Conversely, a Δ*sap4-sap6* mutant, but not a Δ*sap1-sap3* mutant, causes less tissue damage during disseminated infection compared to wild type (97). The *SAP* members have also been investigated for individual contributions to *C. albicans* biology. For example, further characterization of *SAP5* has confirmed its requirement for epithelial cell damage, and demonstrated a Sap5-dependent degradation of E-Cadherin between epithelial cells, facilitating the beginning steps of *C. albicans* invasion (198). The *SAP*s therefore play a role during various stages of *C. albicans* infection, and are regulated by environmental cues.

Morphological shift: *C. albicans* is a polymorphic microbe. One form of *C. albicans* growth is the yeast cell, which is similar in shape and size to cells of the model yeast *Saccharomyces cerevisiae*. Yeast cells divide by budding and are round or slightly ovoid (124). Yeast cell growth is favored by acidic environmental conditions, low surrounding temperatures (less than 37°C), and rich media conditions (18). Because of their small size and less adherent properties than hyphal cells, yeast cells are thought to be important in dissemination of *C. albicans* through the vasculature during bloodstream infections (168).

A second form of *C. albicans* growth is the hyphal cell. Hyphal cells divide by septation and are not easily visually distinguished from one another, as there is no constriction between hyphal cells. Hyphal cells grow in one direction, extending the hyphal length before generating septations between elongated cells. Hyphae express a

number of adhesive proteins not present during yeast-cell growth, and the extending tip secretes high concentrations of SAPs and other degradative enzymes (38, 185). A number of environmental conditions are known to favor hyphal formation, including alkaline pH, high temperature (37°C and higher), presence of CO_2 or serum, and a variety of starvation conditions, including carbon and nitrogen starvation (18, 172). Because of their degradative and adherent properties, hyphae are thought to be important for tissue invasion and destruction during infection.

A third morphological form is the pseudohyphal cell. Pseudohyphal cells divide by budding and look like extremely elongated yeast cells. They can reach hyphal cell lengths but are distinguished from true hyphae by visible constriction between cells. The question of whether pseudohyphae are truly a third, independent morphology, or whether they are an intermediate form based on induction levels has remained in the field for many years. Recent work has suggested that pseudohyphae are intermediates between yeast and hyphae, and are present under weak hyphal-induction signals (36). However, both mechanism and function of pseudohyphal cell formation remain poorly understood.

While the yeast-to-hyphae transition is considered an important virulence factor for *C. albicans* pathogenesis, both yeast cells and hyphal cells are required for virulence. The requirement for yeast-to-hyphae transition in pathogenesis was first demonstrated by mutations in filamentation activators *EFG1* and *CPH1*. An *efg*Δ/Δ *cph*Δ/Δ double mutant strain is unable to form pseudohyphae or hyphae, and is avirulent in a mouse model of disseminated candidiasis (115). The requirement for hyphae-to-yeast transition in pathogenesis was demonstrated by mutations in filamentation repressors *NRG1* and *TUP1*. Deletion of these genes results in constitutive hyphal (*nrg1*Δ/Δ) or pseudohyphal

(*tup1*) cell growth, and both the *nrg1*Δ/Δ and *tup1*Δ/Δ mutant strains display virulence defects in mouse models of disseminated candidiasis (27, 28). In addition to decreased virulence during bloodstream infection, strains unable to transition between morphologies cause less damage to endothelial cells (150) and epithelial cells (197) than wild-type *C. albicans*. The ability to transition from yeast to hyphal cells, and back again, are therefore both required during the course of infection.

Environmental adaptation: *C. albicans* colonizes humans as a commensal microbe, and can be found in such diverse niches as the stomach mucosal lining, the vaginal tract, and the skin. To survive the changes brought about by these different environments, a network of response elements facilitates proper gene expression under each set of conditions. *C. albicans* stress responses to salt stress, oxidative stress, nutrient starvation, tissue architecture, and environmental pH help the cell survive in these various conditions (46, 50, 57, 80, 101, 157, 164). Most environmental factors that require active change in gene expression also influence cell morphology. For example, the Rim101 pathway regulates genes required for growth at alkaline pH conditions as well as the alkaline-induced yeast-to-hyphal transition (204). The numerous regulatory networks promote an environmental flexibility of *C. albicans* that allows it to colonize numerous niches in its human host.

C. albicans adaptation to new environments is critical for its ability to colonize the diverse mucosa on which it lives. These environments can quickly change, such as areas within the mouth, which decrease by 0.7 pH units for up to 120 minutes after eating (87), or the vaginal cavity, which changes from a normally acidic pH of 4-5 to a neutral pH of 6.5-7 during menstruation (32, 103). The microbe itself can experience a change in

environmental pH if moving through the GI tract, which varies from oral cavity (resting pH 6.7) to stomach (pH 2-4) to the small intestine (pH 8). This dissertation focuses on two processes required for continued growth of *C. albicans* in neutral or alkaline environments, and the role of these processes in pathogenesis. The first is the trafficking of endosomes to the vacuole via the endosomal sorting complex required for transport (ESCRT) pathway. This pathway serves to acquire nutrients in alkaline environments, such as iron (202), and is also important in signal attenuation via receptor degradation (166, 179). The second is the Rim101 transcriptional activation pathway. This pathway directly governs expression of genes required for growth at neutral-alkaline environments, including genes involved in nutrient acquistion, morphology, and cell wall composition (47, 50). This dissertation investigates the intersection of these two processes at a single molecule involved in both pathways, Snf7. It also describes a role for the ESCRT pathway during *C. albicans* pathogenesis independent of the Rim101 pathway. Together, these studies contribute novel characterization of the molecular interactions of these pathways as well as the role of ESCRT function during *in vitro* and *in vivo C. albicans* infections. These two pathways are discussed in detail below.

II. The ESCRT pathway:

The endosomal sorting complex required for transport (ESCRT) pathway functions in membrane scission when the cytoplasmic machinery does not have access to the external side of a given membrane bud neck. Several processes result in formation of a bud neck inaccessible to the cytoplasmic machinery (Figure 1). The ESCRT complex is required for the final membrane scission event, which often results in separation of two independent, membrane-bound vesicles.

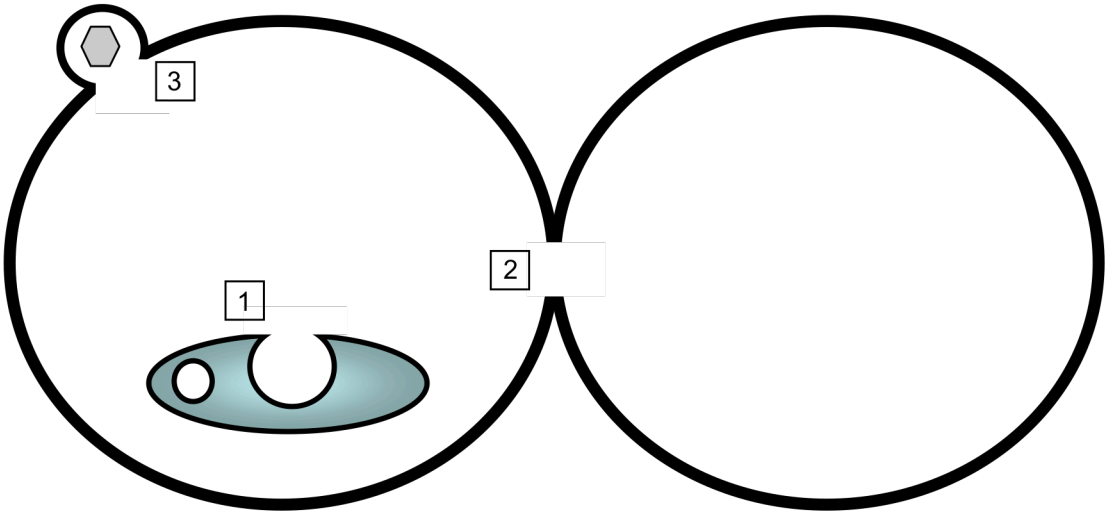

Figure 1. Known functions of the ESCRT pathway. A model of a cell, with the plasma membrane represented by the thick black line. The ESCRT complex is required for the membrane scission steps during (1) multivesicular body (MVB) formation, (2) cytokinesis, and (3) viral budding. ESCRT function in MVB formation has been described in yeast and metazoan systems, but ESCRT function in cytokinesis and viral budding has not been described in yeast.

Table 1. Homologous genes involved in ESCRT/MVB pathway

Complex	Yeast	Humans
ESCRT-0	*VPS27*	HRS
	HSE1	STAM1, STAM2
ESCRT-I	*VPS23*	Tsg101
	VPS28	VPS28
	VPS37	VPS37A-VPS37D
	MVB12	MVB12
ESCRT-II	*VPS36*	EAP45
	VPS22	EAP30
	VPS25	EAP25
ESCRT-III	*VPS20*	CHMP6
	SNF7/VPS32	CHMP4A-CHMP4C
	VPS2	CHMP2A, CHMP2B
	VPS24	CHMP3
ESCRT-DS	*BRO1*	ALIX
	DOA4	AMSH
	VPS4	VPS4A, VPS4B
	VTA1	
	IST1	

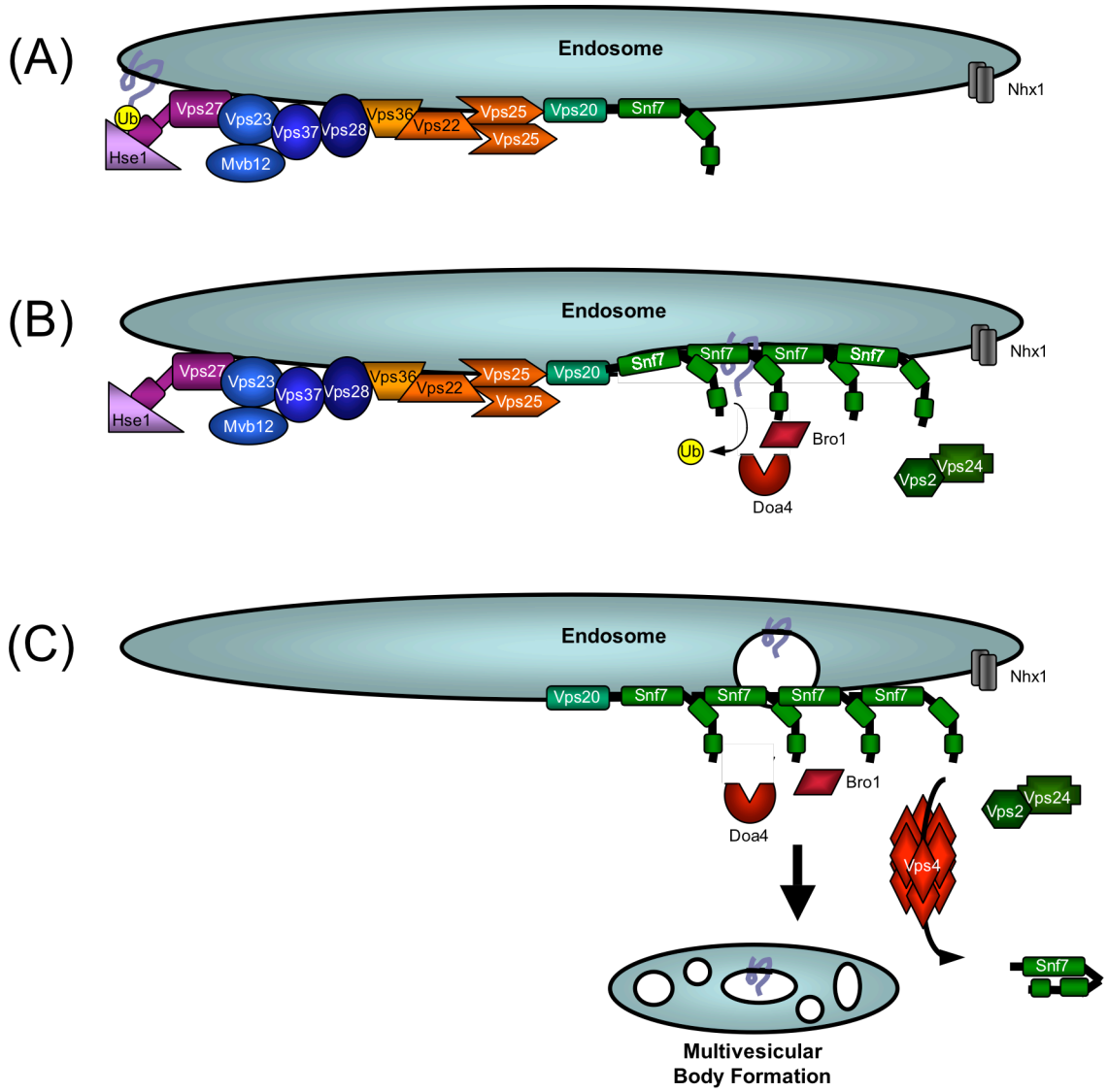

Figure 2. The ESCRT pathway. (A) During formation of an endosomal intralumenal vesicle (ILV), ESCRT-0 (Vps27 and Hse1), ESCRT-I (Vps23, Mvb12, Vps37, and Vps28), and ESCRT-II (Vps36, Vps22, and Vps25) are recruited sequentially to the ubiquitinated cargo protein, and arrive as fully-assembled complexes, followed by ESCRT-IIIa (Vps20 and Snf7). It is unknown when Nhx1 becomes incorporated into the endosome, so it is included at all stages in this model. (B) Snf7 oligomerizes around the cargo protein, eventually recruiting ESCRT-IIIb (Vps2 and Vps24), Bro1, and Doa4. Doa4 deubiquitinates the cargo protein. (C) The AAA-ATPase Vps4 is required to dissociate ESCRT-III from the endosomal membrane. Vps4 forms an oligomeric ring, through which the ESCRT-III monomers are theorized to pass and fold into their "closed," inactive form. The end result is a newly formed ILV containing the cargo protein.

Many of the genes involved were identified through *S. cerevisiae* screens for irregular protein sorting to the vacuole, hence the common name *VPS* for vacuolar protein sorting, although other systems use different nomenclatures (Table 1). The ESCRT pathway was later found to be required for generation of multivesicular bodies (MVBs), a transitional vesicle between the endosome and vacuole. ESCRT pathway mutations display a shared trafficking phenotype called the class E phenotype. This phenotype was originally defined by the missorting of the vacuolar protease carboxypeptidase Y (159), and, later, by the accumulation of the membrane-staining dye FM 4-64 in large aggregates at the vacuolar perimeter (196). These dye aggregates are sometimes called class E exclusion bodies, and represent the prevacuolar complex (PVC), an accumulation of vesicles unable to fuse with the vacuole (196). The ESCRT function in membrane scission is therefore required for proper MVB formation, and thus subsequent endosome-to-vacuole trafficking.

ESCRT function is conserved among all eukaryotes, from yeast to protozoa (*Dictyostelium*) (19) to metazoa (*Drosophila melanogaster, Homo sapiens*) (155, 195). Primitive ESCRT homologs have even been identified in archaea (111, 167), suggesting its evolution precedes the divergence of archaea and eukaryota.

The ESCRT complex is required for membrane scission when the membrane buds away from the cytoplasm (Figure 1). Although originally described in MVB formation, additional roles have since been described for the ESCRT complex. The ESCRT complex is required during cell division (division in archaea, cytokinesis in higher eukarya) for the final abscission of cell membranes (111, 128, 167). Additionally, many enveloped viruses hijack the ESCRT machinery when budding during production of infectious virus. Viral

proteins recruit the ESCRT machinery either to the plasma membrane, where a virion-enveloping vesicle "buds" with the help of ESCRT machinery, or to an MVB which is then facilitates viral release via the exosome pathway (119, 120, 129). Thus, while the ESCRT pathway function has been most meticulously characterized in the context of MVB formation, the ESCRT machinery plays multiple roles in the cell.

During MVB formation, the ESCRT pathway is required to generate intraluminal vesicles (ILVs) within an endosome after endocytosis has occurred. These ILVs form around a specific cargo protein, which has been signaled for degradation by ubiquitination. As multiple ILVs are generated within the endosome, mature MVBs (called late endosomes in some systems) are formed. Mature MVBs fuse with the vacuole, releasing luminal content, including ILVs, into the vacuolar lumen. The acidic environment inside the vacuole, and the degradative enzymes therein, break down the ILVs to recycle their components within the cell. MVB formation is important for recycling plasma-membrane-embedded molecules, such as protein receptors or transporters, which are not accessible by the cytoplasmic proteases. It is also the only identified pathway known to promote fusion of endosomes, via MVB formation, with the vacuole, facilitating delivery of nutrients taken up by endocytosis (202). Thus, the ESCRT pathway generates MVBs, which are important for recycling membrane-embedded molecules and delivering endosomal content to the vacuole.

The ESCRT pathway consists of a number of polyprotein complexes, which interact and result in the formation of an ILV (Figure 2). Much of our understanding of the ESCRT pathway comes from work done in *S. cerevisiae*. These studies have identified ubiquitination as a key signaling modification to both initiate endocytosis and

to subsequently recruit ESCRT components. These studies have also identified four complexes involved: ESCRT-0 (composed of Vps27 and Hse1), ESCRT-I (Vps23, Vps37, Vps28, and Mvb12), ESCRT-II (Vps36, Vps22, and Vps25), and ESCRT-III (Vps20, Snf7/Vps32, Vps24, and Vps2) are required for ILV formation (8, 9, 16, 88). Genetic evidence suggests that these complexes are sequentially recruited to the ubiquitylated cargo protein. ESCRT-III then recruits downstream proteins (called ESCRT-DS in this text) required for the final steps in ILV formation, deubiquitination and disassembly of the ESCRT complexes.

ESCRT-0 is initially recruited through the endosomally-enriched phosphatidylinositol 3-phosphate and through both Vps27- and Hse1-ubiquitin interactions (Figure 2) (16, 184). ESCRT-0 then recruits ESCRT-I through Vps27-Vps23 interactions, and through Vps23-ubiquitin interactions (88, 89). ESCRT-I then recruits ESCRT-II to the endosomal membrane through Vps28-Vps36 interactions (69). The complexes ESCRT-0, ESCRT-I, and ESCRT-II arrive at the endosomal membrane as fully formed complexes, and each individual complex can be purified from the cell cytoplasm, suggesting that these protein complexes do not require further assembly.

The last complex of the pathway, ESCRT-III is thought to play a major role in forming the nascent ILV. ESCRT-III does not arrive fully formed, but is brought in as subcomplexes (Figure 2). The first subcomplex, ESCRT-IIIa, consists of the heterodimer Vps20 and Snf7, which are attracted to the endosomal membrane through Vps25-Vps20 interactions (189). Vps20 is myristolated, and the myristol group adds stability to the protein-membrane interactions (9). Snf7 then recruits more Snf7 molecules, oligomerizing through self-interactions (188). Eventually, the second subcomplex of

ESCRT-III is brought in: a heterodimer of Vps24 and Vps2, attracted through Snf7-Vps24 interactions (9, 188). Biochemical studies suggest that the final ratio of Vps20:Snf7:Vps24:Vps2 is 1:10-15:1:1, or that a total of 10-15 Snf7 molecules are recruited to ESCRT-III for every molecule of Vps20/Vps24/Vps2 (188). The Snf7 oligomers are thought to form filaments that bend the endosomal membrane to form a nascent ILV (74, 110). There is some debate on whether the Snf7 oligomers form a coil, growing outward, or a fence, corralling the cargo proteins to be incorporated into the ILV. Regardless, this oligomerization has been shown to induce membrane budding, both *in vitro* and *in vivo* on artificial vesicles (74, 84).

In addition to requiring an assembly step not observed with other ESCRT complexes, the ESCRT-III proteins require an activation step unique to these complex members. All ESCRT-III members consist of 5-6 alpha helices that span the protein length, and have a basic N-terminal half and acidic C-terminal half. The N-terminal region is required for membrane interaction: a truncated hSnf7-1 containing only the N-terminus constitutively bound to membranes, while a truncated hSnf7-1 containing only the C-terminus remained cytosolic (110). Small angle X-ray scattering data suggest hVps24 has two folding conformations in solution: a closed, globular conformation and an open, extended conformation (104). These properties permit the molecules to fold up in their "inactive" phase when found as monomers in the cytoplasm; in fact, the ability to fold is thought to be required to remain cytosolic (105, 175). The C-terminal helix is thought to play an autoinhibitory role in protein activation, supported by studies demonstrating C-terminal truncations of hVps24 result in trafficking and cytokinesis defects and constitutive hVps24 membrane association (55). This has led to a model in

the field whereby the ESCRT-III monomers in the cytosol are folded, and upon recruitment to the endosomal membrane, the monomers unfold. This makes the C-terminal end available for further interactions, thereby recruiting additional monomers.

ESCRT-III member Snf7 recruits several proteins involved in MVB formation in addition to the Vps24/Vps2 heterodimer. One of these additional proteins is Bro1, a protein involved in deubiquitinating the cargo protein prior to its incorporation into an ILV (136, 140). Snf7 recruits Bro1 by interacting with the Bro1 bro1-domain (92, 122). Bro1 then recruits and activates the deubiquitinase Doa4 (117, 136, 160). *DOA4* overexpression can rescue a *bro1*Δ *S. cerevisiae* strain, suggesting that alternative recruitment mechanisms may also recruit Doa4 to the endosome, and Snf7 has been shown to interact with Doa4 through yeast-two-hybrid interactions (25). Both Bro1 and Doa4 are required for normal MVB formation and vacuolar fusion, but trafficking defects of a Δ*bro1* or Δ*doa4* strain are less severe than those of ESCRT complex members (3, 98, 140). Thus, Snf7 recruits proteins necessary for deubiquitinating cargo protein, and this step is necessary for normal MVB formation.

Another well-characterized interaction of Snf7 is with the AAA-ATPase (ATPase Associated with a variety of Activities) Vps4. Vps4 is required for release of the ESCRT-III complex from the endosomal membrane prior to formation of an independent, membrane-bound ILV inside the endosomal lumen (10). Vps4 interacts with ESCRT-III members through the Vps4 microtubule interacting and transport (MIT) domain (138, 171, 186). After recruitment to the ESCRT-III complex, Vps4 multimerizes to form a double-barrel ring of 12 Vps4 subunits (211). Its ATPase activity provides the energy required to dissociate ESCRT-III subunits from the endosomal membrane (67). The

subunits are hypothesized to pass through the double-barrel Vps4 ring, which facilitates their refolding to the "inactive" form (Figure 2) (76). The energy produced from the ATP hydrolysis is further theorized to be coupled to the final step in membrane scission. Thus, Snf7 interacts with Vps4 to facilitate ESCRT-III recycling and to provide energy for the final step in membrane scission.

Several steps ensure that Vps4 activity is properly regulated. The first is proper Vps4 recruitment through ESCRT-III interactions, as described above. Vps4 oligomerization and ATPase activity are additionally regulated by *IST1* and *VTA1*, respectively (7, 53). The absence of either of these genes leads to weak class E phenotypes, and for simplicity they have been omitted from Figure 1.

The ESCRT machinery is responsible for generating cargo-carrying ILVs as endosomes mature before vacuolar fusion. Several additional processes are also required for normal endosome maturation, most notably membrane lipid concentration and endosomal lumen content. Membrane lipid content is regulated in part by *FAB1*, a lipid kinase that phosphorylates phosphatidylinositol-3-phosphate to the endosome-associated phosphatidylinositol-3,5-bisphosphate (64, 139). Luminal content is influenced by *NHX1*, an endosomal Na^+/H^+ transporter that sequesters sodium ions inside the endosome (24, 135), and vacuolar H^+-ATPases that are also found on late endosomes (91, 118, 194). The genes involved in these processes do not directly interact with the ESCRT machinery, but deletion of *FAB1* or *NHX1* also leads to a class E phenotype. Many other genes are also required for proper endosome maturation and trafficking, such as the endosomal Snap Receptor SNARE *PEP12* required for vesicle fusion and Rab GTPase *VPS21*, but do not result in a class E phenotype when deleted (65, 66, 159). Thus, the ESCRT complex

pathway is only one of several processes required for endosomal maturation and endosome-to-vacuole trafficking.

III. The Rim101 pathway:

The Rim101 pathway is a signaling pathway conserved within the fungal kingdom. To date, homologous pathways have been described in ascomycetes (*S. cerevisiae*, *C. albicans*, *Aspergillus nidulans*, *Yarrowia lipolitica*, *Sclerotinia sclerotiorum*, *Collectotrichum acutatum*, and *Fusarium oxysporum*) (108) (102) (192) (163) (210) (35) (153), and basidiomycetes (*Ustilago maydis* and *Cryptococcus neoformans*) (6) (114). In the ascomycetes, signaling occurs in response to extracellular pH and is required for growth in neutral or alkaline environments. Rim101 signaling has not been described in any non-fungal species.

Rim101 signaling results in the activation of the transcription factor Rim101 (called PacC in some mold species; all genes are referred by *S. cerevisiae*/*C. albicans* nomenclature within this text) (Table 2). Rim101 protein is produced constitutively but its activation occurs only in neutral-alkaline pH conditions (47). Rim101 activation occurs through proteolytic cleavage of its C-terminal end. This reveals a truncated, active N-terminus, which then translocates to the nucleus to govern gene expression changes.

An upstream signaling pathway, called the Rim101 pathway, regulates Rim101 activation (Figure 3). This pathway includes two proteins able to interact with Rim101. The first, Rim20, binds to the C-terminal end of Rim101, through a YPXL binding motif on Rim101 (199, 206). Rim20 also contains a bro1-domain homologous to that of ESCRT-related protein Bro1 (191, 207). The second, Rim13, is the putative protease

Table 2. Homologous genes involved in the Rim101 pH response pathway

Complex	*C. albicans*	*S. cerevisiae*	*A. nidulans*
Activation complex	*RIM21*	*RIM21*	*PALH*
	DFG16	*DFG16*	n/a
	RIM9	*RIM9*	*PALI*
	RIM8	*RIM8*	*PALF*
Unknown	*Orf19.2914 (?)*	*YGR122w*	*PALC*
Processing complex	*SNF7*	*SNF7*	*VPS32*
	RIM20	*RIM20*	*PALA*
	RIM13	*RIM13*	*PALB*
	RIM101	*RIM101*	*PALC*

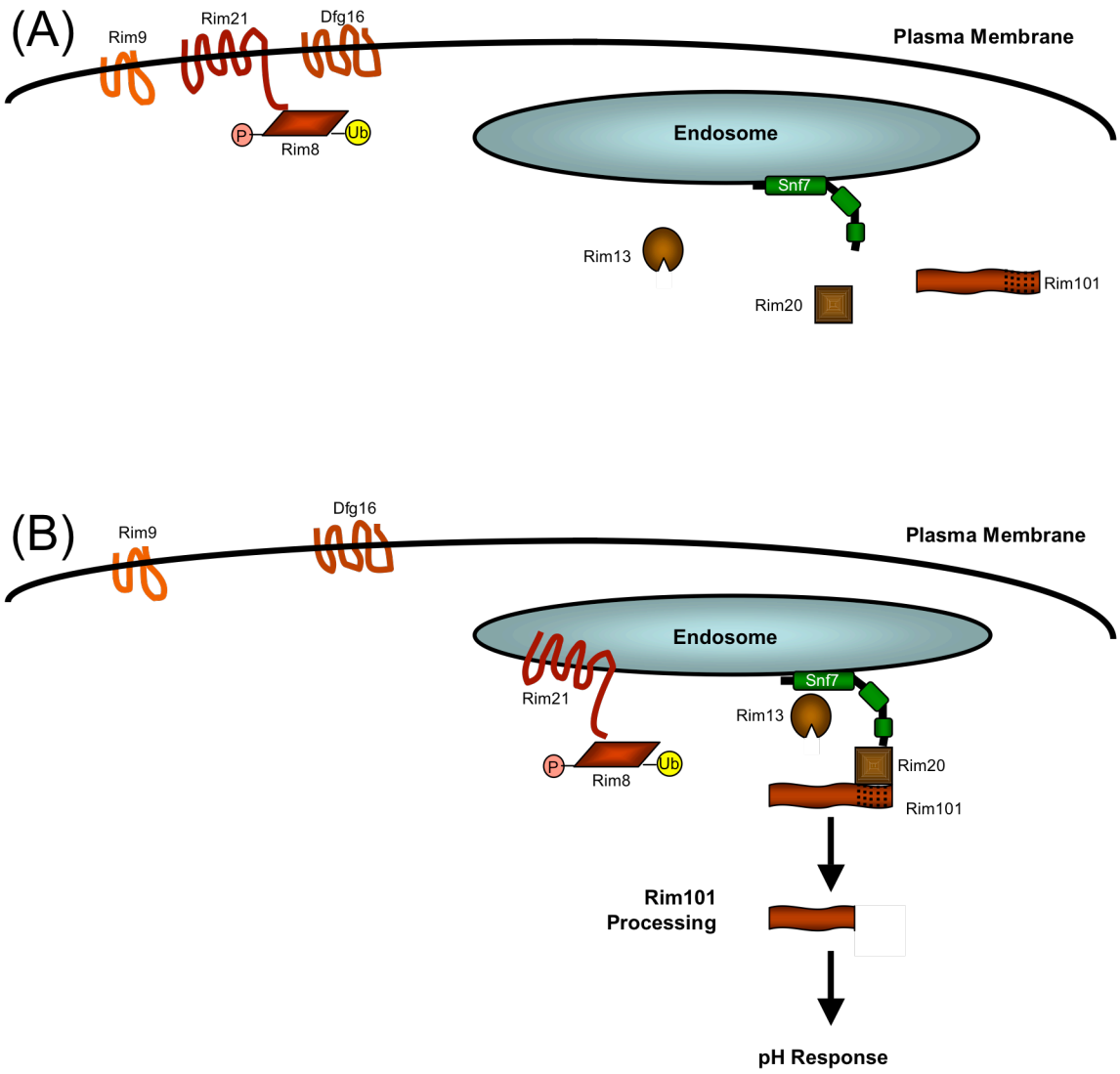

Figure 3. The Rim101 pathway. (A) Rim101 signaling requires three plasma-membrane-spanning proteins, Rim9, Rim21, and Dfg16. Rim21 is the putative receptor. Rim8 is an arrestin-like protein that undergoes ubiquitination and phosphorylation and that can interact with Rim21. The Rim21-Rim8 protein complex is called the signaling complex in this text. Rim13 is the putative protease responsible for Rim101 processing. Rim20, which contains a bro1-domain, is a scaffold protein that interacts with the C-terminal end of Rim101. Snf7, Rim13, and Rim20 are directly required for Rim101 processing. These four proteins are refered to in this text as the processing complex. Rim8 ubiquitination is depicted although not detected in *C. albicans*.

responsible for the proteolysis of Rim101 during activation (62, 107, 187). Rim13 sequence contains some homology to calpain proteases but does not maintain the calcium-binding domain found in true calpains (43). Both Rim20 and Rim13 interact with Rim101 and are necessary for Rim101 activation by proteolysis.

How do Rim13 and Rim20 promote Rim101 processing? Although Rim13 and Rim20 do not interact directly, both proteins interact with Snf7 in *S. cerevisiae* and *Y. lipolytica* (20, 25, 86). These interactions are thought to occur at the endosomal membrane, based on studies showing that ESCRT members upstream of *SNF7* are required for Rim101 processing. ESCRT-I, -II, and -IIIa complexes are required for Rim101 processing in *S. cerevisiae*, although ESCRT-0 member *VP27* is not. These upstream ESCRT proteins do not directly interact with Rim101 processing machinery, but are necessary for Snf7 recruitment to the endosomal membrane (165, 207). Despite producing cytoplasmic Snf7, strains with upstream ESCRT mutations are not able to promote Rim101 processing, suggesting Rim101 processing is dependent on Snf7 localization. Endosomal processing is further supported by colocalization studies demonstrating that Snf7 and Rim20 colocalize in a punctate manner (26). Thus, Snf7 mediates interaction between Rim13 and Rim20 to promote Rim101 processing.

Unlike Rim20, Rim13 has not been localized in *S. cerevisiae*. Studies in *A. nidulans* have shown Rim13 interacts with ESCRT-III member Vps24 through the Rim13 MIT domain in this organism (162). Cell fractionation studies have demonstrated that these interactions occur in the same fraction that contains endosomal marker Pep12. This same study showed that Rim13 did not interact with Snf7, negating the possibility that Rim13 is recruited by Vps24 and passed to Snf7 prior to processing. The differences in

ESCRT-III interaction between *A. nidulans* Rim13 and *S. cerevisiae*/*Y. lipolytica* Rim13 likely represents a slight divergence in signaling pathways among fungal species. However, both models suggest that the protease does interact with ESCRT-III members, and *A. nidulans* studies support that Rim13 is recruited to endosomal fractions through ESCRT-III interactions. These interactions of Rim13, Snf7, Rim20, and Rim101 generate the "processing complex," or protein complex directly involved with Rim101 processing.

In addition to Rim20 and Rim13 activity, several upstream members of the Rim101 pathway are required for Rim101 activation. In *C. albicans* and *S. cerevisiae*, there are three transmembrane proteins localized to the plasma membrane: Rim21, which contains 7 transmembrane domain; Dfg16, which contains 6; and Rim9, which contains 4 (Figure 3) (13, 42, 165, 187). All three are required for normal Rim101 processing. *A. nidulans* contains at least two of the three transmembrane proteins, Rim21 (called PalH) and Rim9 (called PalI) (Table 2) (52). The signal recognized by these putative receptors is not known.

Rim8 is another upstream member required for Rim101 processing (187). Rim8 is a homolog to the mammalian arrestin signaling proteins (79). In *S. cerevisiae* and *A. nidulans*, Rim8 is ubiquitinated; this ubiquitination is pH-dependent in *A. nidulans*, but not in *S. cerevisiae* (78, 79). This ubiquitination promotes Rim8 association with Rim21. Both Rim8 modification and Rim8-Rim21 interactions are required for Rim101 processing. Together, the modified Rim8-Rim21 interactions, possibly in conjuction with Dfg16 and/or Rim9, compose the activation complex, or protein complex thought to receive and transmit the signal to activate Rim101 processing.

The ubiquitination of Rim8 suggests a means of connecting the spatially segregated upstream signaling complex and the endosome-associated processing complex. Ubiquitination of plasma membrane-embedded proteins is one signal to promote protein uptake from the plasma membrane through endocytosis. In *A. nidulans*, Rim21-GFP has been shown to move from plasma membrane localization to internalized cytosolic specks to eventual vacuolar lumen localization (33). Localization of Rim21 is promoted in part by Rim9, which helps maintain plasma membrane-association of Rim21 (33). The role of Rim9 in Rim21 localization has not been studied in other species. Uptake of Rim21-Rim8 may lead to recruitment of downstream ESCRT complexes and subsequent activation of the processing complex. Thus, Rim8 modification may play a role in bringing together the signaling and processing complexes.

Through Western blot analyses, *C. albicans* Rim8 was shown to be modified in an alkaline pH-dependent manner that produces multiple bands larger than the unmodified Rim8 (J. Gomez-Raja, in preparation). All modification can be removed by phosphatase treatment, suggesting that Rim8 undergoes phosphorylation, and that phosphorylation is the cause of all the high-molecular weight bands observed. This is in agreement with *A. nidulans* Rim8 studies, which suggest Rim8 is phosphorylated as well as ubiquitinated; however, no ubiquitin was detected in modified *C. albicans* Rim8. Further studies showed that modified *C. albicans* Rim8 immunoprecipitations simultaneously precipitate Rim21 and Rim101 from crude protein extracts (J. Gomez-Raja, in preparation). This suggests that *C. albicans* Rim8 modification may play a role in Rim101 recruitment to the endosome for processing, and that the activation and processing complexes do become proximal despite spatial separation.

A role for modified Rim8 has been furtherd by research in *S. cerevisiae* demonstrating that Rim8 is ubiquitinated (78). Rim8 ubiquitination facilitates Rim8-Vps23 interactions, which suggests a possible mechanism to bypass ESCRT-0 function in Rim101 processing. ESCRT-0 recruitment to the endosome is dependent on cargo ubiquitination (16), but ESCRT-I members Vps23 and Mvb12 also contain ubiquitination recognition motifs (174, 190), and may therefore be recruited by Rim8 directly. Colocalization studies of Rim8-Vps23 suggest this interaction occurs at the cell perimeter. Thus Rim8 modification has been detected in several fungal species and may recruit ESCRT-I directly to promote Rim101 processing.

A. nidulans studies have uncovered a second protein in the PacC pathway that contains a bro1-domain, PalC. These *A. nidulans* studies have shown PalC interacts with Snf7 through its bro1-domain. Localization studies at alkaline pH have shown PalC has a spotted pattern that is dependent on Rim21, closest to the cell perimeter (63). A PalC homolog, Rim23, has been found to interact with Snf7 in *Y. lipolytica* (20), but no characterization of Rim23 has been published in *S. cerevisiae* or *C. albicans* literature, although both contain ORFs with significant homology to the *Y. lipolytica RIM23* sequence (*YGR122w* and *ORF19.2914*, respectively). The studies on PalC localization, in addition to the localization of Rim8 and Vps23 near the cell perimeter in *S. cerevisiae*, suggest an alternative site for Rim101 processing: at or near the plasma membrane. This theory posits that, like enveloped viruses, Rim101 signaling machinery bypass ESCRT-0 to redirect ESCRT complex recruitment, and subsequently the Rim101 processing complex, to the plasma membrane. However, the studies performed in this dissertation

have been based on the prevailing model that Rim101 processing occurs at the endosomal membrane.

How could ESCRT-III favor interactions with Rim101 processing machinery, rather than with downstream ESCRT machinery? *S. cerevisiae* colocalization studies have shown that Rim20-Snf7 interactions are pH-dependent. This suggests the processing complex is assembled only under neutral-alkaline conditions. Since the processing complex is theorized to assemble at the endosomal membrane, one factor that may influence interactions at this location is the cargo content taken up by endocytosis. This is represented in our model (Figure 4), whereby endocytosis of the activating complex (Rim21-Rim8) recruits ESCRT complexes and favors processing complex recruitment. Colocalization of Rim20 and Bro1 suggest that processing complex recruitment does not prohibit ESCRT-DS recruitment, however, and the two functions may occur simultaneously at the same endosome (Figure 4) (26). Localization of Rim8-GFP to the vacuole supports this model and suggests the activation complex may be incorporated into MVBs destined for the vacuole (J. Gomez-Raja, in preparation). Thus, endocytosis of the modified Rim8 may favor recruitment of the Rim101 processing complex in addition to recruitment of ESCRT-DS members.

IV. Rim101 processing and *C. albicans* pathogenesis

Rim101 processing is required for wild-type virulence of *C. albicans* (50). A *rim101*Δ/Δ *C. albicans* strain is attenuated in a mouse model of systemic candidiasis, as are strains unable to process Rim101 (48). In *C. albicans*, Rim101 regulates genes associated with a switch to neutral-alkaline pH conditions, which is the pH of many of

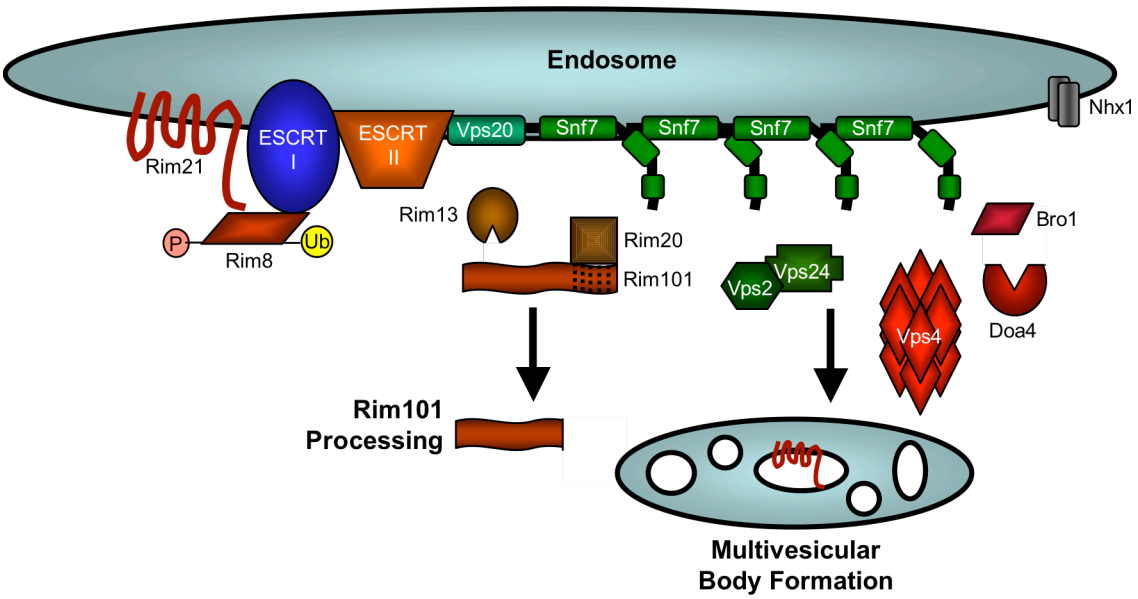

Figure 4. Model of ESCRT pathway and Rim101 pathway interaction at the endosome. The Rim21-Rim8 signaling complex is taken up by endocytosis, likely signaled by Rim8 ubiquitination and/or phosphorylation. These modifications allow Rim8 to recruit ESCRT-I directly, which leads to normal ESCRT-I, -II, and -IIIa formation. The presence of modified Rim8 at the endosomal membrane promotes Rim13 and Rim20 interactions with Snf7, leading to Rim101 processing. Snf7 can simultaneously interact with downstream ESCRT proteins, eventually leading to MVB formation. Rim21 and Rim8 are incorporated into MVBs and are degraded upon MVB fusion with the vacuole.

the host niches. The effect of Rim101 on the cell is pleiotrophic, however, as Rim101 regulates many genes required for microbial survival in the host, as well as genes directly involved in host damage.

Several genes involved in iron acquisition are regulated by Rim101. These genes include the high-affinity iron transporter *FTR1/2* and the ferric reductases *FRE2* and *FRP1* (14). Microbial access to iron is required for growth inside the host, which uses iron sequestration as an antimicrobial defense. The effect of Rim101 on iron-related genes is rational, as the same neutral-to-alkaline environments that lead to Rim101 activation are also iron-depleted. As the environment becomes more alkaline, iron is increasingly found in its insoluble, ferric form, rather than the soluble, ferrous form more easily accessed in acidic conditions. However, Rim101 is not activated by iron starvation, as chelation treatment of iron-replete media does not result in Rim101 processing, and Rim101 is not required for growth in iron-limiting conditions at acidic pH (J. M. Wolf, unpublished data). Rim101 activation does lead to expression of genes necessary to acquire iron in neutral-alkaline environments.

ALS3 is another Rim101-regulated gene shown to play a role in iron acqusition and *C. albicans* pathogenesis. *ALS3* is required to access iron sequestered by ferritin inside the host cell, and has been suggested to bind directly to ferritin (2). An *als3*Δ/Δ *C. albicans* strain cannot damage epithelial cells during *in vitro* assays, possibly due to the inability of this strain to access iron (137). The role of *ALS3* is compounded by its role in adhesion and invasion into host cells, but its ability to bind ferritin when heterologously expressed in *S. cerevisiae* suggests its role in iron acquisition is independent of these

functions. Thus, Rim101-regulated iron-acquisition genes are required for epithelial cell damage.

Rim101 also regulates several genes associated with the cell wall. The pH-dependent expression of cell wall-associated genes was first identified by characterization of *PHR1* and *PHR2* expression (131). This category has since been expanded to include a diverse set of genes, such as *ALS3*, *CHT2* (a chitinase 2 precursor), *ECE1* and *HWP1* (cell wall proteins associated with hyphal growth), *SKN1* (a glucan synthase subunit involved in cell wall biogenesis), *RBR1* (a glycosylphosphatidyl inositol protein) (37, 116, 137), as well as several genes related to nutrient acquisition, such as *FRE2* and *ZRT2*, a high-affinity zinc transporter (137). Some of these genes are up-regulated as part of the Rim101-dependent alkaline-induced filamentation, such as *ECE1* and *HWP1* (137). Some of these genes are up-regulated in response to changing nutritional needs of the cell independent of morphology, such as *FRE2*. Proper expression of these genes is required for wild-type virulence in *in vitro* oral epithelial cell damage assays, and overexpression of these genes can partially rescue the *rim101*Δ/Δ mutant defects. The first contact *C. albicans* has with its outside environment is through cell wall interactions. Thus the cell must constantly fine-tune the composition of cell wall-associated proteins to prepare for changes in morphology, available nutrients, and host cell interactions. Cell wall adjustments governed by Rim101 are required for *C. albicans* pathogenesis.

V. Goals of these studies

The aim of this body of work was to characterize the Rim101-dependent and -independent role of the ESCRT pathway in *Candida albicans*. Work was done to

understand the molecular interactions involving Snf7 (Chapter 2) as well as to understand the role of individual ESCRT members in Rim101 processing (Chapter 3). I further investigated a role for endosomal maturation in Rim101 processing using the *nhx1*Δ/Δ mutant (Chapter 4). These studies helped identify ESCRT complex members uninvolved with Rim101 processing, which in turn facilitated the study of ESCRT function and endosomal maturation during *C. albicans* pathogenesis (Chapters 3 and 4).

CHAPTER 2

I. Introduction

C. albicans is a common cause of nosocomial, hematogenously disseminated systemic infection, which has an attributable mortality of up to 50% even with antifungal therapy (148, 149). The success of *C. albicans* as a pathogen is principally due to its success as a human commensal. As a commensal, *C. albicans* colonizes diverse surfaces, including the oral, intestinal, or vaginal mucosa in at least 80% of the adult human population (149, 182). While *C. albicans* primarily causes non-life-threatening infections at these sites, life-threatening systemic infections can arise through escape of commensals from mucosal sites (4, 121). Thus, *C. albicans* must be able to thrive in diverse host environments in order to survive as a commensal and cause disease as a pathogen.

One environmental condition that varies markedly in sites colonized by *C. albicans* is pH. *C. albicans* can survive and thrive in the most acidic host sites, such as the stomach and vaginal cavity, and the most alkaline sites, such as the intestinecolon. *C. albicans* can grow over a wide pH range *in vitro* (pH 2-10), demonstrating the flexibility of *C. albicans* in the face of environmental pH. The ability to adapt to distinct environmental pH is critical for survival and pathogenesis for several reasons. First, environmental pH is a potent inducer of the *C. albicans* yeast-to-hyphae transition, which is crucial for pathogenesis (47, 48, 70, 112, 113). Second, the expression profile of gene families relevant to pathogenesis, such as the secreted aspartyl protease family, is regulated by extracellular pH (14, 22). Third, environmental pH affects the kinetics of extracellular enzymes, including virulence factors (22). Fourth, environmental pH affects nutrient uptake, as many plasma membrane transporters use the proton gradient, which is

not maintained at alkaline pH (93). Nutrient solubility is also affected in neutral-alkaline environments, making their uptake more difficult (11, 14, 82). Therefore, in order to survive and infect the host, *C. albicans* must respond appropriately to environmental pH.

Several distinct pH-sensing systems have been identified that are required for adaptation of *C. albicans* to neutral-alkaline pH environments (47, 49-51, 99, 153, 173). One system, the Rim101 signal transduction pathway, regulates activity of the transcription factor Rim101. A similar pH-dependent Rim101/PacC pathway has been detected in a number of ascomycetes and basidiomycetes, including *Saccharomyces cerevisiae*, *Aspergillus nidulans*, and *Ustillago maydis* (6, 102, 147). Rim101 is activated at neutral-alkaline pH by the proteolytic removal of an inhibitory C-terminal domain (Figure 1) (47). Proteolytic activation requires upstream members, including Rim13, which acts as the putative protease (107), and Rim20, which interacts with a PEST-like motif in the Rim101 C-terminal domain (199, 206). Rim101 activation also requires Snf7, which interacts with Rim13 and Rim20. (20, 25, 86, 206). Therefore, Snf7 is predicted to facilitate interaction between the protease Rim13 and its substrate Rim101 via Rim20. Rim101 activation is required for growth in neutral-alkaline environments and is required for *C. albicans* virulence in animal models of both systemic and mucosal disease (48, 49, 126, 153, 158, 198). Thus, the sensing and adaptation to environmental pH through the Rim101 pathway is essential for *C. albicans* pathogenesis.

Another response to alkaline pH in yeast is an increased reliance on endocytosis and vacuolar acidification for nutrient acquisition (68, 132). Because alkaline conditions do not generate a favorable proton gradient, plasma membrane transporters are shut down and cells rely on the internal vacuolar proton gradient. In fact, endocytosis and vacuolar

acidification are essential processes for fungal growth in alkaline but not acidic environments (132). To deliver endosomes containing extracellular material to the vacuole, cells use the endocytic sorting complex required for transport (ESCRT) pathway. This pathway consists of the cytoplasmic protein complexes, ESCRT-0, -I, and -II, that are sequentially recruited to ubiquitylated cargo proteins at endocytic vesicle membranes (Figure 5) (203). This then recruits the ESCRT-III heterodimer Vps20-Snf7 (8, 9, 16, 88, 89), which initiates Snf7 oligomerization (188). Vps20-Snf7 then recruits the second half of ESCRT-III, the Vps2-Vps24 heterodimer (8), which recruits downstream ESCRT members, including Bro1 and Vps4. Bro1 recruits a deubiquitinase which removes ubiquitin from the cargo protein, while Vps4 is an AAA-ATPase that dissociates ESCRT-III from the endosomal membrane, promoting multivesicular body (MVB) formation and fusion with the vacuole (61, 208). Using the ESCRT pathway, cells are able to acquire and deliver nutrients to the vacuole, where the internal proton gradient facilitates delivery of cargo nutrients to the cytoplasm of the cell (142, 143).

ESCRT-I and -II, as well as Vps20 and Snf7, are required for Rim101 processing (207). Although strains lacking ESCRT-I and –II do not recruit Snf7 to the endosomal membrane, Snf7 is expressed. This suggests that Snf7 must be localized to the endosomal membrane for its function in the Rim101 pathway, where it may serve as a scaffold for the Rim101 processing machinery at the membrane surface. This idea is supported by the colocalization of Rim101 pathway member Rim20 with Snf7 in a punctate pattern when cells are grown in alkaline conditions (26). Thus, Snf7 localization is important for function both in the ESCRT and in the Rim101 pathways.

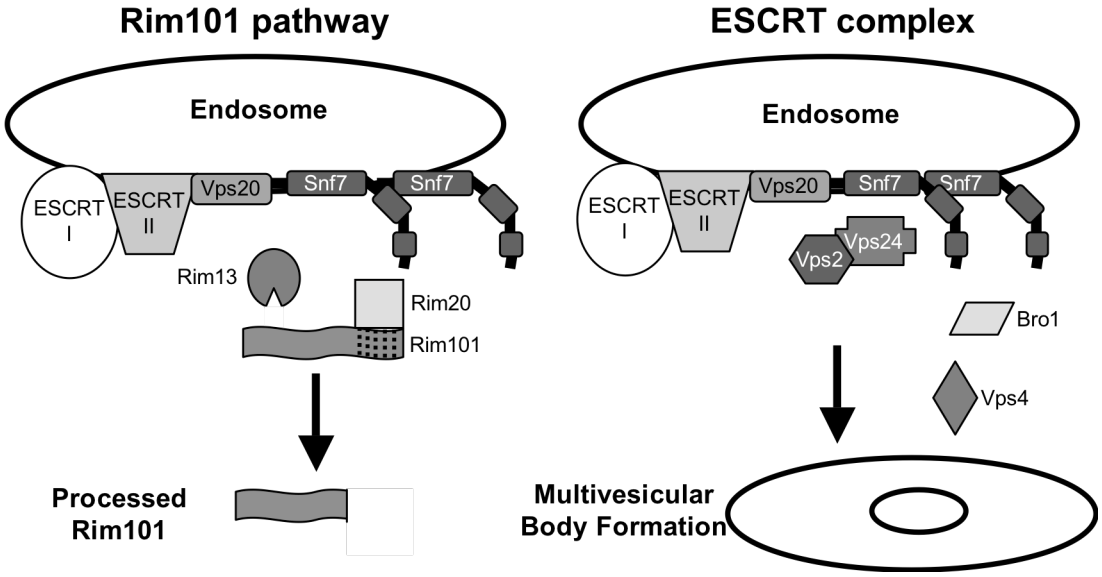

Figure 5. Model of Snf7 role in Rim101 processing and in ESCRT complex functions. On the left, ESCRT-I and –II recruitment of Vps20-Snf7 to the endosomal membrane leads to Snf7 interaction with the protease Rim13 and scaffold protein Rim20. Rim20 interacts with the C-terminal PEST-like domain of Rim101 (red dashes), and these interactions lead to Rim101 processing to its active form. On the right, ESCRT-I and –II recruitment of Vps20-Snf7 leads to downstream recruitment of Vps2/Vps24 and Bro1. Vps4 interacts with Snf7 to facilitate ESCRT-III dissociation from the membrane, and these interactions lead to multivesicular body formation.

In addition to colocalizing, Snf7 and Rim20 interact through the yeast two-hybrid and split-ubiquitin assays (86, 136). Snf7-Rim20 interactions likely occur through the Rim20 bro1-domain. The bro1-domain was first identified in the ESCRT pathway member Bro1 as a Snf7-interaction domain. (92, 122). As both Bro1 and Rim20 act as scaffold proteins, Bro1 and Rim20 have been proposed to act as adaptors, promoting downstream Snf7 function toward the ESCRT pathway or the Rim101 pathway, respectively (26).

Because Snf7 is required for both ESCRT-mediated MVB formation and for Rim101 activation, we wanted to more precisely characterize the role of Snf7 in these two processes in *C. albicans*. We hypothesized that the function of Snf7 in the ESCRT and Rim101 pathways is distinct. To test this hypothesis, we generated a series of *snf7* mutant alleles and identified specific alleles whose products disrupted the ESCRT pathway, the Rim101 pathway, or both pathways. Phenotypic analyses of our alleles have revealed that Snf7 function in the ESCRT pathway is separable from Snf7 function in the Rim101 pathway. Further analyses of these alleles have uncovered a slight variation in the bro1-domain interactions at the C-terminal end of Snf7.

II. Materials and methods

a. Strains and plasmids: All *C. albicans* strains from this study are derived from BWP17 (204) and are listed in Table 3. To generate the *SNF7* complementation plasmid pDDB426, wild-type *SNF7* sequence was amplified by the PCR from BWP17 genomic DNA using primers 5' SNF7 comp and 3' SNF7 comp (Table 4). The resulting PCR product and NotI/EcoRI-digested pDDB78 were transformed into *S. cerevisiae* to

Table 3. Strains used in Chapter 2 studies.

Name	Genotype	Reference
BWP17	*ura3::λimm434/ura3::λimm434 arg4::hisG/arg4::hisG his1::hisG/his1::hisG*	(204)
DAY5	*ura3::λimm434/ura3::λimm434 arg4::hisG/arg4::hisG his1::hisG/his1::hisG rim101::ARG4/rim101::URA3-dpl200*	(204)
DAY185	*ura3::λimm434/ura3::λimm434 ARG4::URA3::arg4::hisG/arg4::hisG HIS1::DDB78::his1::hisG/his1::hisG*	(48)
DAY534	*ura3::λimm434/ura3::λimm434 arg4::hisG/arg4::hisG his1::hisG/his1::hisG snf7::ARG4/snf7::URA3-dpl200*	(98)
DAY537	*ura3::λimm434/ura3::λimm434 arg4::hisG/arg4::hisG his1::hisG/his1::hisG vps4::ARG4/vps4::URA3-dpl200*	(98)
DAY763	*ura3::λimm434/ura3::λimm434 arg4::hisG/arg4::hisG HIS1::DDB78::his1::hisG/his1::hisG snf7::ARG4/snf7::URA3-dpl200*	(98)
DAY980	*ura3::λimm434/ura3::λimm434 arg4::hisG/arg4::hisG SNF7-V5::HIS1::DDB427::his1::hisG/his1::hisG snf7::ARG4/snf7::URA3-dpl200*	This study
DAY981	*ura3::λimm434/ura3::λimm434 arg4::hisG/arg4::hisG snf7-1::HIS1::DDB428::his1::hisG/his1::hisG snf7::ARG4/snf7::URA3-dpl200*	This study
DAY982	*ura3::λimm434/ura3::λimm434 arg4::hisG/arg4::hisG snf7-2::HIS1::DDB429::his1::hisG/his1::hisG snf7::ARG4/snf7::URA3-dpl200*	This study
DAY983	*ura3::λimm434/ura3::λimm434 arg4::hisG/arg4::hisG snf7-3::HIS1::DDB430::his1::hisG/his1::hisG snf7::ARG4/snf7::URA3-dpl200*	This study
DAY984	*ura3::λimm434/ura3::λimm434 arg4::hisG/arg4::hisG snf7-4::HIS1::DDB431::his1::hisG/his1::hisG snf7::ARG4/snf7::URA3-dpl200*	This study
DAY985	*ura3::λimm434/ura3::λimm434 arg4::hisG/arg4::hisG snf7-5::HIS1::DDB432::his1::hisG/his1::hisG snf7::ARG4/snf7::URA3-dpl200*	This study
DAY986	*ura3::λimm434/ura3::λimm434 arg4::hisG/arg4::hisG snf7-6::HIS1::DDB433::his1::hisG/his1::hisG snf7::ARG4/snf7::URA3-dpl200*	This study
DAY987	*ura3::λimm434/ura3::λimm434 arg4::hisG/arg4::hisG snf7-8::HIS1::DDB434::his1::hisG/his1::hisG snf7::ARG4/snf7::URA3-dpl200*	This study
DAY988	*ura3::λimm434/ura3::λimm434 arg4::hisG/arg4::hisG snf7-9::HIS1::DDB435::his1::hisG/his1::hisG snf7::ARG4/snf7::URA3-dpl200*	This study
DAY989	*ura3::λimm434/ura3::λimm434 arg4::hisG/arg4::hisG snf7-10::HIS1::DDB436::his1::hisG/his1::hisG snf7::ARG4/snf7::URA3-dpl200*	This study
DAY990	*ura3::λimm434/ura3::λimm434 arg4::hisG/arg4::hisG snf7-11::HIS1::DDB437::his1::hisG/his1::hisG snf7::ARG4/snf7::URA3-dpl200*	This study
DAY991	*ura3::λimm434/ura3::λimm434 arg4::hisG/arg4::hisG snf7-12::HIS1::DDB438::his1::hisG/his1::hisG snf7::ARG4/snf7::URA3-dpl200*	This study
DAY992	*ura3::λimm434/ura3::λimm434 arg4::hisG/arg4::hisG snf7-13::HIS1::DDB439::his1::hisG/his1::hisG snf7::ARG4/snf7::URA3-dpl200*	This study
DAY993	*ura3::λimm434/ura3::λimm434 arg4::hisG/arg4::hisG snf7-14::HIS1::DDB440::his1::hisG/his1::hisG snf7::ARG4/snf7::URA3-dpl200*	This study
DAY994	*ura3::λimm434/ura3::λimm434 arg4::hisG/arg4::hisG snf7-15::HIS1::DDB441::his1::hisG/his1::hisG snf7::ARG4/snf7::URA3-dpl200*	This study
DAY995	*ura3::λimm434/ura3::λimm434 arg4::hisG/arg4::hisG snf7-16::HIS1::DDB442::his1::hisG/his1::hisG snf7::ARG4/snf7::URA3-dpl200*	This study
DAY996	*ura3::λimm434/ura3::λimm434 arg4::hisG/arg4::hisG snf7-17::HIS1::DDB443::his1::hisG/his1::hisG snf7::ARG4/snf7::URA3-dpl200*	This study
DAY997	*ura3::λimm434/ura3::λimm434 arg4::hisG/arg4::hisG snf7-18::HIS1::DDB444::his1::hisG/his1::hisG snf7::ARG4/snf7::URA3-dpl200*	This study
DAY998	*ura3::λimm434/ura3::λimm434 arg4::hisG/arg4::hisG snf7-19::HIS1::DDB445::his1::hisG/his1::hisG snf7::ARG4/snf7::URA3-dpl200*	This study
DAY999	*ura3::λimm434/ura3::λimm434 arg4::hisG/arg4::hisG snf7-20::HIS1::DDB446::his1::hisG/his1::hisG snf7::ARG4/snf7::URA3-dpl200*	This study
DAY1000	*ura3::λimm434/ura3::λimm434 arg4::hisG/arg4::hisG snf7-21::HIS1::DDB447::his1::hisG/his1::hisG snf7::ARG4/snf7::URA3-dpl200*	This study
DAY1001	*ura3::λimm434/ura3::λimm434 arg4::hisG/arg4::hisG snf7-22::HIS1::DDB448::his1::hisG/his1::hisG snf7::ARG4/snf7::URA3-dpl200*	This study
DAY1002	*ura3::λimm434/ura3::λimm434 arg4::hisG/arg4::hisG snf7-23::HIS1::DDB449::his1::hisG/his1::hisG snf7::ARG4/snf7::URA3-dpl200*	This study
DAY1003	*ura3::λimm434/ura3::λimm434 arg4::hisG/arg4::hisG snf7-24::HIS1::DDB450::his1::hisG/his1::hisG snf7::ARG4/snf7::URA3-dpl200*	This study
DAY1004	*ura3::λimm434/ura3::λimm434 arg4::hisG/arg4::hisG snf7-25::HIS1::DDB451::his1::hisG/his1::hisG snf7::ARG4/snf7::URA3-dpl200*	This study
DAY1005	*ura3::λimm434/ura3::λimm434 arg4::hisG/arg4::hisG snf7-26::HIS1::DDB452::his1::hisG/his1::hisG snf7::ARG4/snf7::URA3-dpl200*	This study
DAY1006	*ura3::λimm434/ura3::λimm434 arg4::hisG/arg4::hisG snf7-27::HIS1::DDB453::his1::hisG/his1::hisG snf7::ARG4/snf7::URA3-dpl200*	This study
DAY1007	*ura3::λimm434/ura3::λimm434 arg4::hisG/arg4::hisG snf7-28::HIS1::DDB454::his1::hisG/his1::hisG snf7::ARG4/snf7::URA3-dpl200*	This study

DAY1008	*ura3::λimm434/ura3::λimm434 arg4::hisG/arg4::hisG snf7-29::HIS1::DDB455::his1::hisG/his1::hisG snf7::ARG4/snf7::URA3-dpl200*	This study
DAY1009	*ura3::λimm434/ura3::λimm434 arg4::hisG/arg4::hisG snf7-30::HIS1::DDB456::his1::hisG/his1::hisG snf7::ARG4/snf7::URA3-dpl200*	This study
DAY1010	*ura3::λimm434/ura3::λimm434 arg4::hisG/arg4::hisG snf7-31::HIS1::DDB457::his1::hisG/his1::hisG snf7::ARG4/snf7::URA3-dpl200*	This study
DAY1011	*ura3::λimm434/ura3::λimm434 arg4::hisG/arg4::hisG snf7-32::HIS1::DDB458::his1::hisG/his1::hisG snf7::ARG4/snf7::URA3-dpl200*	This study
DAY1012	*ura3::λimm434/ura3::λimm434 arg4::hisG/arg4::hisG snf7-33::HIS1::DDB459::his1::hisG/his1::hisG snf7::ARG4/snf7::URA3-dpl200*	This study
DAY1013	*ura3::λimm434/ura3::λimm434 arg4::hisG/arg4::hisG snf7-34::HIS1::DDB460::his1::hisG/his1::hisG snf7::ARG4/snf7::URA3-dpl200*	This study
DAY1014	*ura3::λimm434/ura3::λimm434 arg4::hisG/arg4::hisG snf7-35::HIS1::DDB461::his1::hisG/his1::hisG snf7::ARG4/snf7::URA3-dpl200*	This study
DAY1015	*ura3::λimm434/ura3::λimm434 arg4::hisG/arg4::hisG snf7-36::HIS1::DDB462::his1::hisG/his1::hisG snf7::ARG4/snf7::URA3-dpl200*	This study
DAY1016	*ura3::λimm434/ura3::λimm434 arg4::hisG/arg4::hisG snf7-37::HIS1::DDB463::his1::hisG/his1::hisG snf7::ARG4/snf7::URA3-dpl200*	This study
DAY1017	*ura3::λimm434/ura3::λimm434 arg4::hisG/arg4::hisG snf7-38::HIS1::DDB464::his1::hisG/his1::hisG snf7::ARG4/snf7::URA3-dpl200*	This study
DAY1018	*ura3::λimm434/ura3::λimm434 arg4::hisG/arg4::hisG snf7-39::HIS1::DDB465::his1::hisG/his1::hisG snf7::ARG4/snf7::URA3-dpl200*	This study
DAY1019	*ura3::λimm434/ura3::λimm434 arg4::hisG/arg4::hisG snf7-40::HIS1::DDB466::his1::hisG/his1::hisG snf7::ARG4/snf7::URA3-dpl200*	This study
DAY1020	*ura3::λimm434/ura3::λimm434 arg4::hisG/arg4::hisG snf7-41::HIS1::DDB467::his1::hisG/his1::hisG snf7::ARG4/snf7::URA3-dpl200*	This study
DAY1021	*ura3::λimm434/ura3::λimm434 arg4::hisG/arg4::hisG snf7-42::HIS1::DDB468::his1::hisG/his1::hisG snf7::ARG4/snf7::URA3-dpl200*	This study
DAY1022	*ura3::λimm434/ura3::λimm434 arg4::hisG/arg4::hisG snf7-43::HIS1::DDB469::his1::hisG/his1::hisG snf7::ARG4/snf7::URA3-dpl200*	This study
DAY1023	*ura3::λimm434/ura3::λimm434 arg4::hisG/arg4::hisG snf7-44::HIS1::DDB470::his1::hisG/his1::hisG snf7::ARG4/snf7::URA3-dpl200*	This study
DAY1024	*ura3::λimm434/ura3::λimm434 arg4::hisG/arg4::hisG snf7-45::HIS1::DDB471::his1::hisG/his1::hisG snf7::ARG4/snf7::URA3-dpl200*	This study
DAY1025	*ura3::λimm434/ura3::λimm434 arg4::hisG/arg4::hisG snf7-46::HIS1::DDB472::his1::hisG/his1::hisG snf7::ARG4/snf7::URA3-dpl200*	This study
DAY1026	*ura3::λimm434/ura3::λimm434 arg4::hisG/arg4::hisG snf7-47::HIS1::DDB473::his1::hisG/his1::hisG snf7::ARG4/snf7::URA3-dpl200*	This study
DAY1027	*ura3::λimm434/ura3::λimm434 arg4::hisG/arg4::hisG snf7-48::HIS1::DDB474::his1::hisG/his1::hisG snf7::ARG4/snf7::URA3-dpl200*	This study
DAY1028	*ura3::λimm434/ura3::λimm434 arg4::hisG/arg4::hisG snf7-49::HIS1::DDB475::his1::hisG/his1::hisG snf7::ARG4/snf7::URA3-dpl200*	This study
DAY1029	*ura3::λimm434/ura3::λimm434 arg4::hisG/arg4::hisG snf7-50::HIS1::DDB476::his1::hisG/his1::hisG snf7::ARG4/snf7::URA3-dpl200*	This study
DAY1113	*ura3::λimm434/ura3::λimm434 arg4::hisG/arg4::hisG his1::hisG/his1::hisG vps4::ARG4/vps4::dpl200*	This study
DAY1114	*ura3::λimm434/ura3::λimm434 arg4::hisG/arg4::hisG SNF7-V5::HIS1::DDB427::his1::hisG/his1::hisG vps4::ARG4/vps4::dpl200*	This study
DAY1115	*ura3::λimm434/ura3::λimm434 arg4::hisG/arg4::hisG snf7-6::HIS1::DDB433::his1::hisG/his1::hisG vps4::ARG4/vps4::dpl200*	This study
DAY1116	*ura3::λimm434/ura3::λimm434 arg4::hisG/arg4::hisG snf7-15::HIS1::DDB441::his1::hisG/his1::hisG vps4::ARG4/vps4::dpl200*	This study
DAY1117	*ura3::λimm434/ura3::λimm434 arg4::hisG/arg4::hisG snf7-20::HIS1::DDB446::his1::hisG/his1::hisG vps4::ARG4/vps4::dpl200*	This study
DAY1126	*ura3::λimm434/ura3::λimm434 arg4::hisG/arg4::hisG his1::hisG/his1::hisG snf7::ARG4/snf7::dpl200*	This study
DAY1127	*ura3::λimm434/ura3::λimm434 arg4::hisG/arg4::hisG his1::hisG/his1::hisG snf7::ARG4/snf7::dpl200 RIM101-V5::URA3::DDB478::RIM101/RIM101*	This study
DAY1128	*ura3::λimm434/ura3::λimm434 arg4::hisG/arg4::hisG SNF7::HIS1::DDB426::his1::hisG/his1::hisG snf7::ARG4/snf7::dpl200 RIM101-V5::URA3::DDB478::RIM101/RIM101*	This study

Table 4. Primers used in Chapter 2 studies

Primer name	Sequence 5'-3'
5' Snf7-HpaI-V5	TGTATCAAGAGAAGAAGAGTTACCACAATTCCCATCTGTTGGTAAGCCTATCCCTAACCC
3' Snf7-HpaI-V5	CTTCATCTTCATCTTCTTCTACTACTGGAGCTTTCTTGTTATGGTGATGGTGATGATGAC
5' Snf7 comp	AAGCTCGGAATTAACCCTCACTAAAGGGAACAAAAGCTGGGCCTCATTGAGCAACTTGAG
3' Snf7 comp	ACGACGGCCAGTGAATTGTAATACGACTCACTATAGGGCGTAATCGACATTAAAGGACTC
5' Snf7.1	TAGTAAACAGGCCTAGGATCGCGGGAGCTTTTTTTGGAGGAAATAGCCA
3' Snf7.1	TGGCTATTTCCTCCAAAAAAAGCTCCCGCCATCCTAGGCCTGTTTACTA
5' Snf7.2	GGCCTAGGATGTGGGGATATGCTGCTGGAGGAAATAGCCAACAAAA
3' Snf7.2	TTTTGTTGGCTATTTCCTCCAGCAGCATATCCCCACATCCTAGGCC
5' Snf7.3	ATTTTTTTGGAGGAAATAGCGCAGCAAAGAAAGATTTACCAAAGAA
3' Snf7.3	TTCTTTGGTAAATCTTTCTTTGCTGCGCTATTTCCTCCAAAAAAAT
5' Snf7.4	TTGGAGGAAATAGCCAACAAGCGCGGCAGCTTTACCAAAGAAGGCAATAGT
3' Snf7.4	ACTATTGCCTTCTTTGGTAAAGCTGCCGCTTGTTGGCTATTTCCTCCAA
5' Snf7.5	AACAAAAGAAAGATTTACCAGCGGCGGCAATAGTGGAATTGCGAGA
3' Snf7.5	TCTCGCAATTCCACTATTGCCGCCGCTGGTAAATCTTTCTTTTGTT
5' Snf7.6	TACCAAAGAAGGCAATAGTGGCATTGGCAGCACACATACAAACACTAAACAA
3' Snf7.6	TTGTTTAGTGTTTGTATGTGTGCTGCCAATGCCACTATTGCCTTCTTTGGTA
5' Snf7.7	CAATAGTGGAATTGCGAGAAGCCATAGCAACACTAAACAAGAAGAAGAA
3' Snf7.7	TTCTTCTTCTTGTTTAGTGTTGCTATGGCTTCTCGCAATTCCACTATTG
5' Snf7.8	AACACATACAAACACTAAACGCGGCGGCGAACCATTTGCAACAGCAAAT
3' Snf7.8	ATTTGCTGTTGCAAATGGTTCGCCGCCGCGTTTAGTGTTTGTATGTGTT
5' Snf7.9	ACAAGAAGAAGAACCATTTGGCAGCGGCAATGGATGACCAAGAT
3' Snf7.9	AACTGATCTTGGTCATCCATTGCCGCTGCCAAATGGTTCTTCTTCTTGT
5' Snf7.10	AGAACCATTTGCAACAGCAAGCGGCTGCCCAAGATCAGTTGGCCAGAAA
3' Snf7.10	TTTCTGGCCAACTGATCTTGGGCAGCCGCTTGCTGTTGCAAATGGTTCT
5' Snf7.11	TGCAACAGCAAATGGATGACGCAGCTGCGTTGGCCAGAAAATATGTTAG
3' Snf7.11	CTAACATATTTTCTGGCCAACGCAGCTGCGTCATCCATTTGCTGTTGCA
5' Snf7.12	ATGACCAAGATCAGTTGGCCGCAGCAGCTGTTAGTTCAAAACAAACAAC
3' Snf7.12	GTTGTTTGTTTTGAACTAACAGCTGCTGCGGCCAACTGATCTTGGTCAT
5' Snf7.13	CCAGAAAATATGTTAGTTCAGCAGCAACAACTTTAGCTAAAAGTGC
3' Snf7.13	GCACTTTTAGCTAAAGTTGTTGCTGCTGAACTAACATATTTTCTGG
5' Snf7.14	CAAAACAAACAACTTTAGCTGCAGCTGCTTTAAAAAGAAAAAAGGG
3' Snf7.14	CCCTTTTTTCTTTTTAAAGCAGCTGCAGCTAAAGTTGTTTGTTTTG
5' Snf7.15	CAACTTTAGCTAAAAGTGCTGCAGCAGCAAAAAAGGGGTATGAATCTAA
3' Snf7.15	TTAGATTCATACCCCTTTTTTGCTGCTGCAGCACTTTTAGCTAAAGTTG

5' Snf7.16	AGTGCTTTAAAAAGAGCAGCGGGGTATGCATCTAATCTATTAAAA
3' Snf7.16	TTTTAATAGATTAGATGCATACCCCGCTGCTCTTTTTAAAGCACT
5' Snf7.17	GAATCTAATCTATTAGCAGTGGCAAACGCGATTGAAACTTTGGAA
3' Snf7.17	TTCCAAAGTTTCAATCGCGTTTGCCACTGCTAATAGATTAGATTC
5' Snf7.18	GTGGAAAACCAGATTGCAACTGCGGCAACACAATTAATT
3' Snf7.18	ACTAATTAATTGTGTTGCCGCAGTTGCAATCTGGTTTTCCAC
5' Snf7.19	ACCAGATTGAAACTTTGGAAGCAGCAGCAATTAGTATCGAAGGAGCAAA
3' Snf7.19	TTTGCTCCTTCGATACTAATTGCTGCTGCTTCCAAAGTTTCAATCTGGT
5' Snf7.20	CTTTGGAAACACAATTAATTGCTGCCGCAGGAGCAAACTTGAACTTGGA
3' Snf7.20	TCCAAGTTCAAGTTTGCTCCTGCGGCAGCAATTAATTGTGTTTCCAAAG
5' Snf7.21	AAGGAGCAAACTTGAACTTGGCAACTGCGGCAGCTATGAAACAAGGAG
3' Snf7.21	TTTGCTCCTTGTTTCATAGCTGCCGCAGTTGCCAAGTTCAAGTTTGCTCCTT
5' Snf7.22	ACTTGGAAACTATGAAAGCTGCGGCAGCAGGAGCAAAGGCCATGAAACA
3' Snf7.22	TGTTTCATGGCCTTTGCTCCTGCTGCCGCAGCTTTCATAGTTTCCAAGT
5' Snf7.23	ATGAAACAAGGAGCAAAGGCCATGAAACAAATACATGGGGAATAC
3' Snf7.23	GTATTCCCCATGTATTGCTGCCATGGCCGCTGCTCCTTGTTTCAT
5' Snf7.24	CAAAGGCCATGAAACAAATAGCTGCGGCATACGATGTAGACAAAGTTGA
3' Snf7.24	TCAACTTTGTCTACATCGTATGCCGCAGCTATTTGTTTCATGGCCTTTG
5' Snf7.25	CAAATACATGGGGAATACGCTGTAGCCGCAGTTGAAGATACTATGGATG
3' Snf7.25	CATCCATAGTATCTTCAACTGCGGCTACAGCGTATTCCCCATGTATTTG
5' Snf7.26	AATACGATGTAGACAAAGTTGCAGCTACTGCGGATGAAATAAGAGAACAA
3' Snf7.26	TTGTTCTCTTATTTCATCCGCAGTAGCTGCAACTTTGTCTACATCGTATT
5' Snf7.27	CAAAGTTGAAGATACTATGGCTGCAATAGCAGAACAAGTAGAGTTAGCC
3' Snf7.27	GGCTAACTCTACTTGTTCTGCTATTGCAGCCATAGTATCTTCAACTTTG
5' Snf7.28	TACTATGGATGAAATAAGAGCAGCAGTAGCGTTAGCCGATGAAATCAGT
3' Snf7.28	ACTGATTTCATCGGCTAACGCTACTGCTGCTCTTATTTCATCCATAGTA
5' Snf7.29	CAAGTAGAGTTAGCCGCTGCAATCAGTGCAGCTATATCGAGGCCC
3' Snf7.29	GGGCCTCGATATAGCTGCACTGATTGCAGCGGCTAACTCTACTTG
5' Snf7.30	ATGAAATCAGTGAAGCTATAGCGGCGCCCGTTGGTAATGAATTTGT
3' Snf7.30	ACAAATTCATTACCAACGGGCGCCGCTATAGCTTCACTGATTTCAT
5' Snf7.31	CTATATCGAGGCCCGTTGGTAATGAATTTGTTGATGAAGATGAATT
3' Snf7.31	AATTCATCTTCATCAACAAATGCAGCACCAACGGGCCTCGATATAG
5' Snf7.32	CCGTTGGTAATGAATTTGTTGCTGCAGATGAATTGGACGAAGAATT
3' Snf7.32	AATTCTTCGTCCAATTCATCTGCAGCAACAAATTCATTACCAACGG
5' Snf7.33	GTAATGAATTTGTTGATGAAGCTGCATTGGACGAAGAATTGAAAGA
3' Snf7.33	TCTTTCAATTCTTCGTCCAATGCAGCTTCATCAACAAATTCATTAC
5' Snf7.34	TTGTTGATGAAGATGAATTGGCCGCAGCATTGAAAGAGTTGGAGGCAGA
3' Snf7.34	TCTGCCTCCAACTCTTTCAATGCTGCGGCCAATTCATCTTCATCAACAA

5' Snf7.35	AAGATGAATTGGACGAAGAAGCGGCAGCGTTGGAGGCAGAAGCTAAAGA
3' Snf7.35	TCTTTAGCTTCTGCCTCCAACGCTGCCGCTTCTTCGTCCAATTCATCTT
5' Snf7.36	TGGACGAAGAATTGAAAGAGGCGGCGGCAGAAGCTAAAGAACA
3' Snf7.36	TCTTGTTCTTTAGCTTCTGCCGCCGCCTCTTTCAATTCTTCGTCCA
5' Snf7.37	TTGAAAGAGTTGGAGGCAGCAGCTGCAGCACAAGAACAAGAACATAGA
3' Snf7.37	TCTATGTTCTTGTTCTTGTGCTGCAGCTGCTGCCTCCAACTCTTTCAA
5' Snf7.38	TGGAGGCAGAAGCTAAAGAAGCAGCAGCAGAACATAGAGTGCCAGCTCA
3' Snf7.38	TGAGCTGGCACTCTATGTTCTGCTGCTGCTTCTTTAGCTTCTGCCTCCA
5' Snf7.39	AAGCTAAAGAACAAGAACAAGCAGCTGCAGTGCCAGCTCAAAAGGCAAA
3' Snf7.39	TTTGCCTTTTGAGCTGGCACTGCAGCTGCTTGTTCTTGTTCTTTAGCTT
5' Snf7.40	GAACATAGAGTGCCAGCTGCAGCGGCAGCACCACAACCTGTATCAAGA
3' Snf7.40	TCTTGATACAGGTTGTGGTGCTGCCGCTGCAGCTGGCACTCTATGTTC
5' Snf7.41	TGCCAGCTCAAAAGGCAAAAGCAGCACCTGTATCAAGAGAAGAAGA
3' Snf7.41	TCTTCTTCTCTTGATACAGGTGCTGCTTTTGCCTTTTGAGCTGGCA
5' Snf7.42	AGGCAAAACCACAACCTGTAGCAGCAGAAGAAGAGTTACCACAATT
3' Snf7.42	AATTGTGGTAACTCTTCTTCTGCTGCTACAGGTTGTGGTTTTGCCT
5' Snf7.43	AACCACAACCTGTATCAAGAGCAGCAGCGTTACCACAATTCCCATCTGT
3' Snf7.43	ACAGATGGGAATTGTGGTAACGCTGCTGCTCTTGATACAGGTTGTGGTT
5' Snf7.44	CAAGAGAAGAAGAGTTACCAGCATTCCCATCTGTTGGTAAGCC
3' Snf7.44	GGCTTACCAACAGATGGGAATGCTGGTAACTCTTCTTCTCTTG
5' Snf7.45	ATCATCACCATCACCATAACGCGGCAGCTCCAGTAGTAGAAGAAGA
3' Snf7.45	TCTTCTTCTACTACTGGAGCTGCCGCGTTATGGTGATGGTGATGAT
5' Snf7.46	AAGAAAGCTCCAGTAGTAGCAGCAGCTGAAGATGAAGAAGCATTG
3' Snf7.46	TTTCAATGCTTCTTCATCTTCAGCTGCTGCTACTACTGGAGCTTTCTT
5' Snf7.47	CCAGTAGTAGAAGAAGATGCAGCTGCAGAAGCATTGAAAGCATTGCAAG
3' Snf7.47	CTTGCAATGCTTTCAATGCTTCTGCAGCTGCATCTTCTTCTACTACTGG
5' Snf7.48	GAAGAAGATGAAGATGAAGCAGCAGCGGCAGCATTGCAAGCTGAAATG
3' Snf7.48	CATTTCAGCTTGCAATGCTGCCGCTGCTGCTTCATCTTCATCTTCTTC
5' Snf7.49	GAAGAAGCATTGAAAGCAGCGGCAGCTGCAATGGGATTATGATGTGTT
3' Snf7.49	AACACATCATAATCCCATTGCAGCTGCCGCTGCTTTCAATGCTTCTTC
5' Snf7.50	TAATTAGTATCGAAGGAGCAAACTTGAACTTGGAAACTATGAAAGCTAT
3' Snf7.50	ATAGCTTTCATAGTTTCCAAGGCCGCGGCTGCTCCTTCGATACTAATTA

generate pDDB426 by *in vivo* recombination (130). Plasmid pDDB426, and all additional plasmids generated by *in vivo* recombination in *S. cerevisiae,* were recovered from *S. cerevisiae* and transformed into DH5α *E. coli* by electroporation for amplification.

To generate an epitope-tagged *SNF7* allele, the V5-His6 tag was amplified in the PCR from the pTRACER-EF plasmid (Invitrogen) using primers 5' Snf7-V5 and 3' Snf7-V5. The resulting PCR product and HpaI-digested pDDB426 were transformed into *S. cerevisiae* to generate pDDB427. Purified pDDB427 was digested with NruI and transformed into DAY534 to generate DAY980.

To generate the *snf7* alanine scanning alleles, two overlapping PCR products were generated using plasmid pDDB427 as template. For example, *snf7-1* was amplified from pDDB427 in two PCR reactions, the first using primers 5' SNF7 comp and 3' snf7-1, and the second using primers 5' snf7-1 and 3' SNF7 comp (Table 4). The two PCR products and NotI/EcoRI digested pDDB78 were transformed into *S. cerevisiae* to generate plasmid pDDB428 by *in vivo* recombination. This approach was used to generate plasmids pDDB428-pDDB476. Purified plasmids were digested with NruI and transformed into *C. albicans* strain DAY534 to generate DAY981-DAY1029. The *snf7* alleles lacking the V5 epitope (*snf7-20.1*, *snf7-35.1*, *snf7-48.1*, *snf7-47.1*, and *snf7-49.1*) were generated using the same approach except pDDB426 as the template sequence to produce pDDB481, 483, 485, 494, and 495, respectively. All mutant *snf7* alleles were sequenced to ensure only specifically engineered mutations were present.

Specific *snf7* alleles were transformed into the *vps4*Δ/Δ background as follows. First, the *vps4*Δ/Δ strain DAY537 (98) was plated on 5-FOA-containing YPD plates to select for loss of the *URA3* marker through homologous recombination to generate

DAY1113. DAY1113 was transformed with pDDB427, 433, 441, and 446 to generate DAY1114-1117.

To generate a Ura marker plasmid, first *C. albicans URA3* was amplified from pGEM-URA3 using primers pRS/pGEMT-5 and pRS/pGEMT-3 (183). The resulting PCR product and NgoMI-linearized pRS314 (178) were transformed into *S. cerevisiae* to generate pDDB76 by *in vivo* recombination. Next, pDDB200 (107) was digested with PvuII and the *RIM101* containing fragment was purified. The purified product and NotI-digested pDDB76 were transformed into *S. cerevisiae* to generate pDDB477 by *in vivo* recombination (130). Finally, the V5 epitope sequence was amplified from pTRACER-EF in a PCR using primers AgeI 5' V5 and AGEI 3' V5 (107) and the resulting PCR product was transformed with AgeI-digested pDDB477 into *S. cerevisiae* to generate pDDB478.

Specific *snf7* mutant alleles were expressed with *RIM101-V5* as follows. First, the *snf7*Δ/Δ strain DAY534 (98) was plated on 5-FOA-containing YPD plates to select for loss of the *URA3* marker through homologous recombination to generate DAY1126. DAY1126 was then transformed with BstEII-digested pDDB478 to generate DAY1127. DAY1127 was then transformed with pDDB427, 426, 437, 461, 433, 458, 471, 472, 473, 474, 475, 440, 441, 443, 455, 476, 429, 446, 481, 483, 485, 494 and 495 to generate DAY1151, DAY1128 – DAY1144, DAY1148 – DAY1150, DAY1213, and DAY1214 respectively.

To generate prototrophic *vps4*Δ/Δ, *bro1*Δ/Δ, and *rim20*Δ/Δ mutant strains, DAY23 (49), DAY537, and DAY653 (98) were transformed with NruI-cut DDB78 and selected on SC-his medium to generate DAY1153, DAY1155, and DAY1156.

b. Growth and filamentation assays: Strains were regularly propagated in YPD medium (2% Bacto Peptone, 1% yeast extract, 2% dextrose). To test for growth phenotypes, YPD was buffered with 150mM HEPES to pH 9 with NaOH or contained 150mM lithium chloride. M199 medium (Gibco BRL) was buffered with 150mM HEPES and pH-adjusted as described in the text. Transformants were selected on synthetic medium (SC, 0.67% yeast nitrogen base with ammonium sulfate and without amino acids, 2% dextrose) supplemented as required for the auxotrophic requirements for the cells (1). To select for Ura- transformants, strains were streaked on synthetic complete medium containing 0.1% 5-FOA (MP Biomedicals). All media, except that selecting for Ura+ transformants, was supplemented with 80µg of uridine per ml. Solid medium contained 2% Bacto-agar.

c. FM 4-64 staining: 25µl of a YPD overnight culture was inoculated into 1ml M199 pH 8 medium and incubated at 30˚C for 4.5 hours. 2µl of 16mM FM 4-64 (Invitrogen) in DMSO was added to each tube and the cells were incubated on ice for 15 minutes. Cells were then washed and resuspended in 1ml fresh M199 pH 8 medium and incubated at 30˚C for 90 minutes. 80µl of cells were transferred to a tube containing 10µl each of 100mM NaN_3 and 100mM NaF. Cells were stored on ice and examined by fluorescent microscopy.

d. Protein preparation: 50ml YPD medium was inoculated from an overnight culture to an OD_{600} 0.05 - 0.07 and grown to an OD_{600} 0.5 - 0.7. Cells were washed with 1mM phenylmethylsulphonyl fluoride (PMSF) and then resuspended in radioimmunoprecipitation assay buffer (50mM Tris pH 8, 150mM NaCl, 1% NP-40, 3mM EDTA, 0.5% deoxycholate, 0.1% SDS) with protease inhibitors (1 mM PMSF,

10mM dithiothreitol (DTT), 1 ug/ml each of leupeptin, aprotinin, and pepstatin). Cells were lysed by glass bead disruption by vortexing four times for two minutes each. Cell debris was removed by 15 minutes centrifugation at 13000 x g. Supernatants were collected and protein concentration was determined by Bradford assay (Bio-Rad).

e. Cell fractionation: 0.6ml overnight cultures were diluted into 100ml M199 medium at pH 4 or pH 8 and grown roughly 6 hours at 30°C. 5 OD_{600} cells were washed in cold 10mM NaF/10mM NaN_3 and pelleted. Cells were resuspended in 10mM Tris pH 7.5/100mM EDTA/0.5% β-mercaptoethanol/10mM NaN_3/10mM NaF and shaken 20 minutes at 37°C. Cells were collected and resuspended in isotonic S buffer (40mM Tris pH 7.5/1.2M sorbitol/0.5mM $MgCl_2$/10mM NaN_3/10mM NaF/800μg/ml yeast lytic enzyme (MPBio)). Spheroplasts were gently pelleted and resuspended in Lysis Buffer (50mM Tris pH 7.5/0.2M sorbitol/2mM EDTA) containing 10mM DTT and protease inhibitors (1mM PMSF, 1μg/ml each of leupeptin, aprotinin, and pepstatin) and homogenized with 30 dounces in a glass homogenizer. Cell debris was removed by centrifugation for 10 minutes at 500 x g to generate the cleared homogenate. 100μl of the supernatant was removed and saved at -80°C as total sample. The remainder of the supernatant was centrifuged 15 minutes at 13,000 x g. The supernatant was removed and stored at -80°C and the pellets were washed twice with 1mL Lysis buffer, centrifuged 15 minutes at 13,000 x g, and resuspended in 0.5ml lysis buffer. 50μl sample from each fraction (supernatant and pellet, as well as cleared homogenate) was used for Western blot analysis.

f. Western blot analysis: 50μl of crude protein or cell fractionation sample was separated by SDS-polyacrylamide gel electrophoresis (SDS-PAGE). Resolving gels were

made to 12% or 6% polyacrylamide for Rim101 or Snf7 visualization, respectively. Protein was transferred to a nitrocellulose membrane and blots were blocked 1 hour at room temperature with 5% milk in Tris-buffered saline containing 0.05% Tween-20 (TBS-T). Blots were probed in blocking solution containing a 1:5000 monoclonal anti-V5-HRP (Invitrogen) antibody. Blots were washed with TBS-T, incubated with ECL reagent (Amersham), and exposed to film.

g. Immunofluorescence: Cells were grown to mid-log phase and fixed with 4% formaldehyde for 15 minutes. Spheroplasts were generated using 5µg/ml yeast lytic enzyme (YLE) (MPBio) in Solution B (100mM potassium phoshate pH 7.5, 1.2M sorbitol) for 15 minutes. Cells were pelleted at 0.5 x g for 5 minutes, washed twice in 1ml Solution B, and spotted onto polylysine-coated slides. Samples were blocked 10 minutes with 5% BSA and incubated 1 hour with 1:100 anti-V5 antibody. This was followed by a 1 hour incubation with 1:200 anti-mouse IgG conjugated to alexafluor 488 (Invitrogen). Cells were visualized on a Zeiss Imager.M1 microscope and images were captured using Axiovision Release 4.6.3 software.

h. Filamentation assays: For filamentation assays on solid medium, 3µl of overnight YPD cultures was spotted onto M199 pH 8 agar plates. Plates were incubated 5-7 days at 37°C and photographed. For liquid filamentation assays, overnight YPD cultures were inoculated 1:100 into M199 pH 8 medium and grown for 4 hours at 37°C. 500µl of cells were fixed with 1ml ethanol 30 minutes at 23°C. Cell morphology was analyzed microscopically and at least 300 cells per sample were counted.

i. FaDu cell damage assay: The FaDu cell line of oral epithelial cells (ATCC) was grown in 24-well tissue culture dishes and incubated at 37°C 5% CO_2 in Modified

Eagle Medium (MEM) with 10% final concentration FBS and 5 ml antibiotic/antimycotic cocktail (Invitrogen). At 90% monolayer confluence, FaDu cells were incubated in 0.5 ml medium containing 0.5μCi ^{51}Cr for 16 hours. After washing the FaDu cells with PBS, $1x10^5$ *C. albicans* cells were added in MEM with 10% FBS and 5ml antibiotic cocktail and incubated 10 hours. Some FaDu cells were untreated to measure spontaneous ^{51}Cr release. After incubation, 0.5 ml of supernatant was moved to a 13 ml glass (supernatant) tube. 0.5ml 6M NaOH was added to FaDu cells and moved to a separate (debris) tube. The remaining cells were removed to the debris tube in 0.5ml Liftaway (RPI Corp). Specific release was calculated as [(2*supernatant)-(2*spontaneous release)]/[(2*total)-(2*spontaneous release)].

III. Results

To determine how Snf7 functions in the Rim101 and vacuolar transport pathways, we first generated a V5 epitope-tagged *SNF7* allele. Since C-terminal Snf7-V5 fusions were not functional (data not shown), we used the internal HpaI site to generate an in-frame fusion. This *SNF7-V5* allele fully complemented the endocytosis and growth defects observed in the *snf7*Δ/Δ strain (Figures 6 and 7, Table 6), demonstrating that Snf7-V5 is functional.

We predicted that distinct domains of Snf7 contribute to vacuolar transport and Rim101 activation. To address this hypothesis, we used alanine scanning mutagenesis to generate a series of mutant *snf7-V5* alleles. Alanine residues were substituted at up to three charged residues within a span of five amino acids. Using this approach, 49 alleles were generated in the *SNF7-V5* background that span the length of the 226 residues of Snf7 protein (Table 5). To determine if these alleles impact Snf7 function in the vacuolar

Table 3 Mutant Snf7 sequences.

Allele	WT sequence[1]	Allele	WT sequence
snf7-1	1-MWGYF	*snf7-26*	125-VEDTM
snf7-2	3-GYFFG	*snf7-27*	129-MDEIR
snf7-3	10-SQQKK	*snf7-28*	133-REQVE
snf7-4	12-QKKDL	*snf7-29*	140-DEISE
snf7-5	17-PKKAI	*snf7-30*	146-ISRPV
snf7-6	22-VELRE	*snf7-31*	151-GNEFV
snf7-8	32-NKKKN	*snf7-32*	155-VDEDE
snf7-9	38-LQQQM	*snf7-33*	157-EDELD
snf7-10	41-QMDDQ	*snf7-34*	160-LDEEL
snf7-11	44-DQDQL	*snf7-35*	163-ELKEL
snf7-12	49-ARKYV	*snf7-36*	166-ELEAE
snf7-13	55-SKQTT	*snf7-37*	169-AEAKE
snf7-14	61-AKSAL	*snf7-38*	173-EQEQE
snf7-15	64-ALKRK	*snf7-39*	176-QEHRV
snf7-16	68-KKGYE	*snf7-40*	182-AQKAK
snf7-17	77-KVENQ	*snf7-41*	186-KPQPV
snf7-18	82-IETLE	*snf7-42*	190-VSREE
snf7-19	86-ETQLI	*snf7-43*	192-REEEL
snf7-20	90-ISIEG	*snf7-44*	196-LPQFP
snf7-50	95-ANLNL	*snf7-45*	202-VNKKA
snf7-21	100-ETMKA	*snf7-46*	209-VEEDE
snf7-22	105-AMKQG	*snf7-47*	212-DEDEE
snf7-23	111-KAMKQ	*snf7-48*	215-EEALK
snf7-24	116-IHGEY	*snf7-49*	220-ALQAE
snf7-25	120-YDVDK		

[1] # represents the N-terminal Snf7 residue. Underlined residues represent those targeted for mutation to alanine in the mutant *snf7* alleles.

transport pathway, Rim101 pathway, or both pathways, the alleles were transformed into a *snf7*Δ/Δ mutant and tested for complementation of vacuolar transport and Rim101 processing defects (referred to as ESCRT-dependent and Rim101-dependent phenotypes in following text, although we recognize that Rim101-dependent phenotypes also depend on upstream ESCRT function).

To determine if a given mutation affected Snf7 protein stability, we performed Western blot analysis on crude protein extracts from our mutant strains. All strains containing an alanine-scanning allele produced abundant Snf7 protein (Figure 9). However, we noted that specific alleles revealed differences in mobility, such as *snf7-29*, *snf7-40*, and *snf7-47*. These differences are likely due to alterations of SDS binding, however we cannot rule out the possibility that the altered mobilities are due to disruption of an as-yet-unknown Snf7 post-translational modification. Regardless, these results indicate that the alanine scanning alleles are expressed and that phenotypes observed in the mutant alleles are not due to the instability of the Snf7 protein.

When grown on rich YPD medium, the wild-type strain and the *snf7*Δ/Δ + *SNF7-V5* strain grew comparably (Figure 7). However, the *snf7*Δ/Δ mutant grew slower, as reported previously (98). All of the *snf7*Δ/Δ + *snf7* alanine scanning allele strains rescued this growth defect on rich medium. This result, and the fact that Snf7 protein is expressed at similar levels in all strains, suggests that none of the *snf7* alleles is a true null.

a. *snf7* alleles affecting vacuolar transport: We first analyzed the *snf7* alleles for ESCRT-dependent phenotypes. Endocytosis is required to move plasma membrane components to the vacuole and can be monitored using the fluorescent lipophilic dye, FM 4-64 (196). In wild-type and *snf7*Δ/Δ +*SNF7-V5* cells, FM 4-64 associated with the

plasma membrane, was taken up by endocytosis, and was ultimately localized to the vacuolar membrane, resulting in the ring-like pattern around the vacuole (Figure 6). In *snf7*Δ/Δ cells, FM 4-64 associated with the plasma membrane and was taken up by endocytosis, but was unable to localize to the vacuole, resulting in a more diffuse staining pattern and the apparent formation of class E-like exclusion bodies around the perimeter of the vacuole (Figure 6). These exclusion bodies likely consist of endosomes unable to fully mature to MVBs and thus unable to efficiently fuse with the vacuole (96). We next tested a *rim20*Δ/Δ mutant, which does not process Rim101 but has no detected role in MVB formation (48, 98). This strain localized FM 4-64 to the vacuole like wild-type, as previously reported. We also tested a *bro1*Δ/Δ strain, which affects MVB formation but has no detected role in Rim101 processing (98 and data not shown). The *bro1*Δ/Δ mutant showed stronger vacuolar staining than the *snf7*Δ/Δ mutant but similarly displayed class E-like bodies around the periphery of the vacuole and cytoplasmic punctate spots not observed in wild-type cells (Figure 6). This suggests that *bro1*Δ/Δ mutants have a defect in vacuolar trafficking, but that this defect is not as severe as the *snf7*Δ/Δ mutant, as previously described in *C. albicans* and homologous *S. cerevisiae* mutants (98, 140). Finally, we tested a *vps4*Δ/Δ strain, which also had a defect in vacuolar trafficking that was less pronounced than the *snf7*Δ/Δ mutant defect, as reported previously (98). Thus Snf7 and downstream ESCRT proteins, but not Rim101 pathway members, are required for FM 4-64 localization to the vacuole.

The *snf7*Δ/Δ + *snf7* alanine scanning alleles were assayed for FM 4-64 localization and characterized as nonfunctional, partially functional, or fully functional. Nonfunctional alleles were defined as those that have a staining pattern that mimics the

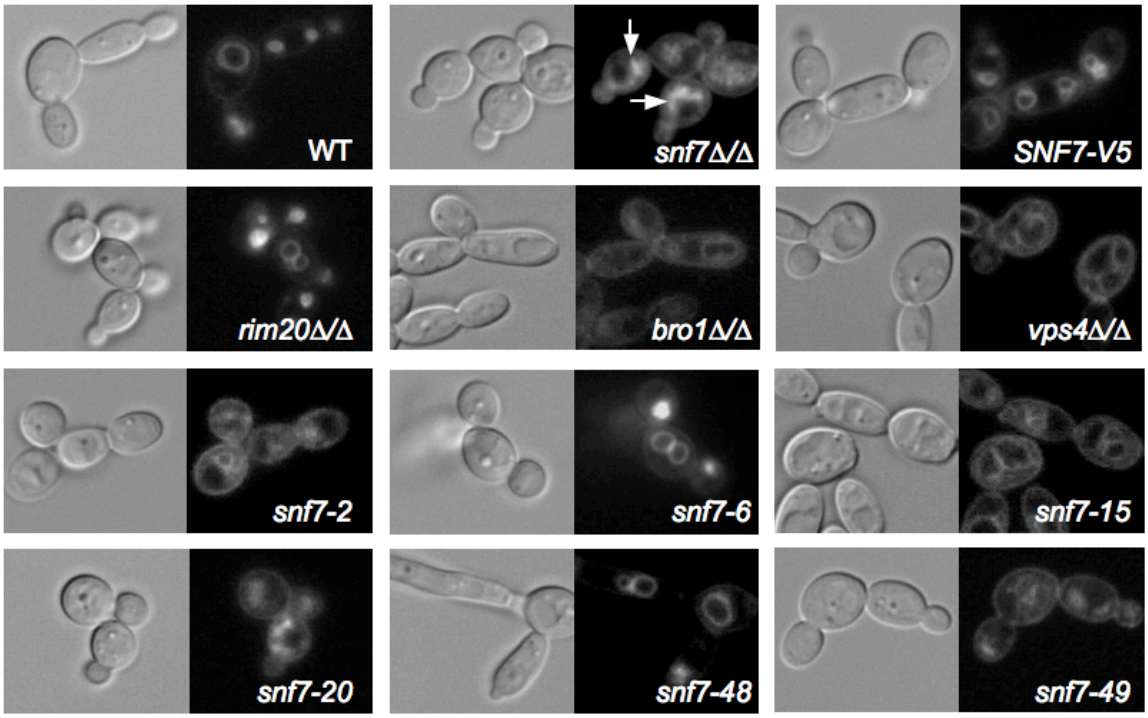

Figure 6. FM 4-64 localization in control strains and *snf7* mutants. Strains used include WT (DAY185), *snf7*Δ/Δ (DAY763), *snf7*Δ/Δ + *SNF7-V5* (DAY980), *rim20*Δ/Δ (DAY1153), *bro1*Δ/Δ (DAY1156), *vps4*Δ/Δ (DAY1155), *snf7*Δ/Δ + *snf7-2* (DAY982), *snf7*Δ/Δ + *snf7-6* (DAY986), *snf7*Δ/Δ + *snf7-15* (DAY994), *snf7*Δ/Δ + *snf7-20* (DAY 999), *snf7*Δ/Δ + *snf7-48* (DAY1027), and *snf7*Δ/Δ + *snf7-49* (DAY1028). Strains were grown at 30°C to mid-log phase in M199 (pH 8) medium and exposed to FM 4-64 for 15 minutes. Cells were washed and incubated in fresh M199 pH 8 medium for 90 minutes at 30°C. Cells were placed on ice and NaF and NaN_3 added prior to photographing. Arrows indicate Class E-like accumulations in *snf7*Δ/Δ strain.

*snf7*Δ/Δ strain, such as *snf7-2* and *snf7-20* (Figure 6). Partially functional alleles were those that showed some vacuolar staining but variously retained FM 4-64 in the cytoplasm or had slightly aberrant vacuolar staining patterns, such as *snf7-15* and *snf7-49*. We noted similar patterns between some partially functional alleles, such as *snf7-15*, and the *vps4*Δ/Δ strain, which had less a severe FM 4-64 trafficking defect than the *snf7*Δ/Δ mutant (Figure 6). Fully functional alleles were defined as those that localized FM 4-64 to the vacuole similar to the *snf7*Δ/Δ +*SNF7-V5* strain, such as *snf7-6* and *snf7-48*. Thus, we were able to test the ESCRT-dependent function of our *snf7* alleles and identified several alleles from each of three categories among our *snf7* alleles (Figure 10).

b. *snf7* alleles affecting the Rim101 pathway: We next analyzed the alanine scanning *snf7* alleles for Rim101-dependent phenotypes with five-fold serial dilution growth assays. Rim101 activation is required for growth on YPD buffered to pH 9 and on YPD containing lithium chloride (LiCl) (Figure 7). These growth defects are also observed on streaked agar plates (Figure 8). On YPD pH 9 medium, the wild-type and *snf7*Δ/Δ + *SNF7-V5* strains grew similarly, but the *snf7*Δ/Δ strain did not produce isolated colonies (Figure 7). The *rim20*Δ/Δ mutant also displayed a growth defect, although not as severe as the *snf7*Δ/Δ strain. Both the *bro1*Δ/Δ and *vps4*Δ/Δ mutant strains were able to form wild-type-sized colonies on this alkaline medium (Figure 7). Thus, Snf7 and downstream Rim101 pathway members are required for alkaline growth, and downstream ESCRT pathway members are not.

The *snf7*Δ/Δ + *snf7* alanine scanning alleles showed a range of growth phenotypes on alkaline medium that were categorized as nonfunctional, partially functional, or fully functional. Nonfunctional alleles were defined as those that, like the *snf7*Δ/Δ mutant,

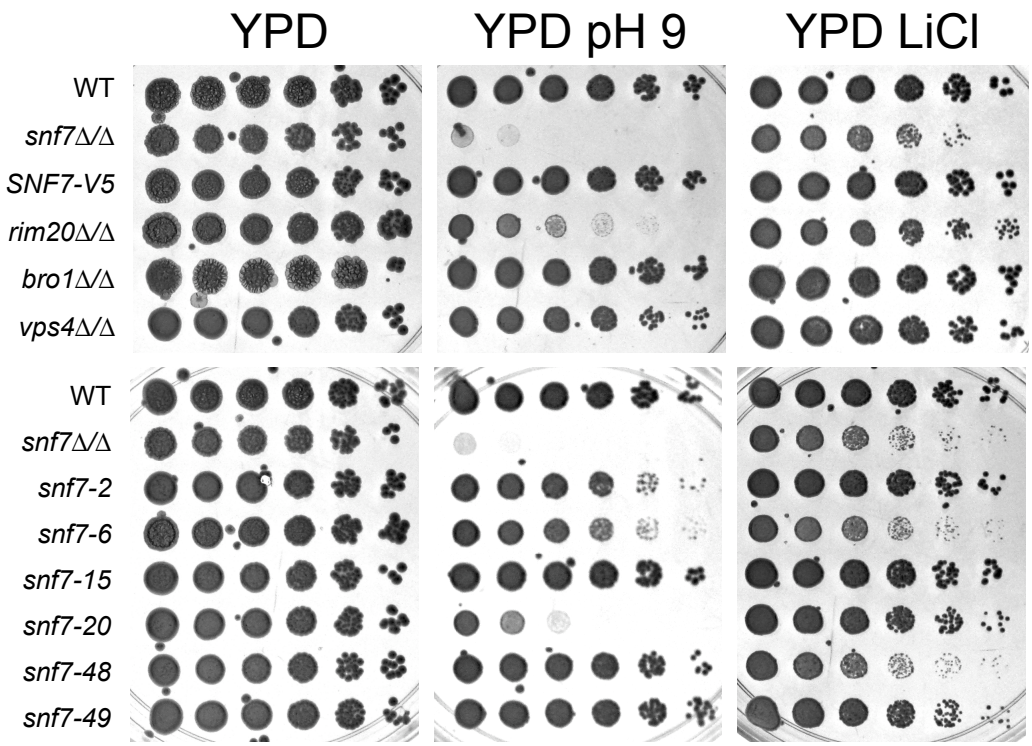

Figure 7. Growth phenotypes of control strains and *snf7* mutants. Strains pictured include the wild-type (WT) (DAY185), *snf7*Δ/Δ (DAY763), *snf7*Δ/Δ + *SNF7-V5* (DAY980), *rim20*Δ/Δ (DAY1153), *bro1*Δ/Δ (DAY1156), *vps4*Δ/Δ (DAY1155), *snf7*Δ/Δ + *snf7-2* (DAY982), *snf7*Δ/Δ + *snf7-6* (DAY986), *snf7*Δ/Δ + *snf7-15* (DAY994), *snf7*Δ/Δ + *snf7-20* (DAY 999), *snf7*Δ/Δ + *snf7-48* (DAY1027), and *snf7*Δ/Δ + *snf7-49* (DAY1028). Strains were grown on YPD, YPD pH 9, and YPD + LiCl for two days at 37ºC prior to photographing.

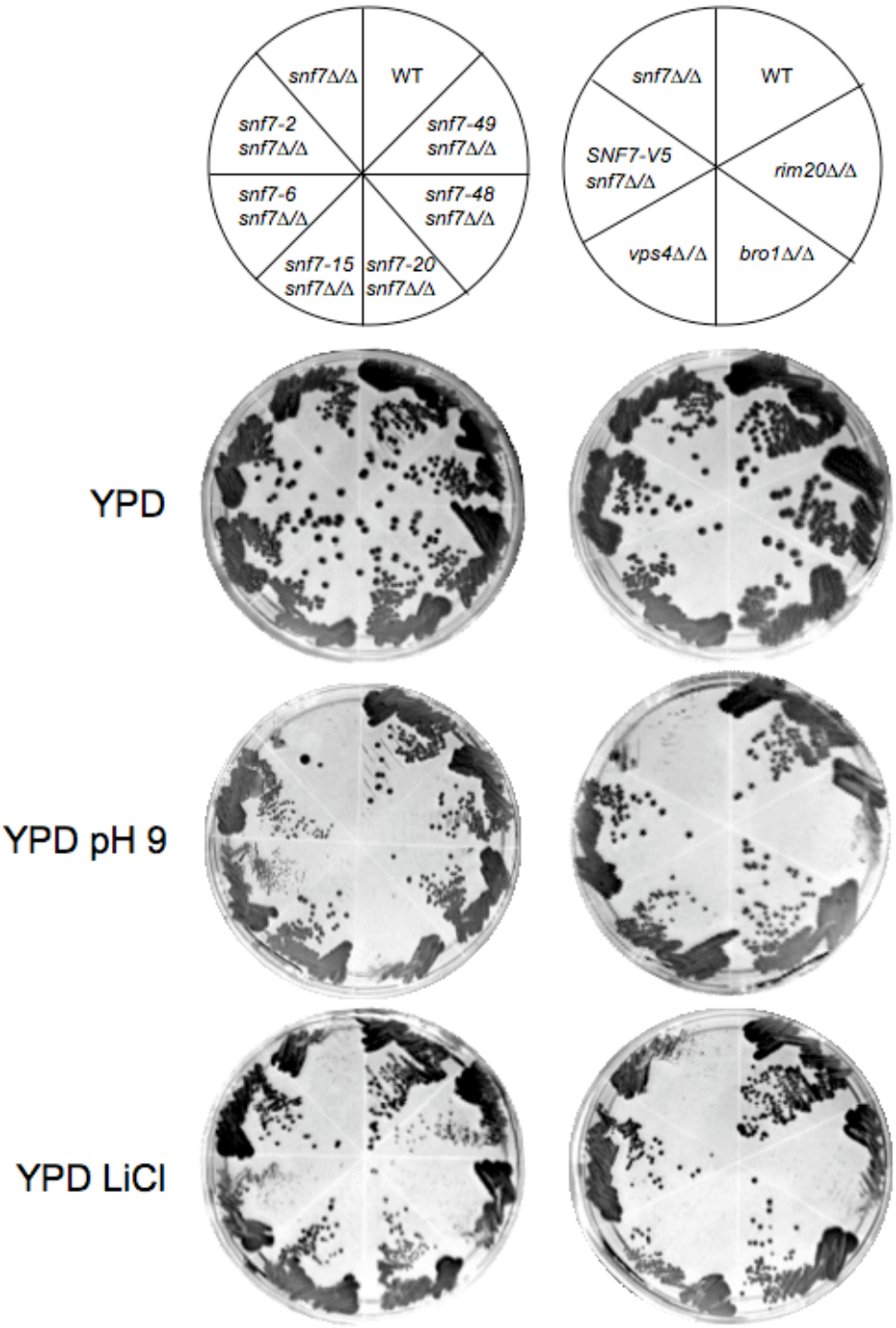

Figure 8. Growth phenotypes of control strains and *snf7* mutants (streaks). Strains pictured include the wild-type (WT) (DAY185), *snf7*Δ/Δ (DAY763), *snf7*Δ/Δ + *SNF7-V5* (DAY980), *rim20*Δ/Δ (DAY1153), *bro1*Δ/Δ (DAY1156), *vps4*Δ/Δ (DAY1155), *snf7*Δ/Δ + *snf7-2* (DAY982), *snf7*Δ/Δ + *snf7-6* (DAY986), *snf7*Δ/Δ + *snf7-15* (DAY994), *snf7*Δ/Δ + *snf7-20* (DAY 999), *snf7*Δ/Δ + *snf7-48* (DAY1027), and *snf7*Δ/Δ + *snf7-49* (DAY1028). Strains were grown on YPD, YPD pH 9, and YPD + LiCl for two days at 37ºC prior to photographing.

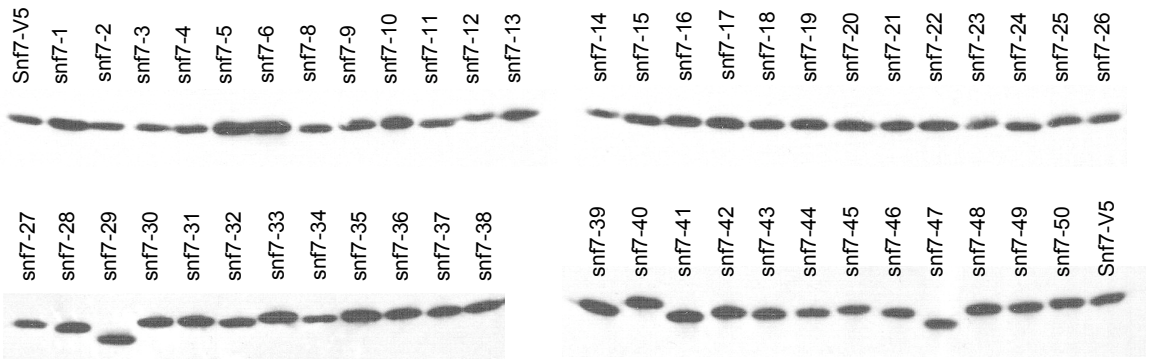

Figure 9. Mutant *snf7* alleles produce detectable protein. 250µg protein collected from mid-log cultures was loaded for each sample and run on 10% SDS-PAGE. Blots were probed with anti-V5-HRP antibody. Protein loading was normalized to anti-tubulin signal (data not shown).

were unable to form individual colonies after two days growth, such as *snf7-20* (Figure 7). Partially functional alleles were defined as those that could form isolated colonies smaller than the colonies produced by the *snf7*Δ/Δ + *SNF7-V5* strain, such as *snf7-2* and *snf7-6*, and, to a lesser degree, *snf7-48* and *snf7-49* (Figures 7 and 8). Fully functional alleles were defined as those that could form isolated colonies similar in size to those produced by the *snf7*Δ/Δ + *SNF7-V5* strain, such as *snf7-15.* We identified several alleles from all three categories among our *snf7* alleles using this Rim101-dependent growth assay (Figure 10).

We next assayed growth on LiCl medium. On LiCl medium, the wild-type and *snf7*Δ/Δ + *SNF7-V5* strains grew similarly and the *snf7*Δ/Δ mutant had a severe defect, forming only pinprick sized colonies (Figure 7). The *rim20*Δ/Δ mutant strain showed a slightly less severe growth defect, forming only very small colonies, while the *bro1*Δ/Δ and *vps4*Δ/Δ mutant strains showed no growth defects on LiCl medium (Figure 7). Thus, Snf7 and downstream Rim101 pathway members, but not downstream ESCRT members, are required for LiCl growth.

The *snf7*Δ/Δ + *snf7* alanine scanning alleles again showed a range of growth phenotypes on LiCl medium that were categorized as nonfunctional, partially functional, or fully functional. Nonfunctional alleles were defined as those whose colonies grew similarly to the *snf7*Δ/Δ mutant, such as *snf7-6* and *snf7-48*. Partially functional alleles were defined as those that promoted colony growth of a size intermediate between the *snf7*Δ/Δ +*SNF7-V5* and the *snf7*Δ/Δ strains, such as *snf7-2*, *snf7-20* and *snf7-49* (Figure 7). Fully functional alleles were defined as those that grew similarly to the *snf7*Δ/Δ

+*SNF7-V5* strain, such as *snf7-15*. Again, we identified several alleles from all three categories among our *snf7* alleles using this assay (Figure 10).

While most *snf7* alanine scanning alleles conferred similar growth defects on both pH 9 medium and LiCl medium (Figure 10), we did note that certain alleles showed variation between these two assays. For example, *snf7-48* was scored as partially functional on pH 9 medium but as nonfunctional on LiCl medium (Figures 7 and 10). However, no allele was fully functional in one growth assay and nonfunctional in the other. Thus, we infer that the few observed differences between these two growth assays reflect sensitivities between the growth assays. Alleles that conferred clear growth defects on both pH 9 and LiCl media were candidates for Rim101 pathway disruption.

We noted that some alleles displayed both ESCRT-dependent defects and Rim101-dependent defects, such as *snf7-20*, while some alleles displayed ESCRT-dependent defects yet showed no detectable Rim101-dependent defects, such as *snf7-15*. Conversely, some alleles showing no ESCRT-dependent defects conferred Rim101-dependent defects, such as *snf7-6* and *snf7-48* (Figure 10). Thus among these *snf7* alleles, we have identified candidate alleles with differential ESCRT-and Rim101-dependent phenotypes that are strong candidates for separation of function.

c. Filamentation-related *snf7* phenotypes: Vesicle trafficking and Rim101 activation are both required for filamentation, a critical virulence trait of *C. albicans* (15, 31, 98, 144). We wished to further investigate the role of these processes and their relative contributions to filamentation. Since Snf7 is required for both ESCRT trafficking and Rim101 processing, we predicted that *snf7* alanine scanning alleles defective in either ESCRT function or Rim101 activation would show defects in filamentation. To test this

possibility, we assayed the *snf7* alanine scanning alleles for filamentation in liquid and solid M199 pH 8 medium.

We first assessed filamentation using a quantitative liquid assay. Strains were incubated four hours in M199 pH 8 medium and germ tube formation was assessed for each strain. The wild-type strain produced ~95% germ tubes (Table 6). The *snf7*Δ/Δ mutant produced < 0.01% germ tubes under these conditions, while the complemented *snf7*Δ/Δ + *SNF7-V5* strain rescued germ tube production. The *rim101*Δ/Δ and *rim20*Δ/Δ mutant strains were both severely deficient in germ tube production, with no detectable germ tubes after a four-hour incubation (Table 6). The *bro1*Δ/Δ strain produced wild-type levels of germ tubes, while the *vps4*Δ/Δ strain produced ~80% germ tubes. Nonfunctional alleles were those that produced < 5% germ tubes, such as *snf7-6*. Partially functional alleles were those that produced an intermediate number, 5-90%, of germ tubes, such as *snf7-15* and *snf7-48* with 78% and 88% germ tubes respectively. Fully functional alleles were defined as those that formed >90% germ tubes like the *snf7*Δ/Δ +*SNF7-V5*. We noted that some alleles with filamentation defects also conferred ESCRT-dependent defects, such as *snf7-15*; that some also conferred Rim101-dependent defects, such as *snf7-48*; and that some also conferred defects in both, such as *snf7-20*. We did not find any alleles conferring solely filamentation defects. Although both Rim101- and ESCRT-related defects are reported to affect filamentation, we noted fewer pheonotypic defects in this assay than in the FM 4-64 assay or growth assays (Figure 10).

We also assessed colony filamentation by spotting strains on solid alkaline or acidic medium and measuring the ability of the strains to form peripheral filamentation. On alkaline medium, the wild-type and *snf7*Δ/Δ + *SNF7-V5* strains formed peripheral

Table 6. Filamentation Assays of *snf7* mutants.

Strain	Genotype	Alkaline agar filamentation	Acidic agar filamentation	% Germ Tubes[1]
DAY185	WT	+	-	96 ± 3
DAY763	*snf7*Δ/Δ	-	+	0 ± 0
DAY980	*SNF7-V5*	+	-	96 ± 1
DAY25	*rim101*Δ/Δ	-	-	0 ± 0
DAY537	*vps4*Δ/Δ	±	+	82 ± 2
DAY982	*snf7-2*	+	-	2 ± 2
DAY986	*snf7-6*	-	-	1 ± 1
DAY994	*snf7-15*	+	-	78 ± 4
DAY999	*snf7-20*	-	-	13 ± 7
DAY1028	*snf7-48*	+	-	86 ± 6

[1] % germ tube formation ± standard deviation from 2 independent experiments

filamentous rings (Table 6). The *snf7*Δ/Δ, *rim20*Δ/Δ, and *rim101*Δ/Δ mutants did not produce a ring of peripheral filaments, as expected due to the inability of these strains to process Rim101. The *bro1*Δ/Δ strain produced a wild-type filamentation pattern, and the *vps4*Δ/Δ mutant produced an erratic ring of peripheral filaments, as previously reported (98). The *snf7*Δ/Δ + *snf7* alanine scanning alleles were assayed and categorized as functional or nonfunctional, as no intermediate phenotypes were observed. Nonfunctional alleles were defined as alleles that did not produce peripheral filaments, such as *snf7-6* and *snf7-20*. Fully functional alleles produced filamentous rings similar to those observed in the *snf7*Δ/Δ +*SNF7-V5* strain, such as *snf7-2, snf7-15*, and *snf7-48*.

On acidic solid medium, neither the wild-type, *snf7*Δ/Δ + *SNF7-V5*, *rim101*Δ/Δ, *rim20*Δ/Δ, nor the *bro1*Δ/Δ strains formed peripheral filaments (Table 6). However, we noted that both the *snf7*Δ/Δ and *vps4*Δ/Δ strains formed robust filaments. None of the mutant *snf7* alanine alleles promoted acidic filamentation, supporting our previous premise that no *snf7* mutation results in completely abolished Snf7 function. Because both Snf7 and Vps4 are required for ESCRT function and Rim101 plays no role in ESCRT function (98), our data suggest that vacuolar transport influences filamentation at acidic pH.

In order to define regions that may function specifically in either the ESCRT or Rim101 pathways, we mapped the results of the phenotypic assays in relation to the position of *snf7* alanine scanning alleles (Figure 10). Alleles were classified into categories based on their phenotypic profile. These included alleles that showed either no phenotypic defects or a mild defect in a single Rim101-dependent assay (Group A), alleles that showed only ESCRT-dependent defects (Group B), alleles that showed only

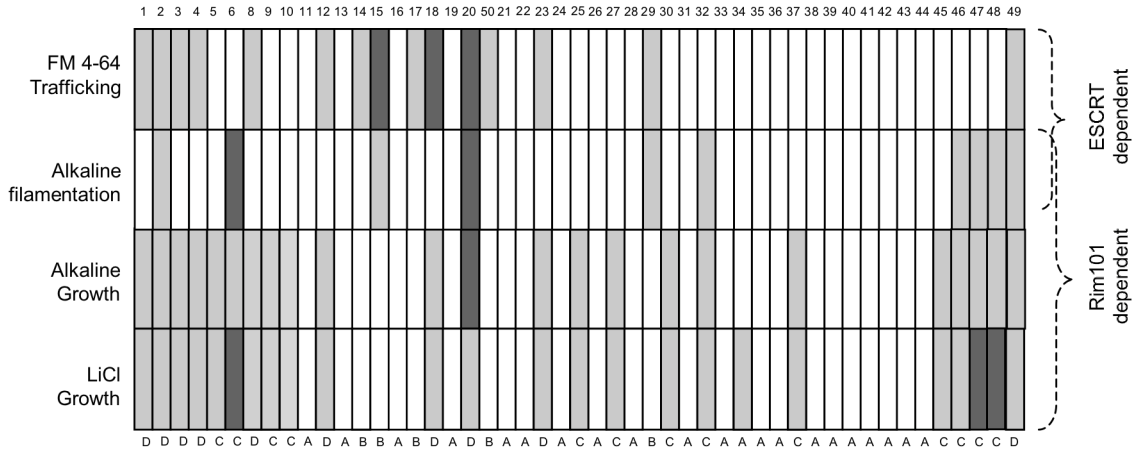

Figure 10. Comparison of mutant *snf7* alleles facilitates categorization into functional groups. The cartoon represents the N- to C-terminal sequence of Snf7, with the alleles placed in order along the protein sequence. Assays are listed to the left of each row while *snf7* mutant allele number is listed above each column. Rim101- and ESCRT-dependent assays are labeled to the right side. White blocks indicate the mutant *snf7* allele behaves like wild-type *SNF7*, dark grey blocks indicate the mutant allele behaves like *snf7Δ/Δ,* and light grey blocks indicate an intermediate phenotype. For FM 4-64 trafficking, the output is specific vacuolar staining. For alkaline filamentation, the output is percent germ tube formation. For alkaline and LiCl growth assays, the output is colony size.

Rim101-dependent defects (Group C), and alleles that showed both ESCRT- and Rim101-dependent defects (Group D). We then used these groups as a guide for investigating the mechanisms behind our alanine scanning *snf7* allele phenotypes.

d. Snf7 protein localization: In wild-type cells, Snf7 cycles between the cytoplasm and endosomal membrane, and its release requires Vps4. We tested Snf7 localization using cell fractionations to separate the membrane-bound organelles, including endosomes, from the cytoplasm. We first used plasma membrane protein Pma1 and cytoplasmic protein Pgk1, which localized to the pellet or supernatant fraction, respectively (data not shown), as control proteins for our fractionation protocol. Snf7-V5 was observed in both pellet and supernatant (Figure 11A), indicating that Snf7-V5 is able to cycle on and off endosomal membranes, as reported in *S. cerevisiae* (10). Snf7-V5 localization in a *vps4*Δ/Δ background resulted in a strong pellet signal but no supernatant signal, indicating that Snf7-V5 is unable to dissociate from endosomal membranes in the absence of Vps4, also as reported in *S. cerevisiae* (10). This inability to dissociate is independent of extracellular pH (data not shown). We further confirmed a Vps4-dependent Snf7 release from endosomes using immunofluorescence. Snf7-V5 fluorescence in a wild-type background showed staining throughout the cytoplasm as well as concentrated spots, which likely represent foci of Snf7 endosomal recruitment (Figure 11B). Snf7-V5 fluorescence in a *vps4*Δ/Δ background showed little cytoplasmic staining and 1 or 2 very highly concentrated spots, which likely are class E-like compartments. These two methods confirm that Snf7 localization is regulated similarly to previously described systems.

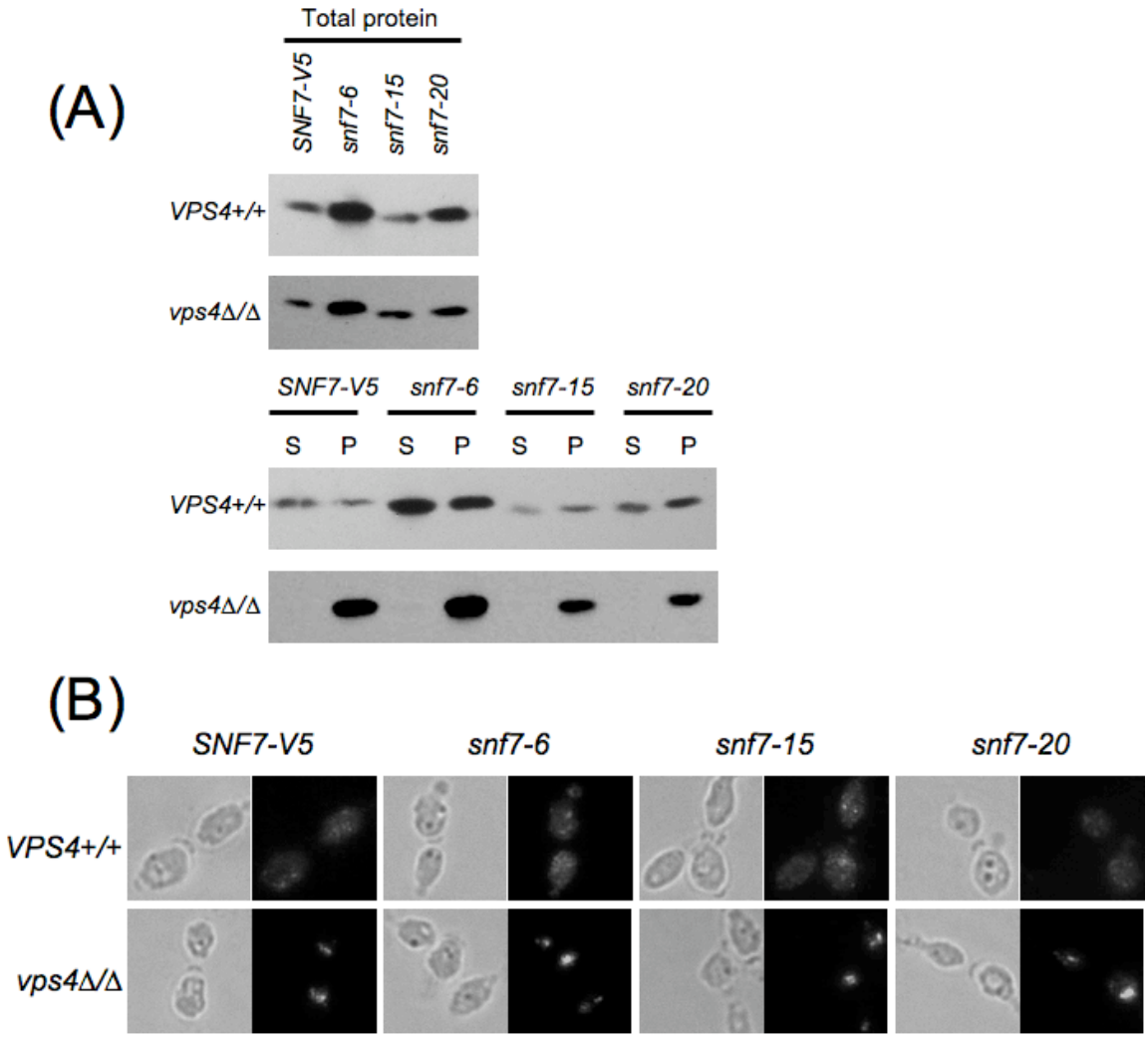

Figure 11. Snf7 localization remains normal in alanine scanning *snf7* mutants. (A) Snf7 localization remains normal in alanine scanning *snf7* mutants during cell fractionation. Mid-log cultures were gently lysed and separated by centrifugation to generate a cytoplasm-containing supernatant (S) and an organelle-containing pellet (P). 50uL of each fraction was run on 10% SDS-PAGES. Blots were probed with anti-V5-HRP antibody. (B) Snf7 localization remains normal in alanine scanning *snf7* mutants during immunofluorescence. Strains were grown to mid-log phase in M199 (pH 8) medium, fixed with 4% formaldehyde, spheroplasted, and attached to polylysine-treated wells for immunofluorescence. Samples were treated with anti-V5 antibody, followed by anti-mouse-IgG-alexafluor 488 (green).

We identified seventeen Group D *snf7* alleles that affected Snf7 function in both the Rim101 and ESCRT pathways. Two simple models can explain the Group D phenotypes. In the first model, Group D alleles are defective in overall Snf7 function due to a failure of Snf7 protein to interact with the upstream ESCRT pathway member Vps20 or with Snf7 itself. Vps20 has been shown to facilitate initial Snf7 endosomal association, followed by the formation of a Snf7 lattice through Snf7-Snf7 interactions (8, 188). Thus, *snf7* alleles unable to interact with either Vps20 or itself would not be able to properly localize, and would be expected to have a defective phenotype in any assay for Snf7 function. In the second model, Group D alleles are defective in overall Snf7 function due to disruption of a Snf7 region required for interaction with downstream components of both pathways. For example, Snf7 interacts with Bro1 and Rim20 via a bro1-domain found in both proteins (92, 199). To distinguish between these two possible explanations, Snf7 protein from the Group D alleles was localized through cell fractionations.

We predicted that if Group D alleles affected upstream Snf7 interactions, Snf7 protein would not be properly recruited to the endosomal membrane. To test this, we introduced the Group D alleles into a *vps4*Δ/Δ strain, in which Snf7 protein is unable to dissociate from the endosomal membrane. If the Group D allele blocked recruitment to the endosome, Snf7 should be detected only in the supernatant fraction. If the Group D allele blocked downstream interactions with members of both pathways, Snf7 should be enriched in the pellet fraction. Strains containing *snf7-20* showed primarily pellet-associated Snf7 (figure 11A), indicating that normal recruitment and retention of Snf7 in a *vps4*Δ/Δ background was retained. Results for the other Group D strains were similar to *snf7-20* (data not shown). We used immunofluorescence to confirm that *snf7-20*

expression leads to normal Snf7 protein localization in both a *VPS4*+/+ and *vps4*Δ/Δ background (Figure 11B). This suggests the mutations in these alleles affect an epitope necessary for downstream Snf7 function in both the Rim101 and ESCRT pathway.

We identified five Group B alleles that affected only ESCRT-dependent Snf7 function. Because Rim101 function requires endosomal Snf7 localization, and because these alleles did not affect Rim101 function, we predicted that alleles in this category affected interactions with downstream ESCRT pathway members, such as Vps2, Vps24, or Vps4. Because we had noted a similar FM 4-64 staining pattern between the *snf7-15* and *vps4*Δ/Δ strains (Figure 6), we considered *snf7-15* to be a strong candidate for interrupted Snf7-Vps4 interactions. To test this possibility, we investigated Snf7-15 localization by cell fractionation. Alanine scanning alleles affecting Snf7-Vps4 interactions should have enriched Snf7 protein in the pellet fraction, as the *vps4*Δ/Δ strain does, while mutant alleles not affecting Snf7-Vps4 interactions should have Snf7 in both the pellet and supernatant fractions, as the wild-type strain (Figure 11A). Snf7-15 protein was found in both pellet and cytoplasmic fractions, suggesting that Snf7-Vps4 interactions are not inhibited in this strain. We expected Group C alleles, which conferred only Rim101-dependent defect, would promote Snf7 protein localization similar to wild-type and we detected both pellet- and supernatant-associated Snf7 protein in all Group C alleles, such as *snf7-6* (Figure 11A). Normally regulated Snf7 protein localization from both the *snf7-6* and *snf7-15* alleles was confirmed with immunofluorescence (Figure 11B). Thus, we did not find any *snf7* alleles that significantly affected protein localization patterns.

e. Rim101 processing and localization: We identified thirteen Group C alleles that disrupted only Rim101-dependent Snf7 function, including *snf7-6* and *snf7-48*. Because Snf7 interacts with Rim101 processing machinery, we predicted that alleles in this category would produce less active, processed Rim101, and that this decrease would explain the phenotypic defects observed in our screens. To test this prediction, we used Western blot analysis to investigate Rim101 processing in *snf7*Δ/Δ *RIM101-V5* strains containing mutant *snf7* alleles (Figure 12A). We noted that the *SNF7-V5* strain contained less processed Rim101 (both 74 and 65 kDa forms) and more full-length Rim101 compared to wild-type cells. However, similar results were observed using an untagged *SNF7* complementation strain (Figure 12B), suggesting that decreased Rim101 processing in the *SNF7-V5* strain is not due to the V5 epitope.

We tested all *snf7* mutant alleles for their ability to promote Rim101 processing. As expected, all Group A and Group B alleles, such as *snf7-35* and *snf7-15* respectively, processed Rim101 similarly to the *SNF7-V5* strain. (Figure 12A). We expected Group C alleles, which conferred only Rim101-dependent defects, to show decreased levels of Rim101 processing compared to the *SNF7-V5* strain. However, we found only one allele, *snf7-6*, that abolished Rim101 processing, similar to the *snf7*Δ/Δ strain (Figure 12A). Other Group C alleles, such as *snf7-48*, processed levels of Rim101 similar to the *SNF7-V5* strain. We expected Group D alleles, which conferred both ESCRT- and Rim101-dependent defects, to also have decreased levels of Rim101 processing compared to the *SNF7-V5* strain. This was observed for all Group D alleles, including *snf7-20* (Figure 12A). Thus, while alleles in Group B and Group D behaved as expected, a decrease in processed Rim101 does not explain the growth defects seen in all Group C alleles.

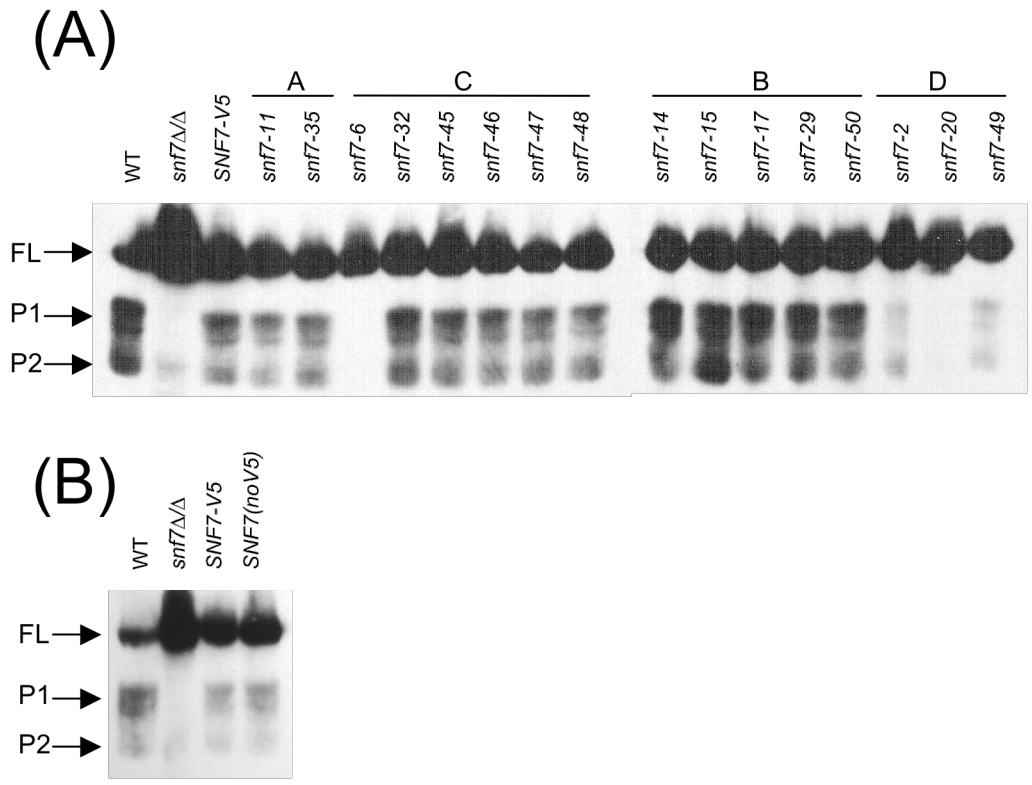

Figure 12. Rim101 processing is affected by some *snf7* mutants. (A) Strains were grown to mid-log phase in M199 pH 8 medium before protein preparation. Equivalent protein amounts were analyzed by Western blotting analysis. FL: full length Rim101 (85 kDa); P1: processed form 1 of Rim101, the active form (74 kDa); P2: processed form 2 of Rim101, with unknown function (65 kDa) (B) Rim101 processing is decreased in the presence of only one *SNF7* allele regardless of V5 epitope.

We considered two models to explain the processing seen in Group C alleles. First, Group C *snf7* alleles that process Rim101 do not promote translocation to the nucleus. Second, Group C *snf7* alleles have Rim101 processing defects that were missed at steady-state growth. To test these models, we generated alanine scanning *snf7* alleles without the V5 epitope and expressed them into a *snf7*Δ/Δ *RIM101-V5* strain. We grew our strains in acidic medium to mid-log phase and shifted them to alkaline medium for 30 minutes to investigate the initial stages of alkaline adaptation. We then tested Rim101 localization through immunofluorescence and Rim101 processing through Western blot analysis.

In a strain with wild-type *SNF7* grown at pH 4, Rim101-V5 showed cytoplasmic staining (data not shown). This same strain shifted to pH 8 showed V5 staining that colocalized with the DNA stain DAPI (Figure 13A), indicating nuclear localization of Rim101-V5 in these cells. The *snf7*Δ/Δ strain, which does not process Rim101, showed cytoplasmic V5 staining with no specific DAPI colocalization, indicating cytoplasmic retention of Rim101-V5 in this strain. We next analyzed the *snf7*Δ/Δ mutant complemented with wild-type *SNF7* or the Group A allele *snf7-35.1.* As expected, strains containing either the wild-type *SNF7* allele or the *snf7-35.1* allele displayed wild-type Rim101-V5 staining patterns (Figure 13A), indicating nuclear localization of Rim101 in these strains. This correlates well with the robust processing promoted by these alleles (Figure 13A).

Next, we tested the Group D alleles *snf7-20.1* and *snf7-49.1*. The *snf7-20.1* allele conferred severe growth defects (Figure 7) and contained no processed, active Rim101 (Figure 12A). Cells expressing *snf7-20* displayed a V5 staining pattern similar to the

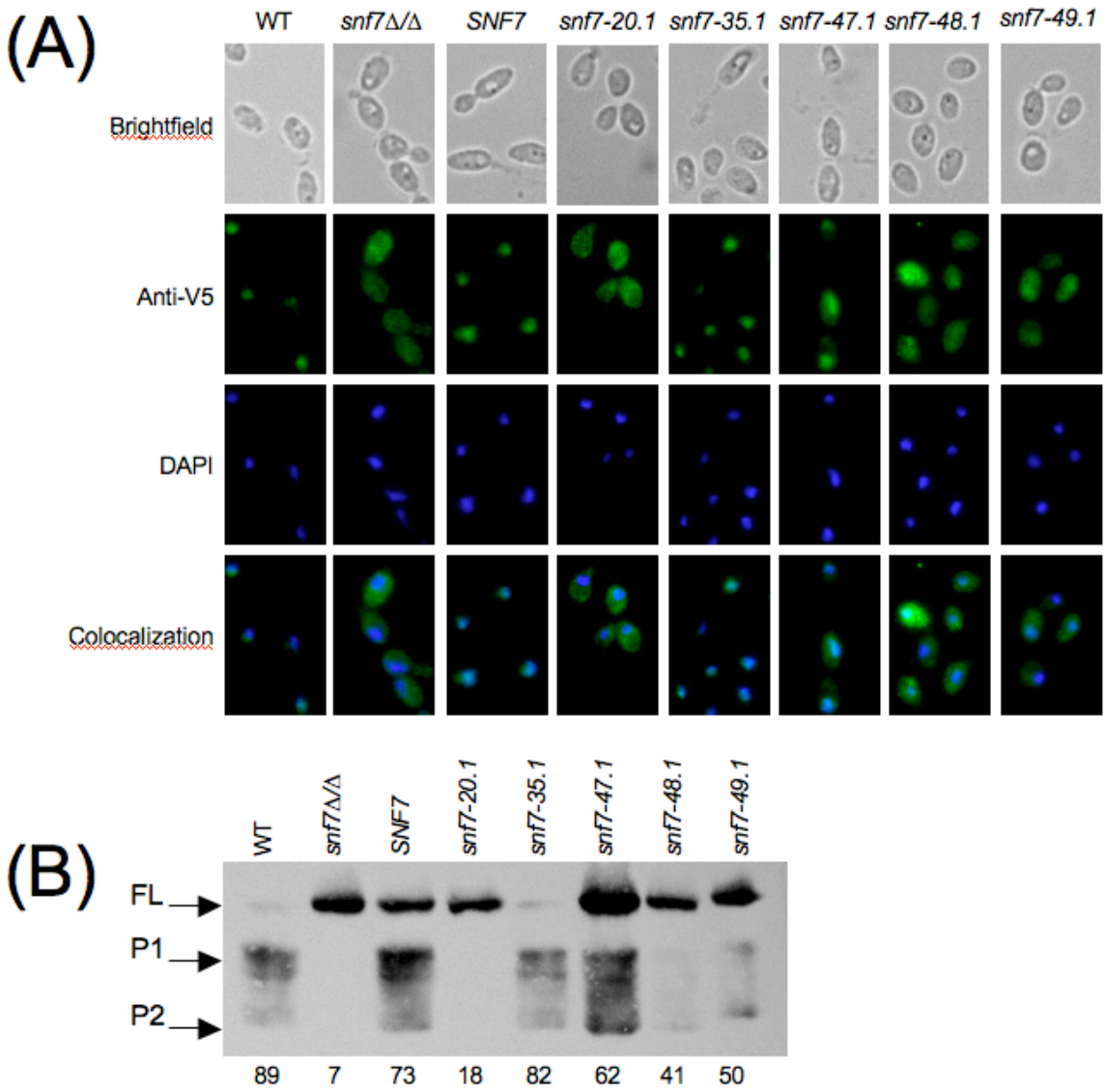

Figure 13. Rim101 localization in alanine scanning *snf7* mutants. (A) Rim101 localization in Group C alleles may be impaired after a shift to alkaline pH. Strains were grown to mid-log phase in M199 pH 4 medium and shifted to pH 8 for 30 minutes. Strains were fixed with 4% formaldehyde, spheroplasted, and attached to polylysine-treated wells for immunofluorescence. Samples were treated with anti-V5 antibody, followed by anti-mouse-IgG-alexafluor 488 (green). Nuclei were visualized by DAPI staining (blue). Strains investigated include *SNF7+/+ RIM101-V5* (WT) (DAY1212), *snf7*Δ/Δ *RIM101-V5* (DAY1127), *snf7*Δ/Δ *SNF7 RIM101-V5* (DAY1128), *snf7*Δ/Δ *snf7-20.1 RIM101-V5* (DAY1148), *snf7*Δ/Δ *snf7-35.1 RIM101-V5* (DAY1149), *snf7*Δ/Δ *snf7-47.1 RIM101-V5* (DAY1213), *snf7*Δ/Δ *snf7-48.1 RIM101-V5* (DAY1150) and *snf7*Δ/Δ *snf7-49.1 RIM101-V5* (DAY1214). (B) Rim101 processing in Group C alleles may be impaired after a shift to alkaline pH. Strains were grown as in 8A before protein preparation. Equivalent protein amounts were analyzed by Western blotting analysis. Numbers under each column represent percent P1 signal over total Rim101 (FL + P1 + P2) signal.

*snf7*Δ/Δ strain, with no DAPI colocalization, indicating non-nuclear localization in these cells. The *snf7-49* allele conferred intermediate growth defects (Figure 7) and decreased active Rim101 (Figure 12). Cells expressing *snf7-49.1* displayed an intermediate V5 staining pattern with both DAPI-overlapping and non-DAPI overlapping staining (Figure 13A). This indicated partial nuclear localization and partial cytoplasmic retention of Rim101 in this strain. Thus, the Rim101-V5 localization in these Group D strains correlated with the growth phenotype and Rim101 processing observed.

We then tested the Group C alleles *snf7-47.1* and *snf7-48.1* that conferred Rim101-dependent defects yet had normal Rim101 processing (Figures 7 and 12 and data not shown). Strains expressing either of these alleles displayed strong cytoplasmic V5 compared with *snf7-35.1* and wild-type *SNF7* strains. While some cells showed slight V5 colocalization with DAPI, all cells maintained cytoplasmic staining (Figure 12A). We noted a stronger cytoplasmic staining pattern in the *snf7-48.1* strain compared to the *snf7-47.1* strain, which correlated with the slight difference in Rim101-dependent phenotypic defects observed between these strains (data not shown). This indicates partial nuclear localization and partial cytoplasmic retention of Rim101-V5 in the *snf7-47.1* and *snf7-48.1* strains.

To determine how Rim101 processing is affected during adaptation to alkaline pH by these *snf7* alleles, we also examined Rim101 processing following a 30 minute shift to alkaline pH. As previously observed (Figure 12), the wild-type strain processed Rim101-V5 and the *snf7*Δ/Δ strain did not (Figure 13B). Also, addition of *SNF7* or the Group A *snf7-35.1* allele restored processing. Both Group D alleles, *snf7-20.1* and *snf7-49.1*,

conferred processing defects. Thus, these alleles promoted similar Rim101 processing under steady state and adaptive growth conditions.

However, we found that the Group C allele *snf7-48.1* had considerably less Rim101-V5 processing than wild-type after a 30-minute shift to pH 8 compared to wild-type cells or compared to steady state growth at pH 8 (Figure 13B). This suggests that processing occurs more slowly in a *snf7-48* strain, but active Rim101 levels eventually reach wild-type levels. We observed more processed Rim101 in the *snf7-47.1* strain, but noted that this strain still had less processed Rim101 (P1 + P2) relative to the amount of total Rim101 (FL + P1 + P2) than the control (Figure 13B). When we tested our 13 Group C alleles, we observed a decrease in processed Rim101 relative to total Rim101 in 7 of 13 Group C alleles (unpublished data). Taken together, these data suggest that many Group C alleles, including *snf7-48*, fail to process Rim101 at the same rate as wild-type, but that Rim101-dependent phenotypic defects become less pronounced as processed Rim101 accumulates in the cell during steady-state growth.

f. Epithelial cell damage. *C. albicans* causes epithelial cell damage, and this damage requires active Rim101 (137, 198). We wished to test the ability of our mutant *snf7* alleles to mediate epithelial cell damage in a Rim101-dependent and Rim101-independent manner. To do this, we utilized a radiolabeled FaDu oropharyngeal epithelial cell line. When incubated with the wild-type *C. albicans* strain, we observed ~45% specific release (Figure 14A). We observed significantly less damage when the FaDu cells were incubated with the *rim101*Δ/Δ or *snf7*Δ/Δ strains. The addition of the *SNF7-V5* allele rescued most, but not all, of the damage defect in the *snf7*Δ/Δ strain (Figure 14A). Because the mutant *snf7* alleles were generated in the *SNF7-V5* background, we

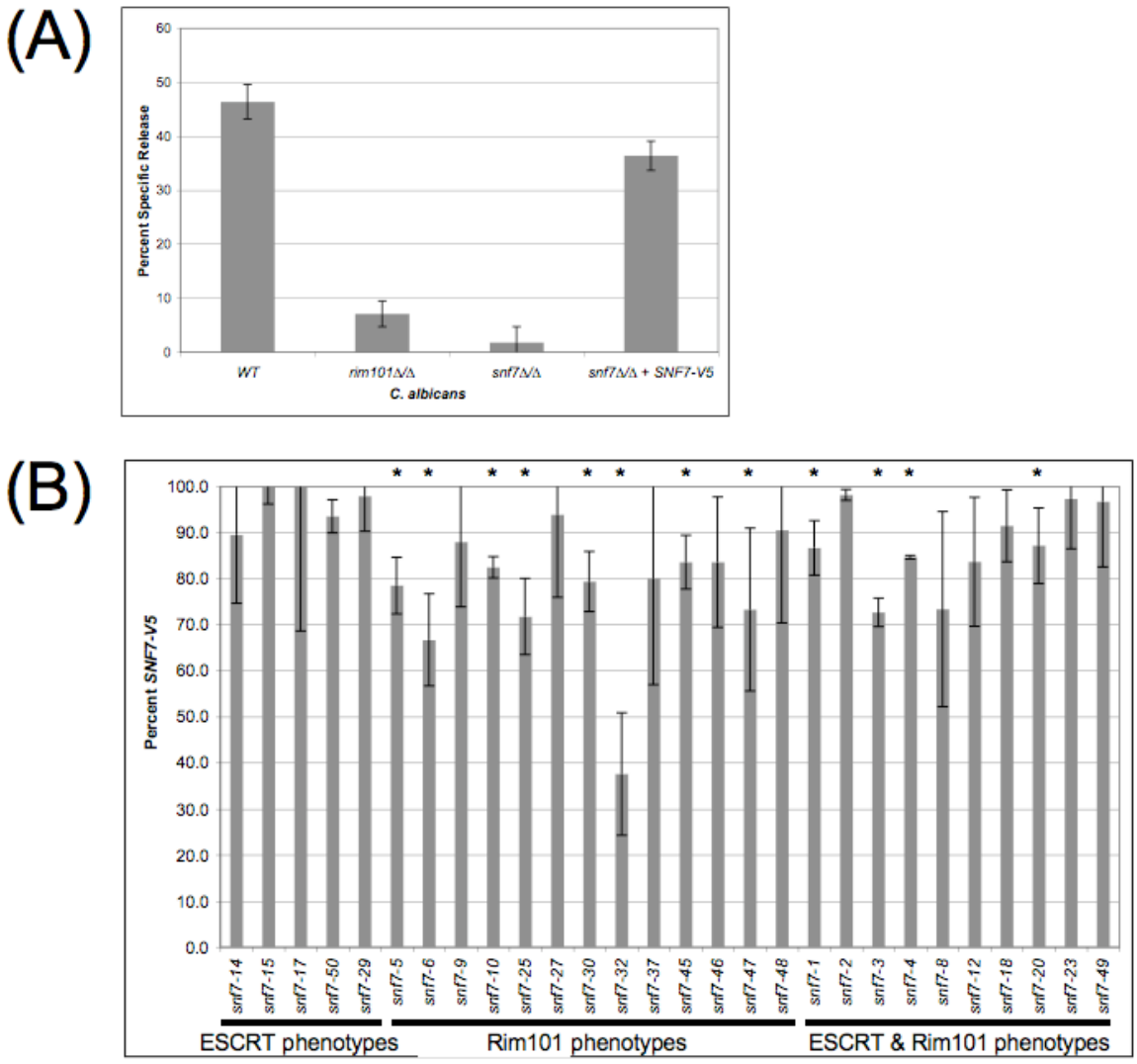

Figure 14. *C. albicans*-mediated FaDu cell damage is affected by Rim101-dependent defects. (A) Both the *rim101*Δ/Δ mutant and *snf7*Δ/Δ mutant have severe FaDu cell damage defects, and the *SNF7-V5* allele rescues most of the *snf7*Δ/Δ defect. FaDu cell monolayers were Cr^{51}-labeled overnight, then washed and incubated with $1x10^5$ cells/mL *C. albicans* for 10 hours. Strains were tested in triplicate during each assay and compared with media-alone wells to measure specific Cr^{51} release. The assay was repeated at least three times; the figure denotes one representative assay. (B) Only mutant *snf7* alleles with Rim101-dependent defects have damage defects. Assays were run as described in (A), and mutant *snf7* allele damage was compared to *SNF7-V5* damage. Each strain was tested in triplicate during each assay, and assays were repeated twice for each mutant *snf7* allele.

measured epithelial damage mediated by these mutant alleles and compared it to damage mediated by *SNF7-V5*.

We predicted that the Group C alleles, which conferred only Rim101-dependent defects, would cause decreased epithelial cell damage due to their Rim101-related phenotypes. We tested thirteen Group C alleles, of which eight caused less damage than the *SNF7-V5* allele ($p < 0.05$) (Figure 14B). We noted that *snf7-6*, the only Group C allele to completely abolish Rim101 processing, did not have the strongest damage defect. In fact, none of the Group C alleles were as diminished in damage as the *rim101*Δ/Δ, suggesting that all alleles maintained at least low levels of Rim101 activity. Overall, 62% of Group C alleles caused less FaDu cell damage than the *SNF7-V5* allele.

Endocytosis plays an important role in receptor down-regulation and nutrient acquisition. We predicted that full ESCRT function would be required for wild-type epithelial cell damage. However, because the Group B allele growth and filamentation defects were less severe than the Group C defects, we predicted the Group B alleles would play a lesser role in epithelial cell damage than the Group C alleles. In fact, we did not see a significant decrease in damage in any of the five alleles tested (Figure 14B). This suggests either that the ESCRT pathway does not contribute to FaDu cell damage or that the *snf7* alanine mutations do not abolish ESCRT function to levels that affect *C. albicans*-epithelial cell interactions.

Finally, we tested the Group D alleles, which conferred both ESCRT- and Rim101-dependent defects. Four of ten Group D alleles tested caused decreased FaDu cell damage ($p < 0.05$), and none of the defects were more severe than those conferred by

the Group C alleles (Figure 14B). Thus 40% of the Group D alleles caused less damage than the *SNF7-V5* allele, likely due to Rim101-dependent defects.

IV. Discussion

Adaptation of *C. albicans* to a neutral-alkaline environment requires several cellular responses. One critical response is the activation of the transcription factor Rim101, which regulates gene expression in an extracellular pH-dependent manner. Another cellular change is the dependence on endocytosis and endosomal trafficking for uptake of otherwise inaccessible nutrients. Snf7 protein plays a pivotal role in both of these processes, and is therefore essential for the cellular adaptation to a neutral-alkaline environment. We investigated the role of Snf7 in these two distinct processes using alanine scanning mutagenesis, which allowed us to examine the function of discrete regions of Snf7. Our analyses demonstrate that Snf7 function in the Rim101 pathway is separable from Snf7 function in the ESCRT pathway.

a. Separation of function and identification of functional domains: Our phenotypic results allowed us to characterize the mutant *snf7* alleles as nonfunctional, partially functional, or fully functional, with respect to the different phenotypic assays. To disrupt discrete domains, each mutation changed up to three amino acids. While we did not test Snf7 interactions directly due to the failure to generate functional tagged constructs, disruption of a interaction domain remains the simplest explanation for many of our partially complementary alleles.

The largest number of alleles (21) was classified into Group A, the group of alleles conferring no defects or only one Rim101-dependent phenotypic defect. Of the 21

alleles included in this group, 19 have no apparent defect in any phenotypic assay tested. The largest cluster of Group A alleles was a span of 25 amino acids in the C-terminal half of the protein. The J-Pred software program (44) predicted six alpha-helices spanning the coding sequence (Figure 10),which is similar to the predicted human Snf7 structures (175). We aligned our phenotypic data with the predicted helical structures to correlate Snf7 structures and function. Interestingly, the cluster of Group A alleles coincided with a region containing no predicted helices, suggesting that this lack of defined structure may increase tolerance for mutation in this region. The functional importance of the identified helices may explain their conservation of through evolutionary time, while the less conserved unstructured regions suggest a linker sequence function.

We noted regions where adjacent alleles displayed similar phenotypic effects. There was one cluster of Group D alleles at the N-terminus, indicating that this region of Snf7 is important for Rim101 and ESCRT functions. This region may function in Snf7 recruitment to the endosomal membrane through upstream interactions or it could be involved with a common downstream interaction. Because Snf7-bro1-domain interactions are the only common interactions yet identified between the *C. albicans* Rim101 and ESCRT pathways, and because Snf7-bro1-domain interactions have been mapped to the C-terminal end of Snf7 (see below), this region is more likely to be involved in upstream Snf7 function, such as recruitment by Vps20 or self-oligomerization. These N-terminal Group D alleles caused intermediate phenotypes, suggesting partial Snf7 activity, which may explain why we didn't observe differences in Snf7 localization (Figure 11 and data not shown).

The majority of Group B alleles fell within the second predicted alpha helix, which spans residues 58-94 and encompasses *snf7-14* through *snf7-20*. CHMP3, the human Vps24 homolog, has a helical structure related to CHMP4a, one of three human Snf7 homologs, and the second alpha helix of CHMP3 is important for self-interactions (133, 175). We predict this region of Snf7 is important for an ESCRT-specific interaction, such as with the Vps2/Vps24 heterodimer or Vps4, which are necessary for endosomal trafficking but do not prevent Rim101 processing (207). We demonstrated that Snf7-15 is able to cycle between endosome and cytoplasm by cell fractionation and immunofluorescence. These data indicate that Snf7-15 does not abolish Vps4 interactions. Failure of *snf7-14*, *snf7-15*, or *snf7-17* to efficiently self-oligomerize or to interact with downstream ESCRT-III members could account for the aberrant FM 4-64 trafficking seen in these strains (Figure 6), although the normal Snf7 protein localization pattern observed (Figure 11) indicates that minimally some Snf7 recycling occurs. Rim101-dependent growth and Rim101 processing appear normal in these strains, indicating that Rim101 activation is supported by the endosome-associated Snf7 present in these strains.

Strikingly, many Group C alleles, which affect only Rim101-dependent phenotypes, cluster at the C-terminal alpha helix of Snf7. The clustering of Group C alleles over this helix suggests that this structure may be specific for Snf7 interaction with Rim101 pathway proteins. Thus, this region of Snf7 is also a good candidate for interaction with a Rim101 pathway member, such as Rim13 or Rim20. The bro1-domain of the human Bro1 homolog (ALIX) was shown to interact with the C-terminal end of all three human Snf7 homologs, CHMP4a, 4b, and 4c (122). The CHMP4 region important

for ALIX interactions corresponds to the C-terminal Group C cluster of *C. albicans* Snf7. This suggests the C-terminal region of Snf7 may be important for interactions with bro1-domain-containing proteins. However, we predicted that disrupting Snf7-bro1-domain interactions would affect both Rim101- and ESCRT-dependent phenotypes, which was only observed at the very C-terminal mutation, *snf7-49*. Why would mutations affecting interactions with one bro1-containing protein, Rim20, not affect interactions with another bro1-containing protein, Bro1? One possibility is that different bro1-containing proteins interact at this site using slightly different residues; residues changed in *snf7-48* may interrupt only Rim20 interactions, while those changed in *snf7-49* may interrupt both Rim20 and Bro1 interactions. This is supported by the fact that while all ALIX-CHMP4 interactions occurred at the C-terminal end of CHMP4, the critical residues for interaction varied between the three CHMP4 homologs (122). Alternatively, the residues involved may be important for both Rim20 and Bro1 interactions, but the minor phenotypic defects of a failed Snf7-Bro1 interaction were not detected by our system for alleles other than *snf7-49*. The importance of this region for overall protein function is emphasized by the failure of our C-terminally tagged Snf7 to fully complement a *snf7*Δ/Δ strain (data not shown). A third possibility is that the C-terminal Group C cluster interacts with an unidentified Rim101 pathway member in *C. albicans*. In *A. nidulans*, *Yarrowia lipolytica*, and *S. cerevisiae*, an additional Rim101 pathway member, PalC/Rim23, has been identified which contains a bro1-domain and is able to interact with Snf7 (20, 63, 191). We identified *C. albicans* orf19.2914 through a blast search with ScRim23 sequence. If Orf19.2914 interacts with Snf7 through its bro1-domain, this interaction

should occur at the Snf7 C-terminus, either in conjunction with Rim20 or on separate molecules of Snf7, which oligomerizes on the endosomal membrane.

Abnormal Snf7-Rim20 or Snf7-Rim13 interactions are possible explanations for Group C phenotypes. However, it is possible that Rim13 interacts with a domain of Snf7 that also interacts with an ESCRT pathway member. A human homolog of Rim13, Calpain 7, was shown to interact with CHMP4b and CHMP4c through a microtubule interacting and trafficking (MIT) domain (176). Vps4-ESCRT III member interactions also occur through a MIT domain at the N-terminus of Vps4 (171, 193). Calpain 7 contains two MIT domains, while Vps4 contains one. However, while the *A. nidulans* Rim13 homolog, PalB, has recently been shown to interact with an ESCRT-III member through an MIT domain, no MIT domains were identified in *S. cerevisiae* or *C. albicans* Rim13 (162). While this does not rule out a shared Snf7-interaction domain between Rim13 and an ESCRT pathway member, it suggests that *C. albicans* Rim13 may interact with Snf7 in a manner not conserved among ESCRT pathway member interactions. Group C alleles, such as *snf7-6*, may affect these Rim13-Snf7 interactions.

b. Effects on Rim101 processing and regulation: Several mutant *snf7* alleles caused Rim101-dependent phenotypes without causing overt ESCRT-specific phenotypes (Group C alleles). As described above, *snf7-6* may interrupt a domain necessary for Snf7 interactions with Rim101 processing machinery. We predict that the C-terminus of Snf7 interacts with the bro1-domain of Rim20. Thus, we predict that *snf7-6* interrupts interaction with putative protease Rim13. Surprisingly, several C-terminal mutant alleles (*snf7-45*, *-46*, *-47*, and *-48*) showed Rim101-dependent defects but had Rim101 processing at levels comparable to the complemented strain during steady-state growth.

We found that these strains have a Rim101 processing defect when shifted briefly to alkaline pH, indicating these strains have a kinetic defect not observed during steady-state growth. Therefore, defective Rim101 processing accounts for all Group C allele phenotypes.

Our phenotypic analyses, combined with structural and biochemical analyses, have allowed us to generate a model of Snf7 interactions (Figure 15). Our model posits that after Snf7 has been recruited to the endosomal membrane, Snf7-Rim13 interactions occur at the region containing *snf7-6*, and that disruption of this region results in abrogation of Rim101 processing. Further, Snf7-Rim20 interactions occur at the C-terminal end, in a region spanning the area required for Snf7-Bro1 interactions. We can predict essential residues for Snf7-bro1 domain interaction by aligning *C. albicans* Snf7 with *H. sapiens* Snf7 proteins. *McCollough et al.* found three critical residues required for bro1-domain interaction with hSnf7-1 (Figure 15B) (122). Our work suggests these residues remain critical, but that Rim20-Snf7 interaction requires the entire sequence while Bro1-Snf7 interaction requires only the very C-terminal sequence. Rim20 and Bro1 colocalization has been observed under alkaline conditions (26), suggesting that Rim101 processing and ESCRT function can occur simultaneously at the same Snf7 oligomerization site. Thus, in alkaline conditions, an undetermined factor, such as modified Rim8/PalF (79), may promote Rim20-Snf7 interactions over Bro1-Snf7 interactions.

c. Effects on epithelial cell damage: Our data support the idea that Rim101 is necessary for wild-type levels of epithelial cell damage (Figure 14A). As we predicted, the majority of Group C *snf7* alleles conferred reduced damage. We noted that the allele

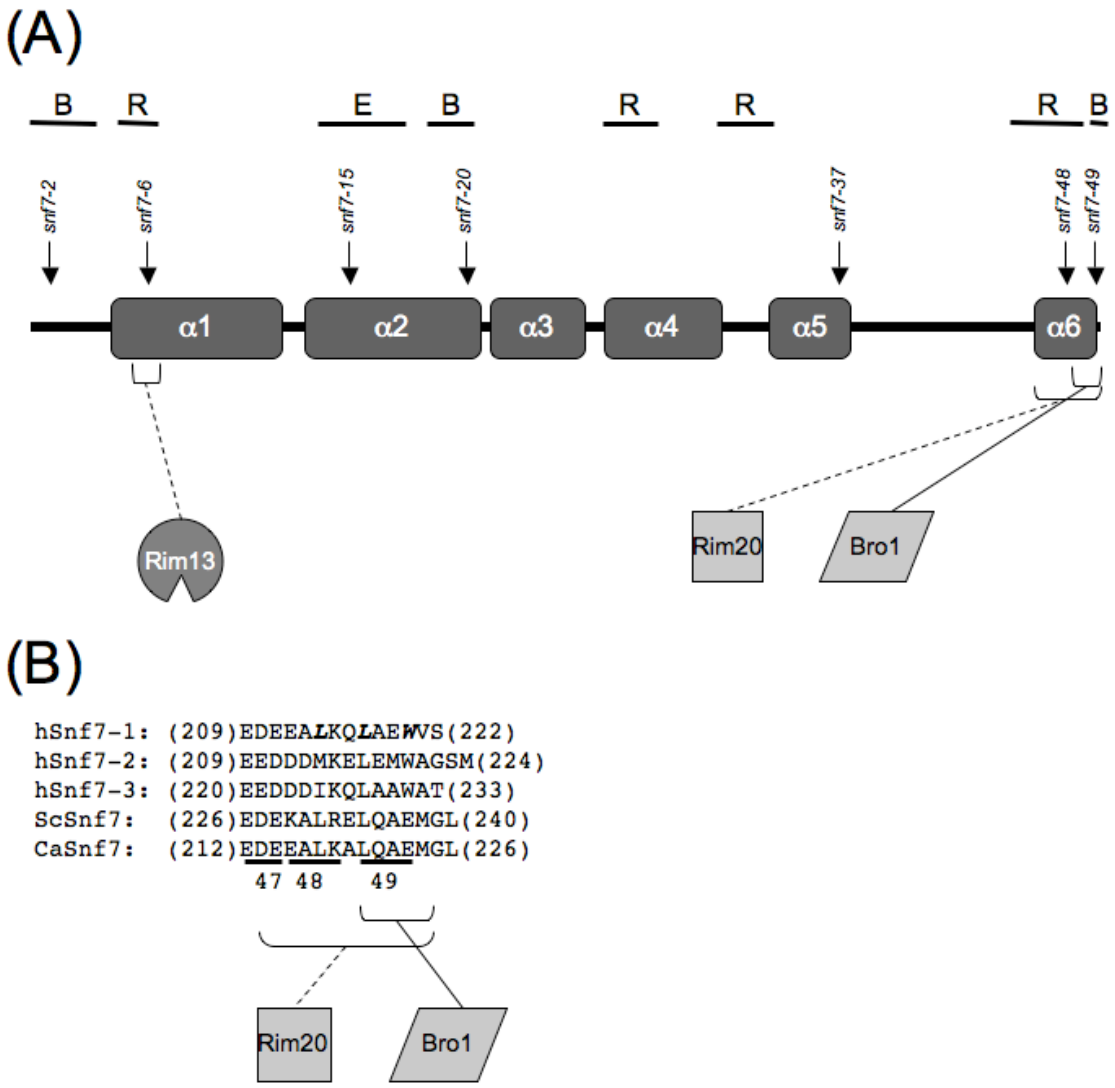

Figure 15. Model of Snf7 interactions. (A) Snf7 interacts with ESCRT member Bro1, or Rim101 members Rim13 and Rim20, through distinct interaction domains. Putative Snf7 helical structure is shown with several *snf7* alleles marked for reference. Also noted are the domains predicted from our studies to be involved in ESCRT-specific (E), Rim101-specific (R), or both (B) processes. Solid lines represent interactions conserved in other species. Dashed lines represent interactions predicted from our data. (B) Alignment of Snf7 C-terminal sequence with *snf7* allele numbers noted below. Mutation of bold residues abolished hSnf7-1-Bro1 domain interactions (122). *C. albicans snf7* mutation of these residues has differential effects on bro1-domain protein interaction. Abbreviations: h, human; Sc, *S. cerevisiae*; Ca, *C. albicans*.

snf7-6, which abolished all Rim101 processing, caused more damage than the *rim101*Δ/Δ mutant. One explanation for this result is that the *snf7-6* allele processes very low levels of Rim101 undetectable by Western blot analysis. However, we favor the model that full-length Rim101 can mediate partial damage. This idea is supported in an endothelial cell damage model where a *rim8*Δ/Δ mutant caused less host cell damage than the *rim101*Δ/Δ mutant (48). Further, the fact that the Group C *snf7* alleles are not as deficient as the *snf7*Δ/Δ strain supports the idea that these alleles are at least partially functional.

We were surprised to find that Group B alleles did not affect host cell damage in this model. MVB formation and vesicle trafficking are important for cell physiology. Several explanations may account for this observation. First, ESCRT function and MVB formation may not play an important role during epithelial cell damage. Epithelial cell damage depends on the ability of *C. albicans* to filament, and no Group B allele affected filamentation as severely as the Group C alleles. Second, ESCRT function may be important for acquiring nutrients, such as iron, for which the cells are not starved during the course of these assays. Third, the alleles may not fully knock down ESCRT function, as most *snf7* alleles affecting solely ESCRT function conferred intermediate FM 4-64 trafficking defects (Figure 6). Regardless, our data suggest that ESCRT function does not play a role during epithelial cell damage.

d. Effects on filamentation: Numerous redundant signals play a role in the regulation of filamentation, including temperature, nutrient availability, and cell density. Defects in both vesicle trafficking and pH sensing have been shown to affect hyphal formation (15, 49, 73, 144). Few of our alanine scanning *snf7* alleles conferred strong defects in filamentation, which is consistent with the observation that few *snf7* alleles

completely abolished Snf7 function. We were surprised to observe acidic filamentation of the *snf7*Δ/Δ and *vps4*Δ/Δ strains, suggesting that MVB trafficking may play an inhibitory function under acidic conditions. This was particularly remarkable as *snf7*Δ/Δ and *vps4*Δ/Δ strains have opposite effects on Rim101 processing: a *snf7*Δ/Δ strain is unable to process Rim101 and a *vps4*Δ/Δ strain constitutively processes Rim101 (77, 98). Although these null mutations have opposite effects on Rim101 processing, they have similar effects on ESCRT trafficking: both null mutations result in accumulation of endosomes unable to fuse with the vacuole. This suggests that aberrant ESCRT function results in acidic filamentation independent of Rim101 processing.

The intimate relationship between endocytosis and signal transduction has been established in various signaling pathways in many different organisms (94, 152, 200), however, much remains unknown regarding the exact nature of these relationships. Endocytosis can serve to downregulate receptors, to promote extended downstream signaling through "signaling endosomes," or to generate physical proximity between members of a signaling pathway. The Rim101 pathway is likely a case of the latter model, with the signaling complex brought proximal to the processing complex to promote Rim101 processing. When Rim101 and ESCRT pathway members intersect remains unclear. The work done here demonstrates several functional regions of Snf7 that are specific for the Rim101 pathway, and suggests that bro1-domain containing proteins may interact at slightly divergent, though overlapping Snf7 sites, leaving open the possibility that Rim13 and Rim20 interact with a single Snf7 monomer to facilitate Rim101 processing early in MVB formation.

CHAPTER 3

I. Introduction

Candida albicans is a ubiquitous opportunistic pathogen that colonizes most healthy human individuals as part of their commensal flora (149, 182). In both disease and non-disease states, *C. albicans* colonizes diverse mucosal surfaces of its host, including the oral cavity, gastrointestinal tract, and female urogenital tract (148). These niches can vary widely in pH, osmolarity, and in available nutrients. *C. albicans* can therefore survive in a wide variety of environmental niches within its human host.

To adapt to these specific niches, *C. albicans* must be able to activate specific signal transduction pathways and concomitantly terminate other pathways to properly regulate gene expression. One mechanism of signal termination is degradation of signaling receptors by way of the vacuole. Thus, niche adaptation requires tight regulation of signal activation and termination, and receptor degradation is one mechanism to terminate signal propagation.

Prior to vacuolar degradation, the receptor protein is internalized through endocytosis, where it is subsequently incorporated into the endosomal lumen as an interluminal vesicle (ILV). Formation of the ILV requires the endosomal sorting pathway required for transport (ESCRT) complex pathway (9, 166, 188). ILVs increase in number, generating a multivesicular body (MVB), which then fuses with and releases its luminal content into the vacuole for degradation. MVBs therefore allow for transmembrane receptor downregulation and contribute to signal transduction arrest during adaptation to new environments.

The ESCRT complex is a collection of heterogeneous polyprotein complexes recruited to the endosomal membrane by the post-translational modification pattern, frequently ubiquitination, of the receptor (or cargo) protein and the membrane lipid content (89). There are four core polyprotein complexes (Figure 16): ESCRT-0 (Vps27 and Hse1), ESCRT-I (Mvb12, Vps23, Vps37, and Vps28), ESCRT-II (Vps36, Vps22, Vps25), and ESCRT-III (Vps20, Snf7, Vps2, and Vps24) (8, 9, 16, 45, 88, 89). These complexes are recruited sequentially, and while ESCRT-0, -I, and -II are recruited as fully formed complexes, ESCRT-III arrives as two separate heterodimers (8). The first heterodimer, ESCRT-IIIa (Vps20-Snf7), facilitates nucleation of additional Snf7 monomers around the ubiquitinated cargo protein (188), and Snf7 oligomerization is thought to mediate membrane involution necessary for ILV formation (67, 74, 188). The second heterodimer, ESCRT-IIIb (Vps2-Vps24), caps the Snf7 oligomer (8, 188) and recruits downstream proteins such as Bro1, Doa4, and Vps4 (10, 140). Bro1 and Doa4 are required to deubiquitinate the cargo protein before its incorporation into the ILV. Vps4, an AAA-ATPase, catalyzes ESCRT-III dissociation from the membrane and formation of the ILV (9, 10). Therefore, the ESCRT complex machinery is necessary for ILV and MVB formation.

In addition to forming MVBs, the ESCRT-III member Snf7 plays a direct role in signal transduction in *C. albicans* and other fungi (98, 207). Snf7 interacts with the processing components necessary to proteolytically activate the transcription factor Rim101. Snf7 interacts with Rim20 (25, 86), a scaffold protein that binds Rim101 (206), and with Rim13 (20, 86), the putative protease responsible for Rim101 processing (Figure 16) (107). Activation of Rim101 is required for adaptation to neutral-alkaline

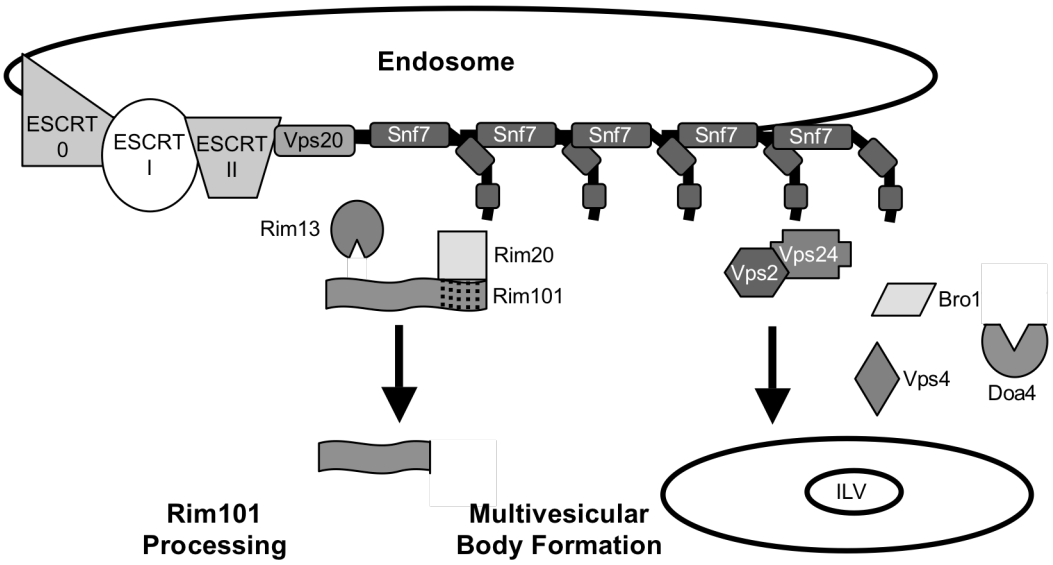

ESCRT-0	ESCRT-I	ESCRT-II	ESCRT-III	ESCRT-DS
Vps27	**Mvb12**	**Vps36**	**Vps20**	**Vps4**
Hse1	Vps23	**Vps22**	**Snf7**	Vti1
	Vps37	Vps25	Vps2	**Bro1**
	Vps28		Vps24	**Doa4**

Figure 16. Model of ESCRT pathway and Rim101 pathway intersection. The Rim101 pathway intersects with the ESCRT pathway. ESCRT-0, -I, -II, and -III complexes are recruited to the endosomal membrane. ESCRT-III member Snf7 can interact either with Rim101 pathway members, resulting in proteolytic activation of Rim101, or with downstream ESCRT members, resulting in MVB formation. Yeast ESCRT complex components are listed below, and bolded members are those investigated in this study.

environments (49), and this activation is thought to be mediated by Snf7 recruitment of Rim13 and Rim20. Snf7 is therefore required for both MVB formation and Rim101 processing in *C. albicans*.

Snf7 localization is important for both MVB and Rim101 functions of Snf7 and is dependent on the upstream ESCRT complex members. In *S. cerevisiae*, mutations in ESCRT components upstream of *SNF7* fail to recruit Snf7 to the endosomal membrane and are unable to form MVBs. These mutants are also unable to process Rim101 (165, 207). ESCRT component mutations downstream of *SNF7* are able to process Rim101 like wild-type (165, 207). The *S. cerevisiae vps27*Δ mutant was likewise able to process Rim101, demonstrating that ESCRT-0 is not required for Rim101 processing in *S. cerevisiae*, but that ESCRT-I, -II, and the first ESCRT-III heterodimer are required (165, 207). This suggests Snf7 must be recruited to the endosome for both MVB-specific or Rim101-specific function. Snf7 and Rim20 exhibit alkaline pH-dependent colocalization in a punctate pattern reminiscent of endosomal staining (26), suggesting that extracellular environment can influence Snf7 interactions. Snf7 therefore acts as a molecular hub at the endosome that can coordinate MVB-specific or Rim101-specific functions.

The role of ESCRT components in *C. albicans* Rim101 processing is relatively unexplored. Mutants in *C. albicans* ESCRT-I, -II, and -IIIa components displayed filamentation defects when tested for Rim101-dependent filamentation (207), suggesting these genes are required for Rim101-dependent phenotypes. However, no ESCRT-0 *C. albicans* mutants have been tested for filamentation or Rim101 processing. Thus, the critical ESCRT complexes for *C. albicans* Rim101 processing are not fully understood.

We wished to investigate the role of the ESCRT function in *C. albicans* pathogenesis. Previous studies have suggested that ESCRT function plays a role in bloodstream candidiasis independent of Rim101 activation, but did not fully decoupled the two processes (40). We hypothesized that, like *S. cerevisiae*, ESCRT-0 would not be required for Rim101 processing, and would therefore be an ideal candidate to study MVB-specific contributions of the ESCRT pathway. Here, we generated a collection of ESCRT component mutants to characterize Rim101- and ESCRT-dependent phenotypes. We then used these mutants to investigate the role of ESCRT function in epithelial cell damage and *C. albicans* virulence. Our results demonstrate a role for ESCRT complex function in *C. albicans* pathogenesis in addition to its role in Rim101 activation.

II. Materials and Methods

a. Media and growth conditions: All *C. albicans* strains were routinely passaged in YPD (1% yeast extract, 2% w/v Bacto Peptone, 2% w/v dextrose) supplemented with 80μg/ml uridine (Sigma). To select for Arg^+, Ura^+, or His^+ transformants, synthetic medium (0.67% yeast nitrogen base plus ammonium sulfate and without amino acids; 2% dextrose; 80 μg of uridine per ml) was used, supplemented as required by the auxotrophic needs of the cells. To test for Rim101-dependent growth phenotypes, YPD was buffered with 150 mM HEPES to pH 9 with NaOH or contained 150 mM LiCl. For alkaline-induced filamentation assays, M199 medium (GibcoBRL) was buffered with 150 mM HEPES and pH-adjusted to pH 4 or pH 8 and supplemented with 80 μg/ml uridine. For serum-induced filamentation assays, 4% bovine calf serum (BCS) was supplemented

with 80 μg/ml uridine. For determining CFUs from mouse tissue, YPD was supplemented with 1μg/ml ampicillin (company).

b. Strain manipulation: All strain manipulations were performed in the BWP17 genetic background and are listed in Table 7. All knockouts were engineered by subsequent rounds of allelic exchange with PCRs using a set of disrupt (DR) primers specific for the targeted gene (Table 8). For example, to generate the *vps27*Δ/Δ strain (DAY 1177), the *vps27::ARG4* cassette was amplified in a PCR using Vps27 5DR and Vps27 3DR primers and pRS-ARGΔSpe (pDDB246) template to generate the homozygous mutant DAY1176. DAY1176 was transformed with the *vps27::URA3-dpl200* cassette, which was amplified in a PCR using Vps27 5DR and Vps27 3DR primers and pRS-URA3-dpl200 (pDDB57) template, to generate the heterozygous mutant DAY1177. To generate a prototrophic His^+ strain, DAY1177 (or other heterozygous knockout strain) was transformed with NruI-digested pDDB78 plasmid to generate DAY1160. To express *RIM101-V5* in the *vps*Δ/Δ strain (or other heterozygous knockout strain), NruI-digested pDDB233 plasmid was transformed into DAY1177 to generate DAY1178. For the *VPS27* complementation vector, genomic *VPS27* plus promoter and terminator sequence was amplified in a PCR using Vps27 5comp and Vps27 3comp primers and DAY1 genomic DNA as a template. This sequence was transformed into *S. cerevisiae* along with NotI- EcoRI-digested pDDB78, where the two DNA fragments recombined to form pDDB501 (130). NruI-digested pDDB501 was recovered and transformed into DAY1177 to generate DAY1264.

Growth assays: Overnight YPD cultures were diluted 1:20 in sterile water and diluted subsequently 1:5 into sterile water using a 96-well sterile plate. 5μl of each

Table 7. Strains used in Chapter 3 studies.

Name	Genotype				Ref
BWP17	*ura3::λimm434* *ura3::λimm434*	*arg4::hisG* *arg4::hisG*	*his1::hisG* *his1::hisG*		(204)
DAY25	*ura3::λimm434* *ura3::λimm434*	*arg4::hisG* *arg4::hisG*	*HIS1::DDB78::his1::hisG* *his1::hisG*		(48)
DAY185	*ura3::λimm434* *ura3::λimm434*	*ARG4::URA3::arg4::hisG* *arg4::hisG*	*HIS1::DDB78::his1::hisG* *his1::hisG*		(48)
DAY534	*ura3::λimm434* *ura3::λimm434*	*arg4::hisG* *arg4::hisG*	*his1::hisG* *his1::hisG*	*snf7::ARG4* *snf7::URA3-dpl200*	(98)
DAY537	*ura3::λimm434* *ura3::λimm434*	*arg4::hisG* *arg4::hisG*	*his1::hisG* *his1::hisG*	*vps4::ARG4* *vps4::URA3-dpl200*	(98)
DAY568	*ura3::λimm434* *ura3::λimm434*	*arg4::hisG* *arg4::hisG*	*RIM101-V5::HIS1::DDB233:::his1::hisG* *his1::hisG*	*vps4::ARG4* *vps4::URA3-dpl200*	(98)
DAY576	*ura3::λimm434* *ura3::λimm434*	*arg4::hisG* *arg4::hisG*	*RIM101-V5::HIS1::DDB233:::his1::hisG* *his1::hisG*	*vps4::ARG4* *vps4::URA3-dpl200*	(98)
DAY653	*ura3::λimm434* *ura3::λimm434*	*arg4::hisG* *arg4::hisG*	*his1::hisG* *his1::hisG*	*bro1::ARG4* *bro1::URA3-dpl200*	(98)
DAY763	*ura3::λimm434* *ura3::λimm434*	*arg4::hisG* *arg4::hisG*	*HIS1::DDB78::his1::hisG* *his1::hisG*	*snf7::ARG4* *snf7::URA3-dpl200*	(98)
DAY1155	*ura3::λimm434* *ura3::λimm434*	*arg4::hisG* *arg4::hisG*	*HIS1::DDB78::his1::hisG* *his1::hisG*	*vps4::ARG4* *vps4::URA3-dpl200*	This study
DAY1156	*ura3::λimm434* *ura3::λimm434*	*arg4::hisG* *arg4::hisG*	*HIS1::DDB78::his1::hisG* *his1::hisG*	*bro1::ARG4* *bro1::URA3-dpl200*	This study
DAY1157	*ura3::λimm434* *ura3::λimm434*	*arg4::hisG* *arg4::hisG*	*HIS1::DDB78::his1::hisG* *his1::hisG*	*vps20::ARG4* *vps20::URA3-dpl200*	This study
DAY1158	*ura3::λimm434* *ura3::λimm434*	*arg4::hisG* *arg4::hisG*	*HIS1::DDB78::his1::hisG* *his1::hisG*	*doa4::ARG4* *doa4::URA3-dpl200*	This study
DAY1159	*ura3::λimm434* *ura3::λimm434*	*arg4::hisG* *arg4::hisG*	*HIS1::DDB78::his1::hisG* *his1::hisG*	*bro1::ARG4* *bro1::URA3-dpl200*	This study
DAY1160	*ura3::λimm434* *ura3::λimm434*	*arg4::hisG* *arg4::hisG*	*HIS1::DDB78::his1::hisG* *his1::hisG*	*vps27::ARG4* *vps27::URA3-dpl200*	This study

DAY1161	*ura3::λimm434* *ura3::λimm434*	*arg4::hisG* *arg4::hisG*	*HIS1::DDB78::his1::hisG* *his1::hisG*	*vps28::ARG4* *vps28::URA3-dpl200*	This study
DAY1162	*ura3::λimm434* *ura3::λimm434*	*arg4::hisG* *arg4::hisG*	*HIS1::DDB78::his1::hisG* *his1::hisG*	*vps36::ARG4* *vps36::URA3-dpl200*	This study
DAY1163	*ura3::λimm434* *ura3::λimm434*	*arg4::hisG* *arg4::hisG*	*HIS1::DDB78::his1::hisG* *his1::hisG*	*mvb12::ARG4* *mvb12::URA3-dpl200*	This study
DAY1176	*ura3::λimm434* *ura3::λimm434*	*arg4::hisG* *arg4::hisG*	*his1::hisG* *his1::hisG*	*vps27::ARG4* *VPS27*	This study
DAY1177	*ura3::λimm434* *ura3::λimm434*	*arg4::hisG* *arg4::hisG*	*his1::hisG* *his1::hisG*	*vps27::ARG4* *vps27::URA3-dpl200*	This study
DAY1178	*ura3::λimm434* *ura3::λimm434*	*arg4::hisG* *arg4::hisG*	*RIM101-V5::DDB233::his1::hisG* *his1::hisG*	*vps27::ARG4* *vps27::URA3-dpl200*	This study
DAY1181	*ura3::λimm434* *ura3::λimm434*	*arg4::hisG* *arg4::hisG*	*his1::hisG* *his1::hisG*	*vps28::ARG4* *VPS28*	This study
DAY1182	*ura3::λimm434* *ura3::λimm434*	*arg4::hisG* *arg4::hisG*	*his1::hisG* *his1::hisG*	*vps28::ARG4* *vps28::URA3-dpl200*	This study
DAY1183	*ura3::λimm434* *ura3::λimm434*	*arg4::hisG* *arg4::hisG*	*RIM101-V5::DDB233::his1::hisG* *his1::hisG*	*vps28::ARG4* *vps28::URA3-dpl200*	This study
DAY1186	*ura3::λimm434* *ura3::λimm434*	*arg4::hisG* *arg4::hisG*	*his1::hisG* *his1::hisG*	*vps36::ARG4* *VPS36*	This study
DAY1187	*ura3::λimm434* *ura3::λimm434*	*arg4::hisG* *arg4::hisG*	*his1::hisG* *his1::hisG*	*vps36::ARG4* *vps36::URA3-dpl200*	This study
DAY1188	*ura3::λimm434* *ura3::λimm434*	*arg4::hisG* *arg4::hisG*	*RIM101-V5::DDB233::his1::hisG* *his1::hisG*	*vps36::ARG4* *vps36::URA3-dpl200*	This study
DAY1191	*ura3::λimm434* *ura3::λimm434*	*arg4::hisG* *arg4::hisG*	*his1::hisG* *his1::hisG*	*mvb12::ARG4* *MVB12*	This study
DAY1192	*ura3::λimm434* *ura3::λimm434*	*arg4::hisG* *arg4::hisG*	*his1::hisG* *his1::hisG*	*mvb12::ARG4* *mvb12::URA3-dpl200*	This study
DAY1193	*ura3::λimm434* *ura3::λimm434*	*arg4::hisG* *arg4::hisG*	*RIM101-V5::DDB233::his1::hisG* *his1::hisG*	*mvb12::ARG4* *mvb12::URA3-dpl200*	This study
DAY1196	*ura3::λimm434* *ura3::λimm434*	*arg4::hisG* *arg4::hisG*	*his1::hisG* *his1::hisG*	*vps22::ARG4* *VPS22*	This study
DAY1197	*ura3::λimm434* *ura3::λimm434*	*arg4::hisG* *arg4::hisG*	*his1::hisG* *his1::hisG*	*vps22::ARG4* *vps22::URA3-dpl200*	This study

DAY1200	*ura3::λimm434* *ura3::λimm434*	*arg4::hisG* *arg4::hisG*	*his1::hisG* *his1::hisG*	*hse1::ARG4* *HSE1*	This study
DAY1201	*ura3::λimm434* *ura3::λimm434*	*arg4::hisG* *arg4::hisG*	*his1::hisG* *his1::hisG*	*hse1::ARG4* *hse1::URA3-dpl200*	This study
DAY1212	*ura3::λimm434* *ura3::λimm434*	*arg4::hisG* *arg4::hisG*	*RIM101-V5::DDB233::his1::hisG* *his1::hisG*	*rim101::ARG4* *rim101::URA3-dpl200*	This study
DAY1217	*ura3::λimm434* *ura3::λimm434*	*arg4::hisG* *arg4::hisG*	*HIS1::DDB78::his1::hisG* *his1::hisG*	*vps22::ARG4* *vps22::URA3-dpl200*	This study
DAY1218	*ura3::λimm434* *ura3::λimm434*	*arg4::hisG* *arg4::hisG*	*HIS1::DDB78::his1::hisG* *his1::hisG*	*hse1::ARG4* *hse1::URA3-dpl200*	This study
DAY1219	*ura3::λimm434* *ura3::λimm434*	*arg4::hisG* *arg4::hisG*	*RIM101-V5::DDB233::his1::hisG* *his1::hisG*	*bro1::ARG4* *bro1::URA3-dpl200*	This study
DAY1221	*ura3::λimm434* *ura3::λimm434*	*arg4::hisG* *arg4::hisG*	*RIM101-V5::DDB233::his1::hisG* *his1::hisG*	*hse1::ARG4* *hse1::URA3-dpl200*	This study
DAY1222	*ura3::λimm434* *ura3::λimm434*	*arg4::hisG* *arg4::hisG*	*RIM101-V5::DDB233::his1::hisG* *his1::hisG*	*vps22::ARG4* *vps22::URA3-dpl200*	This study
DAY1264	*ura3::λimm434* *ura3::λimm434*	*arg4::hisG* *arg4::hisG*	*VPS27::HIS1::DDB501::his1::hisG* *his1::hisG*	*vps27::ARG4* *vps27::URA3-dpl200*	This study
L24	*ura3::λimm434* *ura3::λimm434*	*arg4::hisG* *arg4::hisG*	*his1::hisG* *his1::hisG*	*frp1::ARG4* *frp1::URA3-dpl200*	This study

Table 8. Primers used in Chapter 3 studies.

Vps27 5DR	AATACTTATTAATTTCACATATAATATCATTTCATTAGTAGTAGGAAATACCTTTATATTTTTCCCAGTCACGACGTT
Vps27 3DR	AGAAGTAGAAGTTTGGCTAAATATTTCTAGATAAGCAAAAATTATTGCCAACTTTTATTAGTGGAATTGTGAGCGGATA
Hse1 5DR	TTTGCCTCCTCCCACTATTAATCAATTAGTAACCCCGATCATCAATTCCTTACCAACAACCTTTCCCAGTCACGACGTT
Hse1 3DR	AGTACTACAGCTTTATACTTCTTTCAATAGAAGAATATTAGTGAGACGTGTATTATATGACTGGAATTGTGAGCGGATA
Mvb12 5DR	GCAACCAACGAACGAACGAACGAACGAGCGAACCTATAAACACATACATTCACAACAACATTTCCCAGTCACGACGTT
Mvb12 3DR	TTATACTATTAATAATATGACCCATCTATTTACAAAAAAAAAAACGTTTCATTATAATTCAGTGGAATTGTGAGCGGATA
Vps28 5DR	TTTCTTTAGTGTTTTGTTTATCCTTAGTCATAGAACAATCAACTTTGATTTATTGCCATTTTTCCCAGTCACGACGTT
Vps28 3DR	ATCGTATAAGCAAGAAACAGAGTATCCAACCAAACAGATAATTGTGTATTGTGTATATTAGTGGAATTGTGAGCGGATA
Vps36 5DR	TAGATGGGGAGTGGGAGCGAGTCAGATCTAATCTCTTATATATAGAAAAACCTCAATATTTTTCCCAGTCACGACGTT
Vps36 3DR	ATTAATACATAGTTCTATATATATGTCCATTTTTTTTTTTAAAAAAAACATATTACTTTAGTGGAATTGTGAGCGGATA
Vps22 5DR	ATTTTGATTAAAAGAGAAATCAAATCTTTATCTATCTTCCTATCACTTAACTATACTATTTTTCCCAGTCACGACGTT
Vps22 3DR	GGACAAGAAAAACTCAATAAAGAATAAGAAGTAAGTATGCCTGTATATATTTATTATTTAGTGGAATTGTGAGCGGATA
Vps20 5DR	TTATCAGGAACTGTAATTTGCTATCATAATCAATATAGATCTAATACATTCAAATTGACATTTCCCAGTCACGACGTT
Vps20 3DR	ATGTAAATGCAAAAATTTATTATTAAGTGTATTATGACTCACATAGAATTATGTTGTTGGGTGGAATTGTGAGCGGATA
Doa4 5DR	TTCGTACACTTTCTGATTCCAAACTAAATTACCACCAACTCTAACTTTTGTTCTTTGAAGTTTCCCAGTCACGACGTT
Doa4 3DR	GGGACACCACCCCAAGTTTCAATTTATTGACAAAAATAAATCTATGAGTTCTATTTAATAGTGGAATTGTGAGCGGATA
Vps27 5det	CCAGACGATATCAAACCTCC
Vps27 3det	CGAAAAAGATTAACACTACG
Hse1 5det	CCTCTGCTTATTCCAATTAGAACC
Hse1 3det	CGGTCAAGAAATCAAGGCTGACCC
Mvb12 5det	TCTCCAATCAAAGTGTTGTC
Mvb12 3det	GGTGTTCATCTTCCGATTAG
Vps28 5det	CGTCTGTGAATCTCATGGTG
Vps28 3det	CTCAAAGTTAGCATCGGACA
Vps36 5det	GACAAGAATAAGACCACGAG
Vps36 3det	CTCAACGTTATTTTTCTTC
Vps22 5det	GGCTCTGTATGGTCAATGAATAGC
Vps22 3det	CCCATCAATGGAATGGAAATCC
Vps20 5det	GAGGGGGATCAAGTTGCAAA
Vps20 3det	CCTTCCTGATTTTGCAAGAC
Doa4 5det	AAAATAAAGGAAATCCTGCA
Doa4 3det	ACGGCGAAATACACATAAAT
Vps27 5comp	AAGCTCGGAATTAACCCTCACTAAAGGGAACAAAAGCTGGCCTCTTCTTATCCAGTTTACTG
Vps27 3comp	ACGACGGCCAGTGAATTGTAATACGACTCACTATAGGGCGTTAATGAATTAATGATTTCTCC

dilution was spotted onto YPD, YPD + LiCl, and YPD pH 9 plates and stored 2 days at 37°C. For growth assays in iron-limiting conditions, 200 μM bathophenanthrolinedisulfonic acid (BPS) was added to YPD agar medium. Plates were photographed with a Canon Powershot A560 camera and adjusted in Adobe Photoshop Elements 2.0.

c. Filamentation assays: Strains were grown in 3 ml YPD overnight at 30°C. For alkaline-induced filamentation assays, 3μL overnight cultures were spotted onto M199 pH 8 agar and incubated 5 days at 37°C. Plates were photographed with a Canon Powershot A560 camera and adjusted in Adobe Photoshop Elements 2.0. For serum-induced filamentation, 3μL overnight cultures were spread on 4% BCS plates and incubated 24 hours at 37°C. Filamentation was visualized on a Zeiss Imager.M1 microscope and images were captured using Axiovision Release 4.6.3 software or as described under the growth assays.

d. Protein preparations: Strains were growth to mid-log phase in 40 mL M199 pH 4 medium and either collected directly for protein preparation or collected and resuspended in 40 mL M199 pH 8 for 30 minutes before collecting. Cells were collected by centrifugation, washed in 1 mM phenylmethylsulphonyl fluoride (PMSF), and cell pellets were resuspended in radioimmunoprecipitation assay buffer (50 mM Tris pH 8, 150 mM NaCl, 1% NP-40, 3 mM ethylenediaminetetraacetic acid, 0.5% deoxycholate, 0.1% sodium laurel sulfate) with protease inhibitors (1 mM PMSF, 10 mM dithiothreitol, 1μg/ml each of aprotinin, pepstatin, and leupeptin). Cells were lysed by glass bead disruption by vortexing 4 times at 4°C. Lysates were then cleared by centrifugations at 15,000 x g for 15 minutes at 4°C to remove cell debris.

e. Western blot analysis: 50 μl protein preparation was separated by SDS-polyacrylamide gel electrophoresis (SDS-PAGE) in an 8% resolving gel. Gels were transferred to a nitrocellulose membrane and blocked 1 hour at room temperature with 5% dry milk dissolved in Tris-buffered saline containing 0.05% Tween-20 (TBS-T). Membranes were incubated with blocking solution containing 1:5000 monoclonal anti-V5-HRP conjugate antibody (Invitrogen). Membranes were washed 3 times in TBS-T, incubated with ECL reagent (Amersham), and exposed to film.

f. Epithelial cell damage assay: FaDu cells (ATCC) were plated in 24-well tissue culture dishes and incubated at 37°C 5% CO_2 in Modified Eagle Medium (MEM) with 10% final concentration FBS and 5 ml Antibiotic/Antimycotic cocktail (Invitrogen). At 90% monolayer confluence, cells were incubated in 0.5 ml medium containing 0.5μCi Cr^{51} for 16 hours. After washing FaDu cells with PBS, $1x10^5$ cells were added in MEM with 10% FBS and 5 ml Antibiotic cocktail (Invitrogen) and incubated 10 hours. Some FaDu were uninfected to measure spontaneous Cr^{51} release. 0.5 ml supernatant was moved to a 13 ml glass tube. 0.5 ml 6M NaOH was added to FaDu cells and moved to a separate tube. Final monolayer removed to the debris tube in 0.5 ml Liftaway (RPI corp). Specific release was calculated as [(2*supernatant)-(2*spontaneous release)]/[(2*total)-(2*spontaneous release)]. All samples were run in triplicate for each individual assay.

g. Oropharyngeal candidiasis mouse model: 4- to 6-week old Balb/c mice were obtained from Charles River (Wilmington, MA). On day -1, mice were immunosuppressed with 0.2mg/g cortisone acetate. On day 0, 50μL of $1x10^5$ cells/ml (low dose) or $1x10^6$ cells/ml (high dose) *C. albicans* cell suspensions were inoculated onto a sterilized cotton ball and incubated 1 hour in the oral cavity of mice anesthetized

with 100μg/g ketamine, 20μg/g xylozine-HCL, and 2.8μg/g acepromazine. On day 3, 10 mice per *C. albicans* strain were sacrificed, and tongue, small intestine, large intestine, and kidney weighed and saved in 2 ml PBS. Tissues were homogenized and plated in 10^0, 10^{-1} and 10^{-2} dilutions on YPD + amp plates. Plates were incubated at 37°C overnight. On day 3, 10 mice per *C. albicans* strain were re-immunosuppressed with cortisone as described for day -1. On day 6, the remaining mice were sacrificed and organs homogenized and plated as described for day 3. Colonies were counted from YPD + amp plates and calculated to represent CFUs/g tissue.

III. Results

We hypothesized that MVB formation plays a role in *C. albicans* pathogenesis independent of Rim101 processing. To test this hypothesis, we generated and characterized strains with mutations in individual members of the ESCRT-0 (Vps27, Hse1), ESCRT-I (Mvb12, Vps28), ESCRT-II (Vps36, Vps22), or ESCRT-III (Vps20, Snf7) complexes, as well as mutations in components that act downstream of *SNF7* in the ESCRT pathway (Vps4, Bro1, Doa4) (referred to as ESCRT-DS in this text) (Figure 16 and Table 7). All deletion mutations were made using sequential rounds of allelic exchange and confirmed by PCR (Figure 17 and data not shown). We then tested these mutant strains for ESCRT-dependent or Rim101-dependent phenotypes.

a. ESCRT deletion mutations and ESCRT-dependent phenotypic defects. We first tested whether ESCRT homologs in *C. albicans* play a role in endosomal trafficking using the lipophilic dye FM 4-64 to visualize internalized vesicle trafficking. Following a 45-60 minute chase, wild-type cells showed strong staining of the vacuole, with little-to-

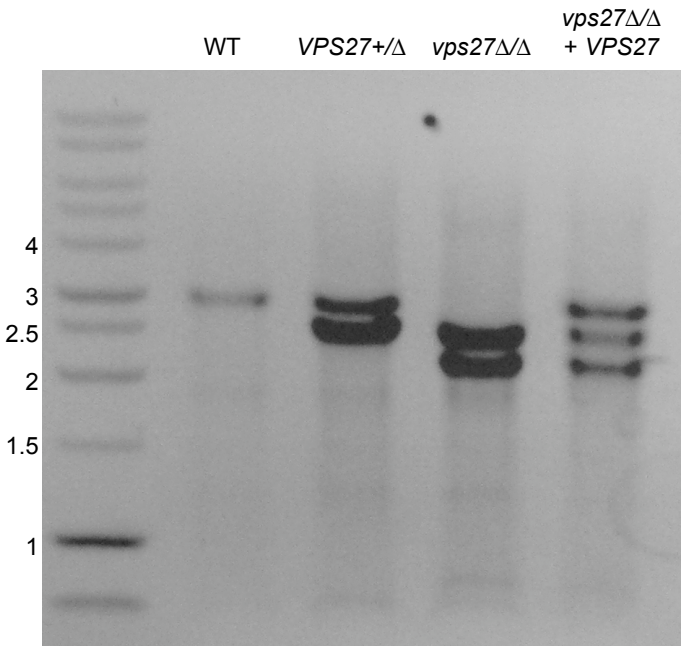

Figure 17. PCR genotyping of *vps27*Δ/Δ strains. *VPS27* was amplified in a PCR using Vps27 5-det and Vps27 3-det primers (Table 2). Band sizes expected were wild-type *VPS27* (2.9 kB), *vps27::ARG4* (2.5 kB), and *vps27::URA3-dpl200* (2.1 kB). Strains shown are wild-type (DAY185), *VPS27*+/Δ (DAY 1176), *vps27*Δ/Δ (DAY1160), and *vps27*Δ/Δ + *VPS27* (DAY1264).

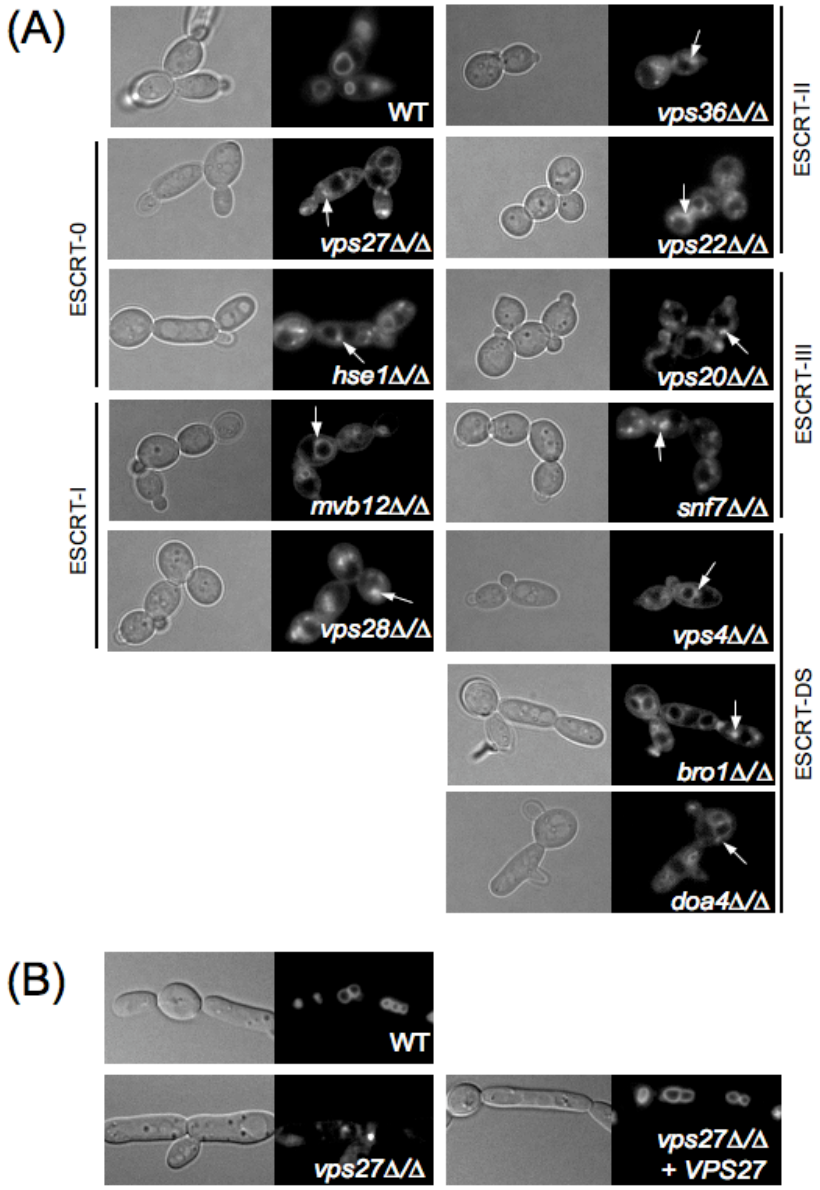

Figure 18. FM 4-64 trafficking defects of *C. albicans* ESCRT mutants. (A) FM 4-64 confirms trafficking defects of ESCRT mutant strains. Exponentially growing cultures were exposed to 16 mM FM 4-64 for 15 minutes on ice. Cells were washed with M199 pH 8 and resuspended in fresh medium and grown for 60 minutes at 30°C. 80 µl culture was then added to 10 mM NaF and 10 mM NaN_3 (final concentrations) before microscopically observing cells. Strains investigated include WT (DAY185), *vps27*Δ/Δ (DAY1160), *hse1*Δ/Δ (DAY 1218), *mvb12*Δ/Δ (DAY1162), *vps28*Δ/Δ (DAY1161), *vps36*Δ/Δ (DAY1163), *vps22*Δ/Δ (DAY1217), *vps20*Δ/Δ (DAY1157), *snf7*Δ/Δ (DAY763), *vps4*Δ/Δ (DAY1155), *bro1*Δ/Δ (DAY1156), and *doa4*Δ/Δ (DAY1158). Arrows point to class E-like exclusion bodies within the cell. (B) The *vps27*Δ/Δ strain is complemented with an exogenous copy of *VPS27*. FM 4-64 staining was performed as in Figure 3A. Strains investigated include WT (DAY185), *vps27*Δ/Δ (DAY1160), and *vps27*Δ/Δ + *VPS27* (DAY1264).

no cytoplasmic staining (Figure 18A). Although the *mvb12*Δ/Δ, *vps4*Δ/Δ, *bro1*Δ/Δ, and *doa4*Δ/Δ strains displayed weaker defects than the other ESCRT mutants tested, all strains lacking ESCRT components displayed staining patterns containing accumulation of perivacuolar staining, indicating that all mutations generated led to formation of class E-like exclusion bodies (Figure 18A). In *S. cerevisiae*, most ESCRT components were initially identified as Class E *vps* mutants, due to the formation of a "class E exclusion body" around the vacuole perimeter, which consists of accumulated immature and/or incomplete MVBs unable to fuse with the vacuole (159). This demonstrates that the homologs identified in *C. albicans* play a similar role in endosomal trafficking as they do in other organisms. We concluded that all ESCRT components identified play a role in MVB trafficking.

b. Rim101-dependent phenotypic defects. We next tested whether ESCRT homologs in *C. albicans* have Rim101-dependent growth defects. Overnight YPD cultures were diluted 1:50 in PBS and fivefold dilutions were spotted onto YPD, YPD pH 9, or YPD + LiCl agar medium. After two days at 37°C, all strains grew robustly on YPD, with similar colony formation numbers at higher dilutions, indicating that each dilution set represented roughly equivalent numbers of cells (Figure 19). Thus, all mutants were able to grow well on rich medium and at a physiologically relevant temperature.

We observed robust growth of the wild-type strain and poor growth of the *rim101*Δ/Δ strain (Figure 19) on YPD, YPD pH 9, and YPD + LiCl. The *vps27*Δ/Δ and the *hse1*Δ/Δ strains, which lack individual ESCRT-0 components, grew similarly to wild type on both YPD pH 9 and YPD + LiCl. Thus, ESCRT-0 is not required for Rim101-

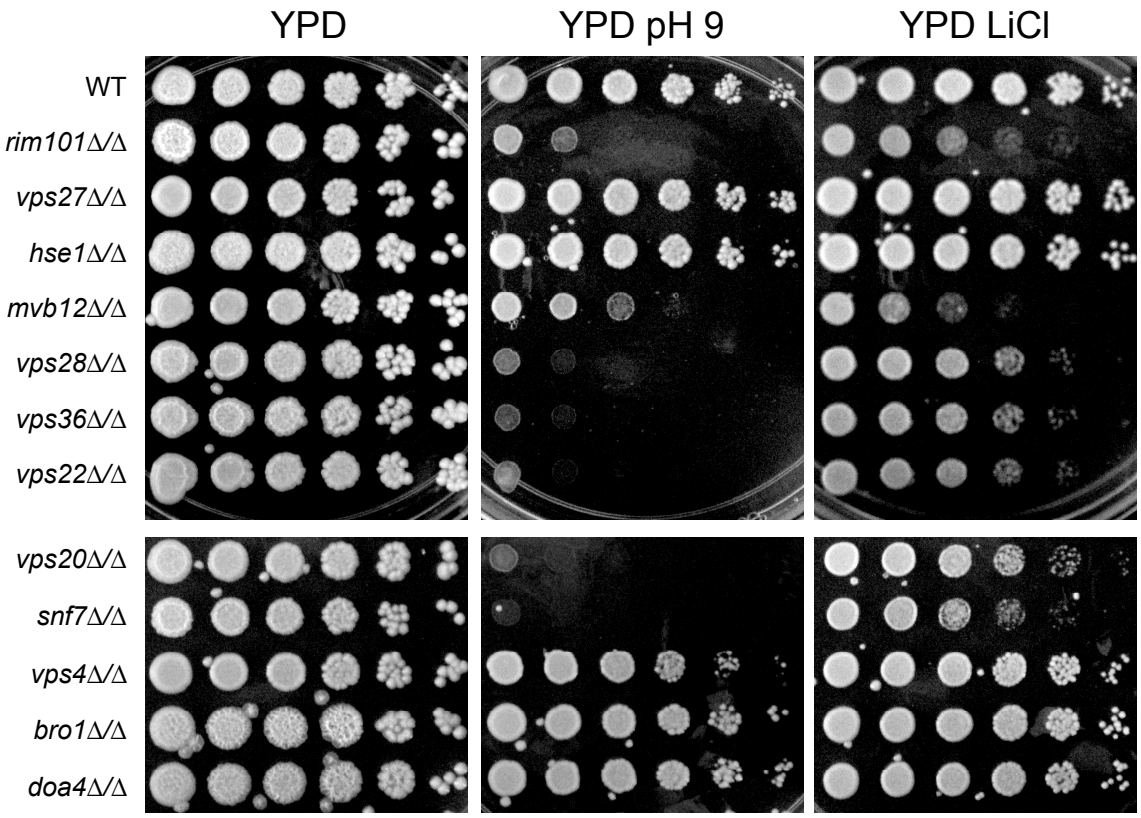

Figure 19. ESCRT-I, -II, and -III mutants, but not ESCRT-0 or -DS mutants, have Rim101-dependent defects. Overnight YPD cultures were diluted 1:50 in PBS and fivefold dilutions were spotted onto YPD, YPD pH 9, or YPD + LiCl agar medium. Plates were incubated at 37°C for two days before photographing. Strains investigated include WT (DAY185), *vps27*Δ/Δ (DAY1160), *hse1*Δ/Δ (DAY 1218), *mvb12*Δ/Δ (DAY1162), *vps28*Δ/Δ (DAY1161), *vps36*Δ/Δ (DAY1163), *vps22*Δ/Δ (DAY1217), *vps20*Δ/Δ (DAY1157), *snf7*Δ/Δ (DAY763), *vps4*Δ/Δ (DAY1155), *bro1*Δ/Δ (DAY1156), and *doa4*Δ/Δ (DAY1158).

dependent growth on these conditions.

As predicted, all strains lacking ESCRT-I (*mvb12*Δ/Δ or *vps28*Δ/Δ), ESCRT-II (*vps22*Δ/Δ or *vps36*Δ/Δ), or either member of the ESCRT-III heterodimer (*vps20*Δ/Δ or *snf7*Δ/Δ) components grew poorly on both YPD pH 9 and YPD + LiCl (Figure 19). This is consistent with previously reported *S. cerevisiae* and *C. albicans* data (207). In fact, we noted that all but the *mvb12*Δ/Δ mutant grew more poorly than the *rim101*Δ/Δ mutant on YPD pH 9, suggesting that these ESCRT pathway members play Rim101-dependent and -independent roles during alkaline growth. Although displaying an alkaline growth defect, the *mvb12*Δ/Δ mutant grew slightly better than the *rim101*Δ/Δ strain on this medium, suggesting an intermediate role in Rim101-dependent alkaline growth. All ESCRT-I, -II, and -IIIa mutants tested therefore displayed a growth defect on alkaline medium. Similar growth between these mutants and the *rim101*Δ/Δ mutant on YPD + LiCl suggests these components play only a Rim101-dependent role during LiCl growth. We noted an exception of the ESCRT-I *mvb12*Δ/Δ mutant, which grew slightly worse than *rim101*Δ/Δ levels (Figure 19), suggesting that Mvb12 contributes to LiCl growth in a Rim101-dependent and -independent manner.

We did not observe Rim101-dependent growth defects in any ESCRT-DS mutant strain (*vps4*Δ/Δ, *bro1*Δ/Δ, or *doa4*Δ/Δ) (Figure 19). This is consistent with *S. cerevisiae* and our previously unpublished results, which demonstrated that strains lacking *VPS4* constitutively process Rim101. Neither Δ*bro1* nor Δ*doa4 S. cerevisiae* mutations prevent Rim101 processing, and a *bro1*Δ/Δ strain did not confer filamentation defects (207). Both the *bro1*Δ/Δ and *doa4*Δ/Δ strains grew well on alkaline medium, supporting a model where these members are not required for Rim101-dependent growth.

We then investigated the role of various ESCRT components in Rim101-dependent filamentation. We expected that ESCRT-I, -II, and -III would be required for Rim101 processing, and thus have filamentation defects in these conditions, but that ESCRT-0 and ESCRT-DS components would not be required for Rim101-dependent alkaline-induced filamentation. To test this hypothesis, we spotted 3 μl overnight YPD culture onto M199 pH 8 plates and incubated them at 37°C. After 6 days, a ring of filamentation was apparent around the periphery of the wild-type colony (Figure 20 and Table 9). No filamentation was observed around the *rim101*Δ/Δ strain. We noted wild-type filamentation around the *hse1*Δ/Δ (ESCRT-0), *vps27*Δ/Δ (ESCRT-0), *bro1*Δ/Δ (ESCRT-DS), and *doa4*Δ/Δ (ESCRT-DS) mutant colonies. We noted intermediate filamentation, indicated by a shorter filament radius or uneven filamentous periphery, around the *mvb12*Δ/Δ (ESCRT-I), and *vps4*Δ/Δ (ESCRT-DS) colonies, respectively. No filamentation was observed around the *vps28*Δ/Δ (ESCRT-I), *vps36*Δ/Δ (ESCRT-II), *vps22*Δ/Δ (ESCRT-II), *vps20*Δ/Δ (ESCRT-III), or *snf7*Δ/Δ (ESCRT-III) colonies (Figure 20). Thus, the mutant strains with the most severe filamentation defects were those with Rim101-dependent defects.

We next tested whether the ESCRT mutants affected filamentation at acidic pH. *C. albicans* does not normally filament in acidic conditions, but we have found that both *snf7*Δ/Δ and *vps4*Δ/Δ strains form peripheral filamentation on M199 pH 4 agar (205).We hypothesized that acidic filamentation may be suppressed by an ESCRT function, and that other ESCRT knockout mutants would similarly show acidic filamentation. However, when we spotted 3 μL overnight YPD culture onto M199 pH 4 plates, only the *snf7*Δ/Δ and *vps4*Δ/Δ strains showed uniform peripheral rings after incubation at 37°C

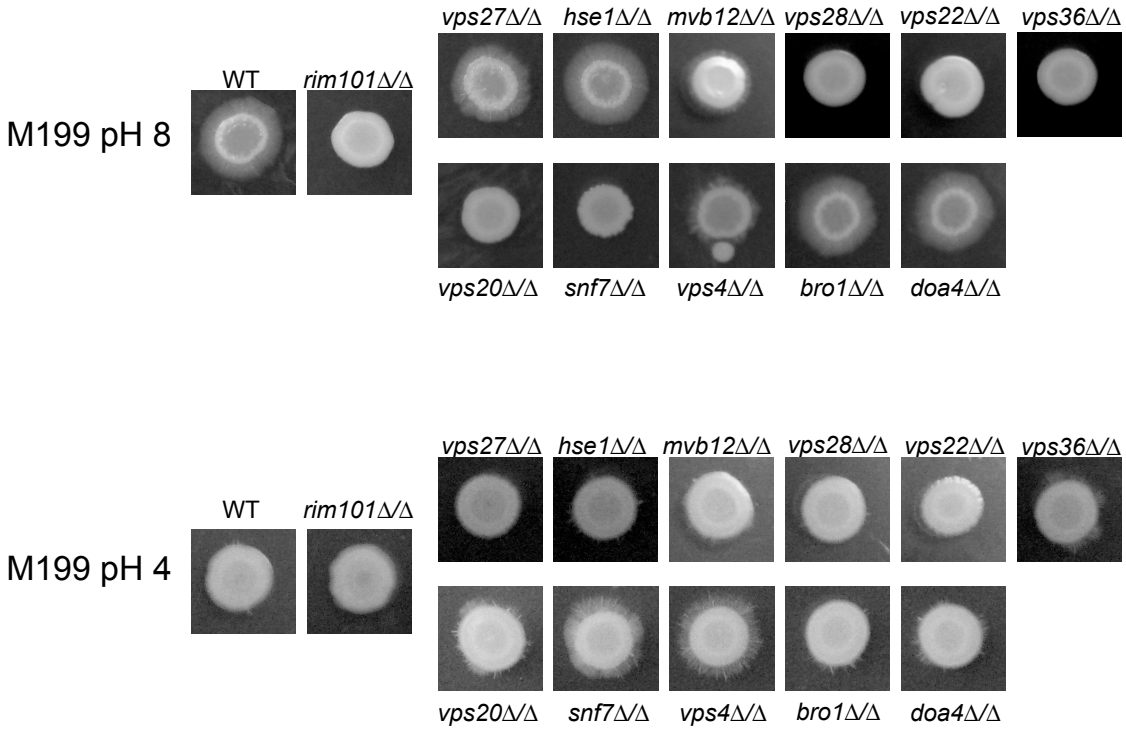

Figure 20. ESCRT mutant filamentation phenotypes. (A) ESCRT-I, -II, and -III mutant strains, but not ESCRT-0 mutant strains, have alkaline-induced filamentation defects. 3 μl overnight YPD cultures were spotted on M199 pH 8 agar plates, and plates were incubated 6 days at 37°C before photographing. (B) Several ESCRT mutant strains have aberrant acidic filamentation. 3 μl overnight YPD cultures were spotted onto M199 pH 4 agar plates, and plates were incubated 6 days at 37°C before photographing.

Table 9. ESCRT mutant filamentation assays.

Strain	Genotype	Alkaline agar filamentation	Acidic agar filamentation	BCS agar filamentation
DAY185	WT	+	-	+
DAY25	*rim101*Δ/Δ	-	-	-
DAY1160	*vps27*Δ/Δ	+	-	+
DAY1218	*hse1*Δ/Δ	+	-	+
DAY1162	*mvb12*Δ/Δ	±	-	-
DAY1161	*vps28*Δ/Δ	-	-	-
DAY1163	*vps36*Δ/Δ	-	±	-
DAY1217	*vps22*Δ/Δ	-	-	-
DAY1157	*vps20*Δ/Δ	-	±	-
DAY763	*snf7*Δ/Δ	-	±	-
DAY1155	*vps4*Δ/Δ	±	±	+
DAY1156	*bro1*Δ/Δ	+	-	+
DAY1158	*doa4*Δ/Δ	+	-	+

(Figure 20 and Table 9). We did note smaller areas of filamentation in uneven patches around the periphery of the *vps36*Δ/Δ, *vps20*Δ/Δ, *bro1*Δ/Δ, and *doa4*Δ/Δ colonies. Thus, Snf7 and Vps4 play the most critical roles in inhibiting acidic filamentation, and other ESCRT components play little-to-no role.

Finally, we tested whether the ESCRT mutations affected serum-induced filamentation. A *rim101*Δ/Δ strain is unable to filament on 4% bovine calf serum (BCS) agar after 24 hour incubation at 37°C. We streaked 2 μl overnight YPD culture onto 4% BCS agar. After 24 hours, the wild-type strain had produced a thick mesh of hyphae, while the *rim101*Δ/Δ strain was observed only in yeast form (Table 9). All ESCRT-0 and ESCRT-DS mutant strains were observed to form wild type-like hyphal cells, while all ESCRT-I, -II, and -IIIa mutant strains were only observed as yeast cells (Table 9). This further confirms that ESCRT-I, -II, and -IIIa are required for Rim101 processing and that ESCRT-0 and ESCRT-DS are not required for Rim101 processing in *C. albicans*.

c. Rim101 processing. We hypothesized that the Rim101-dependent growth and filamentation defects were due to Rim101 processing defects. To test this, we transformed a *RIM101-V5* allele into each of the mutant strains. We grew these strains to mid-log phase and collected protein for Western blot analysis. After growth in M199 pH 8 medium, we observed distinct Rim101-V5 bands in the wild-type strain: the full-length, unprocessed 84-kDa band (FL); the processed, active 78-74-kDa bands (P1), and the processed 65-kDa band of unknown function (P2) (Figure 21A). We noted similar banding patterns in the two ESCRT-0 knockout strains, *vps27*Δ/Δ and *hse1*Δ/Δ (Figure 21A). All ESCRT-I, -II, and -III knockout strains tested showed neither P1 nor P2 processed forms, indicating no Rim101 processing occurs in these strains (Figure 21A).

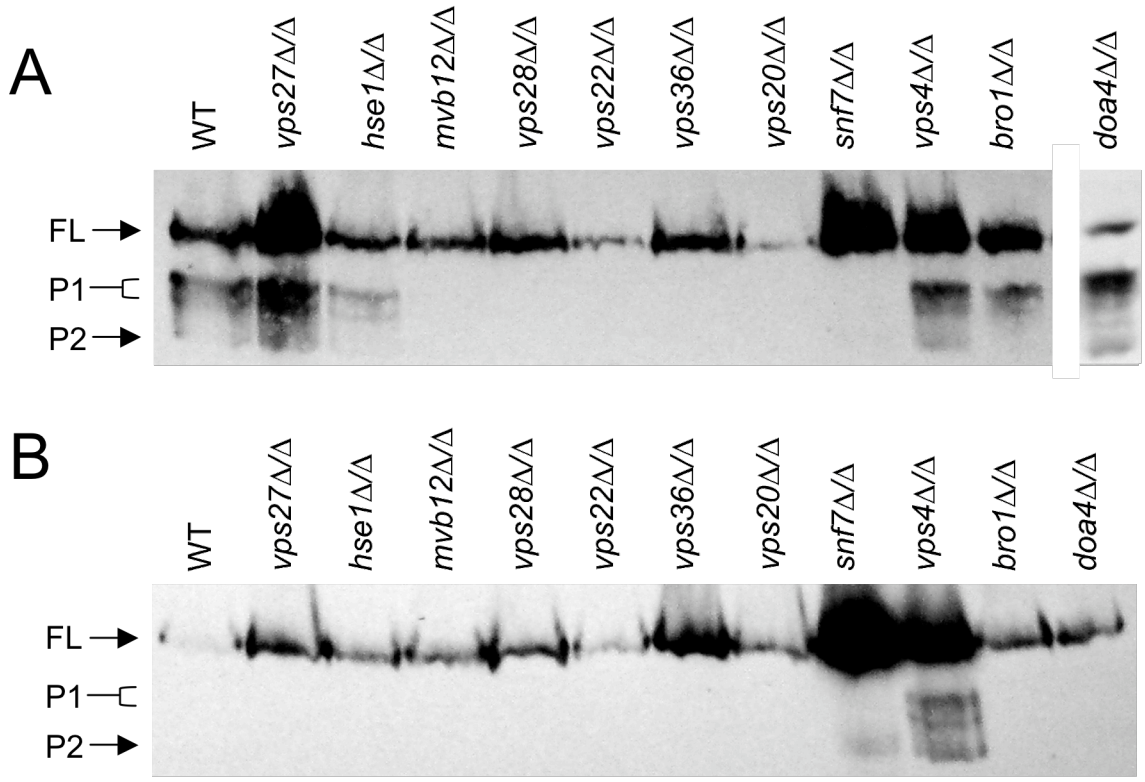

Figure 21. Rim101 processing in ESCRT mutants. (A) ESCRT mutants show Rim101 processing defects after growth in acidic pH and shift to alkaline pH. 200 μl overnight YPD cultures were inoculated into 50 ml M199 pH 4 and grown 4.5 hours at 30°C. Cell pellets were then collected and resuspended in 50 ml M199 pH 8 for 30 minutes growth at 30°C. Crude protein preparations were made from the cultures and run on an 8% resolving gel before transfer to a nitrocellulose membrane. Rim101-V5 was detected after 1 hour incubation with anti-V5-HRP antibody (Invitrogen), using ECL luminescence developing kit. Wild-type Rim101 is processed from full-length size (85 kDa; FL) to active size (74 kDa; P1) and size of unknown function (65 kDa; P2). Strains investigated include WT (DAY1212), *vps27*Δ/Δ (DAY1178), *hse1*Δ/Δ (DAY 1221), *mvb12*Δ/Δ (DAY1193), *vps28*Δ/Δ (DAY1183), *vps36*Δ/Δ (DAY1188), *vps22*Δ/Δ (DAY1222), *vps20*Δ/Δ (DAY1257), *snf7*Δ/Δ (DAY568), *vps4*Δ/Δ (DAY576), *bro1*Δ/Δ (DAY1219), and *doa4*Δ/Δ (DAY1260). (B) Only *vps4*Δ/Δ mutant strain constitutively processes Rim101 at acidic pH. 200 μl overnight YPD culture was inoculated into 50 ml M199 pH 4 and grown 5 hours at 30°C. Protein preparations and Western analysis was done as in Figure 21A.

The *vps4*Δ/Δ, *bro1*Δ/Δ, and *doa4*Δ/Δ strains, whose products all act downstream of Snf7 recruitment to the endosome, showed the same banding pattern as the wild-type strain (Figure 21A). The growth defects observed could therefore be explained by the ability of the mutant strains to process Rim101.

We further hypothesized that Rim101 processing may be improperly activated by ESCRT mutations. This has been shown to be true for ESCRT-DS member *VPS4* in *S. cerevisiae* (77) and *C. albicans* (J. M. Wolf, unpublished data). To test this, we analyzed the *RIM101-V5* expressing strains by Western analysis after growth in M199 pH 4 medium. We observed only full-length Rim101 in the wild type, as well as all other mutant strains except the *vps4*Δ/Δ mutant strain (Figure 21B). The *vps4*Δ/Δ strain displayed the P1 and P2 banding signals also observed in alkaline growth, indicating improper Rim101 activation. No other ESCRT-DS mutation affected Rim101 processing in acidic growth condition.

d. Iron-specific growth defects. Rim101 is known to activate genes involved in acquiring iron, which is insoluble in alkaline environments (11). Studies in several *C. albicans* ESCRT mutants demonstrated that members of ESCRT-I, -II, and -III are required for transporting hemoglobin to the vacuole (202), including the ESCRT-IIIb member *VPS2*. We therefore hypothesized that the ESCRT pathway plays a role in iron acquisition independent of Rim101 processing.

To test this hypothesis, we grew strains up overnight in YPD + 50 μM BPS. We diluted overnight cultures 1:50 and and fivefold dilutions were spotted onto YPD or YPD + 150 μM BPS agar medium and incubated at 37°C. After three days, all strains were growing robustly on YPD medium. On YPD + BPS, the wild-type strain showed

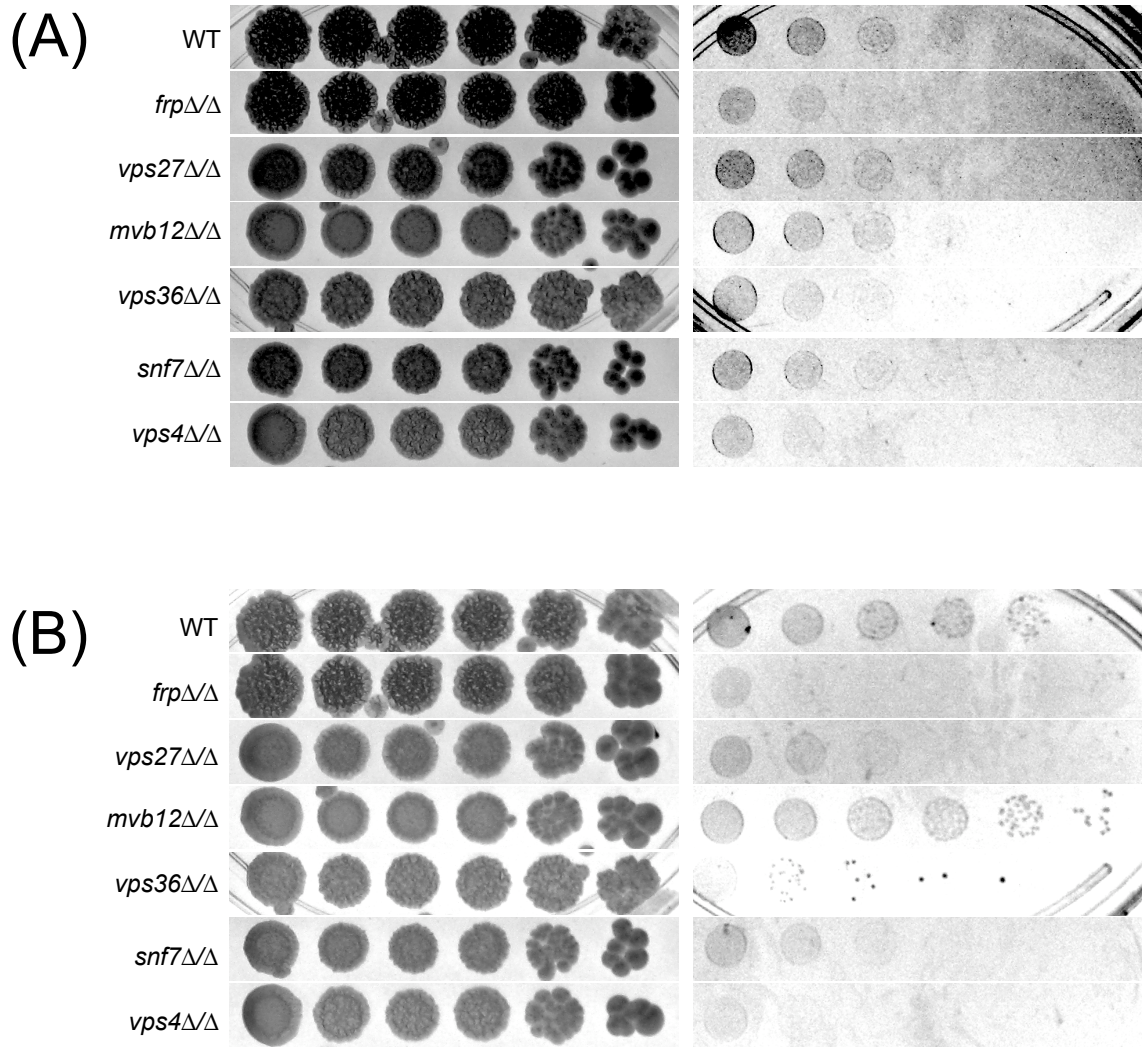

Figure 22. ESCRT mutants have growth defects on iron-depleted medium. Overnight YPD cultures were diluted 1:50 in PBS and fivefold dilutions were spotted onto YPD and YPD + BPS agar plates. Plates were incubated at 37°C for two days before photographing. Strains investigated include wild type (DAY185), *frp1*Δ/Δ (L24), *vps27*Δ/Δ (DAY1160), *mvb12*Δ/Δ (DAY1193), *vps36*Δ/Δ (DAY1183), *snf7*Δ/Δ (DAY568), and *vps4*Δ/Δ (DAY576).

moderate growth through the fourth dilution. *FRP1* is a Rim101-induced ferric reductase required for growth on YPD + BPS, and the *frp1*Δ/Δ mutation conferred a growth defect, growing only to the second dilution (Figure 22A). The *vps27*Δ/Δ (ESCRT-0) strain and *mvb12*Δ/Δ (ESCRT-I) strain showed an intermediate growth defect, growing to the third dilution. The *vps36*Δ/Δ (ESCRT-II) mutant and *snf7*Δ/Δ (ESCRT-III) mutant showed growth defects similar to the *frp*Δ/Δ strain, while the *vps4*Δ/Δ (ESCRT-DS) mutant showed the most severe growth defect, growing only on the first dilution spot (Figure 22A). Differences between the wild type strain and the mutant strains, including *vps27*Δ/Δ, become more apparent after prolonged incubation of the plates at room temperature (Figure 22B). These data show that ESCRT-II, -III, and –DS members are required for growth on iron-limited media, and suggest that ESCRT-0 and -I are also required, though less stringently, for growth on iron-limited media. From these data we concluded that the ESCRT pathway contributes to iron acquisition in both a Rim101-dependent and -independent manner.

e. Epithelial cell damage. We next wished to investigate the role of the ESCRT pathway in mediating epithelial cell damage. Epithelial cells line the skin and all mucosal surfaces, and are the primary cell type on which *C. albicans* resides as a commensal. *C. albicans* has been observed to cause damage to the epithelia by mediating its own endocytosis by the epithelial cells while germinating, rupturing the epithelial cell and releasing cytoplasmic contents into the supernatant (145, 151). By radiolabeling a monolayer of FaDu oropharyngeal epithelial cells, damage can be monitored by measuring the radioactivity released to the culture supernatant. We utilized our

characterized ESCRT mutants to ask the question: does the ESCRT pathway play a role in damaging epithelial cells?

We observed epithelial cell damage after incubating FaDu monolayer cultures with wild-type *C. albicans*, with a typical assay resulting in 30-50% specific ^{51}Cr release (48). To facilitate comparison between assays, we normalized the assays to wild-type damage, and compared the amount of damage induced by the mutant strains to the wild type. Epithelial damage was diminished when incubating cultures with a *rim101*Δ/Δ strain (Figure 23A), resulting in an average of 3% wild-type damage. While we found that the ESCRT-0 *hse1*Δ/Δ mutant was not statistically different from the wild type, we observed ~35% decrease compared to wild-type damage in the *vps27*Δ/Δ infected FaDu cells (P=0.0006). After incubating FaDu with the ESCRT-I, -II, and –III mutant strains, we observed strong decreases in damage relative to wild-type damage, although the *mvb12*Δ/Δ mutant caused more damage than the other ESCRT-I member (Figure 23B). The *vps4*Δ/Δ, *bro1*Δ/Δ, and *doa4*Δ/Δ strains all showed approximately 35-40% decrease in damage compared to wild type, similar to the *vps27*Δ/Δ strain. The *vps27*Δ/Δ, *bro1*Δ/Δ, and *doa4*Δ/Δ strains did not affect Rim101-dependent phenotypes or Rim101 processing, but did affect FM 4-64 trafficking, which suggests ESCRT function plays a role in *C. albicans*-mediated epithelial cell damage. The similar phenotypes among ESCRT members not affecting Rim101 processing suggests ESCRT function, though not *HSE1*, may play an independent role in mediating epithelial damage through vesicle trafficking.

f. Oropharyngeal candidiasis mouse model of disease. We hypothesized that ESCRT function plays a role during an *in vivo* infection setting. We tested this hypothesis using an oropharyngeal candidiasis mouse model, which facilitates *C. albicans*-oral

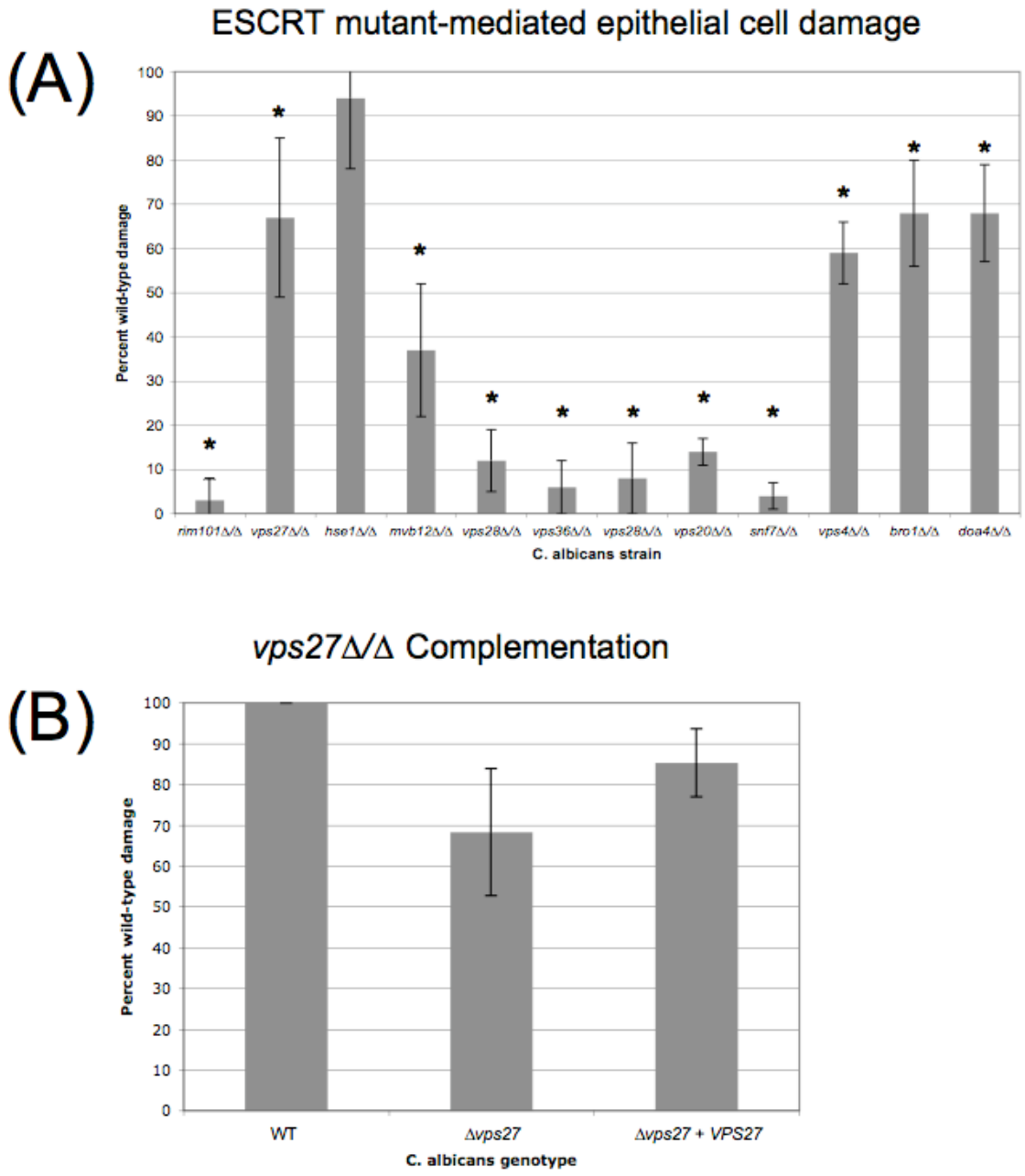

Figure 23. ESCRT mutants have FaDu epithelial cell damage defects. (A) ESCRT mutants show defects in damaging FaDu epithelial cells. 10^5 *C. albicans* cells were incubated 10 hours with ^{51}Cr-labeled FaDu cells. Supernatant was collected and compared to uninfected FaDu cells to determine specific release. Samples were run in triplicate for each assay. Graph shows damage conferred by each mutant relative to a simultaneously tested wild-type strain. Mutants were tested minimally in three separate assays. *, P<0.05. (B) The *vps27*Δ/Δ strain damage defect is complemented with a copy of *VPS27*.

epithelial cell interactions in an *in vivo* setting. Cortisone-immunosuppressed mice were infected orally with wild-type, *rim101*Δ/Δ, *vps27*Δ/Δ, or *snf7*Δ/Δ *C. albicans*. 10 mice per strain were sacrificed at 3 days post-infection (DPI) and at 6 DPI. Mouse tongues were harvested to assess oral fungal burden and mice were weighed daily. These procedures allowed us to assess both fungal burden and mouse morbidity.

We first assessed the fungal burden of mice infected with $5x10^3$ CFUs at 3 DPI. The oral cavity of mice infected with the wild-type strain showed an average fungal burden of $4x10^4$ CFUs/gm. A significant decrease was observed between the wild-type strain and the three mutant *C. albicans* strains (P=0.033, P=0.038, P=0.033 for *rim101*Δ/Δ, *vps27*Δ/Δ, and *snf7*Δ/Δ strains, respectively) (Figure 24A). Mice infected with the *vps27*Δ/Δ strain carried a log less CFU/gm tongue compared to mice infected with the wild type. The *rim101*Δ/Δ and *snf7*Δ/Δ strains showed a sharp decreases in fungal burden, with both strains nearly two logs lower burden than wild type. The fact that all mutants colonized to lower burden levels suggests that all three genes play a role in *C. albicans* pathogenesis. Additionally, both the *rim101*Δ/Δ and *snf7*Δ/Δ strains colonized the oral cavity at a significantly lower burden than the *vps27*Δ/Δ strain (P=0.032, P=0.024 for *rim101*Δ/Δ and *snf7*Δ/Δ strain, respectively) (Figure 24A). Thus, both Rim101 processing and ESCRT function are necessary for wild-type levels of *in vivo* tongue colonization, but defects in Rim101 processing result in more severe virulence defects than defects in ESCRT function.

At 6 DPI, all mice infected with the wild-type strain were still colonized, although the fungal burden decreased by approximately a log, to $4x10^3$ CFUs/gm. All mice infected with the *rim101*Δ/Δ and *snf7*Δ/Δ strains had cleared the infection to levels below

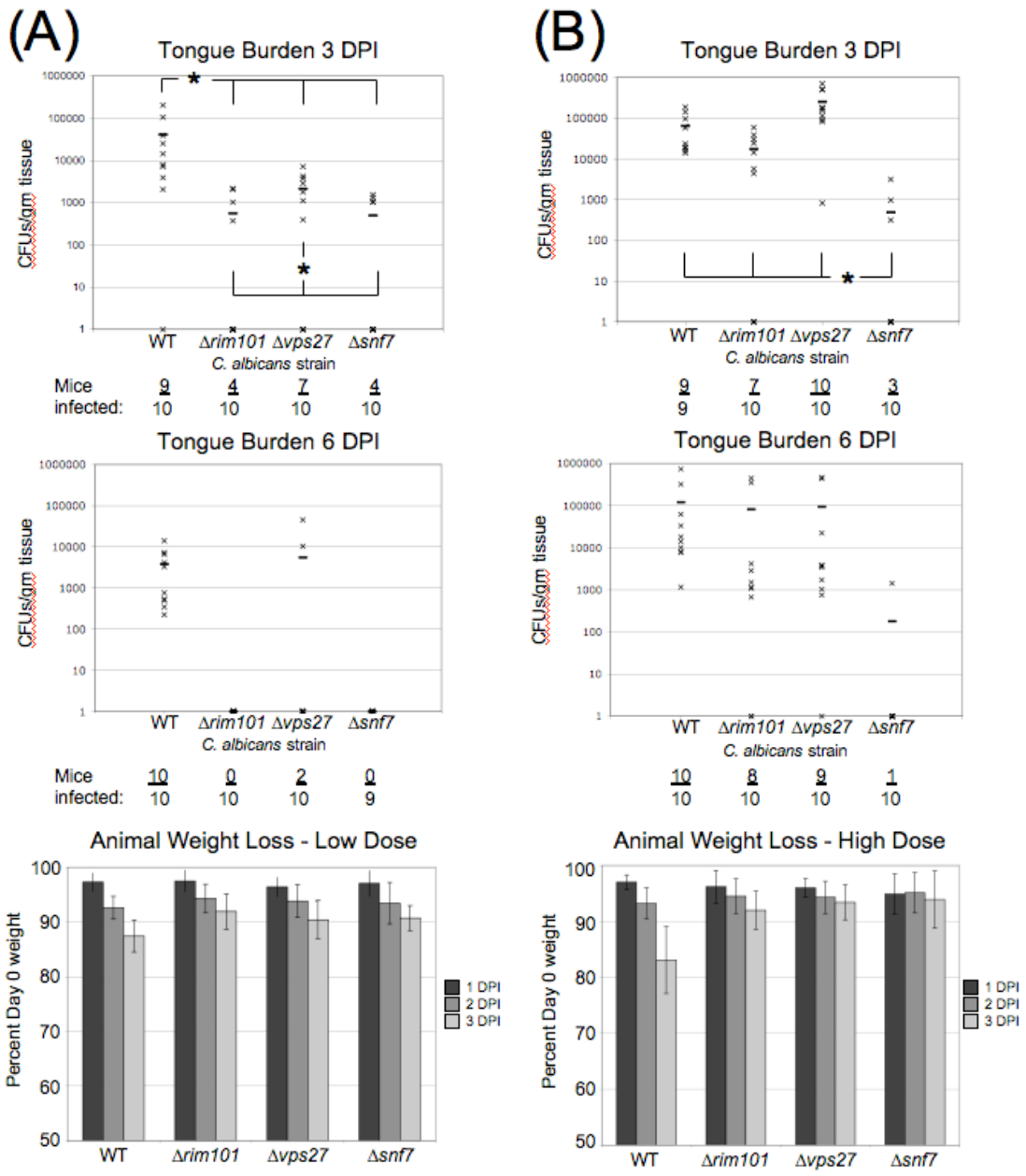

Figure 24. A *vps27*Δ/Δ mutant is attenuated in a mouse model of oral candidiasis. (A) Tongue fungal burden and animal weight loss after low-dose inoculation. Cortisone-immunosuppressed animals were infected with 50 μL of 10^5 CFUs/ml *C. albicans*. At 3 DPI, half the animals were harvested and their tongues collected for fungal cell counts, The other half were resuppressed with cortisone at 3 DPI and harvested at 6 DPI for fungal cell counts. The number of mice with detectable fungal burden per group is noted below each graph. * $P < 0.05$ between indicated groups. (B) Tongue fungal burden and animal weight loss after high-dose inoculation. The experiment was run identically but with an infectious dose of 50 μl of 10^6 CFUs/ml *C. albicans*.

a detectable threshold for this assay, and all but two mice infected with the *vps27*Δ/Δ strain had also cleared the infection (Figure 24A). This indicates that both Rim101 processing and ESCRT function are necessary for maintaining infection, and that Rim101 processing plays a more important role in maintenance than ESCRT function.

During the course of infection, we weighed the mice as a measure of mouse morbidity. Mice with oral candidiasis can lose weight quickly. Mice infected with all of the four *C. albicans* strains lost weight over the course of the experiment. However, by 6 DPI, mice infected with the wild-type strain had lost significantly more weight than mice infected with any of the three mutant strains (P=0.002, P=0.028, P=0.008 for *rim101*Δ/Δ, *vps27*Δ/Δ, and *snf7*Δ/Δ strains, respectively) (Figure 24A). There was no significant difference in weight loss between mice infected with the *rim101*Δ/Δ, *vps27*Δ/Δ, and *snf7*Δ/Δ strains. This suggests that weight loss correlates with fungal burden, and that mice more heavily colonized will manifest disease symptoms more quickly than those less heavily colonized.

We hypothesized that the decreased burden among mutant strains may be due to poor initial colonization by the *C. albicans* cells, and that the decreased burden observed in mutant strains might be overcome with a higher initial inoculum. To address this possibility, we infected mice with a ten-fold higher inoculum ($5x10^4$ CFUs) and again assessed fungal burden at 3 DPI and 6 DPI. At 3 DPI, the wild-type oral cavity contained an average of $6x10^4$ CFUs/gm, which was comparable to the wild-type colonization level in the lower dose experiment (Figure 24B). Mice infected with the *rim101*Δ/Δ strain showed a significant decrease in burden compared to those infected with wild type (P=0.021), but with an average of $2x10^4$ CFUs/gm. However, the *rim101*Δ/Δ-infected

mice at the higher dose were colonized with two logs higher burden than the *rim101*Δ/Δ-infected mice at the lower dose. Mice infected with the *vps27*Δ/Δ strain showed a significantly higher burden than those infected with wild-type (P=0.015), $2x10^5$ CFUs/gm, which was also approximately two logs higher than mice infected with a lower dose of *vps27*Δ/Δ (Figure 24B). Mice infected with the *snf7*Δ/Δ strain showed a significant decrease in fungal burden than wild-type-infected mice (P=0.004), and at $5x10^2$ CFUs/gm, is comparable to the *snf7*Δ/Δ-infected mice in the lower dose experiment. Because an increase in the wild-type inoculum did not increase the fungal burden, this suggests there are a finite number of sites within the mouse oral cavity for *C. albicans* to reside. We were able to increase the burden of the *rim101*Δ/Δ- and *vps27*Δ/Δ-infected mice, supporting our hypothesis. However, the *snf7*Δ/Δ strain did not increase in burden with an increased inoculum, suggesting that the *snf7*Δ/Δ is unable to access those sites that are available.

We next looked at mice infected with the higher dose at 6 DPI. At 6 DPI, mice infected with the wild-type strain exhibited a fungal burden of $1x10^5$ CFUs/gm. Mice infected with the *rim101*Δ/Δ or *vps27*Δ/Δ strain showed no significant difference from wild-type in oral fungal burden with an average of $8x10^4$ and $9x10^4$ CFUs/gm, respectively (P=0.486, P=0.146 for *rim101*Δ/Δ and *vps27*Δ/Δ strains, respectively) (Figure 24B). This suggests that Rim101 processing and ESCRT function contribute independently to maintaining colonization levels during infection. All mice but one had cleared the *snf7*Δ/Δ strain from their oral cavity by 6 DPI, however, indicating that the effects of Rim101 processing and ESCRT function are additive, and when both are defective, the cells cannot maintain infection in the host. Alternatively, the *snf7*Δ/Δ

mutant may have additional defects unrelated to either Rim101 or ESCRT function that decrease viability of this strain.

We then analyzed weight loss during the course of the infection with a higher inoculum. All mice again lost weight over the course of the infection, but this weight loss was not significant in *snf7*Δ/Δ-infected mice (Figure 24B). While *rim101*Δ/Δ- and *vps27*Δ/Δ-infected mice lost weight, mice infected with wild-type *C. albicans* lost a significantly larger amount of weight than any of the mutant strains (P=0.0005, P=0.0001, P=0.0004 for *rim101*Δ/Δ, *vps27*Δ/Δ, and *snf7*Δ/Δ mutants, respectively) (Figure 24B). Thus, although mice infected with the wild-type, *rim101*Δ/Δ, or *vps27*Δ/Δ strains are colonized to similar levels, mice infected with wild-type *C. albicans* show significantly more morbidity than mice infected with either mutant strain. This supports our hypothesis that the ESCRT pathway plays a Rim101-independent role during *C. albicans* pathogenesis.

g. VPS27 complementation. We wished to confirm that the *vps27*Δ/Δ phenotypes observed were due to *VPS27* specific mutation. To do this, we transformed the *vps27*Δ/Δ strain with a *VPS27*-containing plasmid and compared it to the deletion mutant in several assays. Addition of *VPS27* reverted the trafficking phenotype to a wild-type staining pattern (Figure 18B). The reversion strain partially rescued the *vps27*Δ/Δ epithelial cell damage defect, causing significantly more damage than the *vps27*Δ/Δ strain (P=0.008) (Figure 23B), although still significantly less damage than the wild-type strain. This partial rescue could be due to position effects, haploinsufficiency, or insufficient promoter sequence inclusion in the construct. However, the partial damage rescue and

full FM 4-64 trafficking rescue lead us to conclude that the defects observed with this strain are indeed due to *VPS27* deletion.

IV. Discussion

We have used a series of mutants in the ESCRT pathway to investigate the role of individual ESCRT protein components in both Rim101 processing and MVB trafficking in *C. albicans*. We found that ESCRT-I, -II, and -IIIa components play a role in proteolytically processing the transcription factor Rim101, but that ESCRT-0 and several components downstream of ESCRT-III are not required for Rim101 processing. Our *in vitro* epithelial cell damage studies suggest that ESCRT function plays an independent role in epithelial cell damage, and our *in vivo* studies suggest ESCRT function is required for normal *C. albicans* virulence. Our data demonstrate that Vps27 is required for wild-type colonization levels when orally administered to mice at a relatively low dose, but that this colonization defect can be overcome by administering a higher inoculum dose. However, even when mice are colonized with similar numbers of wild-type and *vps27*Δ/Δ *C. albicans*, wild-type infected mice lose significantly more weight than knockout-infected mice. Thus, ESCRT function is required for normal colonization and morbidity associated with *C. albicans* infection independent of Rim101.

a. ESCRT complex relationship with Rim101 processing. Are all ESCRT complexes required for Rim101 processing? ESCRT complex function plays a role in activating the transcription factor Rim101 in a number of fungi, including *C. albicans*, *S. cerevisiae*, and *A. fumagatus*, by recruiting the processing machinery to the endosomal membrane. Work done in *S. cerevisiae* demonstrated that the ESCRT-0 member Vps27

does not play a role in Rim101 activation, and suggested that the same may hold true in *C. albicans*. Our investigation of many ESCRT knockout mutants establishes that neither Vps27 nor Hse1, the other ESCRT-0 member, are required for Rim101-dependent growth or Rim101 processing (Figures 17 and 19). While it is possible that *C. albicans* contains redundant *VPS27* or *HSE1* homologs, this is seems unlikely, as both *vps27*Δ/Δ and *hse1*Δ/Δ strains displayed FM 4-64 trafficking defects associated with ESCRT defects. If redundant homologs existed, these homologs would likely act in both ESCRT and Rim101 function. Thus, ESCRT-0 is not required for Rim101 processing in *C. albicans*.

How could Rim101 processing bypass ESCRT-0 yet require ESCRT-I, -II, and -IIIa? One possibility is that ESCRT-I, -II, and -IIIa are recruited directly by the upstream Rim101 signaling molecules, Rim21 and Rim8. Rim21 (PalH), a transmembrane protein found at the plasma membrane, interacts with ubiquitinated Rim8 (PalF) in *Aspergillus nidulans* (79), and the Rim21-Rim8 complex is thought to act as a surrogate "receptor" in alkaline conditions, initiating endocytosis and subsequent ESCRT complex assembly. Rim8 ubiquitination has recently been documented in *S. cerevisiae*, and ubiquitinated Rim8 can interact directly with ESCRT-I member Vps23 (78). This suggests that the Rim21-Rim8 complex bypasses ESCRT-0 by recruiting ESCRT-I directly. ESCRT-I recruitment appears to be mediated through Rim8 mimicry of ESCRT-0 component Vps27, as Rim8 interacts with Vps23 through a Rim8 SXP motif similar to the Vps27 PSAP motif known to interact with Vps23 (78). However, Rim8 ubiquitination in *S. cerevisiae* is pH-independent, and thus does not explain how the cell can activate Rim101 only in neutral-alkaline conditions. Recently, our lab has shown that *C. albicans* Rim8 is phosphorylated in an alkaline-dependent manner (J. Gomez-Raja, in preparation), and

this modified Rim8 may be important for activating Rim101 processing machinery. Other systems are known to recruit ESCRT-I directly, bypassing ESCRT-0, to assemble the core ESCRT complexes at diverse cellular locations for distinct function such as cytokinesis and viral budding (12, 120, 128). Direct recruitment of ESCRT-I by Rim101 signaling members is likely conserved across fungi containing Rim101.

We had previously observed the *snf7*Δ/Δ mutant to have stronger Rim101-dependent growth defects than the *rim101*Δ/Δ mutant, suggesting a contribution of MVB trafficking to alkaline and LiCl growth. Because of the common function among ESCRT-I, -II, and –IIIa members, we expected ESCRT-I, -II, and -IIIa mutants to have growth defects similar to the *snf7*Δ/Δ mutant. This is largely what we observed, with the stronger phenotype on YPD pH 9 agar suggesting that ESCRT function is more important during alkaline adaptation than LiCl adaptation. While the *snf7*Δ/Δ mutant had a slightly worse phenotype than other ESCRT complex mutants, this can be explained by the propensity of Snf7 to associate with membranes even in the absence of ESCRT recruitment (110). Because ESCRT complex mutants express *SNF7*, they may retain low levels of Snf7 function.

Growth phenotypes differed between ESCRT-I complex members. We tested mutants in two of four identified ESCRT-I complex members, the *mvb12*Δ/Δ strain and the *vps28*Δ/Δ strain. The *vps28*Δ/Δ strain grew similarly to the ESCRT-II mutant strains on Rim101-dependent media. However, while the *mvb12*Δ/Δ strain displayed a growth defect on alkaline medium, it was not as severe a defect as the *rim101*Δ/Δ growth defect. Additionally, the *mvb12*Δ/Δ strain demonstrated an intermediate filamentation defect, as it was able to produce peripheral filaments, but shorter filaments than those observed

with the wild-type strain. Mvb12 has been suggested to regulate ESCRT-I recruitment (39, 45), and may play a role in recognizing ubiquitylated cargo (141, 174). The partial endocytic sorting defect combined with the partial Rim101-dependent phenotype suggests that Mvb12 is required for wild-type levels of ESCRT-III recruitment but that ESCRT-III (including Snf7) is partially recruited in an Δ*mvb12* strain. Confoundingly, the *mvb12*Δ/Δ strain grew worse than the other ESCRT mutant strains on LiCl-supplemented medium. Because ESCRT-0 mutant strains displayed no LiCl growth defects, this is not likely due to the lesser role of *MVB12* in MVB formation. Thus, *MVB12* may play an additional, non-ESCRT-dependent role within the cell, which may explain the discrepancies in mutant strain phenotypes.

Several studies have been performed using a mutation within a single ESCRT complex subunit as representative of behavior of the complex. The phenotypic differences between the *mvb12*Δ/Δ and *vps28*Δ/Δ mutant strains highlight the hazard in this assumption. Our data highlight the fact that molecular subunits of a complex do not have the same effect on function, and valuable information may be missed using a single representative mutation.

b. ESCRT function in pathogenesis. Previous studies from our lab have studied several *snf7* separation-of-function alleles during *C. albicans* epithelial cell damage (205). These studies suggested that the Snf7 function in the ESCRT pathway does not contribute to epithelial cell damage. However, many of these alleles were partial ESCRT-function disruptions and the assay may not have been sensitive enough to detect differences with these partial disruptions. Thus, our previous experiments included several caveats and were not wholly conclusive.

The *vps27*Δ/Δ, *hse1*Δ/Δ, *vps4*Δ/Δ, *bro1*Δ/Δ, and *doa4*Δ/Δ mutant strains were all able to grow like wild-type on Rim101-dependent media, and all but the *vps4*Δ/Δ presented normal Rim101-dependent filamentation. Thus, we expected these strains to be the most representative of independent ESCRT function during *C. albicans* pathogenesis. The similar decreases in the *vps27*Δ/Δ, *bro1*Δ/Δ, and *doa4*Δ/Δ mutants in the FaDu epithelial cell damage assay suggest the defect may be due to the common ESCRT function of these genes. The slightly larger decrease of the *vps4*Δ/Δ mutant may be due to the dysregulation of Rim101 processing in this strain (Figure 6).

We were surprised to see a difference between ESCRT-0 members in the FaDu epithelial cell damage assay. The *vps27*Δ/Δ strain caused consistently lower damage than the wild-type strain, while the *hse1*Δ/Δ strain was indistinguishable from the wild-type strain. Because the *hse1*Δ/Δ strain showed a trafficking defect (Figure 3), it is unlikely that a second, redundant *HSE1* homolog exists in *C. albicans*. Vps27 binds both endosomal ubiquitylated cargo proteins and the endosomal phosyphatydyl-insolisol-3-phosphate membrane lipid surface, while Hse1 has only been demonstrated to bind to some ubiquitylated cargo (16, 125). Hse1 may therefore play an accessory role to Vps27 function in ESCRT complex trafficking. To the best of our knowledge, this is the first demonstration that Hse1 is not necessary for all Vps27-dependent phenotypes.

Previous studies have looked at the role of ESCRT complex proteins in *C. albicans* infection using a bloodstream infection mouse model (41). However, the ESCRT complex members studied, Vps28 and Snf7/Vps32, function in both Rim101 processing and MVB trafficking. These genes were knocked out and the mutant strains were found to be less pathogenic than the *rim101*Δ/Δ strain. These findings suggest that

ESCRT function plays a role in *C. albicans* pathogenesis, but do not truly study ESCRT function independent from Rim101 function. The *vps27*Δ/Δ and *hse1*Δ/Δ strains used here study ESCRT function wholly uncoupled from Rim101 processing.

Data from our OPC mouse model suggest that the ESCRT pathway plays a Rim101-independent role in pathogenesis. The *vps27*Δ/Δ strain was defective in colonizing the tongue at a lower inoculum. The colonization defect was overcome with an increased inoculum, but similar fungal burden was not an indication of similar disease states, as mice infected with wild-type *C. albicans* lost significantly more weight than mice infected with the *vps27*Δ/Δ strain. Thus, ESCRT plays a role both in establishing colonization during infection (at low doses) and in disease-associated morbidity (at high doses). We compared the wild-type and *vps27*Δ/Δ in several assays for filamentation, adherence, and growth, and observed no differences to account for morbidity differences (J. M. Wolf, data not shown). However, our studies of ESCRT mutant growth suggest a broader role for ESCRT function in iron-poor growth conditions than have been reported. Iron sequestration is a potent antimicrobial defense by the host, and Vps27 function may be required for wild-type growth in the iron-depleted environment of the host.

c. *C. albicans* niche size. Are fungal colonization levels dependent on inocula concentrations? Both lower and higher dose inocula lead to similar fungal burden with the wild-type strain, while a higher dose inocula lead to a higher fungal burden with the mutant strains. However, mutant strain burden did not increase much beyond wild-type levels, if at all (Figure 24). This potential upper limit of fungal colonization suggests there exist a finite number of sites where *C. albicans* can grow within its host.

We were able to rescue colonization defects of both the *vps27*Δ/Δ and *rim101*Δ/Δ strains to wild-type levels by increasing the inocula dose. However, we observed similar wild-type colonization numbers at 3 DPI in animals infected with low- or high-dose inocula. These facts indicate that *C. albicans* has a limited niche size in the oral cavity. We manipulated the niche size of our animals with cortisone and tetracycline treatments, and different manipulations could alter this niche size. However, given a set of conditions in a host niche, there is an upper threshold to the *C. albicans* burden the host can bear.

Our studies have shown *C. albicans* requires a fully functional ESCRT complex for wild-type pathogenic levels during *in vitro* and *in vivo* pathogenesis. Understanding the ESCRT complex function in *C. albicans* presents opportunities to molecularly characterize a nontraditional signal transduction cascade and to investigate the mechanism of ESCRT function during *C. albicans* interactions with the host.

CHAPTER 4

I. Introduction

Regulating sodium homeostasis is vital for a cell survival. Maintaining a low sodium concentration facilitates a gradient that can be used for nutrient symport; it also prevents the cell from succumbing to osmolaric stress in high salt environments.

Several families of sodium pumps have been characterized in yeast as part of the response network to control salt concentrations. Some sodium pumps rely on ATP hydrolysis to pump out excess sodium ions at the plasma membrane, such as *ENA1* in *Saccharomyces cerevisiae* and its homolog, *ENA21*, in *Candida albicans* (57, 75). Others are Na^+/H^+ antiporters also located at the plasma membrane, such as *NHA1*, called *CNH1* in *C. albicans* (154, 181). *S. cerevisiae* contains a single Na^+/H^+ pump found at the endosome, called *NHX1* (135). *NHX1* sequesters sodium ions inside the endosome, which is hypothesized to regulate vesicle volume, turgor, and pH in addition to salinity (29, 135). *C. albicans* has a single candidate homolog, *orf19.4201*, with 59% identity to *ScNHX1*. Thus, *NHX1* is an endosomal Na^+/H^+ pump in *S. cerevisiae* and possibly in *C. albicans*.

In *S. cerevisiae*, *NHX1* has been shown to play a role during growth in high salt or acidic media. Nhx1 protein levels increase when cells are grown in high sodium medium, and the Δ*nhx1* strain exhibits sodium sensitivity (135). *NHX1* can also sequester potassium ions, suggesting the pump may have a broad specificity (29). Additionally, *NHX1* plays a role in both cytoplasmic and vacuolar pH homeostasis, and both the cytoplasm and vacuole of Δ*nxh1* strain are more acidic than those of the wild-type (~0.5 and ~1 pH unit lower, respectively) (29). The dysregulated pH of these organelles leads

to a growth defect when the *nhx1*Δ strain is grown in acidic conditions. Thus, *NHX1* plays a role in both salt stress and acidic stress adaptation in *S. cerevisiae*.

In addition to playing a role in sodium sequestration, *NHX1* plays a role in endosomal trafficking in *S. cerevisiae* (24, 29, 135). Cells lacking *NHX1* have endosomes that are unable to properly mature and fuse with the vacuole. This leads to the improper sorting of vacuolar proteases and the accumulation of the membrane dye FM 4-64 around the vacuolar periphery, called a class E exclusion body (196). The mechanism for *NHX1* contribution to endosome maturation is not fully understood, but is theorized to be at least partially due to control of the endosomal luminal contents (29). Thus *NHX1* acts as a sodium pump and is required for normal endosomal sorting in *S. cerevisiae*.

Many genes in *S. cerevisiae* and *C. albicans* are required for endosomal sorting. Some of these genes, when mutated, produce similar phenotypes as *nhx1*Δ cells, by improperly sorting vacuolar enzymes and FM 4-64 (159). Most of these genes are part of the endosomal sorting complex required for transport, or ESCRT, complex pathway. The ESCRT pathway generates multivesicular bodies (MVBs) from endosomes and is also required for endosomal maturation (84). Thus both *NHX1* and ESCRT pathway members are required for normal endosomal sorting.

Several of the ESCRT pathway members play an additional role in cellular signal transduction and activation of the transcription factor, Rim101 (147). Rim101 is a transcription factor whose proteolytic activation is required for growth and filamentation in neutral-alkaline pH conditions. Its activation is regulated by an upstream signaling pathway, whose members interact with ESCRT machinery. This is most evident with the ESCRT member Snf7, which directly interacts with the processing machinery responsible

for activating Rim101. However, other ESCRT members are required to recruit Snf7 to the endosomal membrane, the putative site of Rim101 activation (8, 9, 88). ESCRT dissociation is mediated by Vps4, and this dissociation further regulates Rim101 activation (10, 77). Thus, ESCRT members promote and regulate Rim101 processing in addition to vesicle trafficking.

Based on its class E phenotype and its role in alkalinizing organelles in *S. cerevisiae*, we hypothesized that *C. albicans NHX1* also plays a role in Rim101 processing. We tested this by generating an *nhx1*Δ/Δ *C. albicans* strain and testing for Rim101-dependent phenotypes. We observed a growth defect in LiCl adaptation and serum-induced filamentation, but no defect in alkaline adaptation or alkaline-induced filamentation. We likewise observed no defects in Rim101 processing. These phenotypes may be due to the surprising observation that the *nhx1*Δ/Δ *C. albicans* strain does not share the class E phenotype of the *nhx1*Δ *S. cerevisiae* strain. When tested for its ability to cause epithelial cell damage, however, the *nhx1*Δ/Δ *C. albicans* strain was strongly attenuated compared to wild type. Thus, while *CaNHX1* may play a slightly different role than *ScNHX1*, the role of *CaNHX1* in serum-dependent filamentation makes it a good candidate for future studies.

II. Materials and Methods

a. Media and growth conditions: All strains were routinely passaged using standard YPD (1% yeast extract, 2% w/v Bacto Peptone, 2% w/v dextrose) with 80 μg/ml uridine supplemented. Prototrophic mutants were selected on synthetic complete medium (0.67% yeast nitrogen base plus ammonium sulfate and without amino acids, 2%

dextrose, 80 μg of uridine per ml) supplemented for the remaining auxotrophic needs of the strain. Rim101-dependent growth phenotypes were tested using YPD buffered with 150 mM HEPES to pH 9 with NaOH or YPD supplemented with 150 mM LiCl. Alkaline-induced filamentation was tested on M199 medium (GibcoBRL) buffered with 150 mM HEPES, supplemented with 80 μg/ml uridine, and pH-adjusted to pH 4 or pH 8. Serum-induced filamentation was tested on 4% bovine calf serum (BCS) supplemented with 80 μg/ml uridine.

b. Strain manipulation: All strains generated during these studies and the primers used for PCR amplification are listed in Tables 10 and 11, respectively. Homologous recombination of prototrophic markers were transformed into the BWP genetic background and selected on appropriately supplemented media. The first *NHX1* allele was knocked out using a PCR generated with NHX1 5DR and NHX1 3DR primers and pRS-URA3-dpl200 (pDDB57) as template to generate the heterozygous *NHX1*+/Δ strain DAY1261. The homozygous *nhx1*Δ/Δ strain was generated using a PCR with the same primers but pRS-ARGΔSpe (pDDB246) template to generate DAY1262. DAY1262 was made prototrophic by addition of the *HIS1*-carrying DDB78 to generate DAY1159. To express *RIM101-V5* in the *nhx1*Δ/Δ strain, DAY1262 was transformed with NruI-digested DDB233 to generate DAY1263. The *NHX1* complementation vector was generate in this way: first *NHX1* plus promoter and terminator sequences were amplified in a PCR using NHX1 5comp and NHX1 3comp primers and BWP17 genomic DNA as template. This PCR was transformed into *Saccharomyces cerevisiae* along with NotI-EcoRI-double digested DDB78, where *in vivo* recombination led to DDB505

Table 10. Strains used in Chapter 4 studies.

Name	Genotype				Ref
BWP17	*ura3::λimm434* *ura3::λimm434*	*arg4::hisG* *arg4::hisG*	*his1::hisG* *his1::hisG*		(204)
DAY25	*ura3::λimm434* *ura3::λimm434*	*arg4::hisG* *arg4::hisG*	*HIS1::DDB78::his1::hisG* *his1::hisG*		(48)
DAY185	*ura3::λimm434* *ura3::λimm434*	*ARG4::URA3::arg4::hisG* *arg4::hisG*	*HIS1::DDB78::his1::hisG* *his1::hisG*		(48)
DAY568	*ura3::λimm434* *ura3::λimm434*	*arg4::hisG* *arg4::hisG*	*RIM101-V5::HIS1::DDB233::his1::hisG* *his1::hisG*	*snf7::ARG4* *snf7::URA3-dpl200*	(98)
DAY1159	*ura3::λimm434* *ura3::λimm434*	*arg4::hisG* *arg4::hisG*	*HIS1::DDB78::his1::hisG* *his1::hisG*	*nhx1::ARG4* *nhx1::URA3-dpl200*	This study
DAY1160	*ura3::λimm434* *ura3::λimm434*	*arg4::hisG* *arg4::hisG*	*HIS1::DDB78::his1::hisG* *his1::hisG*	*vps27::ARG4* *vps27::URA3-dpl200*	Chapter 3
DAY1212	*ura3::λimm434* *ura3::λimm434*	*arg4::hisG* *arg4::hisG*	*RIM101-V5::HIS1::DDB233::his1::hisG* *his1::hisG*	*nhx1::ARG4* *nhx1::URA3-dpl200*	Chapter 2
DAY1261	*ura3::λimm434* *ura3::λimm434*	*arg4::hisG* *arg4::hisG*	*his1::hisG* *his1::hisG*	*nhx1::ARG4* *NHX1*	This study
DAY1262	*ura3::λimm434* *ura3::λimm434*	*arg4::hisG* *arg4::hisG*	*his1::hisG* *his1::hisG*	*nhx1::ARG4* *nhx1::URA3-dpl200*	This study
DAY1263	*ura3::λimm434* *ura3::λimm434*	*arg4::hisG* *arg4::hisG*	*RIM101-V5::HIS1::DDB233::his1::hisG* *his1::hisG*	*nhx1::ARG4* *nhx1::URA3-dpl200*	This study
DAY1267	*ura3::λimm434* *ura3::λimm434*	*arg4::hisG* *arg4::hisG*	*NHX1::HIS1::DDB505::his1::hisG* *his1::hisG*	*nhx1::ARG4* *nhx1::URA3-dpl200*	This study

Table 11. Primers used in Chapter 4 studies.

Nhx1 5DR	CATTATAAAGTTGTTGTCTAGTTTTGAACACGTAATTGAGGATCAAAAAAGAAAACAAGATTTCCCAGTCACGACGTT
Nhx1 3DR	AAATCAAATAAATATGTATAATAATTATTATAAAATCAATATATGTGAAATCTATTTGAAGTGGAATTGTGAGCGGATA
Nhx1 5det	CAATAGATTCAATTGAAGCT
Nhx1 3det	AGCATCGGTTTATGTGCCGC
Nhx1 5comp	AAGCTCGGAATTAACCCTCACTAAAGGGAACAAAAGCTGGTAACTATTATACACGACCGC
Nhx1 3comp	ACGACGGCCAGTGAATTGTAATACGACTCACTATAGGGCGAGCACAAGTGATTTGAATGC

circularization. Plasmid was recovered and digested with NruI before being transformed into DAY1262 to generate DAY1267.

c. Growth assays*:* Overnight YPD cultures were diluted 1:20 into sterile water and subsequently diluted 1:5 into sterile water in a sterile 96-well plate. Approximately 5 μl of each dilution was spotted onto YPD, YPD pH 9, YPD + LiCl, M199 pH 4, and M199 pH 8. Plates were incubated for 2 days at 37°C. For CO_2 growth studies, 1 plate each of YPD, M199 pH 4, and M199 pH 8 was incubated at 37°C with atmospheric CO_2 and 1 plate each was incubated in a tissue culture incubator with 5% CO_2.

d. Filamentation assays: Strains were grown in 3 ml YPD overnight at 30°C. For alkaline-induced filamentation assays, 3μL overnight cultures were spotted onto M199 pH 8 agar and incubated 5 days at 37°C. Plates were photographed with a Canon Powershot A560 camera and adjusted in Adobe Photoshop Elements 2.0. For serum-induced filamentation, 3μL overnight cultures were spread on 4% BCS plates and incubated 24 hours at 37°C.

e. Protein preparation: To test for Rim101 activation, 200 μl from overnight YPD cultures was inoculated into 40 ml M199 pH 4 and grown 5 hours at 30°C. Cells were pelleted, resuspended in 40 ml M199 pH 8, and grown 1 hour at 30°C. To test for attenuation of Rim101, 300 μl from overnight YPD cultures was inoculated into 40 ml M199 pH 8 and grown 5.5 hours at 30°C. Cells were pelleted, resuspended in 40 ml M199 pH 4, and grown 1 hour at 30°C. Cells were collected by centrifugation and washed in 1 mM phenylmethylsulphonyl fluoride (PMSF) before cell pellets were resuspended in radioimmunoprecipitation assay buffer (50 mM Tris pH 8, 150 mM NaCl,

1% NP-40, 3 mM ethylenediaminetetraacetic acid, 0.5% deoxycholate, 0.1% sodium laurel sulfate) with protease inhibitors (1 mM PMSF, 10 mM dithiothreitol, 1μg/ml each of aprotinin, pepstatin, and leupeptin). Cells were lysed by glass bead disruption by vortexing 4 times at 4°C. Lysates were cleared by centrifugations at 15,000 x g for 15 minutes at 4°C to remove cell debris. Protein concentration was determined by Bradford assay.

f. Western blot analyses: 500 μg protein was separated by SDS-polyacrylamide gel electrophoresis (SDS-PAGE) using 8% resolving gels. Protein was transferred to a nitrocellulose membrane and blocked 1 hour at room temperature with 5% dry milk dissolved in Tris-buffered saline containing 0.05% Tween-20 (TBS-T). Blots were incubated with blocking solution containing 1:5000 monoclonal anti-V5-horse radish peroxidase conjugate antibody (Invitrogen). Blots were washed 3 times in TBS-T, incubated with ECL reagents (Amersham), and exposed to film.

g. Epithelial cell damage assay: FaDu cells (ATCC) were plated in 24-well tissue culture dishes and incubated at 37°C 5% CO_2 in Modified Eagle Medium (MEM) with 10% final concentration FBS and 5 ml Antibiotic/Antimycotic cocktail (Invitrogen). At 90% monolayer confluence, cells were incubated in 0.5 ml medium containing 0.5μCi Cr^{51} for 16 hours. After washing FaDu cells with PBS, $1x10^5$ cells were added in MEM with 10% FBS and 5 ml Antibiotic cocktail (Invitrogen) and incubated 10 hours. Some FaDu cells were untreated to measure spontaneous Cr^{51} release. 0.5 ml supernatant was moved to a 13 ml glass tube. 0.5 ml 6M NaOH was added to FaDu cells and moved to a separate tube. Final monolayer removed to the debris tube in 0.5 ml Liftaway (RPI corp).

Specific release was calculated as [(2*supernatant)-(2*spontaneous release)]/[(2*total)-(2*spontaneous release)]. All samples were run in triplicate for each individual assay.

III. Results

Based on BLAST results demonstrating 59% sequence identity at the protein level, *C. albicans* has a single candidate homolog, *orf19.4201*, which we will call *NHX1*. *NHX1* was deleted in two subsequent rounds of homologous recombination (Figure 25) and was made prototrophic by incorporation of the *HIS1*-expressing plasmid pDDB78.

a. FM 4-64 trafficking phenotype. *S. cerevisiae nhx1*Δ mutants have a defect in trafficking FM 4-64 dye to the vacuole. Based on homology to *S. cerevisiae NHX1*, we hypothesized that *C. albicans NHX1* would have a similar FM 4-64 defect. We investigated FM 4-64 trafficking after a 60-minute chase period in a wild-type, *vps27*Δ/Δ, and *nhx1*Δ/Δ strain. The wild-type strain showed a specific staining of the vacuolar membrane (Figure 26). The *vps27*Δ/Δ strain, known to have an FM 4-64 trafficking defect due to its role in the ESCRT pathway (196), showed little vacuolar staining, but an accumulation of fluorescent spots around the vacuolar perimeter. These bright spots are likely class E-like exclusion bodies, which are aggregations of vesicles unable to properly fuse with the vacuole. The *nhx1*Δ/Δ strain showed cells with wild-type patterns of vacuolar staining. We hypothesized that the *nhx1*Δ/Δ trafficking defect may be more readily apparent with a shorter chase period, and investigated FM 4-64 trafficking after a 30-minute chase. However, we did not observe a difference from the 60-minute chase (J. M. Wolf, data not shown). Thus, unlike *S. cerevisiae*, the *C. albicans nhx1*Δ/Δ mutant does not have a detectable FM 4-64 trafficking defect.

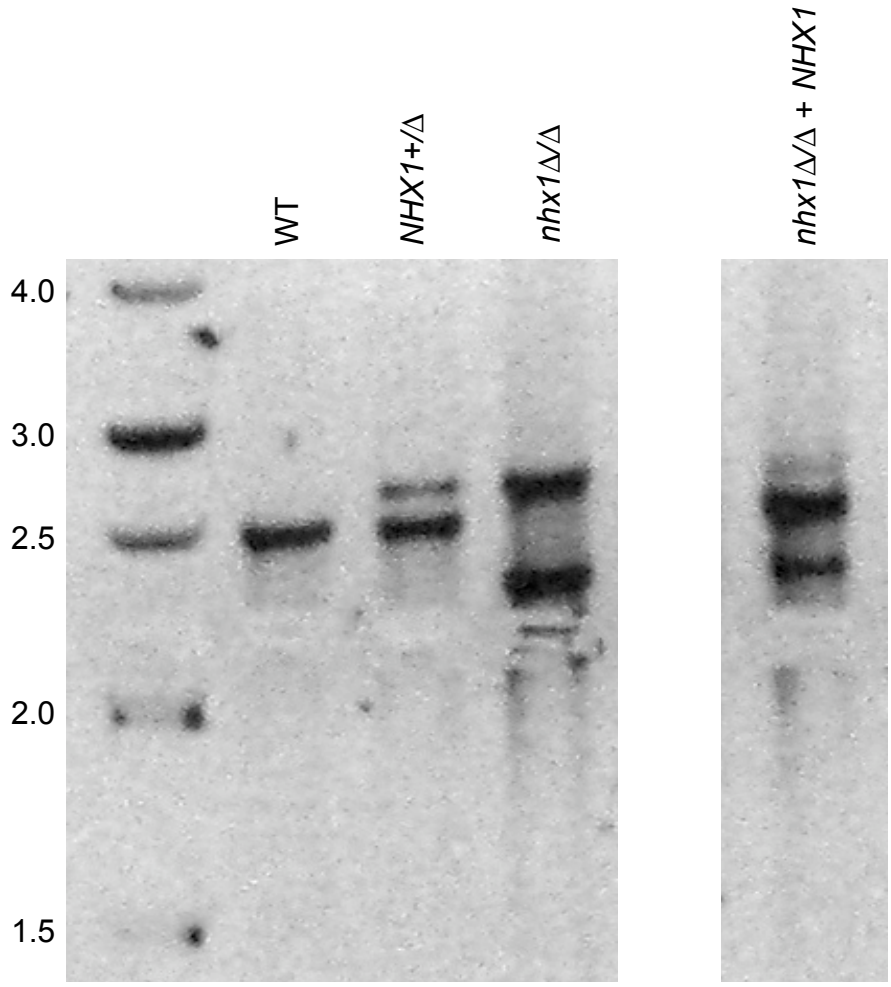

Figure 25. PCR verification of strain genotype. *NHX1* was amplified in a PCR using Nhx1 5-det and Nhx1 3-det primers (Table 11). Band sizes expected were wild-type *NHX1* (2.5 kB), *nhx1::ARG4* (2.6 kB), and *nhx1::URA3-dpl200* (2.3 kB). Strain shown are wild type (DAY185), *NHX1*+/Δ (DAY), *nhx1*Δ/Δ (DAY1159), and *nhx1*Δ/Δ + *NHX1* (DAY1267).

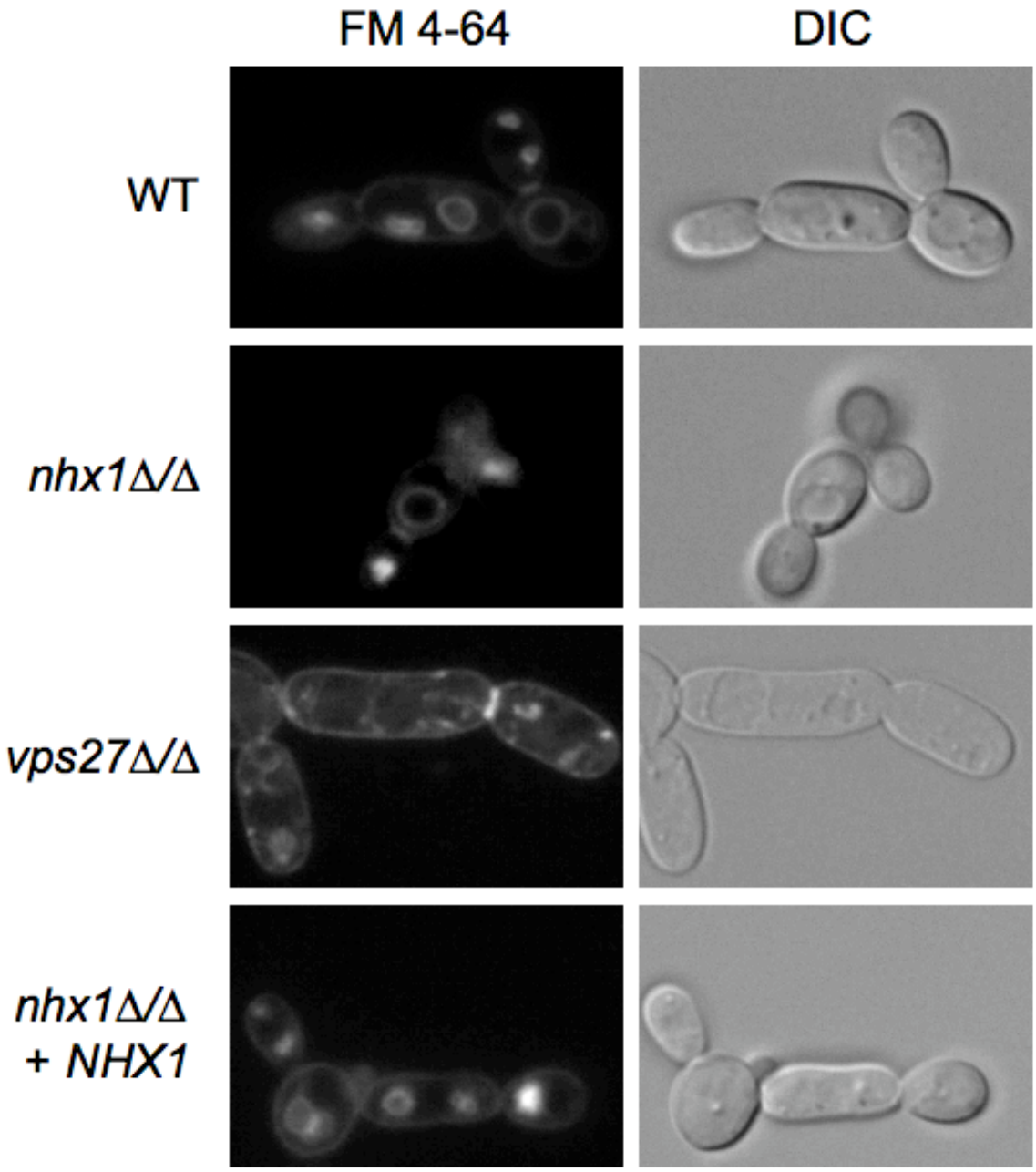

Figure 26. The *nhx1*Δ/Δ mutation does not affect FM 4-64 trafficking in *C. albicans*. 16mM FM 4-64 was exposed to exponentially growing cultures on ice. After 15 minutes, cells were washed with M199 pH 8, resuspended in fresh medium, and grown for 60 minutes at 30°C. 80 µl of culture was added to 10 mM NaF and 10 mM NaN_3 (final concentrations) before observing the cells under the microscope. Strains investigated include (DAY185), *vps27*Δ/Δ (DAY1160), *nhx1*Δ/Δ (DAY1159), and *nhx1*Δ/Δ + *NHX1* (DAY1267).

b. Rim101-dependent growth phenotypes. Because Nhx1 regulates the endosomal lumen in *S. cerevisiae*, we hypothesized that it may play a role in Rim101 processing. We tested this by plating five-fold serial dilutions on media requiring Rim101 processing for growth.

On YPD buffered to pH 9, the wild-type strain was able to grow and form robust colonies at the highest dilution. The *rim101*Δ/Δ strain had a severe growth defect, both in cell number and in colony size, compared to the wild-type strain (Figure 27). The *nhx1*Δ/Δ strain grew similar to the wild-type strain, indicating that *NHX1* is required for adaptation to alkaline pH.

On YPD containing 150 mM LiCl, the wild-type strain was again able to form robust colonies at the highest dilution. The *rim101*Δ/Δ strain was also able to grow at the highest dilution, but the colonies were noticeably smaller than the wild-type colonies (Figure 27). The *nhx1*Δ/Δ strain was also able to grow to the highest dilution, where it formed colonies smaller than the wild-type strain but larger than the *rim101*Δ/Δ strain. Thus, *NHX1* is required for growth in high concentrations of LiCl.

c. Rim101-dependent filamentation phenotypes. Rim101 processing is required for alkaline-induced filamentation. We tested the role of *NHX1* in alkaline filamentation by spotting 3 μl of an overnight YPD culture onto M199 pH 8 and incubating at 37°C. After 6 days incubation, the wild-type strain had formed a ring of filaments around the initial colony. The *rim101*Δ/Δ strain was able to grow, but did not form any filaments around the colony (Figure 28A). The *nhx1*Δ/Δ strain did form a peripheral ring of filamentation, and these filaments were similar in length to those of the wild-type strain. Thus, *NHX1* is not required for alkaline-induced filamentation.

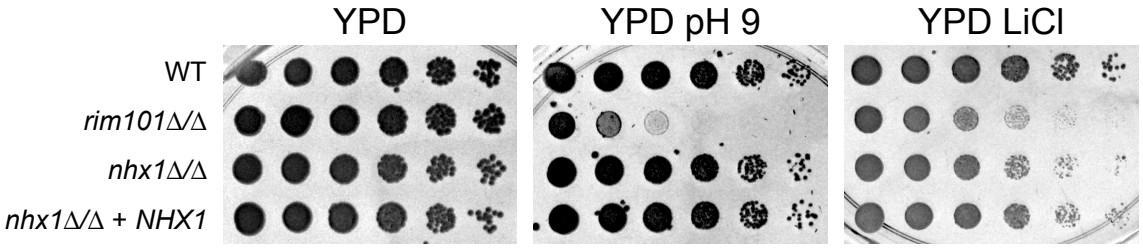

Figure 27. *NHX1* is not required for Rim101-dependent phenotypes. Overnight YPD cultures were diluted 1:50 in PBS and fivefold dilutions were spotted onto YPD, YPD pH 9, or YPD + LiCl agar medium. Plates were incubated at 37°C for two days before photographing. Strain investigated include WT (DAY185), *rim101*Δ/Δ (DAY25), *nhx1*Δ/Δ (DAY1159), and *nhx1*Δ/Δ + *NHX1* (DAY1267).

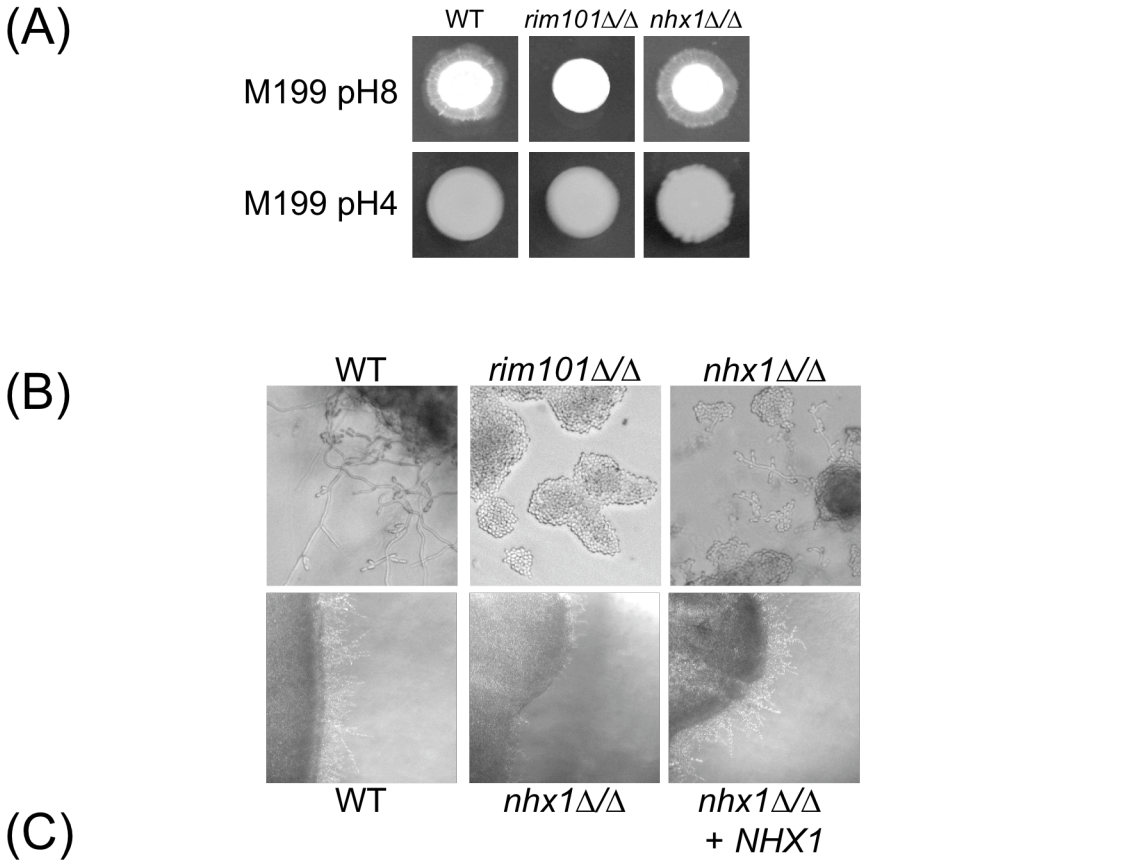

Figure 28. *NHX1* is not required for alkaline-induced filamentation but is required for serum-induced filamentation. (A) 3 μl overnight YPD cultures were spotted on M199 pH 8 or M199 pH 4 agar plates, and plates were incubated 6 days at 37°C before photographing. (B) 2 μl overnight YPD cultures were spotted on 4% BCS agar plates, and plates were incubated 16 hours at 37°C before photographing. (C) 1 x 10^5 cells were incubated in 1 ml tissue culture medium alone (MEM + 10% FBS + antibiotic cocktail) or in medium with a confluent layer of FaDu epithelial cells for 10 hours at 37°C with 5% CO_2. Strain investigated include WT (DAY185), *rim101*Δ/Δ (DAY25), *nhx1*Δ/Δ (DAY1159), and *nhx1*Δ/Δ + *NHX1* (DAY1267).

Rim101 processing is also required for serum-induced filamentation. We tested the role of *NHX1* in serum filamentation by streaking 2 μl of an overnight YPD culture onto 4% BCS agar and incubating at 37°C. After 1 day, the wild-type strain was observed to form long, branching hyphae, while the *rim101*Δ/Δ strain formed only yeast cells on this medium (Figure 28B). The *nhx1*Δ/Δ strain showed an intermediate filamentation defect on this medium. While long hyphae were observed in this strain, many hyphae ended in clusters of yeast cells, and the hyphae appeared less branched than in the wild-type strain (Figure 28B). This filamentation defect was rescued by addition of an *NHX1* allele (Figure 28B). Thus, *NHX1* is required for wild-type levels of serum-induced filamentation.

d. Rim101 processing. We wished to test whether the LiCl growth defect and serum filamentation defect were in fact due to a defect of the *nhx1*Δ/Δ strain in Rim101 processing. To test this, we transformed the *RIM101-V5* allele into the *nhx1*Δ/Δ strain and collected crude protein preparations for Western blot analysis. We hypothesized that the *nhx1*Δ/Δ strain may have a slight processing defect that affected some, but not all, Rim101-dependent phenotypes.

We first wished to test if the *nhx1*Δ/Δ strain had a defect in processing Rim101. To do this, we transformed the *nhx1*Δ/Δ heterozygote with *RIM101-V5*. We grew the cells in M199 pH 4 medium to exponential phase, then shifted them to M199 pH 8 for 1 hour. We collected protein from these cultures and tested equivalent protein concentrations by Western blot analysis for Rim101-V5 processing. In the wild-type strain at pH 4, we observed full-length Rim101 at 85 kDa and a smaller processed band at 65 kDa, the function of which is unknown (Figure 29A). After a shift to pH 8, we

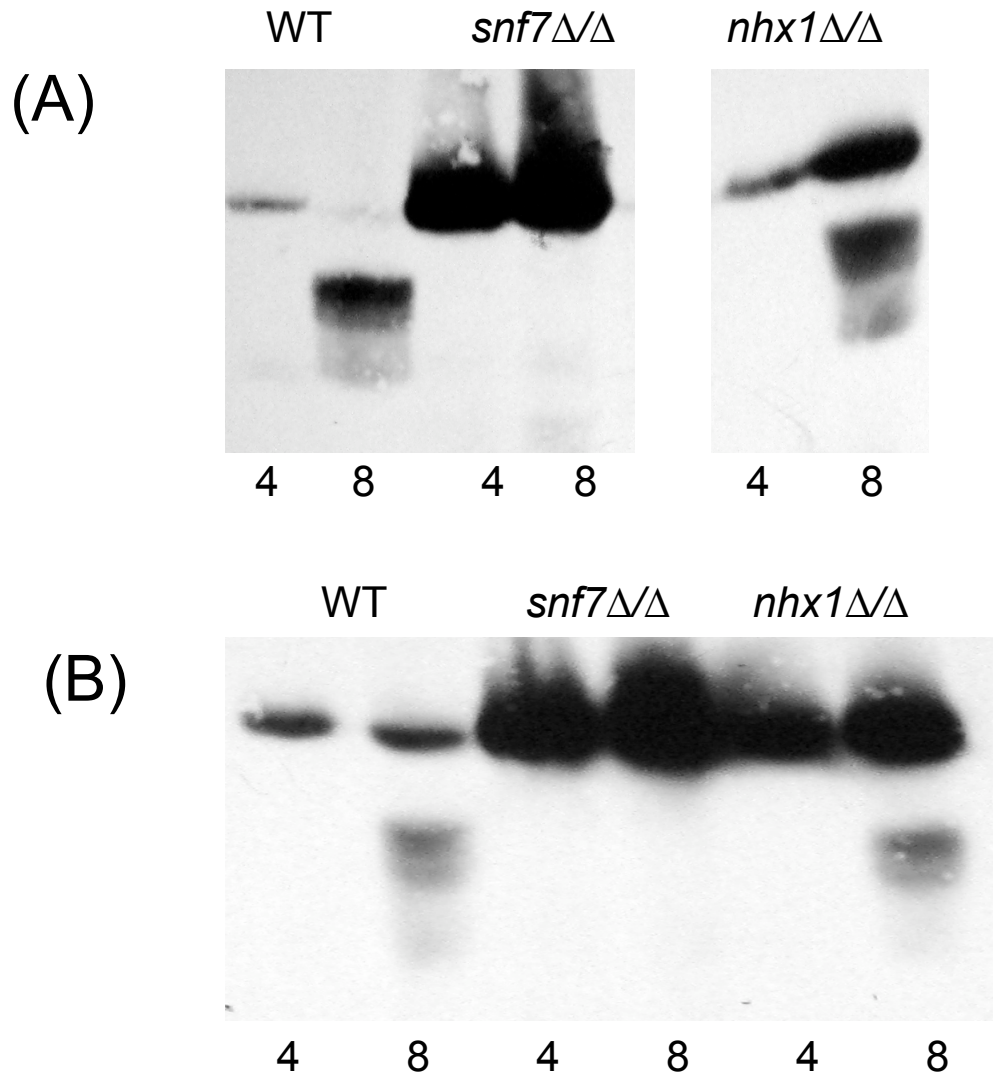

Figure 29. *NHX1* does not play a role in Rim101 processing. (A) 200 μl overnight YPD cultures were inoculated into 50 ml M199 pH 4 and grown 4.5 hours at 30°C. Cell pellets were collected and resuspended in 50 ml M199 pH 8 for 60 minutes growth at 30°C. Crude protein preparations were made from the cultures and run on an 8% resolving gel before transfer to a nitrocellulose membrane. Rim101-V5 was detected after 1 hour incubation with anti-V5-HRP antibody (Invitrogen), using ECL luminescence developing kit. Wild-type Rim101 is processed from full-length size (85 kDa; FL) to active size (74 kDa; P1) and size of unknown function (65 kDa; P2). Strains investigated include wild type (DAY1212), *snf7*Δ/Δ (DAY568), and *nhx1*Δ/Δ (DAY1263). (B) 200 μl overnight YPD cultures were inoculated into 50 ml M199 pH 8 and grown 5 hours at 30°C. Cell pellets were collected and resuspended in 50 ml M199 pH 4 for 60 minutes growth at 30°C. Subsequent steps and strains investigated are identical to those described in panel A.

observed the appearance of the active, 74 kDa band. A *snf7*Δ/Δ strain is unable to process Rim101 to either its 74 kDa or 65 kDa form, as previously reported (REF), and we observed only full-length Rim101 at both ph 4 and pH 8 in this strain. In the *nhx1*Δ/Δ strain, we observed a banding pattern similar to that of the wild-type strain at both pH 4 and pH 8. Thus, *nhx1*Δ/Δ does not affect Rim101 activation after exposure to alkaline environment.

We next hypothesized that the *nhx1*Δ/Δ strain may affect Rim101 signaling attenuation. To test this, we first grew the cells in M199 pH 8 to exponential phase, then shifted them to M199 pH 4 for 1 hour. Again, equivalent protein concentrations were tested by Western blot analysis. In the wild-type strain at pH 8, we observed the same three Rim101 banding pattern as after a one-hour shift, at 85, 74, and 65 kDa (Figure 29B). In the wild-type strain at pH 4, we observed only the full-length band, indicating that all active Rim101 was degraded after a 1-hour shift. In the *snf7*Δ/Δ strain, we observed only the full-length band at both pH 8 and pH 4. In the *nhx1*Δ/Δ strain at pH 8, we observed the same banding pattern as the wild-type strain. We further noted that the *nhx1*Δ/Δ strain had no active Rim101 band after a 1-hour shift to pH 4. This suggests that Nhx1 does not play a role in either activating or attenuating Rim101 processing, and confirms that the observed phenotypic defects (Figures 27 and 28) are not due to Rim101 processing defects.

Although we did not observe any defects in Rim101 processing, we did note a difference in full-length Rim101 signal between the tested strains. In both the acidic-to-alkaline shift (Figure 29A) and the alkaline-to-acidic shift (Figure 29B), the wild-type showed equivalent or less full-length Rim101 in the pH 8 sample than in the pH 4

sample. The *nhx1*Δ/Δ strain, however, displayed equivalent or more full-length Rim101 in the pH 8 sample than in the pH 4 sample. Full-length Rim101 signal was also strongly increased in the *snf7*Δ/Δ sample at both pH 4 and pH 8. This accumulation is independent of the ability to process Rim101, since both the *snf7*Δ/Δ strain and *nhx1*Δ/Δ strain displayed stronger full-length signal than the wild-type strain.

e. Epithelial damage. We wished to test the effect of the *nhx1*Δ/Δ mutation on *C. albicans* interactions with epithelial cells. *C. albicans* damages epithelial cells both by secreting degradative enzymes and by inducing epithelial cell endocytosis, leading to epithelial membrane rupture by filamenting *C. albicans* cells (127, 151). We hypothesized that the *nhx1*Δ/Δ strain would have a slight defect in damaging epithelial cells based on the intermediate serum-induced filamentation defect (Figure 28B). To test this, we incubated 1 x 10^5 *C. albicans* cells/ml with ^{51}Cr-radiolabeled FaDu epithelial cells and measured the amount of radioactivity specifically released into the coculture supernatant. In a representative assay, the wild-type strain caused 30% specific ^{51}Cr release, while the *rim101*Δ/Δ strain did not cause any specific ^{51}Cr release above background levels (Figure 30A). The *nhx1*Δ/Δ strain caused 2% specific ^{51}Cr release ($P < 2^{-5}$). This decrease held over multiple assays, where the *nhx1*Δ/Δ mutant caused an average of 2% the wild-type specific release ($P < 2^{-12}$) (J. M. Wolf, data not shown). This defect was partially rescued by expression of an exogenous copy of *NHX1* (Figure 30B). Therefore, *NHX1* is required for normal epithelial cell damage.

We hypothesized that the epithelial damage defect of the *nhx1*Δ/Δ strain is due to poor growth of the strain in the presence of 5% CO_2. We tested this by plating five-fold dilutions onto two sets of YPD, M199 pH 4, and M199 pH 8 plates. We chose M199

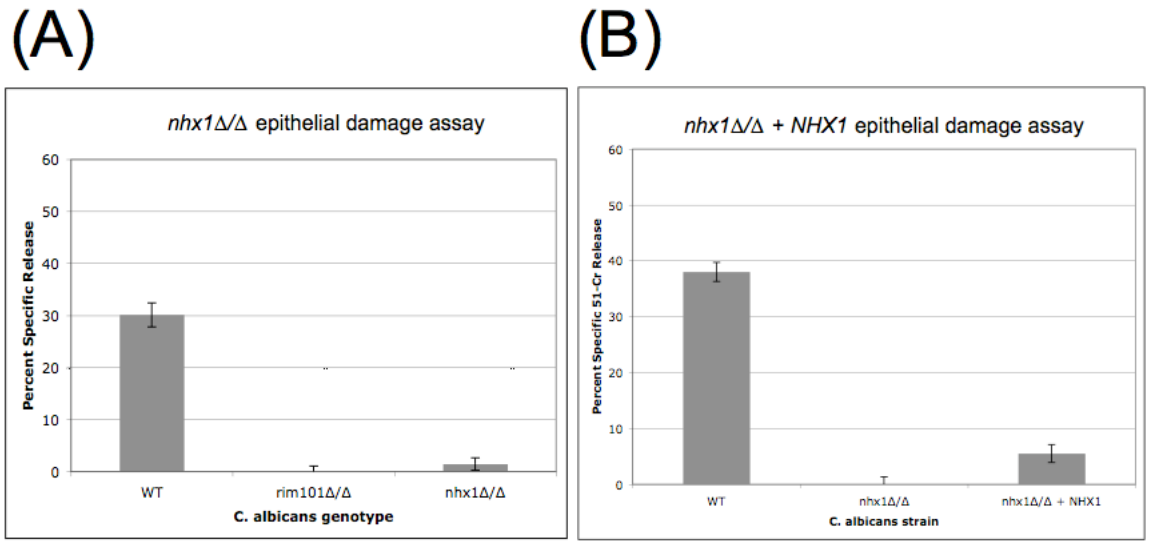

Figure 30. *NHX1* is required for wild-type damage of FaDu epithelial cells. (A) FaDu monolayers were ^{51}Cr-labeled overnight, and then washed and incubated with 10^5 cells/mL *C. albicans* for 10 hours. Strains were tested in triplicate for each individual assay and compared with uninfected wells to measure specific ^{51}Cr release. The assay was repeated three times. A representative assay is pictured. Strains investigated include wild type (DAY185), *rim101*Δ/Δ (DAY25), and *nhx1*Δ/Δ (DAY1159). (B) The reversion mutant only partially complements the *nhx1*Δ/Δ damage defect. The assay was run as described in A. Strains investigated include wild type (DAY185), *nhx1*Δ/Δ (DAY1159), and *nhx1*Δ/Δ + *NHX1* (DAY1267).

because it more closely mimicked the tissue culture medium (DMEM) in which the FaDu experiments were conducted, and we used both pH 4 and pH 8 buffered media because the pH of the DMEM medium visibly decreases during the epithelial cell damage assay. We then incubated one set of plates at 37°C at atmospheric CO_2 concentrations (0.3%) and one set of plates at 37°C at 5% CO_2 for 2 days.

After incubation, we observed robust growth of the wild-type strain on all media, with and without high CO_2 concentrations (Figure 31). We noted no significant growth defects among any of the mutant strains tested, including the *rim101*Δ/Δ and *nhx1*Δ/Δ mutant strains. Growth of the *rim101*Δ/Δ strain on the alkaline M199 plate was expected, as this strain grows but does not filament on M199 pH 8 medium (Figure 28A). This confirms that the defect in filamentation and epithelial cell damage are not due to the *nhx1*Δ/Δ strain incubation in 5% CO_2.

We considered that the *nhx1*Δ/Δ epithelial cell damage defect could be due to poor filamentation in the tissue culture medium. We had observed a serum-induced filamentation defect on 4% BCS plates, and the tissue culture medium contains 10% FBS. We tested this by growing *C. albicans* strains in tissue culture medium with and without the presence of FaDu epithelial cells. Overnight YPD cultures were diluted to 10^5 cells/ml and incubated with and without the presence of FaDu cells. After 10 hours, we observed robust filamentation of the wild type in medium alone, with a noticeable filamentation defect in the *rim101*Δ/Δ strain (Figure 28C). The *nhx1*Δ/Δ strain produced hyphae in the medium alone, but these hyphae were not as long or as branched as the wild-type hyphae. The complemented strain partially rescued this filamentation defect in

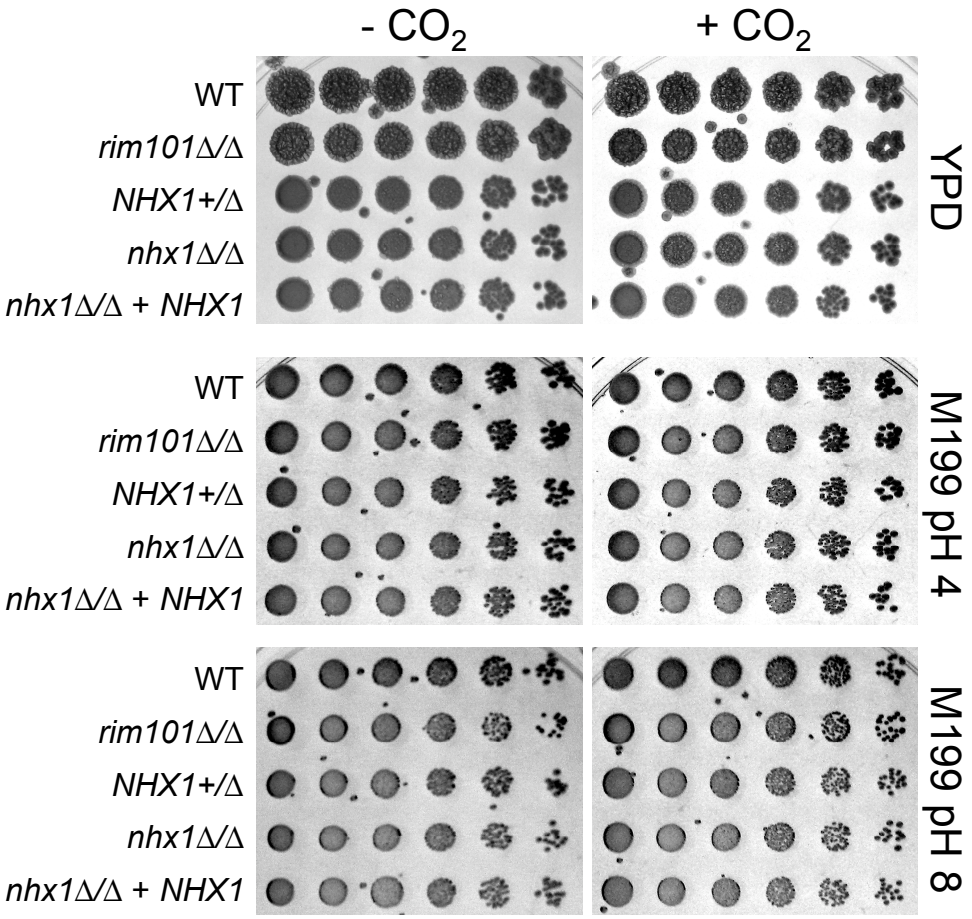

Figure 31. *NHX1* is not required for growth in the presence of CO_2. Overnight YPD cultures were diluted 1:50 in PBS and fivefold dilutions were spotted onto YPD, M199 pH 4, or M199 pH 8. Two sets of plates were generated, with one incubated at 37°C at ambient CO_2 levels, and the other incubated at 37°C at 5% CO_2. Plates were incubated at 37°C for two days before photographing. Strain investigated include WT (DAY185), *rim101*Δ/Δ (DAY25), *NHX1*+/Δ (DAY 1261), *nhx1*Δ/Δ (DAY1159), and *nhx1*Δ/Δ + *NHX1* (DAY1267).

medium alone (Figure 28C). This supports our hypothesis that *NHX1* is required for serum-induced filamentation.

These phenotypes were exacerbated by the presence of FaDu epithelial cells, which caused slower growth of all strains. Wild type filamentation was slightly less robust in the presence of FaDu cells than in medium alone, with slightly shorter and fewer hyphae. The *rim101*Δ/Δ filamentation was visibly decreased from wild-type filamentation. The *nhx1*Δ/Δ filamentation was also noticeably decreased from wild-type filamentation, which was again only partially rescued by the complementation strain (Figure 28C). This filamentation defect in the presence of epithelial cells may explain the decreased damage by the *nhx1*Δ/Δ strain.

IV. Discussion

We had hypothesized the role Nhx1 plays in regulating the endosomal lumen is conserved in *C. albicans* and that this role may affect Rim101 processing. The idea that the internal vesicle environment can regulate external vesicle interactions is not novel to these studies: binding of COPI coat proteins to the early endosome membranes in mammalian cells, has been shown to depend on endosomal lumen pH (5, 72). We were unable to detect an effect of *nhx1*Δ/Δ deletion on Rim101 processing. However, the *C. albicans nhx1*Δ/Δ mutant differed from the previously described *nhx1*Δ *S. cerevisiae* mutant in that the strain did not display a class E phenotype with FM 4-64 staining, suggesting its function may not be conserved, but the increased sensitivity to LiCl suggests CaNhx1 is involved in ion sequestration. Although we did not detect a decrease in Rim101 processing, we did observe a decrease in serum-induced filamentation, which

likely explains why the *nhx1*Δ/Δ mutant strain was severely deficient in damaging epithelial cells.

The increased sensitivity of the *nhx1*Δ/Δ strain to LiCl adaptation supports the idea that *CaNHX1* is a cation pump. Why does the *C. albicans nhx1*Δ/Δ strain not display the class E phenotype observed in *S. cerevisiae*? Although the closest sequence homolog was targeted for mutation, we may have targeted a sodium pump not localized to the endosome. No studies were performed to localize *NHX1* and an increase in salt sensitivity could occur from mutations in numerous sodium pumps. Alternatively, a second *C. albicans* homolog may regulate endosomal ion concentrations, such that the *nhx1*Δ/Δ mutant is more sensitive to sodium stress but not to levels that affect vesicle trafficking. Finally, the *nhx1*Δ/Δ strain may have a trafficking defect undetected in these studies. *NHX1* was not identified in the initial screen for class E trafficking proteins, in part because its phenotypes, while similar, are slightly weaker than other class E mutants (24). Assays such as carboxypeptidase Y secretion and Ste3-GFP trafficking have also been used in *S. cerevisiae* to confirm endosome-to-vacuole trafficking defects, and similar additional trafficking studies could further define the role of *NHX1* in *C. albicans*.

The increased full-length Rim101 observed in the *nhx1*Δ/Δ strain supports the idea that *NHX1* plays a role in endosome-to-vacuole trafficking. Rim101 localizes to the cytoplasm under acidic conditions and to the nucleus when activated by processing (205). However, if Rim101 is processed at the endosome, some Rim101 protein may inadvertently be incorporated into endosome and subsequently degraded. This idea is supported by the increased full-length signal seen in the *snf7*Δ/Δ strain, which has a known trafficking defect. Further support is lent by the observation that Rim101 pathway

member Rim8 has been observed in the vacuole, and that this vacuolar localization is dependent on ESCRT trafficking (J. Gomez-Raja, in preparation). However, future studies must be done to determine whether vacuolar degradation truly plays a part in Rim101 expression.

This is the first study to our knowledge to investigate shut-off of Rim101 processing. Our Western analyses suggest that all active Rim101 is gone from the cell 1 hour after switch to an acidic environment (Figure 29B). This is particularly interesting in light of recently published data on *S. cerevisiae* Rim8 ubiquitination. Rim8 ubiquitination was shown to last up to three hours after switch to an acidic environment (78). Our data suggest that, despite possible signaling, active Rim101 is destroyed quickly after switch to a non-processing environment.

Why did the *nhx1*Δ/Δ strain, which displayed an intermediate filamentation defect, have such a strong epithelial damage defect? *NHX1* may influence virulence traits other than filamentation in *C. albicans.* The *vps4*Δ/Δ *C. albicans* strain is unable to secrete SAPs 4-6 due to its trafficking defects (106). If *NHX* plays a role in trafficking undetected in our studies, the *nhx1*Δ/Δ strain may be attenuated in filamentation and protease secretion. Alternatively, the *C. albicans* filamentation defects observed with serum-containing media may be compounded when fungal cells are incubated with FaDu cells.

How could *NHX1* influence filamentation? Serum-induced filamentation is regulated in part by the cAMP/PKA pathway, which involves cAMP production by the adenylyl cyclase *CYR1* (161). Serum-induced signaling requires *RAS1* activation of *CYR1*, but *CYR1* can also be activated directly by carbon dioxide by way of bicarbonate

production (58, 95). If *CaNHX1* deletion leads to cytoplasmic acidification as observed in *S. cerevisiae*, this may decrease cAMP-inducing bicarbonate ions. One way to test this would be to measure cAMP concentrations within the *nhx1*Δ/Δ strain and compare this to a *cyr1*Δ/Δ strain or an *nce103*Δ/Δ strain. *NCE103* is a carbonic anhydrase that accelerates formation of bicarbonate in solution, and is required for normal filamentation in 5% CO_2 (95). This speculative mechanism requires further experimentation to verify the function of *NHX1* in *C. albicans*. Additionally, this does not fully explain the filamentation defect on BCS agar, which was not incubated in the presence of CO_2.

The function of *NHX1* remains unclear in *C. albicans*. It is clear that *NHX1* plays a role in adaptation to LiCl stress unrelated to Rim101 processing. These studies suggest a role for *NHX1* in serum-induced filamentation, which makes *NHX1* a good candidate for future studies.

CHAPTER 5

These studies were undertaken with several goals in mind. The first was to determine whether *C. albicans* ESCRT and Rim101 pathways were separable. The second was to determine the contribution of the ESCRT pathway to *C. albicans* virulence. Our studies have examined the ESCRT pathway at a molecular level and used these findings to ask questions regarding the ESCRT pathway, the Rim101 pathway, and *C. albicans* pathogenesis.

I. Can the ESCRT and Rim101 pathways be separated?

At the onset of these studies, the model of endosomal Rim101 processing had recently been suggested by several studies of ESCRT mutants. These studies, combined with large-scale interactomes from *S. cerevisiae*, suggested that Rim101 processing and ESCRT complex formation intersected at the molecular hub of Snf7. Mutations in Rim101 processing did not disrupt vesicle trafficking; neither did mutations in ESCRT-IIIb or ESCRT-DS components prohibit Rim101 processing (98, 165, 207). However, the role of Snf7 in directing these downstream interactions was unclear. The molecular dissection of *SNF7* through mutagenesis was conducted to better understand the role of this hub in both pathways.

Snf7 downstream interactions were predicted to function in two simple models. In the first model, Snf7 interacts with Rim101 processing machinery or ESCRT machinery at common Snf7 domains, and thus mutagenesis will disrupt all downstream interactions, signifying no functional separation. In the second model, Snf7 interacts with Rim101 processing machinery or ESCRT machinery at distinct Snf7 domains, and thus

mutagenesis will affect only a specific downstream interaction, signifying functional separation. The studies from Chapter 2 support a more complex blend of these two models, in which Rim20-Snf7 interactions overlap with ESCRT-specific Snf7 interactions but Rim13-Snf7 interactions do not.

The model based on our *snf7* alanine allele work (Figure 15) suggests that Rim13 interacts with a Snf7 domain completely separable from ESCRT function, but that Rim20 interacts with a Snf7 domain shared among bro1-domain containing proteins. This is the first demonstration that the fungal-specific Rim101 pathway interacts with the conserved ESCRT pathway through at least one Snf7 domain not required for MVB forrmation. The bro1-domain has been suggested by others to act as an adaptor domain, mediating interactions between Snf7 and various bro1-domain proteins (Rim20 and Bro1 in fungi; Alix, Brox, and HD-PTP in higher eukaryotes) (26, 54, 85, 122, 146). The C-terminal Snf7 domain mediates bro1-domain interactions in the human ESCRT pathway (122), thus I was not surprised that mutations in this region suggested overlapping function between Rim101 and ESCRT pathways. I attempted to complement our genetic studies with protein interaction studies, but was unable to generate functionally tagged Rim20 or Rim13. This is particularly unfortunate with regards to Rim13, the strongest candidate for separation of Rim101 function, since we identified an allele that would facilitate testing this hypothesis.

The accumulated data presented here demonstrate separation of the ESCRT and Rim101 pathways is possible through several approaches. Our studies on *SNF7* in Chapter 2 demonstrated that discrete Snf7 domains are independently required for ESCRT and Rim101-specific functions. The studies on ESCRT deletion mutants in

Chapter 3 demonstrate that genetic separation of ESCRT function from Rim101 function can also occur upstream and downstream of *SNF7*. Deletion of ESCRT-DS member *VPS4* does not disrupt Rim101 processing but does dysregulate processing to make it signal-independent. However, other ESCRT-DS members, *BRO1* and *DOA4*, neither disrupt nor dysregulate Rim101 processing, and thus are candidates to study ESCRT function independent of Rim101 function in the cell. Additionally, ESCRT function is separable from Rim101 function upstream of Snf7. ESCRT-0 component Vps27 had been previously characterized as dispensable for Rim101 processing in *S. cerevisiae*; here I confirm this in *C. albicans* and expand this characterization to the other ESCRT-0 member, Hse1. Thus, ESCRT function can be disrupted without affecting Rim101 signaling both upstream and downstream of Snf7 and the Rim101 processing complex.

How could ESCRT-I and -II, but not ESCRT-0, be required for Rim101 processing, as demonstrated in Chapter 3? Members of all three complexes interact with ubiquitin (Vps27 and Hse1 in ESCRT-0; Mvb12 and Vps23 in ESCRT-I; Vps36 in ESCRT-II) (16, 69, 88, 94, 174), and no ESCRT complex formation has been reported in the absence of ubiquitin. Thus, the Rim101 signaling complex must either be ubiquitinated directly or mimic ubiquitin structure to recruit downstream complexes. Both the *A. nidulans* and *S. cerevisiae* Rim8 proteins, part of the Rim101 signaling complex, have been reported to undergo ubiquitination (78, 79), and it is likely that this ubiquitination is conserved in *C. albicans* Rim8 based on sequence homology. This ubiquitination may both be a signal for endocytosis and a means of direct Rim8 interaction with ESCRT machinery, thus facilitating a connection between the spatially segregated signaling and processing complexes.

The signal that recruits Rim101 members instead of (or in addition to) ESCRT members remains unknown. It may be that endocytosis of Rim8 and Rim21, shown to interact in *A. nidulans* and *C. albicans* (79), occurs only at alkaline pH, and that this endocytosis recruits downstream Rim101 processing machinery. Data from our lab, however, suggest that Rim8 is degraded via trafficking to the vacuole in both acidic and alkaline environments (J. Gomez-Raja, in preparation), implying that Rim8 undergoes endocytosis and incorporation into MVBs constitutively. Another possibility is that while undergoing constitutive endocytosis, Rim8 receives a pH-specific modification that leads to subsequent recruitment of downstream Rim101 machinery. This seems a more likely possibility, as Rim8 ubiquitination in *S. cerevisiae* is pH-independent (78), but Rim8 phosphorylation is pH-dependent in both *A. nidulans* and *C. albicans* (79). Thus, I favor a model combining these observations, in which Rim8 is constitutively ubiquitinated and taken up by endocytosis and is phosphorylated in a pH-dependent manner to drive Rim101 signaling.

How might Rim8 modification recruit the Rim101 processing complex? Modification of Rim8 may allow it to directly interact with complex members, which, after Rim8 recruitment, are passed to ESCRT-III members (Figure 32A). Rim8 interactions with Rim13 and/or Rim20 may have gone undetected, since large-scale interactomes do not account for possible structural changes induced by post-translational modifications. Another possibility is that Rim8 modification interferes with ESCRT-IIIb capping of Snf7 oligomers, promoting large Snf7 filaments as observed in the *vps4*Δ *S. cerevisiae* strain (Figure 32B). A requirement of large Snf7 oligomer scaffolds for

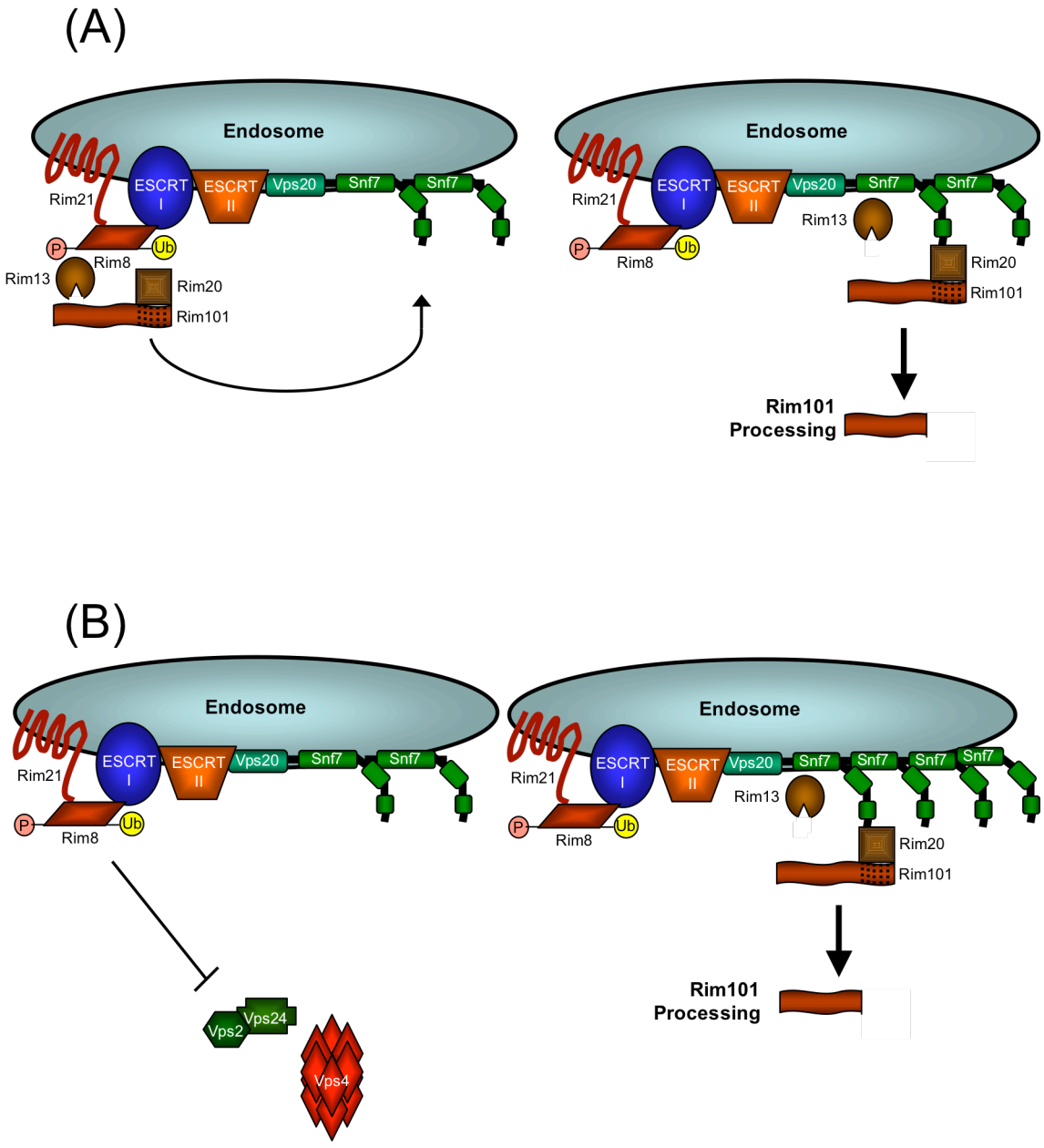

Figure 32. Two possible models of Rim101 processing. (A) Model of direct Rim8 recruitment of the processing complex. After recruiting ESCRT complexes to the endosome, modified Rim8 recruits Rim13 and Rim20 directly. Rim8 passes Rim13 and Rim20 to Snf7, where they form the processing complex and activate Rim101. (B) Model of indirect Rim8 recruitment of the processing complex. Modified Rim8 at the endosome interferes with Vps2, Vps24, and Vps4 recruitment, facilitating large oligomers of Snf7 to form. These large oligomers recruit Rim13 and Rim20, which assemble into the processing complex and activate Rim101.

Rim101 processing would also explain why constitutive Rim101 processing is observed in *vps4*Δ/Δ *C. albicans* and *S. cerevisiae* strains.

Constitutive Rim101 processing in the *vps4*Δ/Δ strain has previously been ascribed to the inability of these cells to dissociate Snf7 from endosomes. Recently, the *vps4*Δ *S. cerevisiae* strain was shown to not only contain more endosomal than cytoplasmic Snf7, but the Snf7 oligomers of this strain were shown to contain more Snf7 than the wild type. I hypothesized that the endosomal lumen could influence ESCRT function, possibly through Snf7 filament size, and thus affect Rim101 processing. Our investigations with the *nhx1*Δ/Δ mutant, however, did not demonstrate a role for Nhx1 in Rim101 processing. Other genes, such as *VMA3* and *VMA5*, may be better candidates, as they directly affect vesicle acidification. Testing a *VMA* role in endosomal acidification would be technically challenging, as these genes also acidify the vacuole, and vacuolar acidification is also necessary for pH adaptation and ion stress response. Thus, endosomal lumen content remains a possible factor in regulating Rim101 processing complex formation.

An unexplored area in the connection between Rim101 processing and the ESCRT pathway is the role played by independent endocytosis processes. Endocytosis is classified into clathrin-dependent endocytosis (CDE) or clatherin-independent endocytosis (CIE). Both CDE and CIE mediate receptor internalization and subsequent vacuolar degradation, and receptors can rely on shared CDE/CIE or on a single endocytosis process for downregulation (134, 177). An interesting question is whether the Rim101 signaling complex relies on CDE, CIE, or both for internalization to signaling endosomes. Determining a role in Rim101 processing for clathrin or another

endocytosis-associated protein, such as caveolin, could both suggest mechanistic roles played by signaling complex members and determine the cellular location of Rim101 processing (discussed in more detail on page 153).

The role of CDE and/or CIE in Rim101 processing will become clearer as the role of these different endocytosis mechanisms in vacuolar trafficking is defined. Interactions between clathrin and Vps27 or Hse1 have been observed in both human cell lines and in *S. cerevisiae* (17, 123, 156). Therefore, CDE proteins are known to interact directly with the ESCRT machinery. These interactions are thought to increase Vps27 concentration at the endosomal membrane, thereby increasing efficiency in recruiting downstream ESCRT complexes (156). Interactions between CIE-associated proteins and the ESCRT pathway have yet to be uncovered. One CIE-associated protein, CIE, has been found localized within MVBs (23), but whether this localization is ESCRT-dependent has yet to be determined.

II. Will the molecular interactions between ESCRT and Rim101 pathways be applicable to all fungi with a Rim101 pathway?

Snf7 or other ESCRT members have been shown to play a role in Rim101 processing in many commonly studied fungi (*C. albicans*, *S. cerevisiae*, *Y. lipolytica*, *A. nidulans*) (21, 98, 162, 207). However, protein interaction partners have likely changed as fungal kingdom members have diverged through evolutionary time. Characterized Rim13 interactions are an illustration of this divergence.

In *A. nidulans*, Rim13 has been shown to interact with ESCRT-IIIb member Vps24, and Snf7/Vps32-Rim13 interactions are not detectable. Rim13-Vps24 interactions

are dependent on the *A. nidulans* Rim13 MIT domain, which has not been identified in either *C. albicans* or *S. cerevisiae* Rim13 (162). Snf7/Vps32 interactions with Rim13 have been identified in *S. cerevisiae* and *Y. lipolytica* (20, 86), and are supported by constitutive Rim101 processing observed in a *vps24*Δ *S. cerevisiae* mutant (77), which would presumably not process Rim101 if Vps24 were required to recruit Rim13. Thus, while ESCRT-III is required to facilitate Rim101 processing, the ESCRT-III member varies between fungal species. Additional differences in pathway interactions among fungal species are likely to be discovered as research continues.

The Rim101 pathway has been suggested to be an antifungal target, as Rim101 is a signaling pathway conserved among fungi that is required for wild-type virulence of *C. albicans* and *A. fumagatus*. However, differences in Rim13-ESCRT-III interactions between species, and the interaction of the human Calpain 7 protease with hVps24 in epithelial cells (209), suggests that the processing complex may not be an ideal antifungal target. Other means of disrupting Rim101 activation, such as targeting the signaling complex, may prove more effective and confer broader specificity. Protease activity is a feasible target for antimicrobial activity, as a recently rediscovered antibacterial drug demonstrates. ADEP-1 works in several Gram-positive bacteria by dysregulating protease activity required for sigma factor activation (30), supporting the viability of the processing complex as a drug target.

III. Where does Rim101 processing occur?

No definitive studies have demonstrated the intracellular location of Rim101 processing. Until recently, most data supported a model in which Rim101 processing

occurs at the endosomal membrane. Several recent finding have proposed a new model, in which Rim101 processing occurs at the plasma membrane. Both hypotheses have supporting data and technical caveats, and neither is conclusive.

Rim101 processing was first suggested to occur at the endosome upon discovery of the ESCRT machinery requirement for processing (165, 207). This was later supported by pH-dependent colocalization of *S. cerevisiae* Snf7 and Rim20 in a spotted pattern within the cell (26), which the authors argued represented intracellular endosomes. However, these colocalizations were performed using C-terminal fluorescently tagged proteins, and Snf7 activity has been shown to be altered by addition of C-terminal tags (205). C-terminal tags interfere with the ability of Snf7 to fold into its closed, inactive form, and lead to constitutive Snf7 active form, which increases Snf7 membrane association. The *vps4*Δ/Δ mutant also has increased membrane-associated Snf7 (Figure 11), which is thought to be the driving mechanism of signal-independent Rim101 processing in this strain. These colocalization studies may therefore be an artifact resulting from increased Snf7 membrane association. However, endosomal processing is further supported by the *A. nidulans* Rim13 cofractionations with endosomal marker Pep12 and *C. albicans* Rim8-GFP trafficking to the vacuole. Thus, data from several fungal species supports Rim101 processing at the endosome.

Rim101 processing at the plasma membrane was first suggested by studies performed in *A. nidulans*. These studies identified a bro1-domain-containing protein, PalC, as a Snf7-interacting protein, and suggested that PalC localizes to cortical structures at or near the plasma membrane (63). Concentrated PalC spots around the cell perimeter are dependent on both pH and upstream signaling member PalH (Rim21).

These data are supported by the colocalization of Rim8 and ESCRT-I member Vps23 at the plasma membrane in *S. cerevisiae* (78). However, both of these studies replied on overexpression constructs with C-terminal fluorescent tags, and both overexpression and sequence additions may drive incorrect localization. For example, human Snf7 shows indiscriminant membrane localization when overexpressed in mammalian cells, although not when expressed at endogenous levels (110). Thus, these data may also have been affected through technique.

Proponents of plasma membrane processing argue the expendability of ESCRT-0 lends support to this theory, based on similar observations in ESCRT-complex-hijacking viruses, such as human immunodeficiency virus (HIV). HIV is one of several viruses that can recruit the ESCRT-I complex directly to the plasma membrane through HIV protein Gag recruitment of ESCRT-I member Vps23. Similar sequence motifs were found to be involved in Vps23 interaction in Vps27, Gag, and Rim8 (16, 78, 120). However, HIV and other enveloped viruses hijack the ESCRT machinery to facilitate virion budding at the plasma membrane, thus utilizing the membrane scission function of the ESCRT complexes. No speculation is made regarding why membrane scission machinery is involved, yet no ESCRT complex formation has been reported that does not utilize ESCRT membrane scission function. In light of *A. nidulans* Rim13 recruitment by ESCRT-IIIb member Vps24, it seems unlikely that Rim101 processing and vesicle formation/membrane scission are not tightly coupled in this organism. Plasma membrane processing also does not explain the ESCRT-dependent accumulation of CaRim8-GFP in the vacuole. The ability of the Rim101 signaling complex to bypass ESCRT-0 is also similar to the recruitment of Vps23 by Cep55 during the final abscission step in

cytokinesis (128). The ESCRT core complexes involved in membrane scission thus can function in various processes after recruitment by ESCRT-0-like adaptor complexes. In light of the above, more evidence currently exists in support of endosomal localization than plasma membrane localization for Rim101 processing.

IV. How does the ESCRT pathway contribute to *C. albicans* virulence?

These studies were undertaken in part to determine what role, if any, the ESCRT pathway plays during *C. albicans* pathogenesis. Previous studies have demonstrated that both *vps28*Δ/Δ and *snf7*Δ/Δ mutant *C. albicans* strains are less virulent than the already attenuated *rim101*Δ/Δ mutant strain (40). The *vps28*Δ/Δ and *snf7*Δ/Δ strains conferred a lower death rate than the *rim101*Δ/Δ strain in a mouse model of bloodstream infection. These strains also had lower fungal burdens in the kidney than the *rim101*Δ/Δ strain, and histological sections demonstrated the *vps28*Δ/Δ and *snf7*Δ/Δ strains had a more pronounced filamentation defect than the *rim101*Δ/Δ strain (40). The authors of this study concluded that the increased defects were due to ESCRT-specific defects in addition to the Rim101-specific defects. While this is a reasonable hypothesis, the authors of the study failed to investigate the ESCRT-dependent defects of the *vps28*Δ/Δ and *snf7*Δ/Δ *C. albicans* strains to verify these defects. I sought to more definitively study ESCRT function independent of Rim101 function in *C. albicans* pathogenesis.

Our studies looked at minimally two members of each ESCRT complex, as well as downstream members required for MVB formation (called ESCRT-DS in this text). By phenotypically screening many ESCRT mutants, I established that mutations in ESCRT-0 components (Vps27 and Hse1) or ESCRT-DS components (Vps4, Bro1, and

Doa4) do not prevent Rim101 processing, although ESCRT-DS member Vps4 dysregulates processing, leading to constitutive Rim101 activation. All of these mutations, except that in *HSE1*, led to decreased epithelial cell damage levels, and these decreases were not statistically different from one another. The only similar function described for these genes is in MVB formation through ESCRT complex formation. From the similar damage decreases and functions described, I conclude that the ESCRT pathway is required for wild-type levels of epithelial cell damage.

The conservation of ESCRT homologs among the eukarya and some archaea suggests this pathway is vital for normal cellular function. ESCRT-0 and ESCRT-DS mutations did not affect growth at alkaline pH or filamentation, however, and thus do not explain the observed damage defects. This leads to the question: What role could the ESCRT pathway play during *C. albicans*-epithelial cell interaction?

ESCRT mutations may affect *C. albicans* ability to withstand epithelial-mediated killing by secretion of antimicrobial peptides, such as histatins or surfactants. ESCRT mutations, but not Rim101 mutations, increase susceptibility to SDS (41), and thus may affect susceptibility to other detergents, such as surfactant. Oral epithelial cells, although not specifically FaDu cells, have been reported to secrete surfactant (109). Thus the ESCRT pathway may affect *C. albicans* survival in conditions untested during these studies.

Alternatively, ESCRT mutations may affect *C. albicans* ability to damage the FaDu cells, either by affecting growth or morphology in an undetected manner or affecting *C. albicans*-epithelial cell interactions. I addressed the first possibility by testing for alkaline growth, alkaline-induced filamentation, and serum-induced filamentation,

resulting in no difference between the ESCRT-0/ESCRT-DS mutants and the wild type. However, the medium used during the cell damage assay is slightly different than those used during phenotyping, and may present additional components that inhibit growth or filamentation. ESCRT-mediated trafficking may play a Rim101-independent role in cell wall maintenance. Cell-wall-anchored proteins, such as the Rim101-regulated Als3, interact with epithelial cell N-cadherin to mediate *C. albicans* endocytosis, which exacerbates epithelial cell damage. The increased sensitivity of the *C. albicans vps28*Δ/Δ and *snf7*Δ/Δ mutants, but not of the *rim101*Δ/Δ mutant, to caspofungin, a cell-wall targeting antifungal, argues an ESCRT-dependent cell wall defect exists in these strains (41). ESCRT mutations may thus alter cell wall components, though not necessarily Als3, and disrupt normal *C. albicans*-epithelial cell interactions.

Further studies on the *vps27*Δ/Δ mutant strain demonstrated that *VPS27* is required for wild-type colonization and maintenance of colonization levels in an *in vivo* oropharyngeal candidiasis mouse model. The mechanism behind *VPS27* function during infection is not known, but several speculations can be made based on our data and previous studies. *VPS27* may be required to establish normal *C. albicans*-epithelial cell interactions in the oral cavity. I have established that a *vps27*Δ/Δ strain causes less damage to epithelial cells. Epithelial damage may be required for the initial colonization of these cells, indicating that less damage results in a lower fungal burden. Alternatively, *VPS27* may be required to traffick nutrients taken up by endocytosis, such as iron, to the vacuole. Our studies in Chapter 3 demonstrate *VPS27* is required for growth in an iron-limited environment. Additionally, plasma membrane receptors Rbt5 and Rbt51 are required for the delivery of hemoglobin to the vacuole, and this delivery depends on

ESCRT machinery (202). The decreased virulence of the *vps27*Δ/Δ strain may be due to a growth defect in the iron-poor environment of the host. Multiple mechanisms may therefore account for the *vps27*Δ/Δ strain defect in *C. albicans* pathogenesis.

Would ESCRT-DS mutants, which also separated ESCRT function from Rim101 processing, display a similar decrease in virulence during infection? As discussed above, the ESCRT pathway can function in multiple cellular processes, with similarly structured proteins recruiting the core ESCRT complexes. *VPS27* is likely specific for endosome-to-vacuole ESCRT function during MVB biogenesis, while several of the ESCRT-DS members have been reported to function in other ESCRT-dependent processes, such as cytokinesis and viral budding. However, neither ESCRT-dependent cytokinesis nor viral budding have been reported in *C. albicans*, suggesting that *BRO1* and *DOA4* function only in MVB formation in *C. albicans*. Based on our analyses of ESCRT gene function, I would predict a similar virulence defect among the *vps27*Δ/Δ, *bro1*Δ/Δ, and *doa4*Δ/Δ mutant strains. Because *VPS4* mutation results in constitutive Rim101 activation, this strain does not fully decouple the two pathways, and mechanisms of *vps4*Δ/Δ virulence defects are hard to distinguish.

The role of *NHX1* in *C. albicans*-epithelial cell interactions is more difficult to define. The serum-induced filamentation defect may be a clue to *C. albicans NHX1* function; however, the mechanism behind the filamentation defect is unclear. The *nhx1*Δ/Δ strain caused no increase over spontaneous epithelial cell damage, similar to the *rim101*Δ/Δ strain. However, Rim101 processing was normal in the *nhx1*Δ/Δ strain, suggesting that *NHX1* plays a role as stringently required as Rim101 processing for epithelial damage, but that this role is Rim101-independent. The lack of an FM 4-64

trafficking defect suggests *NHX1* function may not be conserved between *S. cerevisiae* and *C. albicans*. Thus, while *NHX1* requirement for cell damage has been demonstrated, its role during epithelial cells remains unknown.

With these studies, I have confirmed that the ESCRT pathway is separable from the Rim101 pathway in *C. albicans*. Using this data, I demonstrated that the ESCRT pathway plays an entirely Rim101-independent role in pathogenesis, although this role is smaller than that of Rim101 processing. ESCRT pathway function is required for *in vitro* epithelial cell damage, as well as during *in vivo* infection. I have generated a model based on these results (Figure 33), illustrating the roles played by endosome-associated proteins in MVB formation and Rim101 processing, and subsequent contribution to *C. albicans* virulence.

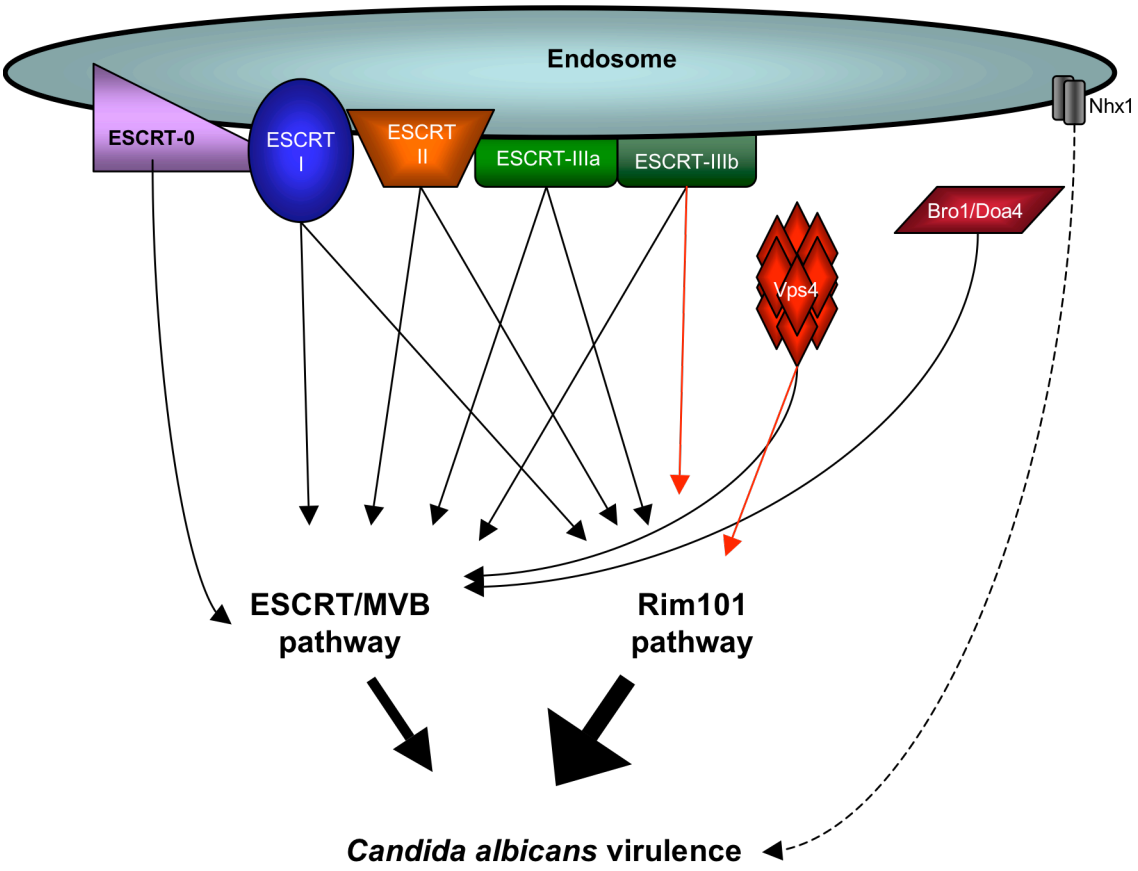

Figure 33. Model of ESCRT complex contributions to pathogenesis. Black arrows drawn from the ESCRT complexes represent a role for that complex in a given pathway. Red arrows drawn from the ESCRT complexes represent a regulatory role for that complex in Rim101 processing. Pathway contribution to *C. albicans* virulence is represented by heavy black arrows. The heavier arrow represents the greater contribution. The dashed arrow represents Nhx1 contribution to virulence by an unknown mechanism.

REFERENCES

1. **Adams, A., D. E. Gottschling, C. A. Kaiser, and T. Stearns.** 1997. Methods in Yeast Genetics, 1997: A Cold Spring Harbor Laboratory Course Manual. Cold Spring Harbor Laboratory Press.
2. **Almeida, R. S., S. Brunke, A. Albrecht, S. Thewes, M. Laue, J. E. Edwards, S. G. Filler, and B. Hube.** 2008. the hyphal-associated adhesin and invasin Als3 of Candida albicans mediates iron acquisition from host ferritin. PLoS Pathog **4:**e1000217.
3. **Amerik, A., N. Sindhi, and M. Hochstrasser.** 2006. A conserved late endosome-targeting signal required for Doa4 deubiquitylating enzyme function. J Cell Biol **175:**825-35.
4. **Andrutis, K. A., P. J. Riggle, C. A. Kumamoto, and S. Tzipori.** 2000. Intestinal lesions associated with disseminated candidiasis in an experimental animal model. J Clin Microbiol **38:**2317-23.
5. **Aniento, F., F. Gu, R. G. Parton, and J. Gruenberg.** 1996. An endosomal beta COP is involved in the pH-dependent formation of transport vesicles destined for late endosomes. J Cell Biol **133:**29-41.
6. **Arechiga-Carvajal, E. T., and J. Ruiz-Herrera.** 2005. The RIM101/pacC homologue from the basidiomycete Ustilago maydis is functional in multiple pH-sensitive phenomena. Eukaryot Cell **4:**999-1008.
7. **Azmi, I., B. Davies, C. Dimaano, J. Payne, D. Eckert, M. Babst, and D. J. Katzmann.** 2006. Recycling of ESCRTs by the AAA-ATPase Vps4 is regulated by a conserved VSL region in Vta1. J Cell Biol **172:**705-17.
8. **Babst, M., D. J. Katzmann, E. J. Estepa-Sabal, T. Meerloo, and S. D. Emr.** 2002. Escrt-III: an endosome-associated heterooligomeric protein complex required for mvb sorting. Dev Cell **3:**271-82.
9. **Babst, M., D. J. Katzmann, W. B. Snyder, B. Wendland, and S. D. Emr.** 2002. Endosome-associated complex, ESCRT-II, recruits transport machinery for protein sorting at the multivesicular body. Dev Cell **3:**283-9.
10. **Babst, M., B. Wendland, E. J. Estepa, and S. D. Emr.** 1998. The Vps4p AAA ATPase regulates membrane association of a Vps protein complex required for normal endosome function. Embo J **17:**2982-93.
11. **Baek, Y. U., M. Li, and D. A. Davis.** 2008. Candida albicans ferric reductases are differentially regulated in response to distinct forms of iron limitation by the Rim101 and CBF transcription factors. Eukaryot Cell **7:**1168-79.
12. **Barajas, D., Y. Jiang, and P. D. Nagy.** 2009. A unique role for the host ESCRT proteins in replication of Tomato bushy stunt virus. PLoS Pathog **5:**e1000705.
13. **Barwell, K. J., J. H. Boysen, W. Xu, and A. P. Mitchell.** 2005. Relationship of DFG16 to the Rim101p pH response pathway in Saccharomyces cerevisiae and Candida albicans. Eukaryot Cell **4:**890-9.
14. **Bensen, E. S., S. J. Martin, M. Li, J. Berman, and D. A. Davis.** 2004. Transcriptional profiling in Candida albicans reveals new adaptive responses to extracellular pH and functions for Rim101p. Mol Microbiol **54:**1335-51.

15. **Bernardo, S. M., Z. Khalique, J. Kot, J. K. Jones, and S. A. Lee.** 2008. Candida albicans VPS1 contributes to protease secretion, filamentation, and biofilm formation. Fungal Genet Biol **45:**861-77.
16. **Bilodeau, P. S., J. L. Urbanowski, S. C. Winistorfer, and R. C. Piper.** 2002. The Vps27p Hse1p complex binds ubiquitin and mediates endosomal protein sorting. Nat Cell Biol **4:**534-9.
17. **Bilodeau, P. S., S. C. Winistorfer, W. R. Kearney, A. D. Robertson, and R. C. Piper.** 2003. Vps27-Hse1 and ESCRT-I complexes cooperate to increase efficiency of sorting ubiquitinated proteins at the endosome. J Cell Biol **163:**237-43.
18. **Biswas, S., P. Van Dijck, and A. Datta.** 2007. Environmental sensing and signal transduction pathways regulating morphopathogenic determinants of Candida albicans. Microbiol Mol Biol Rev **71:**348-76.
19. **Blanc, C., S. J. Charette, S. Mattei, L. Aubry, E. W. Smith, P. Cosson, and F. Letourneur.** 2009. Dictyostelium Tom1 participates to an ancestral ESCRT-0 complex. Traffic **10:**161-71.
20. **Blanchin-Roland, S., G. Da Costa, and C. Gaillardin.** 2008. Ambient pH signalling in the yeast Yarrowia lipolytica involves YlRim23p/PalC, which interacts with Snf7p/Vps32p, but does not require the long C terminus of YlRim9p/PalI. Microbiology **154:**1668-76.
21. **Blanchin-Roland, S., G. Da Costa, and C. Gaillardin.** 2005. ESCRT-I components of the endocytic machinery are required for Rim101-dependent ambient pH regulation in the yeast Yarrowia lipolytica. Microbiology **151:**3627-37.
22. **Borg-von Zepelin, M., S. Beggah, K. Boggian, D. Sanglard, and M. Monod.** 1998. The expression of the secreted aspartyl proteinases Sap4 to Sap6 from Candida albicans in murine macrophages. Mol Microbiol **28:**543-54.
23. **Botos, E., J. Klumperman, V. Oorschot, B. Igyarto, A. Magyar, M. Olah, and A. L. Kiss.** 2008. Caveolin-1 is transported to multi-vesicular bodies after albumin-induced endocytosis of caveolae in HepG2 cells. J Cell Mol Med **12:**1632-9.
24. **Bowers, K., B. P. Levi, F. I. Patel, and T. H. Stevens.** 2000. The sodium/proton exchanger Nhx1p is required for endosomal protein trafficking in the yeast Saccharomyces cerevisiae. Mol Biol Cell **11:**4277-94.
25. **Bowers, K., J. Lottridge, S. B. Helliwell, L. M. Goldthwaite, J. P. Luzio, and T. H. Stevens.** 2004. Protein-protein interactions of ESCRT complexes in the yeast Saccharomyces cerevisiae. Traffic **5:**194-210.
26. **Boysen, J. H., and A. P. Mitchell.** 2006. Control of Bro1-domain protein Rim20 localization by external pH, ESCRT machinery, and the Saccharomyces cerevisiae Rim101 pathway. Mol Biol Cell **17:**1344-53.
27. **Braun, B. R., and A. D. Johnson.** 1997. Control of filament formation in Candida albicans by the transcriptional repressor TUP1. Science **277:**105-9.
28. **Braun, B. R., D. Kadosh, and A. D. Johnson.** 2001. NRG1, a repressor of filamentous growth in C.albicans, is down-regulated during filament induction. Embo J **20:**4753-61.

29. **Brett, C. L., D. N. Tukaye, S. Mukherjee, and R. Rao.** 2005. The yeast endosomal Na+K+/H+ exchanger Nhx1 regulates cellular pH to control vesicle trafficking. Mol Biol Cell **16:**1396-405.
30. **Brotz-Oesterhelt, H., D. Beyer, H. P. Kroll, R. Endermann, C. Ladel, W. Schroeder, B. Hinzen, S. Raddatz, H. Paulsen, K. Henninger, J. E. Bandow, H. G. Sahl, and H. Labischinski.** 2005. Dysregulation of bacterial proteolytic machinery by a new class of antibiotics. Nat Med **11:**1082-7.
31. **Bruckmann, A., W. Kunkel, A. Hartl, R. Wetzker, and R. Eck.** 2000. A phosphatidylinositol 3-kinase of Candida albicans influences adhesion, filamentous growth and virulence. Microbiology **146 (Pt 11):**2755-64.
32. **Brzezinski, A., T. Stern, R. Arbel, G. Rahav, and S. Benita.** 2004. Efficacy of a novel pH-buffering tampon in preserving the acidic vaginal pH during menstruation. Int J Gynaecol Obstet **85:**298-300.
33. **Calcagno-Pizarelli, A. M., S. Negrete-Urtasun, S. H. Denison, J. D. Rudnicka, H. J. Bussink, T. Munera-Huertas, L. Stanton, A. Hervas-Aguilar, E. A. Espeso, J. Tilburn, H. N. Arst, Jr., and M. A. Penalva.** 2007. Establishment of the ambient pH signaling complex in Aspergillus nidulans: PalI assists plasma membrane localization of PalH. Eukaryot Cell **6:**2365-75.
34. **Calderone, R.** 2002. Candida and candidiasis. ASM Press.
35. **Caracuel, Z., M. I. Roncero, E. A. Espeso, C. I. Gonzalez-Verdejo, F. I. Garcia-Maceira, and A. Di Pietro.** 2003. The pH signalling transcription factor PacC controls virulence in the plant pathogen Fusarium oxysporum. Mol Microbiol **48:**765-79.
36. **Carlisle, P. L., M. Banerjee, A. Lazzell, C. Monteagudo, J. L. Lopez-Ribot, and D. Kadosh.** 2009. Expression levels of a filament-specific transcriptional regulator are sufficient to determine Candida albicans morphology and virulence. Proc Natl Acad Sci U S A **106:**599-604.
37. **Castrejon, F., A. Gomez, M. Sanz, A. Duran, and C. Roncero.** 2006. The RIM101 pathway contributes to yeast cell wall assembly and its function becomes essential in the absence of mitogen-activated protein kinase Slt2p. Eukaryot Cell **5:**507-17.
38. **Chen, Y. C., C. C. Wu, W. L. Chung, and F. J. Lee.** 2002. Differential secretion of Sap4-6 proteins in Candida albicans during hyphae formation. Microbiology **148:**3743-54.
39. **Chu, T., J. Sun, S. Saksena, and S. D. Emr.** 2006. New component of ESCRT-I regulates endosomal sorting complex assembly. J Cell Biol **175:**815-23.
40. **Cornet, M., F. Bidard, P. Schwarz, G. Da Costa, S. Blanchin-Roland, F. Dromer, and C. Gaillardin.** 2005. Deletions of endocytic components VPS28 and VPS32 affect growth at alkaline pH and virulence through both RIM101-dependent and RIM101-independent pathways in Candida albicans. Infect Immun **73:**7977-87.
41. **Cornet, M., C. Gaillardin, and M. L. Richard.** 2006. Deletions of the endocytic components VPS28 and VPS32 in Candida albicans lead to echinocandin and azole hypersensitivity. Antimicrob Agents Chemother **50:**3492-5.

42. **Cornet, M., M. L. Richard, and C. Gaillardin.** 2009. The homologue of the Saccharomyces cerevisiae RIM9 gene is required for ambient pH signalling in Candida albicans. Res Microbiol **160:**219-23.
43. **Croall, D. E., and K. Ersfeld.** 2007. The calpains: modular designs and functional diversity. Genome Biol **8:**218.
44. **Cuff, J. A., and G. J. Barton.** 2000. Application of multiple sequence alignment profiles to improve protein secondary structure prediction. Proteins **40:**502-11.
45. **Curtiss, M., C. Jones, and M. Babst.** 2007. Efficient cargo sorting by ESCRT-I and the subsequent release of ESCRT-I from multivesicular bodies requires the subunit Mvb12. Mol Biol Cell **18:**636-45.
46. **Dabas, N., and J. Morschhauser.** 2007. Control of ammonium permease expression and filamentous growth by the GATA transcription factors GLN3 and GAT1 in Candida albicans. Eukaryot Cell **6:**875-88.
47. **Davis, D.** 2003. Adaptation to environmental pH in Candida albicans and its relation to pathogenesis. Curr Genet **44:**1-7.
48. **Davis, D., J. E. Edwards, Jr., A. P. Mitchell, and A. S. Ibrahim.** 2000. Candida albicans RIM101 pH response pathway is required for host-pathogen interactions. Infect Immun **68:**5953-9.
49. **Davis, D., R. B. Wilson, and A. P. Mitchell.** 2000. RIM101-dependent and-independent pathways govern pH responses in Candida albicans. Mol Cell Biol **20:**971-8.
50. **Davis, D. A.** 2009. How human pathogenic fungi sense and adapt to pH: the link to virulence. Curr Opin Microbiol **12:**365-70.
51. **Davis, D. A., V. M. Bruno, L. Loza, S. G. Filler, and A. P. Mitchell.** 2002. Candida albicans Mds3p, a conserved regulator of pH responses and virulence identified through insertional mutagenesis. Genetics **162:**1573-81.
52. **Denison, S. H., S. Negrete-Urtasun, J. M. Mingot, J. Tilburn, W. A. Mayer, A. Goel, E. A. Espeso, M. A. Penalva, and H. N. Arst, Jr.** 1998. Putative membrane components of signal transduction pathways for ambient pH regulation in Aspergillus and meiosis in saccharomyces are homologous. Mol Microbiol **30:**259-64.
53. **Dimaano, C., C. B. Jones, A. Hanono, M. Curtiss, and M. Babst.** 2008. Ist1 regulates vps4 localization and assembly. Mol Biol Cell **19:**465-74.
54. **Doyotte, A., A. Mironov, E. McKenzie, and P. Woodman.** 2008. The Bro1-related protein HD-PTP/PTPN23 is required for endosomal cargo sorting and multivesicular body morphogenesis. Proc Natl Acad Sci U S A **105:**6308-13.
55. **Dukes, J. D., J. D. Richardson, R. Simmons, and P. Whitley.** 2008. A dominant-negative ESCRT-III protein perturbs cytokinesis and trafficking to lysosomes. Biochem J **411:**233-9.
56. **Edmond, M. B., S. E. Wallace, D. K. McClish, M. A. Pfaller, R. N. Jones, and R. P. Wenzel.** 1999. Nosocomial bloodstream infections in United States hospitals: a three-year analysis. Clin Infect Dis **29:**239-44.
57. **Enjalbert, B., G. P. Moran, C. Vaughan, T. Yeomans, D. M. Maccallum, J. Quinn, D. C. Coleman, A. J. Brown, and D. J. Sullivan.** 2009. Genome-wide gene expression profiling and a forward genetic screen show that differential

expression of the sodium ion transporter Ena21 contributes to the differential tolerance of Candida albicans and Candida dubliniensis to osmotic stress. Mol Microbiol **72:**216-28.

58. **Fang, H. M., and Y. Wang.** 2006. RA domain-mediated interaction of Cdc35 with Ras1 is essential for increasing cellular cAMP level for Candida albicans hyphal development. Mol Microbiol **61:**484-96.
59. **Ferwerda, B., G. Ferwerda, T. S. Plantinga, J. A. Willment, A. B. van Spriel, H. Venselaar, C. C. Elbers, M. D. Johnson, A. Cambi, C. Huysamen, L. Jacobs, T. Jansen, K. Verheijen, L. Masthoff, S. A. Morre, G. Vriend, D. L. Williams, J. R. Perfect, L. A. Joosten, C. Wijmenga, J. W. van der Meer, G. J. Adema, B. J. Kullberg, G. D. Brown, and M. G. Netea.** 2009. Human dectin-1 deficiency and mucocutaneous fungal infections. N Engl J Med **361:**1760-7.
60. **Fidel, P. L., Jr.** 2005. Immunity in vaginal candidiasis. Curr Opin Infect Dis **18:**107-11.
61. **Fujita, H., M. Yamanaka, K. Imamura, Y. Tanaka, A. Nara, T. Yoshimori, S. Yokota, and M. Himeno.** 2003. A dominant negative form of the AAA ATPase SKD1/VPS4 impairs membrane trafficking out of endosomal/lysosomal compartments: class E vps phenotype in mammalian cells. J Cell Sci **116:**401-14.
62. **Futai, E., T. Maeda, H. Sorimachi, K. Kitamoto, S. Ishiura, and K. Suzuki.** 1999. The protease activity of a calpain-like cysteine protease in Saccharomyces cerevisiae is required for alkaline adaptation and sporulation. Mol Gen Genet **260:**559-68.
63. **Galindo, A., A. Hervas-Aguilar, O. Rodriguez-Galan, O. Vincent, H. N. Arst, Jr., J. Tilburn, and M. A. Penalva.** 2007. PalC, one of two Bro1 domain proteins in the fungal pH signalling pathway, localizes to cortical structures and binds Vps32. Traffic **8:**1346-64.
64. **Gary, J. D., A. E. Wurmser, C. J. Bonangelino, L. S. Weisman, and S. D. Emr.** 1998. Fab1p is essential for PtdIns(3)P 5-kinase activity and the maintenance of vacuolar size and membrane homeostasis. J Cell Biol **143:**65-79.
65. **Gerrard, S. R., N. J. Bryant, and T. H. Stevens.** 2000. VPS21 controls entry of endocytosed and biosynthetic proteins into the yeast prevacuolar compartment. Mol Biol Cell **11:**613-26.
66. **Gerrard, S. R., B. P. Levi, and T. H. Stevens.** 2000. Pep12p is a multifunctional yeast syntaxin that controls entry of biosynthetic, endocytic and retrograde traffic into the prevacuolar compartment. Traffic **1:**259-69.
67. **Ghazi-Tabatabai, S., S. Saksena, J. M. Short, A. V. Pobbati, D. B. Veprintsev, R. A. Crowther, S. D. Emr, E. H. Egelman, and R. L. Williams.** 2008. Structure and disassembly of filaments formed by the ESCRT-III subunit Vps24. Structure **16:**1345-56.
68. **Giaever, G., A. M. Chu, L. Ni, C. Connelly, L. Riles, S. Veronneau, S. Dow, A. Lucau-Danila, K. Anderson, B. Andre, A. P. Arkin, A. Astromoff, M. El-Bakkoury, R. Bangham, R. Benito, S. Brachat, S. Campanaro, M. Curtiss, K. Davis, A. Deutschbauer, K. D. Entian, P. Flaherty, F. Foury, D. J. Garfinkel, M. Gerstein, D. Gotte, U. Guldener, J. H. Hegemann, S. Hempel, Z. Herman, D. F. Jaramillo, D. E. Kelly, S. L. Kelly, P. Kotter, D. LaBonte, D. C. Lamb,**

N. Lan, H. Liang, H. Liao, L. Liu, C. Luo, M. Lussier, R. Mao, P. Menard, S. L. Ooi, J. L. Revuelta, C. J. Roberts, M. Rose, P. Ross-Macdonald, B. Scherens, G. Schimmack, B. Shafer, D. D. Shoemaker, S. Sookhai-Mahadeo, R. K. Storms, J. N. Strathern, G. Valle, M. Voet, G. Volckaert, C. Y. Wang, T. R. Ward, J. Wilhelmy, E. A. Winzeler, Y. Yang, G. Yen, E. Youngman, K. Yu, H. Bussey, J. D. Boeke, M. Snyder, P. Philippsen, R. W. Davis, and M. Johnston. 2002. Functional profiling of the Saccharomyces cerevisiae genome. Nature **418:**387-91.

69. **Gill, D. J., H. Teo, J. Sun, O. Perisic, D. B. Veprintsev, S. D. Emr, and R. L. Williams.** 2007. Structural insight into the ESCRT-I/-II link and its role in MVB trafficking. Embo J **26:**600-12.
70. **Gow, N. A., A. J. Brown, and F. C. Odds.** 2002. Fungal morphogenesis and host invasion. Curr Opin Microbiol **5:**366-71.
71. **Gow, N. A., M. G. Netea, C. A. Munro, G. Ferwerda, S. Bates, H. M. Mora-Montes, L. Walker, T. Jansen, L. Jacobs, V. Tsoni, G. D. Brown, F. C. Odds, J. W. Van der Meer, A. J. Brown, and B. J. Kullberg.** 2007. Immune recognition of Candida albicans beta-glucan by dectin-1. J Infect Dis **196:**1565-71.
72. **Gu, F., F. Aniento, R. G. Parton, and J. Gruenberg.** 1997. Functional dissection of COP-I subunits in the biogenesis of multivesicular endosomes. J Cell Biol **139:**1183-95.
73. **Gunther, J., M. Nguyen, A. Hartl, W. Kunkel, P. F. Zipfel, and R. Eck.** 2005. Generation and functional in vivo characterization of a lipid kinase defective phosphatidylinositol 3-kinase Vps34p of Candida albicans. Microbiology **151:**81-9.
74. **Hanson, P. I., R. Roth, Y. Lin, and J. E. Heuser.** 2008. Plasma membrane deformation by circular arrays of ESCRT-III protein filaments. J Cell Biol **180:**389-402.
75. **Haro, R., B. Garciadeblas, and A. Rodriguez-Navarro.** 1991. A novel P-type ATPase from yeast involved in sodium transport. FEBS Lett **291:**189-91.
76. **Hartmann, C., M. Chami, U. Zachariae, B. L. de Groot, A. Engel, and M. G. Grutter.** 2008. Vacuolar protein sorting: two different functional states of the AAA-ATPase Vps4p. J Mol Biol **377:**352-63.
77. **Hayashi, M., T. Fukuzawa, H. Sorimachi, and T. Maeda.** 2005. Constitutive activation of the pH-responsive Rim101 pathway in yeast mutants defective in late steps of the MVB/ESCRT pathway. Mol Cell Biol **25:**9478-90.
78. **Herrador, A., S. Herranz, D. Lara, and O. Vincent.** 2009. Recruitment of the ESCRT machinery to a putative seven-transmembrane-domain receptor is mediated by an arrestin-related protein. Mol Cell Biol.
79. **Herranz, S., J. M. Rodriguez, H. J. Bussink, J. C. Sanchez-Ferrero, H. N. Arst, Jr., M. A. Penalva, and O. Vincent.** 2005. Arrestin-related proteins mediate pH signaling in fungi. Proc Natl Acad Sci U S A **102:**12141-6.
80. **Herrero, E., J. Ros, G. Belli, and E. Cabiscol.** 2008. Redox control and oxidative stress in yeast cells. Biochim Biophys Acta **1780:**1217-35.

81. **Horn, D. L., D. Neofytos, E. J. Anaissie, J. A. Fishman, W. J. Steinbach, A. J. Olyaei, K. A. Marr, M. A. Pfaller, C. H. Chang, and K. M. Webster.** 2009. Epidemiology and outcomes of candidemia in 2019 patients: data from the prospective antifungal therapy alliance registry. Clin Infect Dis **48:**1695-703.
82. **Howard, D. H.** 1999. Acquisition, transport, and storage of iron by pathogenic fungi. Clin Microbiol Rev **12:**394-404.
83. **Hruskova-Heidingsfeldova, O.** 2008. Secreted proteins of Candida albicans. Front Biosci **13:**7227-42.
84. **Hurley, J. H.** 2008. ESCRT complexes and the biogenesis of multivesicular bodies. Curr Opin Cell Biol **20:**4-11.
85. **Ichioka, F., R. Kobayashi, K. Katoh, H. Shibata, and M. Maki.** 2008. Brox, a novel farnesylated Bro1 domain-containing protein that associates with charged multivesicular body protein 4 (CHMP4). Febs J **275:**682-92.
86. **Ito, T., T. Chiba, R. Ozawa, M. Yoshida, M. Hattori, and Y. Sakaki.** 2001. A comprehensive two-hybrid analysis to explore the yeast protein interactome. Proc Natl Acad Sci U S A **98:**4569-74.
87. **Jensen, M. E., and C. F. Schachtele.** 1983. Plaque pH measurements by different methods on the buccal and approximal surfaces of human teeth after a sucrose rinse. J Dent Res **62:**1058-61.
88. **Katzmann, D. J., M. Babst, and S. D. Emr.** 2001. Ubiquitin-dependent sorting into the multivesicular body pathway requires the function of a conserved endosomal protein sorting complex, ESCRT-I. Cell **106:**145-55.
89. **Katzmann, D. J., C. J. Stefan, M. Babst, and S. D. Emr.** 2003. Vps27 recruits ESCRT machinery to endosomes during MVB sorting. J Cell Biol **162:**413-23.
90. **Kavanagh, K., and S. Dowd.** 2004. Histatins: antimicrobial peptides with therapeutic potential. J Pharm Pharmacol **56:**285-9.
91. **Kawasaki-Nishi, S., K. Bowers, T. Nishi, M. Forgac, and T. H. Stevens.** 2001. The amino-terminal domain of the vacuolar proton-translocating ATPase a subunit controls targeting and in vivo dissociation, and the carboxyl-terminal domain affects coupling of proton transport and ATP hydrolysis. J Biol Chem **276:**47411-20.
92. **Kim, J., S. Sitaraman, A. Hierro, B. M. Beach, G. Odorizzi, and J. H. Hurley.** 2005. Structural basis for endosomal targeting by the Bro1 domain. Dev Cell **8:**937-47.
93. **King, D. A., D. M. Hannum, J. S. Qi, and J. K. Hurst.** 2004. HOCl-mediated cell death and metabolic dysfunction in the yeast Saccharomyces cerevisiae. Arch Biochem Biophys **423:**170-81.
94. **Kirkin, V., and I. Dikic.** 2007. Role of ubiquitin- and Ubl-binding proteins in cell signaling. Curr Opin Cell Biol **19:**199-205.
95. **Klengel, T., W. J. Liang, J. Chaloupka, C. Ruoff, K. Schroppel, J. R. Naglik, S. E. Eckert, E. G. Mogensen, K. Haynes, M. F. Tuite, L. R. Levin, J. Buck, and F. A. Muhlschlegel.** 2005. Fungal adenylyl cyclase integrates CO2 sensing with cAMP signaling and virulence. Curr Biol **15:**2021-6.

96. **Kranz, A., A. Kinner, and R. Kolling.** 2001. A family of small coiled-coil-forming proteins functioning at the late endosome in yeast. Mol Biol Cell **12:**711-23.
97. **Kretschmar, M., B. Hube, T. Bertsch, D. Sanglard, R. Merker, M. Schroder, H. Hof, and T. Nichterlein.** 1999. Germ tubes and proteinase activity contribute to virulence of Candida albicans in murine peritonitis. Infect Immun **67:**6637-42.
98. **Kullas, A. L., M. Li, and D. A. Davis.** 2004. Snf7p, a component of the ESCRT-III protein complex, is an upstream member of the RIM101 pathway in Candida albicans. Eukaryot Cell **3:**1609-18.
99. **Kullas, A. L., S. J. Martin, and D. Davis.** 2007. Adaptation to environmental pH: integrating the Rim101 and calcineurin signal transduction pathways. Mol Microbiol **66:**858-71.
100. **Kullberg, B. J., and A. M. Oude Lashof.** 2002. Epidemiology of opportunistic invasive mycoses. Eur J Med Res **7:**183-91.
101. **Kumamoto, C. A., and M. D. Vinces.** 2005. Alternative Candida albicans lifestyles: growth on surfaces. Annu Rev Microbiol **59:**113-33.
102. **Lambert, M., S. Blanchin-Roland, F. Le Louedec, A. Lepingle, and C. Gaillardin.** 1997. Genetic analysis of regulatory mutants affecting synthesis of extracellular proteinases in the yeast Yarrowia lipolytica: identification of a RIM101/pacC homolog. Mol Cell Biol **17:**3966-76.
103. **Larsson, P. G., and J. J. Platz-Christensen.** 1991. The vaginal pH and leucocyte/epithelial cell ratio vary during normal menstrual cycles. Eur J Obstet Gynecol Reprod Biol **38:**39-41.
104. **Lata, S., M. Roessle, J. Solomons, M. Jamin, H. G. Gottlinger, D. I. Svergun, and W. Weissenhorn.** 2008. Structural basis for autoinhibition of ESCRT-III CHMP3. J Mol Biol **378:**818-27.
105. **Lata, S., M. Roessle, J. Solomons, M. Jamin, H. G. Gottlinger, D. I. Svergun, and W. Weissenhorn.** 2008. Structural basis for autoinhibition of ESCRT-III CHMP3. J Mol Biol **378:**816-25.
106. **Lee, S. A., J. Jones, S. Hardison, J. Kot, Z. Khalique, S. M. Bernardo, A. Lazzell, C. Monteagudo, and J. Lopez-Ribot.** 2008. Candida albicans VPS4 is Required for Secretion of Aspartyl Proteases and In Vivo Virulence. Mycopathologia.
107. **Li, M., S. J. Martin, V. M. Bruno, A. P. Mitchell, and D. A. Davis.** 2004. Candida albicans Rim13p, a protease required for Rim101p processing at acidic and alkaline pHs. Eukaryot Cell **3:**741-51.
108. **Li, W., and A. P. Mitchell.** 1997. Proteolytic activation of Rim1p, a positive regulator of yeast sporulation and invasive growth. Genetics **145:**63-73.
109. **Ligtenberg, A. J., E. C. Veerman, A. V. Nieuw Amerongen, and J. Mollenhauer.** 2007. Salivary agglutinin/glycoprotein-340/DMBT1: a single molecule with variable composition and with different functions in infection, inflammation and cancer. Biol Chem **388:**1275-89.
110. **Lin, Y., L. A. Kimpler, T. V. Naismith, J. M. Lauer, and P. I. Hanson.** 2005. Interaction of the mammalian endosomal sorting complex required for transport

(ESCRT) III protein hSnf7-1 with itself, membranes, and the AAA+ ATPase SKD1. J Biol Chem **280:**12799-809.

111. **Lindas, A. C., E. A. Karlsson, M. T. Lindgren, T. J. Ettema, and R. Bernander.** 2008. A unique cell division machinery in the Archaea. Proc Natl Acad Sci U S A **105:**18942-6.
112. **Liu, H.** 2002. Co-regulation of pathogenesis with dimorphism and phenotypic switching in Candida albicans, a commensal and a pathogen. Int J Med Microbiol **292:**299-311.
113. **Liu, H.** 2001. Transcriptional control of dimorphism in Candida albicans. Curr Opin Microbiol **4:**728-35.
114. **Liu, O. W., C. D. Chun, E. D. Chow, C. Chen, H. D. Madhani, and S. M. Noble.** 2008. Systematic genetic analysis of virulence in the human fungal pathogen Cryptococcus neoformans. Cell **135:**174-88.
115. **Lo, H. J., J. R. Kohler, B. DiDomenico, D. Loebenberg, A. Cacciapuoti, and G. R. Fink.** 1997. Nonfilamentous C. albicans mutants are avirulent. Cell **90:**939-49.
116. **Lotz, H., K. Sohn, H. Brunner, F. A. Muhlschlegel, and S. Rupp.** 2004. RBR1, a novel pH-regulated cell wall gene of Candida albicans, is repressed by RIM101 and activated by NRG1. Eukaryot Cell **3:**776-84.
117. **Luhtala, N., and G. Odorizzi.** 2004. Bro1 coordinates deubiquitination in the multivesicular body pathway by recruiting Doa4 to endosomes. J Cell Biol **166:**717-29.
118. **Manolson, M. F., B. Wu, D. Proteau, B. E. Taillon, B. T. Roberts, M. A. Hoyt, and E. W. Jones.** 1994. STV1 gene encodes functional homologue of 95-kDa yeast vacuolar H(+)-ATPase subunit Vph1p. J Biol Chem **269:**14064-74.
119. **Martin-Serrano, J., D. Perez-Caballero, and P. D. Bieniasz.** 2004. Context-dependent effects of L domains and ubiquitination on viral budding. J Virol **78:**5554-63.
120. **Martin-Serrano, J., T. Zang, and P. D. Bieniasz.** 2003. Role of ESCRT-I in retroviral budding. J Virol **77:**4794-804.
121. **Mavor, A. L., S. Thewes, and B. Hube.** 2005. Systemic fungal infections caused by Candida species: epidemiology, infection process and virulence attributes. Curr Drug Targets **6:**863-74.
122. **McCullough, J., R. D. Fisher, F. G. Whitby, W. I. Sundquist, and C. P. Hill.** 2008. ALIX-CHMP4 interactions in the human ESCRT pathway. Proc Natl Acad Sci U S A **105:**7687-91.
123. **McCullough, J., P. E. Row, O. Lorenzo, M. Doherty, R. Beynon, M. J. Clague, and S. Urbe.** 2006. Activation of the endosome-associated ubiquitin isopeptidase AMSH by STAM, a component of the multivesicular body-sorting machinery. Curr Biol **16:**160-5.
124. **Merson-Davies, L. A., and F. C. Odds.** 1989. A morphology index for characterization of cell shape in Candida albicans. J Gen Microbiol **135:**3143-52.
125. **Misra, S., and J. H. Hurley.** 1999. Crystal structure of a phosphatidylinositol 3-phosphate-specific membrane-targeting motif, the FYVE domain of Vps27p. Cell **97:**657-66.

126. **Mitchell, B. M., T. G. Wu, B. E. Jackson, and K. R. Wilhelmus.** 2007. Candida albicans strain-dependent virulence and Rim13p-mediated filamentation in experimental keratomycosis. Invest Ophthalmol Vis Sci **48:**774-80.
127. **Moreno-Ruiz, E., M. Galan-Diez, W. Zhu, E. Fernandez-Ruiz, C. d'Enfert, S. G. Filler, P. Cossart, and E. Veiga.** 2009. Candida albicans internalization by host cells is mediated by a clathrin-dependent mechanism. Cell Microbiol **11:**1179-89.
128. **Morita, E., V. Sandrin, H. Y. Chung, S. G. Morham, S. P. Gygi, C. K. Rodesch, and W. I. Sundquist.** 2007. Human ESCRT and ALIX proteins interact with proteins of the midbody and function in cytokinesis. Embo J **26:**4215-27.
129. **Morita, E., and W. I. Sundquist.** 2004. Retrovirus budding. Annu Rev Cell Dev Biol **20:**395-425.
130. **Muhlrad, D., R. Hunter, and R. Parker.** 1992. A rapid method for localized mutagenesis of yeast genes. Yeast **8:**79-82.
131. **Muhlschlegel, F. A., and W. A. Fonzi.** 1997. PHR2 of Candida albicans encodes a functional homolog of the pH-regulated gene PHR1 with an inverted pattern of pH-dependent expression. Mol Cell Biol **17:**5960-7.
132. **Munn, A. L., and H. Riezman.** 1994. Endocytosis is required for the growth of vacuolar H(+)-ATPase-defective yeast: identification of six new END genes. J Cell Biol **127:**373-86.
133. **Muziol, T., E. Pineda-Molina, R. B. Ravelli, A. Zamborlini, Y. Usami, H. Gottlinger, and W. Weissenhorn.** 2006. Structural basis for budding by the ESCRT-III factor CHMP3. Dev Cell **10:**821-30.
134. **Myromslien, F. D., L. M. Grovdal, C. Raiborg, H. Stenmark, I. H. Madshus, and E. Stang.** 2006. Both clathrin-positive and -negative coats are involved in endosomal sorting of the EGF receptor. Exp Cell Res **312:**3036-48.
135. **Nass, R., and R. Rao.** 1998. Novel localization of a Na+/H+ exchanger in a late endosomal compartment of yeast. Implications for vacuole biogenesis. J Biol Chem **273:**21054-60.
136. **Nikko, E., and B. Andre.** 2007. Split-ubiquitin two-hybrid assay to analyze protein-protein interactions at the endosome: application to Saccharomyces cerevisiae Bro1 interacting with ESCRT complexes, the Doa4 ubiquitin hydrolase, and the Rsp5 ubiquitin ligase. Eukaryot Cell **6:**1266-77.
137. **Nobile, C. J., N. Solis, C. L. Myers, A. J. Fay, J. S. Deneault, A. Nantel, A. P. Mitchell, and S. G. Filler.** 2008. Candida albicans transcription factor Rim101 mediates pathogenic interactions through cell wall functions. Cell Microbiol **10:**2180-96.
138. **Obita, T., S. Saksena, S. Ghazi-Tabatabai, D. J. Gill, O. Perisic, S. D. Emr, and R. L. Williams.** 2007. Structural basis for selective recognition of ESCRT-III by the AAA ATPase Vps4. Nature **449:**735-9.
139. **Odorizzi, G., M. Babst, and S. D. Emr.** 1998. Fab1p PtdIns(3)P 5-kinase function essential for protein sorting in the multivesicular body. Cell **95:**847-58.

140. **Odorizzi, G., D. J. Katzmann, M. Babst, A. Audhya, and S. D. Emr.** 2003. Bro1 is an endosome-associated protein that functions in the MVB pathway in Saccharomyces cerevisiae. J Cell Sci **116:**1893-903.
141. **Oestreich, A. J., B. A. Davies, J. A. Payne, and D. J. Katzmann.** 2007. Mvb12 is a novel member of ESCRT-I involved in cargo selection by the multivesicular body pathway. Mol Biol Cell **18:**646-57.
142. **Ohsumi, Y., and Y. Anraku.** 1981. Active transport of basic amino acids driven by a proton motive force in vacuolar membrane vesicles of Saccharomyces cerevisiae. J Biol Chem **256:**2079-82.
143. **Ohsumi, Y., and Y. Anraku.** 1983. Calcium transport driven by a proton motive force in vacuolar membrane vesicles of Saccharomyces cerevisiae. J Biol Chem **258:**5614-7.
144. **Palmer, G. E., M. N. Kelly, and J. E. Sturtevant.** 2005. The Candida albicans vacuole is required for differentiation and efficient macrophage killing. Eukaryot Cell **4:**1677-86.
145. **Park, H., C. L. Myers, D. C. Sheppard, Q. T. Phan, A. A. Sanchez, E. E. J, and S. G. Filler.** 2005. Role of the fungal Ras-protein kinase A pathway in governing epithelial cell interactions during oropharyngeal candidiasis. Cell Microbiol **7:**499-510.
146. **Peck, J. W., E. T. Bowden, and P. D. Burbelo.** 2004. Structure and function of human Vps20 and Snf7 proteins. Biochem J **377:**693-700.
147. **Penalva, M. A., and H. N. Arst, Jr.** 2004. Recent advances in the characterization of ambient pH regulation of gene expression in filamentous fungi and yeasts. Annu Rev Microbiol **58:**425-51.
148. **Perlroth, J., B. Choi, and B. Spellberg.** 2007. Nosocomial fungal infections: epidemiology, diagnosis, and treatment. Med Mycol **45:**321-46.
149. **Pfaller, M. A., and D. J. Diekema.** 2007. Epidemiology of invasive candidiasis: a persistent public health problem. Clin Microbiol Rev **20:**133-63.
150. **Phan, Q. T., P. H. Belanger, and S. G. Filler.** 2000. Role of hyphal formation in interactions of Candida albicans with endothelial cells. Infect Immun **68:**3485-90.
151. **Phan, Q. T., C. L. Myers, Y. Fu, D. C. Sheppard, M. R. Yeaman, W. H. Welch, A. S. Ibrahim, J. E. Edwards, Jr., and S. G. Filler.** 2007. Als3 is a Candida albicans invasin that binds to cadherins and induces endocytosis by host cells. PLoS Biol **5:**e64.
152. **Polo, S., and P. P. Di Fiore.** 2006. Endocytosis conducts the cell signaling orchestra. Cell **124:**897-900.
153. **Porta, A., A. M. Ramon, and W. A. Fonzi.** 1999. PRR1, a homolog of Aspergillus nidulans palF, controls pH-dependent gene expression and filamentation in Candida albicans. J Bacteriol **181:**7516-23.
154. **Prior, C., S. Potier, J. L. Souciet, and H. Sychrova.** 1996. Characterization of the NHA1 gene encoding a Na+/H+-antiporter of the yeast Saccharomyces cerevisiae. FEBS Lett **387:**89-93.
155. **Raiborg, C., T. E. Rusten, and H. Stenmark.** 2003. Protein sorting into multivesicular endosomes. Curr Opin Cell Biol **15:**446-55.

156. **Raiborg, C., J. Wesche, L. Malerod, and H. Stenmark.** 2006. Flat clathrin coats on endosomes mediate degradative protein sorting by scaffolding Hrs in dynamic microdomains. J Cell Sci **119:**2414-24.
157. **Ramirez, M. A., and M. C. Lorenz.** 2007. Mutations in alternative carbon utilization pathways in Candida albicans attenuate virulence and confer pleiotropic phenotypes. Eukaryot Cell **6:**280-90.
158. **Ramon, A. M., A. Porta, and W. A. Fonzi.** 1999. Effect of environmental pH on morphological development of Candida albicans is mediated via the PacC-related transcription factor encoded by PRR2. J Bacteriol **181:**7524-30.
159. **Raymond, C. K., I. Howald-Stevenson, C. A. Vater, and T. H. Stevens.** 1992. Morphological classification of the yeast vacuolar protein sorting mutants: evidence for a prevacuolar compartment in class E vps mutants. Mol Biol Cell **3:**1389-402.
160. **Richter, C., M. West, and G. Odorizzi.** 2007. Dual mechanisms specify Doa4-mediated deubiquitination at multivesicular bodies. Embo J **26:**2454-64.
161. **Rocha, C. R., K. Schroppel, D. Harcus, A. Marcil, D. Dignard, B. N. Taylor, D. Y. Thomas, M. Whiteway, and E. Leberer.** 2001. Signaling through adenylyl cyclase is essential for hyphal growth and virulence in the pathogenic fungus Candida albicans. Mol Biol Cell **12:**3631-43.
162. **Rodriguez-Galan, O., A. Galindo, A. Hervas-Aguilar, H. N. Arst, and M. A. Penalva.** 2008. Physiological involvement in pH signalling of Vps24-mediated recruitment of Aspergillus PalB cysteine protease to ESCRT-III. J Biol Chem.
163. **Rollins, J. A.** 2003. The Sclerotinia sclerotiorum pac1 gene is required for sclerotial development and virulence. Mol Plant Microbe Interact **16:**785-95.
164. **Roman, E., D. M. Arana, C. Nombela, R. Alonso-Monge, and J. Pla.** 2007. MAP kinase pathways as regulators of fungal virulence. Trends Microbiol **15:**181-90.
165. **Rothfels, K., J. C. Tanny, E. Molnar, H. Friesen, C. Commisso, and J. Segall.** 2005. Components of the ESCRT pathway, DFG16, and YGR122w are required for Rim101 to act as a corepressor with Nrg1 at the negative regulatory element of the DIT1 gene of Saccharomyces cerevisiae. Mol Cell Biol **25:**6772-88.
166. **Saksena, S., J. Sun, T. Chu, and S. D. Emr.** 2007. ESCRTing proteins in the endocytic pathway. Trends Biochem Sci **32:**561-73.
167. **Samson, R. Y., T. Obita, S. M. Freund, R. L. Williams, and S. D. Bell.** 2008. A role for the ESCRT system in cell division in archaea. Science **322:**1710-3.
168. **Saville, S. P., A. L. Lazzell, C. Monteagudo, and J. L. Lopez-Ribot.** 2003. Engineered control of cell morphology in vivo reveals distinct roles for yeast and filamentous forms of Candida albicans during infection. Eukaryot Cell **2:**1053-60.
169. **Schaller, M., C. Borelli, H. C. Korting, and B. Hube.** 2005. Hydrolytic enzymes as virulence factors of Candida albicans. Mycoses **48:**365-77.
170. **Schneider, J. J., A. Unholzer, M. Schaller, M. Schafer-Korting, and H. C. Korting.** 2005. Human defensins. J Mol Med **83:**587-95.
171. **Scott, A., J. Gaspar, M. D. Stuchell-Brereton, S. L. Alam, J. J. Skalicky, and W. I. Sundquist.** 2005. Structure and ESCRT-III protein interactions of the MIT domain of human VPS4A. Proc Natl Acad Sci U S A **102:**13813-8.

172. **Sevilla, M. J., and F. C. Odds.** 1986. Development of Candida albicans hyphae in different growth media--variations in growth rates, cell dimensions and timing of morphogenetic events. J Gen Microbiol **132:**3083-8.
173. **Sheth, C. C., E. G. Mogensen, M. S. Fu, I. C. Blomfield, and F. A. Muhlschlegel.** 2008. Candida albicans HSP12 is co-regulated by physiological CO2 and pH. Fungal Genet Biol **45:**1075-80.
174. **Shields, S. B., A. J. Oestreich, S. Winistorfer, D. Nguyen, J. A. Payne, D. J. Katzmann, and R. Piper.** 2009. ESCRT ubiquitin-binding domains function cooperatively during MVB cargo sorting. J Cell Biol **185:**213-24.
175. **Shim, S., L. A. Kimpler, and P. I. Hanson.** 2007. Structure/function analysis of four core ESCRT-III proteins reveals common regulatory role for extreme C-terminal domain. Traffic **8:**1068-79.
176. **Shim, S., S. A. Merrill, and P. I. Hanson.** 2008. Novel Interactions of ESCRT-III with LIP5 and VPS4 and their Implications for ESCRT-III Disassembly. Mol Biol Cell **19:**2661-72.
177. **Sigismund, S., T. Woelk, C. Puri, E. Maspero, C. Tacchetti, P. Transidico, P. P. Di Fiore, and S. Polo.** 2005. Clathrin-independent endocytosis of ubiquitinated cargos. Proc Natl Acad Sci U S A **102:**2760-5.
178. **Sikorski, R. S., and P. Hieter.** 1989. A system of shuttle vectors and yeast host strains designed for efficient manipulation of DNA in Saccharomyces cerevisiae. Genetics **122:**19-27.
179. **Slagsvold, T., K. Pattni, L. Malerod, and H. Stenmark.** 2006. Endosomal and non-endosomal functions of ESCRT proteins. Trends Cell Biol **16:**317-26.
180. **Smolenski, G., P. A. Sullivan, S. M. Cutfield, and J. F. Cutfield.** 1997. Analysis of secreted aspartic proteinases from Candida albicans: purification and characterization of individual Sap1, Sap2 and Sap3 isoenzymes. Microbiology **143 (Pt 2):**349-56.
181. **Soong, T. W., T. F. Yong, N. Ramanan, and Y. Wang.** 2000. The Candida albicans antiporter gene CNH1 has a role in Na+ and H+ transport, salt tolerance, and morphogenesis. Microbiology **146 (Pt 5):**1035-44.
182. **Southern, P., J. Horbul, D. Maher, and D. A. Davis.** 2008. C. albicans colonization of human mucosal surfaces. PLoS ONE **3:**e2067.
183. **Spreghini, E., D. A. Davis, R. Subaran, M. Kim, and A. P. Mitchell.** 2003. Roles of Candida albicans Dfg5p and Dcw1p cell surface proteins in growth and hypha formation. Eukaryot Cell **2:**746-55.
184. **Stahelin, R. V., F. Long, K. Diraviyam, K. S. Bruzik, D. Murray, and W. Cho.** 2002. Phosphatidylinositol 3-phosphate induces the membrane penetration of the FYVE domains of Vps27p and Hrs. J Biol Chem **277:**26379-88.
185. **Stringaro, A., P. Crateri, G. Pellegrini, G. Arancia, A. Cassone, and F. De Bernardis.** 1997. Ultrastructural localization of the secretory aspartyl proteinase in Candida albicans cell wall in vitro and in experimentally infected rat vagina. Mycopathologia **137:**95-105.
186. **Stuchell-Brereton, M. D., J. J. Skalicky, C. Kieffer, M. A. Karren, S. Ghaffarian, and W. I. Sundquist.** 2007. ESCRT-III recognition by VPS4 ATPases. Nature **449:**740-4.

187. **Su, S. S., and A. P. Mitchell.** 1993. Identification of functionally related genes that stimulate early meiotic gene expression in yeast. Genetics **133:**67-77.
188. **Teis, D., S. Saksena, and S. D. Emr.** 2008. Ordered assembly of the ESCRT-III complex on endosomes is required to sequester cargo during MVB formation. Dev Cell **15:**578-89.
189. **Teo, H., O. Perisic, B. Gonzalez, and R. L. Williams.** 2004. ESCRT-II, an endosome-associated complex required for protein sorting: crystal structure and interactions with ESCRT-III and membranes. Dev Cell **7:**559-69.
190. **Teo, H., D. B. Veprintsev, and R. L. Williams.** 2004. Structural insights into endosomal sorting complex required for transport (ESCRT-I) recognition of ubiquitinated proteins. J Biol Chem **279:**28689-96.
191. **Tilburn, J., J. C. Sanchez-Ferrero, E. Reoyo, H. N. Arst, Jr., and M. A. Penalva.** 2005. Mutational analysis of the pH signal transduction component PalC of Aspergillus nidulans supports distant similarity to BRO1 domain family members. Genetics **171:**393-401.
192. **Tilburn, J., S. Sarkar, D. A. Widdick, E. A. Espeso, M. Orejas, J. Mungroo, M. A. Penalva, and H. N. Arst, Jr.** 1995. The Aspergillus PacC zinc finger transcription factor mediates regulation of both acid- and alkaline-expressed genes by ambient pH. Embo J **14:**779-90.
193. **Tsang, H. T., J. W. Connell, S. E. Brown, A. Thompson, E. Reid, and C. M. Sanderson.** 2006. A systematic analysis of human CHMP protein interactions: additional MIT domain-containing proteins bind to multiple components of the human ESCRT III complex. Genomics **88:**333-46.
194. **Umemoto, N., T. Yoshihisa, R. Hirata, and Y. Anraku.** 1990. Roles of the VMA3 gene product, subunit c of the vacuolar membrane H(+)-ATPase on vacuolar acidification and protein transport. A study with VMA3-disrupted mutants of Saccharomyces cerevisiae. J Biol Chem **265:**18447-53.
195. **Vaccari, T., T. E. Rusten, L. Menut, I. P. Nezis, A. Brech, H. Stenmark, and D. Bilder.** 2009. Comparative analysis of ESCRT-I, ESCRT-II and ESCRT-III function in Drosophila by efficient isolation of ESCRT mutants. J Cell Sci **122:**2413-23.
196. **Vida, T. A., and S. D. Emr.** 1995. A new vital stain for visualizing vacuolar membrane dynamics and endocytosis in yeast. J Cell Biol **128:**779-92.
197. **Villar, C. C., H. Kashleva, and A. Dongari-Bagtzoglou.** 2004. Role of Candida albicans polymorphism in interactions with oral epithelial cells. Oral Microbiol Immunol **19:**262-9.
198. **Villar, C. C., H. Kashleva, C. J. Nobile, A. P. Mitchell, and A. Dongari-Bagtzoglou.** 2007. Mucosal tissue invasion by Candida albicans is associated with E-cadherin degradation, mediated by transcription factor Rim101p and protease Sap5p. Infect Immun **75:**2126-35.
199. **Vincent, O., L. Rainbow, J. Tilburn, H. N. Arst, Jr., and M. A. Penalva.** 2003. YPXL/I is a protein interaction motif recognized by aspergillus PalA and its human homologue, AIP1/Alix. Mol Cell Biol **23:**1647-55.
200. **von Zastrow, M., and A. Sorkin.** 2007. Signaling on the endocytic pathway. Curr Opin Cell Biol **19:**436-45.

201. **Watts, H. J., F. S. Cheah, B. Hube, D. Sanglard, and N. A. Gow.** 1998. Altered adherence in strains of Candida albicans harbouring null mutations in secreted aspartic proteinase genes. FEMS Microbiol Lett **159:**129-35.
202. **Weissman, Z., R. Shemer, E. Conibear, and D. Kornitzer.** 2008. An endocytic mechanism for haemoglobin-iron acquisition in Candida albicans. Mol Microbiol **69:**201-17.
203. **Williams, R. L., and S. Urbe.** 2007. The emerging shape of the ESCRT machinery. Nat Rev Mol Cell Biol **8:**355-68.
204. **Wilson, R. B., D. Davis, and A. P. Mitchell.** 1999. Rapid hypothesis testing with Candida albicans through gene disruption with short homology regions. J Bacteriol **181:**1868-74.
205. **Wolf, J. M., and D. A. Davis.** 2009. Mutational Analysis of Candida albicans SNF7 Reveals Genetically Separable Rim101 and ESCRT Functions and Demonstrates Divergence in bro1-domain Protein Interactions. Genetics.
206. **Xu, W., and A. P. Mitchell.** 2001. Yeast PalA/AIP1/Alix homolog Rim20p associates with a PEST-like region and is required for its proteolytic cleavage. J Bacteriol **183:**6917-23.
207. **Xu, W., F. J. Smith, Jr., R. Subaran, and A. P. Mitchell.** 2004. Multivesicular body-ESCRT components function in pH response regulation in Saccharomyces cerevisiae and Candida albicans. Mol Biol Cell **15:**5528-37.
208. **Yeo, S. C., L. Xu, J. Ren, V. J. Boulton, M. D. Wagle, C. Liu, G. Ren, P. Wong, R. Zahn, P. Sasajala, H. Yang, R. C. Piper, and A. L. Munn.** 2003. Vps20p and Vta1p interact with Vps4p and function in multivesicular body sorting and endosomal transport in Saccharomyces cerevisiae. J Cell Sci **116:**3957-70.
209. **Yorikawa, C., E. Takaya, Y. Osako, R. Tanaka, Y. Terasawa, T. Hamakubo, Y. Mochizuki, H. Iwanari, T. Kodama, T. Maeda, K. Hitomi, H. Shibata, and M. Maki.** 2008. Human Calpain 7/PalBH Associates with a Subset of ESCRT-III-related Proteins in its N-terminal Region and Partly Localizes to Endocytic Membrane Compartments. J Biochem **143:**731-745.
210. **You, B. J., and K. R. Chung.** 2007. Phenotypic characterization of mutants of the citrus pathogen Colletotrichum acutatum defective in a PacC-mediated pH regulatory pathway. FEMS Microbiol Lett **277:**107-14.
211. **Yu, Z., M. D. Gonciarz, W. I. Sundquist, C. P. Hill, and G. J. Jensen.** 2008. Cryo-EM structure of dodecameric Vps4p and its 2:1 complex with Vta1p. J Mol Biol **377:**364-77.